UCGE Reports
Number 20332

Department of Geomatics Engineering

Context Aware High Dynamics GNSS-INS for Interference Mitigation

(URL: http://www.geomatics.ucalgary.ca/graduatetheses)

by

Ahmed Mohsen Mohamed Kamel

August, 2011

UNIVERSITY OF CALGARY

Context Aware High Dynamics GNSS-INS for Interference Mitigation

by

Ahmed Mohsen Mohamed Kamel

A THESIS

SUBMITTED TO THE FACULTY OF GRADUATE STUDIES

IN PARTIAL FULFILMENT OF THE REQUIREMENTS FOR THE

DEGREE OF DOCTOR OF PHILOSOPHY

DEPARTMENT OF GEOMATICS ENGINEERING

CALGARY, ALBERTA

August, 2011

Abstract

Autonomous navigation systems used in missiles are mostly dependent on Global Positioning System (GPS) as a primary means of navigation. GPS usage has limitations in terms of missile high dynamics and expected signal interference in the battlefield.

Due to the conflicting bandwidth requirements in Phase/ Frequency Lock Loops (PLLs/ FLLs), a novel FLL-assisted-PLL is proposed for very high dynamic conditions with reduced measurement noise and capabilities to cope with interference. The design is based on fuzzy systems and is used to generate the required Numerical Control Oscillator (NCO) tuning frequency with the information provided by phase and frequency discriminators.

Detailed system design and performance analysis are presented where scenarios include high dynamics and different types and levels of interference are introduced. The designed system is compared also against 3rd order PLLs, with narrow and wide bandwidths, standard FLL-assisted-PLL, in addition to a Kalman Filter (KF) based PLL.

Moreover, to insure robustness of the new system during periods of GPS blockage due to very high interference levels, the system is integrated with additional aiding that can provide external Doppler measurements. Two approaches are introduced to accomplish this. The first approach is to use the measurements available from the missile Inertial Measurement Unit (IMU) as these are not affected by interference. The second approach is to get the benefit from the modern GPS signals such as L2C signal which can be

assumed not to be affected by interference if a narrow band interference signal is aimed at the primary GPS signal L1.

Performance assessments results demonstrate the enhanced performance of the proposed system where better tracking continuity during high dynamics up to 20 g's of acceleration and more accurate measurements in interference free environments and in low and medium interference levels up to jamming-to-signal ratios of 40 dB are achieved for the stand alone system, and at very high interference levels for the aided system.

Acknowledgements

I wish to express my gratitude to my supervisor, Professor Gérard Lachapelle, who was abundantly helpful and offered invaluable assistance, support and guidance.

Deepest gratitude is also due to my co-supervisor Professor Dr. John Nielsen. Without his knowledge and assistance this study would not have been successful.

Special thanks also to Dr. Valérie Renaudin who helped me with her valuable comments, advices and discussions during the thesis progress.

I would like also thank Dr. Daniele Borio for his helpful suggestions during the initial stages of this work.

Sincere thanks also are due to Professor Dr. Mark Petovello who helped me to improve many aspects of the thesis with his helpful comments.

Special thanks to all my graduate student friends in the PLAN Group. Specifically I would like to thank Haris Afzal, Mohamed Tamazin, Shashank Satyanarayana, Pratibha Anantharamu and Peng Xie for sharing literature and their invaluable assistance.

I would also like to convey my thanks to the Egyptian Government for providing me with financial support during my studies at the University of Calgary.

I wish to express my love and gratitude to my beloved parents; although you are thousands of miles away, you were always there whenever I needed you.

This thesis would have never been possible without my loving wife Sara. You were always around at times I was desperate and thought that it would be impossible to continue.

My daughter Nour and my son Mohamed, I owe you lots and lots of fun hours. I could not imagine having done my PhD studies without you; you really gave me the reason to go on.

Table of Contents

List of Tables

List of Figures and Illustrations

List of Symbols, Abbreviations and Nomenclature

Abbreviation	Definition
AI	Artificial Intelligence
AM	Amplitude Modulation
BIOFAM	Binary Input Output Fuzzy Associative Memory
BW	Bandwidth
C/A	Coarse Acquisition
C/N_0	Carrier to Noise Power Density
CB	Citizens Band
CDMA	Code Division Multiple Access
CW	Continuous Wave
CWI	CW Interference
DLL	Delay Lock Loop
DoD	Department of Defense
DSMAC	Digital Scene Matching Area Correlation
E	Early
ECEF	Earth-Centered, Earth-Fixed Coordinates Frame
FAM	Fuzzy Associative Memory
FD	Frequency Discriminator
FFPLL	Fuzzy Frequency Phase Lock Loop
FIS	Fuzzy Inference System
FLC	Fuzzy Logic Controller
FLL	Frequency Lock Loops
FMI	FM Modulation Interference
FSPL	Free Space Path Loss
GNSS	Global Navigation Satellite Systems
GNC	Guidance, Navigation And Control
HPF	High Pass Filter
I	In-Phase
ICD	Interface Control Document
IMU	Inertial Measuring Unit
INS	Inertial Navigation System
IR	Infra Red
J/S	Jamming To Signal Interference Power Ratio
KF	Kalman Filter
L	Late
LNA	Low Noise Amplifier
LOS	Line of Site
MAFE	Maximum Allowed Frequency Error
MEMS	Micro Electro Mechanical System
MF	Membership Function
NCO	Numerically Controlled Oscillator
NF	Noise Figure

NI	National Instruments
P	Prompt
PD	Phase Discriminator
PDF	Probability Density Function
PGM	Precision Guided Munition
PPP	Precise Point Positioning
PI	Proportional Plus Integral
PIT	Predetection Integration Time
PLL	Phase Lock Loop
PRN	Pseudo Random Noise
PSD	Power Spectral Density
Q	Quadrature-Phase
RF	Radio Frequency
RFI	Radio Frequency Interference
SCWI	Swept CW Interference
SD	Standard Deviation
SF	Scale Factor
SV	Space Vehicle
TCXO	Temperature-Compensated Crystal Oscillator
UAV	Unmanned Air Vehicle
UWB	Ultra Wideband
WBN	Wide Band Noise

List of Symbols

Symbol	Definition
A	L1 P signal amplitude
α_k	Rate of change of carrier Doppler
B_n	Loop bandwidth in (Hz)
$C(t)$	Represent C/A code sequence
δf	Filter output frequency error due to noise
$\Delta\phi_k$	Difference between the true carrier phase and the phase of the PLL's NCO
$\Delta\phi_{desired}$	The desired steady-state value of the phase error
Δf	NCO tuning frequency
$\Delta f_{correction}$	Frequency correction signal
Δt_k	The accumulation interval
D	Navigation message data bit sequence
η	Feedback tuning parameter
φ_{o1}	The ambiguous L1 carrier phase
φ_{o2}	The ambiguous L2 carrier phase
Φ	Transition matrix
f_o	Base frequency
f_1	L1 carrier frequency
f_2	L2 carrier frequency
$f_{c\text{-}NCO}$	NCO generated carrier frequency
$f_{d\text{-}INS}$	INS Doppler
f_{Di}^{motion}	Motion Doppler calculated for the frequency f_i
f_e	FLL dynamic stress error.
f_{IF}	Intermediate frequency
f_L	Carrier frequency (Hz)
f_s	Sampling frequency
G_a	Antenna gain (dbic)
h_0, h_{-2}	Allan variance parameters
H	Observation model
J	Jerk stress in g/s
k	Boltzmann's constant
K	Kalman gain
λ_L	GPS carrier wave length
L	Implementation loss
μ	Degree of membership function
N	Filter order
N_f	Noise figure of the receiver including antenna and cable losses (db)
ω_k	Is the carrier Doppler shift

ω_n	Natural radian frequency
P	Error covariance matrix
Q	Dimensionless spread spectrum processing gain adjustment factor
Q	Process noise covariance matrices
R	LOS range to the satellite
R	Measurement noise covariance matrices
σ_θ^2	Variance of the dot-product discriminator
σ_A	1-sigma Oscillator Allan deviation–induced jitter
σ_f	One sigma thermal frequency jitter
σ_j	The phase jitter
σ_t	PLL 1-sigma thermal noise phase jitter
σ_{tFLL}	FLL 1-sigma thermal noise frequency jitter
σ_v	1-sigma Oscillator vibration-induced jitter
S_f	White frequency noise spectral density function amplitude
S_g	Receiver clock's frequency random walk spectral density function amplitude
S_r	Received GPS signal power (dBW)
θ_e	PLL dynamic stress error
T	Predetection integration time
T_o	Thermal noise reference temperature (K)
v_k	The measurement noise
w_k	Process disturbance vector
X	State vector
Z	Update measurements

Chapter One: Introduction

1.1 Background and Motivation

Strategic military dependence on missile technology has been growing rapidly since its first use at the beginning of the twentieth century. The critical requirement regarding missile usage is to lead the missile robustly and accurately from its launch point to its designated end point or target. The missile target could be a certain point on its required orbit in space, or a moving hostile object either flying or rolling on terrain. To achieve this requirement, three operations have to be completed and they are described in literature as the Guidance, Navigation and Control (GNC) process. The GNC process is illustrated in Figure 1-1 and is simply described by dividing it into two main loops (Siouris 2004). The guidance loop has the ability to detect the current target parameters through the guidance sensors and to calculate the error between the desired and actual trajectory. This error is delivered to the guidance computer to generate the guidance commands according to the guidance method used. The guidance command is delivered to the autopilot, which calculates the proper inputs to the actuators to move the missile fins and wings. Missile motion is described as a set of angular rotations and accelerations that are sensed by inertial sensors as a feedback in the autopilot loop to verify the desired manoeuvre of the missile.

Radio Frequency (RF), Infra Red (IR) and optical sensors are examples of different types of guidance sensors that can be used to detect target parameters. Guidance systems can be

categorized into four main categories as shown in Figure 1-2. These categories are command, beam rider, autonomous, and homing guidance (Garnell 1980). A fifth possible category is a combination between two or more of the previous guidance methods such as some types of cruise missiles that switch from autonomous guidance to homing guidance in the terminal phase for more accurate hits. The difference between command guidance and homing guidance is the location of the guidance computer, which can be on the launching station or on missile board, respectively. Beam rider guidance can be classified under the command guidance category, but it requires a direct Line of Site (LOS) between the "beam generator source" and the target.

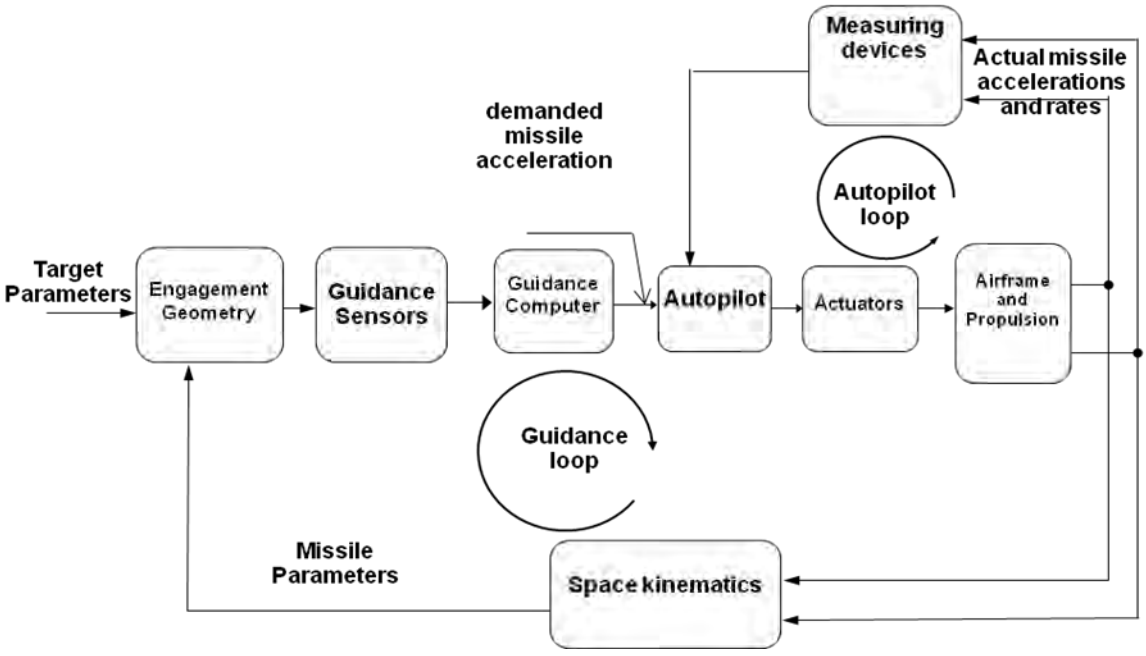

Figure 1-1: Guidance, Navigation and Control (GNC) processes

Both command and homing guidance methods can use RF, IR, or optical sensors and are mostly used for manoeuvring targets. An autonomous guidance system is usually used

when predefined way points are desired or a certain target with known position has to be reached. Different types of sensors can be used for precise navigation such as inertial sensors and Digital Scene Matching Area Correlation (DSMAC) radar.

Global Navigation Satellite Systems (GNSS) are now widely used for precise positioning in civilian and military applications (Kaplan & Hegarty 2006). The Navstar Global Positioning System (Navstar GPS) or simply GPS is the most well-known example of GNSS and was developed by the U.S. Department of Defense (DoD).

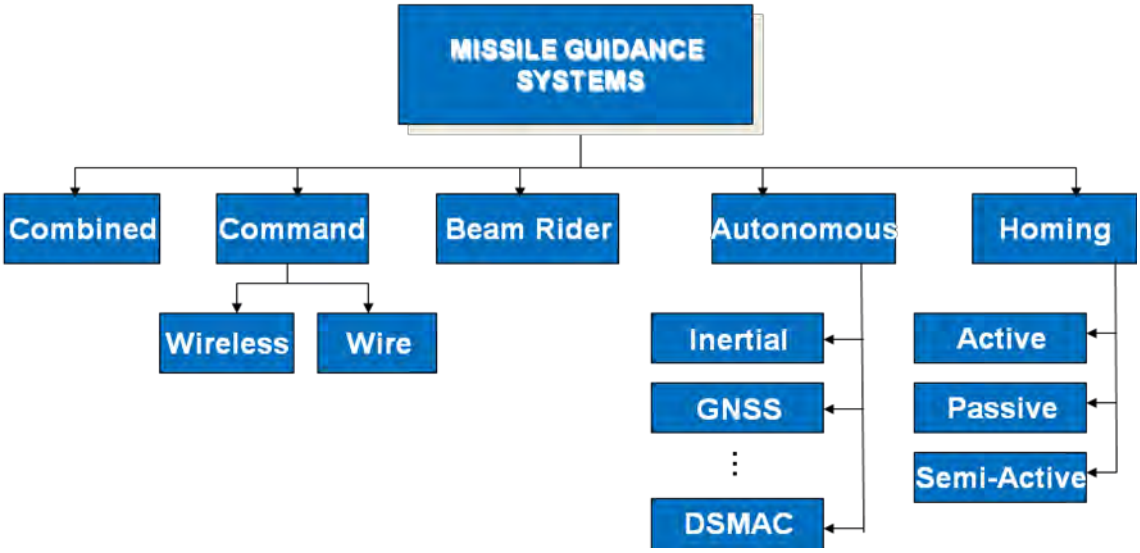

Figure 1-2: Missile Guidance system classification

Recent generations of autonomous guided weapons such as cruise missiles are now heavily dependent on GNSS for midcourse and terminal guidance.

Figure 1-3 (Kamel et al 2011b) is a simple illustration of a GNSS guided cruise missile during the midcourse phase. By using very accurate satellite-navigation updates together with an elementary Inertial Navigation System (INS), a modern cruise missile can achieve autonomous midcourse guidance and deliver a payload to within a few metres of its intended target (Gormley & McMahon 1995). Guided munitions are considered accurate if they can reach their targets within a 12 metre error radius , and considered precise if less than a six metre error is achieved as can be seen in Figure 1-4 (Siouris 2004).

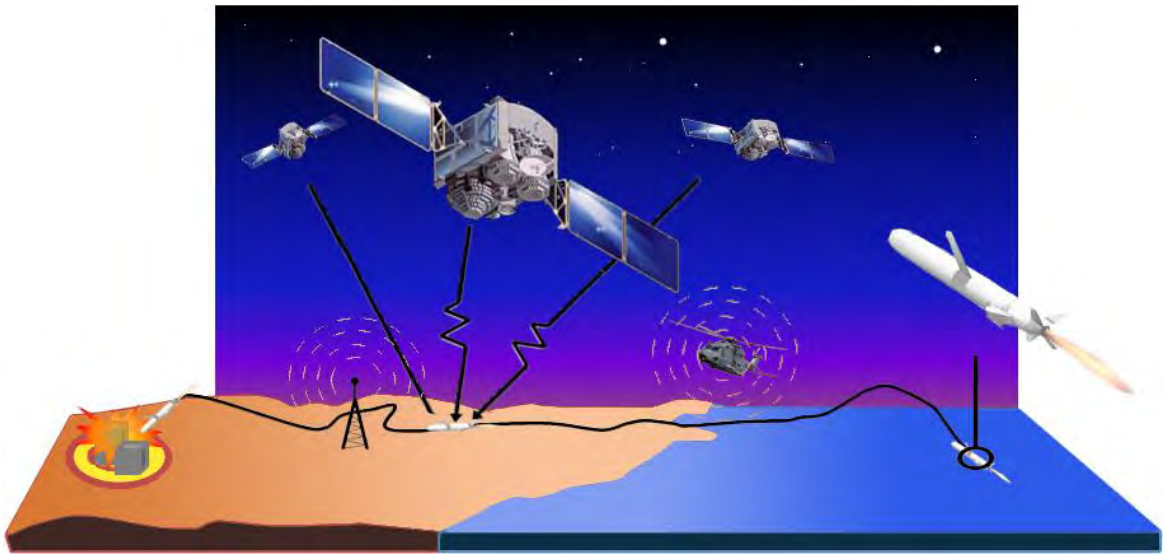

Figure 1-3: Midcourse cruise missile guidance using GNSS

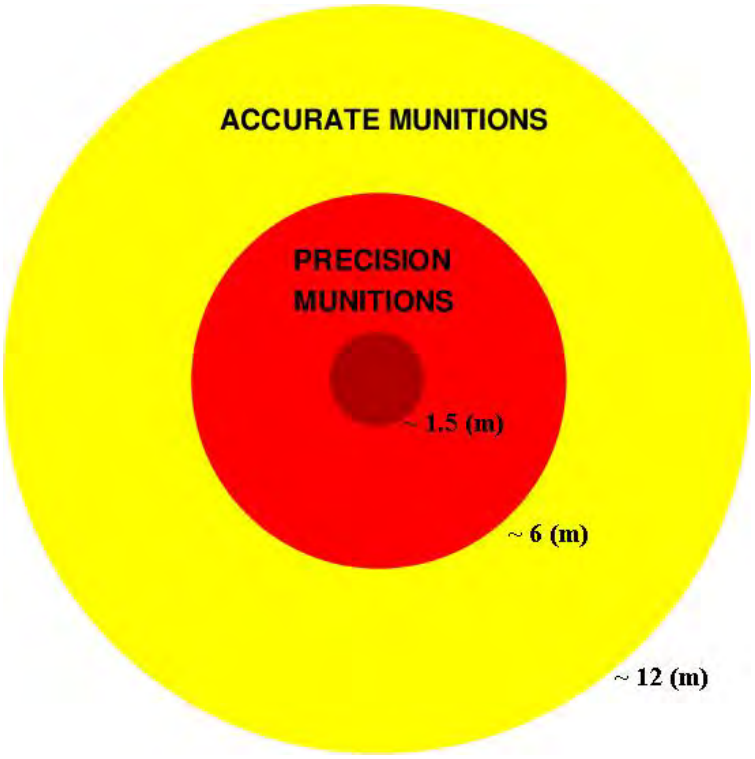

Figure 1-4: Guided munitions accuracy

Due to the very weak GNSS signals near the earth surface (-158.5 dBW for GPS L1 Coarse Acquisition (C/A) signal), high dynamics and possible signal interference are the two main challenges that can threaten GNSS signal tracking for missile applications. To reduce dynamics effects on missile positioning accuracy, an INS can be used as a combined guidance system strategy with GNSS. Several papers in the literature have studied the possible integration schemes between the INS and GPS such as Alban et al (2003). However, even an INS assisted GPS receiver is affected by signal interference depending on the interference threshold and on how the INS and receiver components are fused together. In these conditions, the receiver could lose signal tracking lock and a complete deviation from the required missile trajectory could occur.

This thesis focuses on investigating GPS-based missile guidance system performance under high dynamics and interference effects. As will be discussed in Chapter 2, the GPS receiver tracking requirements for these two effects are conflicting. For this reason, different tracking methods using artificial intelligence with INS aiding and new GNSS signals are proposed to form an integrated context aware navigation unit capable of maintaining acceptable positioning accuracy and robustness in this challenging environment.

1.2 Literature Review and Limitations of Previous Work

The thesis focuses on investigating and improving the performance of autonomous GPS guided missile under the conditions of signal interference and missile high dynamics; for this reason a literature review on types and effects of interference in addition to associated mitigating methods is first required. Missile high dynamics have effects on the GPS signal tracking loops requirements that will be discussed in details in Chapter 2.

GPS, as an example of a GNSS system, is composed of a number of satellites orbiting around the earth at approximately 20,000 km in height and transmitting RF signals with the structure described in the Interface Control Document (ICD) of GPS (GPS.GOV 1993). Those signals carry information used by the receiver on earth to calculate its position. The signal transmitted from each satellite is also modulated with a certain Pseudo Random Noise (PRN) code uniquely identified for this satellite and known by the receiver. Every GPS satellite RF signal suffers from channel loss through its transmission to earth from space and passing through different atmospheric layers. At the receiver's

antenna the signal strength is about -158.5 dBW or 1.4×10^{-16} W, which has a spectral power density that is below that of the ambient thermal noise by about 15 dB. In degraded environments such as foliage or urban canyons, the signal power will be less than that (Misra & Enge 2004). While code correlation in the receiver increases the signals above the background noise floor, the signals are still relatively weak and if the receiver is subjected to intentional or unintentional Radio Frequency Interference (RFI) by a transmitter operating on or near GPS frequencies, tracking will be a challenge. The RFI desensitizes the receiver and if strong enough will deny the receiver acquisition and tracking of the desired GNSS signals (Gerten 2005). Hence, RFI is considered a formidable threat in the operation of a GNSS receiver, especially when used for military applications.

Even though well designed GNSS receivers are robust with regards to interference mitigation, it is essential to suppress unwanted signals as much as possible. Careful design of the antenna can help, by introducing some frequency selectivity against out-of-band interferers (Ward 1994). From a frequency point of view, interferers can either be out-of-band or in-band interferers (Kaplan & Hegarty 2006). An out-of-band interferer is generally an RF source outside the GNSS frequency bands, such as cellular base stations, cell phones, broadcast transmitters, radar, etc. When these signals enter the Low Noise Amplifier (LNA), they can drive it into its non-linear range and the LNA starts to operate as a multiplier or comb generator as it loses its gain and consequently, its Noise Figure (NF) increases. In-band interferers are simply RF sources that transmit inside the GNSS bands (Kaplan & Hegarty 2006). If these interferers are relatively weak, the receiver will

handle them by filtering them out, but from a certain power level and higher, there is not a lot that can be done in a conventional commercial receiver as the receiver will be saturated and will not be working anymore in the linear region.

Table 1-1: Types of interference and typical sources (Kaplan & Hegarty 2006)

Types of Interference		Typical Sources
Wide-band	band-limited Gaussian	Intentional matched bandwidth (BW) noise jammers
	phase/frequency modulation	Television transmitter's harmonics of near-band microwave link transmitters
	Matched spectrum	Intentional matched spectrum jammers, spoofers or near-field of pseudolites.
	Wide-band-pulse	Any type of burst transmitters such as radar or Ultra Wideband (UWB)
Narrow-band	phase/frequency modulation	Intentional chirp jammers or harmonics from an Amplitude Modulation (AM) radio station, Citizens Band (CB) radio, radar harmonics and sub harmonics, or amateur radio transmitter
	swept continuous wave	Intentional Continuous Wave (CW) jammers or FM stations wave transmitter's harmonics
	continuous wave	Intentional CW jammers or near-band unmodulated transmitter's carriers

The interference signal can be wideband or narrow band with respect to the GPS signal; what might be considered wideband interference to the GPS L1 C/A code or L2C might

be narrowband to the P(Y) code, M code, or L5. According to this, various types of RFI and their sources are summarized in Table 1-1 (Kaplan & Hegarty 2006).

1.3 Review on Interference Mitigation Techniques

Interference mitigation techniques can be carried out both spatially and temporally (Ward 1994). Figure 1-5 shows a brief categorization of various interference mitigation techniques (Chang et al 2004, Shanmugam 2007). Spatial processing as will be described in the subsequent paragraph is related to the adaptive antenna signal processing, where as temporal processing can be done before or after the code correlation process through a variety of mitigation techniques that will be described later.

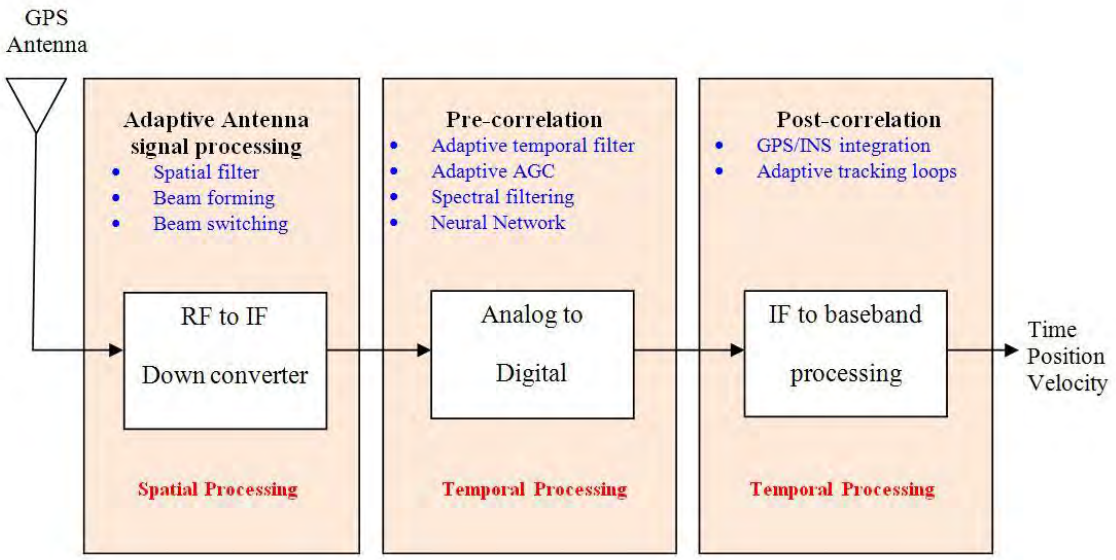

Figure 1-5: Overview of various interference mitigation techniques (Shanmugam 2007)

1.3.1 Spatial Interference Mitigation Technique

Significant interference suppression for a variety of RFI sources can be achieved using spatial processing such as adaptive null steering or beam forming (Brown 2002, Brown & Gerein 2001). However, the issue of system complexity, manufacturing cost and the physical dimension of the missile type under consideration largely limits the application of these techniques. Two techniques called "Null steering" and "Beam forming" are used to control the antenna beam as described in the following paragraphs.

Null Steering: The elements in the antenna array are weighted so that any particular directional signal can be nulled (Cheuk et al 2005). GPS signals are much below the thermal noise level, so any signal that has a power above the thermal noise (i.e., with regards to the Power Spectral Density (PSD)) has to be an interfering signal. In that sense, a null steering antenna adaptively adjusts the weights to place a response null coincident with the bearing of the jammer source. It has a disadvantage of potential reduction of the signal level as well (Zoltowski & Gecan 1995).

Beam Forming: As opposed to null steering, beam forming tries to adjust the antenna in order to maximize the Signal to Noise Ratio (SNR) by steering the antenna beam in the direction of the desired signal or the desired satellite using a Lagrangian type constrained optimizer which maximizes the SNR under the constraint of a null response in the direction of interference (Lin et al 2009). It is however probable that one will end up in a situation where the jammer is in the same direction as the signal source and this is one of the main disadvantages. Figure 1-6 (Malmstrom 2003) is an illustration of the antenna beam forming concept where the antenna beams are formed to be in the satellite

directions. This technique will not prevent the effect of LOS jammers. However, it requires extensive jamming apparatus as illustrated in Figure 1-6 as the jamming signal must come in from several simultaneous bearings.

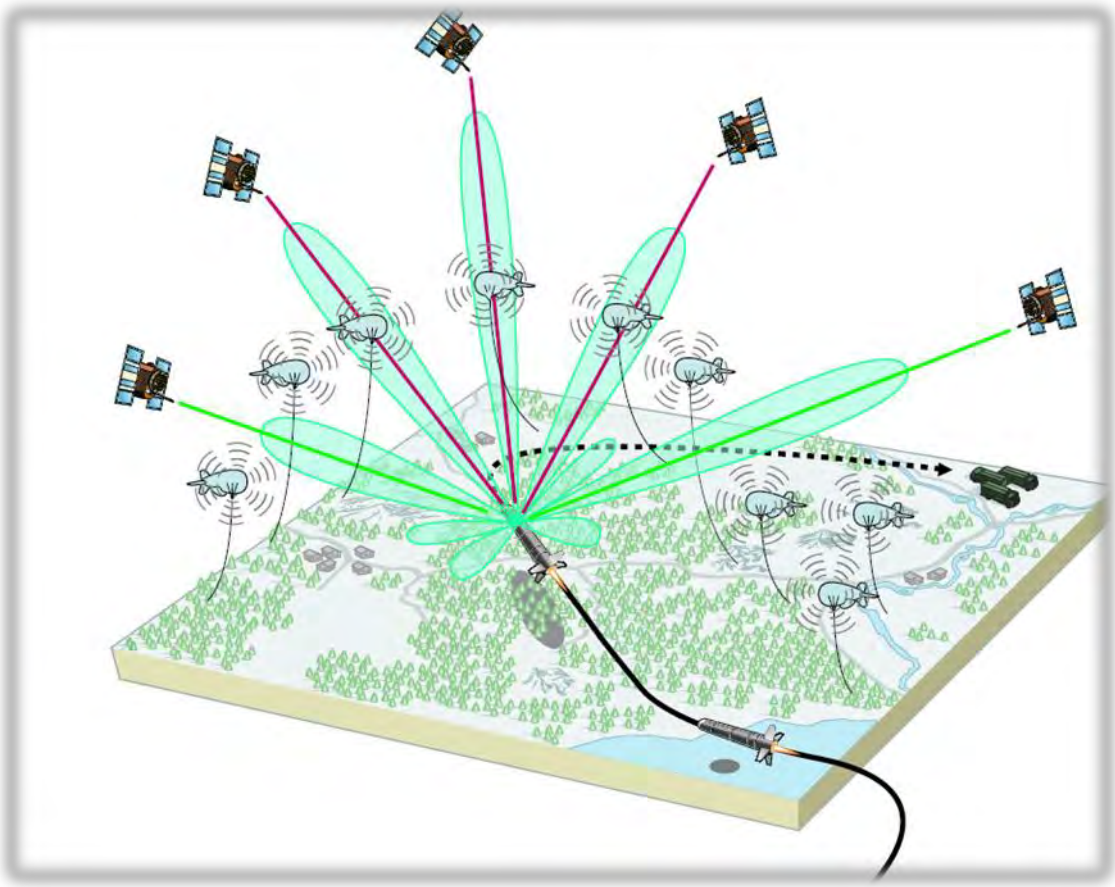

Figure 1-6: GPS antenna beam forming to avoid non-LOS jammers (Malmstrom 2003)

1.3.2 Temporal Interference Mitigation Technique

Temporal processing such as spectral filtering can provide modest interference suppression performance with moderate levels of system complexity (Casbona & Rosen 1999). Temporal processing can be performed prior to or after correlation detection. Prior

to dispreading, the GPS signal has noise-like characteristics. Therefore, any in-band CW interference (CWI) has a relatively narrow spectrum and has strong correlations between samples in which the GPS signals are uncorrelated. For example in the case of a GPS L1 C/A code receiver, the interference of in-band is referred to the frequency between the signal of 1575.42+1.023 MHz and 1575.42-1.023 MHz. It can be discriminated from the GPS signal and suppressed. Depending on the signal domain, jammer features can be sensed and excised.

1.3.2.1 Pre-correlation temporal processing

Adaptive notch filtering and frequency excision techniques are examples of pre-correlation techniques. Adaptive Filtering (Milstein 1988) is effective for narrowband jammers and can be used in applications that require low power and small size. The disadvantage of these methods is that they cannot be used when the jammer does not have a predictable signal structure. When the jammer has a predictable structure, it is possible to subtract the predicted jammer signal from the received signal.

Time-frequency domain filtering attempts to represent the transform of the received signal in such a way that it is possible to easily distinguish between the jammer and the data signal (Giordanengo 2009). Since GPS signals are low power wideband signals, the high power jammer signals can usually be distinguished very easily in the frequency domain by choosing an appropriate threshold. The disadvantage of this technique lies in the fact that the jammer can be effectively separated only if it is sufficiently stronger than the GPS signal, but if it is not significantly stronger than a GPS signal then it is not relevant.

1.3.2.2 Post-correlation temporal processing

Post-correlation techniques are usually referred as adaptive code/carrier tracking loops, which can utilize aiding data from external sensors such as Inertial Measurement Units (IMUs).

Table 1-2: Interference mitigation techniques against several interference types

Interference mitigation techniques	GPS impact	WBN		SCWI		Tone/CW		Pulse		Cost	Size	Retro-fit cost
		1	n	1	n	1	n	1	n			
Spectral Filtering	L	x	x	√	L	√	√	√	√	Low	small	Low
Temporal filtering	L	x	x	√	L	√	√	√	√	Low	small	Low
Spatial Null steering	x	√	L	√	L	√	L	√	L	High	Large	High
Spatial beam forming/switching	x	√	L	√	L	√	L	√	L	High	Large	High
Amplitude canceller	L	√	x	√	x	√	x	√	√	Low	Small	Mid
Axial Nuller	L	√	L	√	L	√	L	√	L	Low	Small	Mid
GPS/INS integration	√	√	√	√	√	√	√	√	√	Mid	Mid	Mid

√ Design capability
L Limited capability
X Little/ No capability

WBN: Wide Band Noise
SCWI: Swept CW Interference
n: multiple jamming sources

After: (Casbona & Rosen 1999)

Interference mitigation techniques against several interference types as well as cost and size are summarized in Table 1-2 (Casbona & Rosen 1999). In this table a comparison is made between many interference mitigation techniques varied between spatial and temporal techniques as described earlier against several interference types such as CW, swept CW interference (SCWI), Wide Band Noise (WBN) and pulsed interference. A comparison is also made against cost, size and retrofit cost of the technique used.

According to this comparison, it is found that the choice of GPS/INS integration as an interference mitigation technique can be considered an optimal solution especially with the fast increasing accuracy of Micro Electro Mechanical Systems (MEMS) in addition to their rapidly decreasing in price.

1.4 Integration of GPS and INS

Inertial coupling between GPS and INS systems provide a good solution for high-rate manoeuvring platforms such as missiles, Precision Guided Munitions (PGMs), Unmanned Air Vehicles (UAVs) and aircrafts. GPS/INS coupling also provides a good and reliable solution for the interference problem as described earlier. The coupling concept is to link the GPS and IMU or INS to allow aiding. Aiding can be performed in several ways (El-Sheimy 2007, Phillips & Schmidt 1996); GPS can be used to periodically update the IMU/INS to establish a minimum bias error. The IMU/INS can provide the position of GPS to improve acquisition and track times, and handle multipath conditions at launch. The GPS and IMU/INS systems can be linked via Kalman techniques (Brown & Hwang 1997) to fuse navigation information and handle short intervals of GPS outage caused by interference or jamming. The levels of performance achieved are dependent on IMU/INS accuracy (and cost) and GPS satellite visibility and are driven generally by miss distance requirements. The complexity and cost of coupling are generally acceptable for manned aircraft, missiles and UAVs that carry both systems. Coupling becomes necessary on missile systems, PGMs, and projectiles to handle the extreme dynamics, rapidly changing GPS visibility and jamming.

The advantages of GPS/INS integration, relative to either GPS or INS alone, can be summarized as follows (Alban et al 2003, Gautier & Parkinson 2003):

1. a high data rate of complete navigation solution including position velocity and attitude,
2. superior short-term and long-term positioning accuracy,
3. improved availability,
4. smoother trajectories,
5. greater integrity, and
6. non significant cost specially when used for military applications.

Based on different data fusion strategies, GPS/INS integrated systems can be divided into three types: loosely coupled GPS/INS, tightly coupled GPS/INS, and ultra-tightly coupled GPS/INS.

In a loosely-coupled integration, the INS and GPS position and velocity are differenced to form the measurement input to a Kalman filter (KF) (Cannon et al 2001), which estimates the INS errors. This technique may be used with any INS and any GPS receiver. However, the gain is limited by the need to account for time-correlated noise on the GPS navigation solution. Also, at least four GPS satellites must be tracked in order to provide the GPS navigation solution with which to calibrate the INS. A block diagram illustration of a loosely coupled integration algorithm is showed in Figure **1-7**.

In a tightly-coupled integration (Wendel & Trommer 2004), the GPS navigation filter is combined into the INS/GPS integration filter which uses the pseudorange and pseudorange rate measurements from the GPS antenna to each satellite, measured by the

GPS receiver and updates the same variables calculated through the INS navigation solution. The INS errors are fed back to correct the inertial navigation equation function. An independent INS navigation solution is maintained, which is corrected to form the integrated navigation solution. A block diagram of a tightly coupled integration algorithm is showed in Figure 1-8.

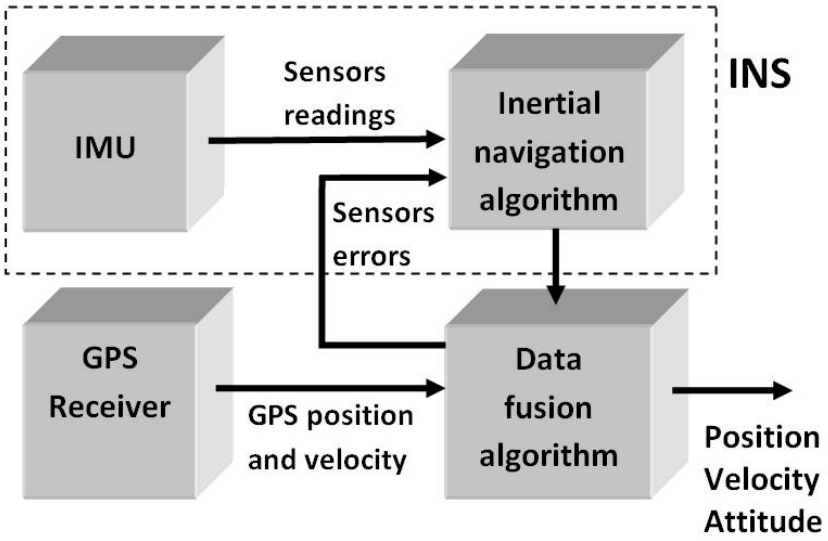

Figure 1-7: Block diagram illustration of a loosely coupled integration algorithm

The final integration architecture is the ultra-tightly coupled (Babu et al 2008, Petovello & Lachapelle 2006, Petovello et al 2007). This combines the INS/GPS integration and GPS signal tracking functions into a single estimation algorithm in which; the INS measurements are fed back into the receiver to decrease GPS signal tracking errors and enhance GPS positioning performance, in addition to helping the receiver tracking loop to retrieve signal lock if it is lost due to interference or jamming. A block diagram illustration of an ultra-tightly coupled integration algorithm is showed in Figure 1-9.

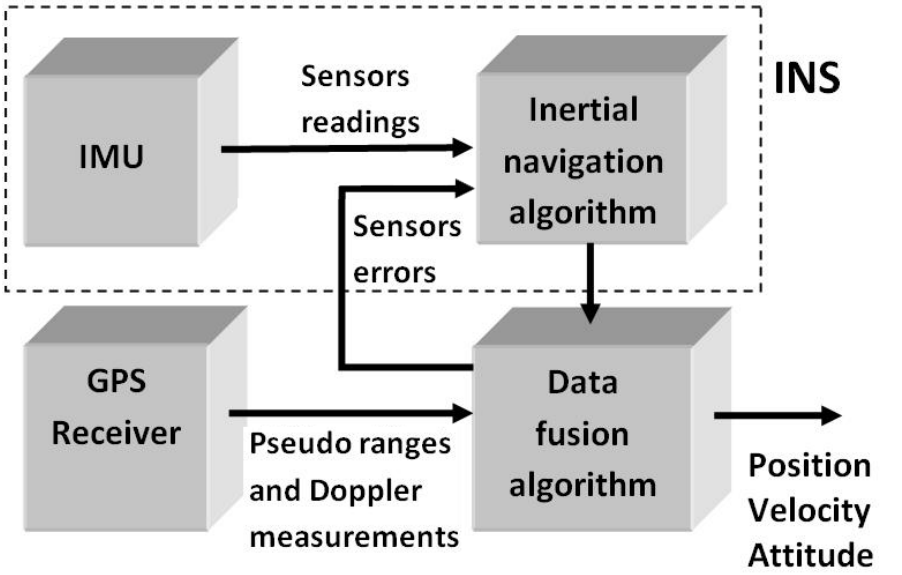

Figure 1-8: Block diagram of a tightly coupled integration algorithm

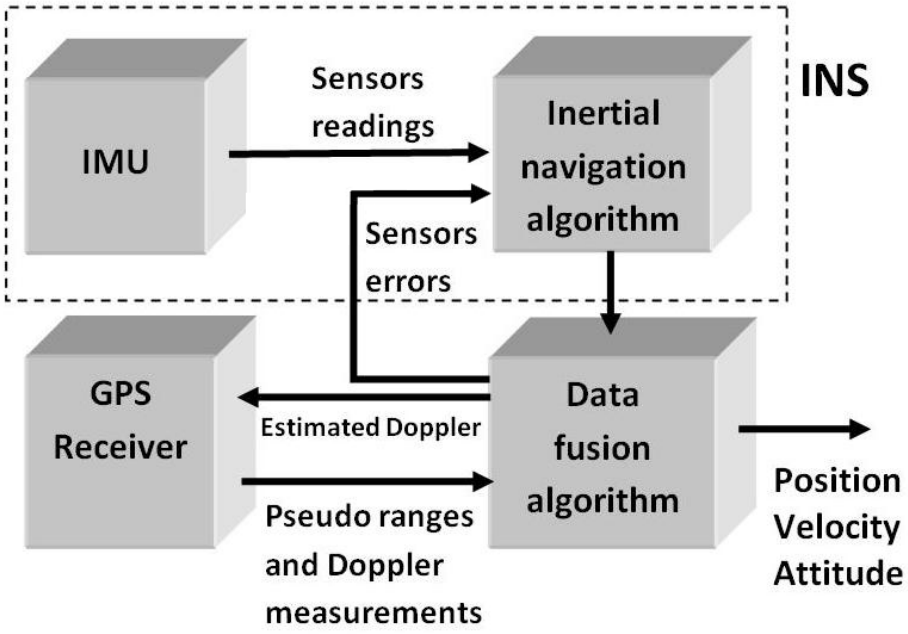

Figure 1-9: Block diagram of an ultra-tightly coupled integration algorithm

1.5 Research Objective and Contributions

Given the lack of non-classified public research directed towards GPS signal tracking during combined events of signal interference and missile high dynamics, this thesis expands the work described in the previous sections by investigating new signal tracking techniques using artificial intelligence such as fuzzy logic and attempts to analyze the performance of existing architectures utilized by different signal tracking schemes such as Phase Lock Loops (PLLs), Frequency Lock Loops (FLLs) and KF based PLLs versus new techniques developed herein in the specific conditions described above. Fuzzy logic was introduced in 1965 by Lotfi Zadeh (Zadeh 1965). It offers a technique for making a decision on partially true or false events and not on a binary decision like in classical logic. The existing applications of fuzzy control range from micro-controller based systems in home applications to advanced flight control systems. The main advantages of using fuzzy are as follows (Zadeh 1965):

- It is implemented based on human operator's expertise, which does not lend itself to being easily expressed in conventional proportional-integral-derivative parameters of differential equations, but rather in situation/action rules.
- For an ill-conditioned or complex plant model, fuzzy control offers ways to implement simple but robust solutions that cover a wide range of system parameters and, to some extent, can cope with major disturbances.

Fuzzy logic based solutions have proven to be successful among control problems researchers and particularly for missile control applications (Kamel & Elsheikh 2004) .

The lack of research in using fuzzy logic techniques in the context of GPS signal tracking introduces it as a novel alternate control loop element that has robust properties ideally suitable for applications and scenarios considered in this research.

The main objective is to design a context aware system that is capable of improving the performance of GPS signal tracking under signal interference and high dynamics conditions by detecting these events and chose the most appropriate tracking configuration from the ones introduced in this research. To achieve this goal, existing enhancement strategies such as INS integration and modern GPS signal tracking such as the use of the L2C signal will be investigated and integrated with the new fuzzy based signal tracking algorithms developed in this research to build a complete system capable of providing the GPS navigation data even with the challenging environments so it can be safely used onboard of missiles, fighters, or UAVs in a battle field. To this end the following goals are pursued:

- Analyze and investigate the performance of the tracking techniques utilized by traditional GPS signal tracking schemes in terms of its accuracy, continuity, and its limitations. Several parameters and their effects on the previous terms have to be studied such as tracking loop filter bandwidth, signal strength and integration time.
- Develop novel tracking algorithms using artificial intelligence that enable efficient GPS signal tracking under GPS signal interference and high dynamic applications.

- Use the previously described benefits of GPS/INS integration with the new tracking algorithms for further performance enhancement.
- Investigate the performance of new GPS signal tracking methods such as the L2C signal under interference and high dynamics conditions and study the benefits of using this signal with the L1 signal in a combined or parallel tracking scheme.

To achieve these goals, a SPIRENT GSS7700 (Spirent 2006) GPS hardware simulator is used due to its availability, capabilities, and accuracy. This hardware has the advantages of producing GNSS RF signals in different and controllable environments in addition to the ability of repeating the exact scenario several times so different environmental effects can be isolated and monitored. The current hardware configuration is capable of producing L1 and L2C frequencies, among other GNSS frequencies, in addition to adjustable additive interference through two separate signal generators. The simulator also is able to produce IMU like measurements with controllable output rate. These measurements are perfectly synchronized with GPS RF signals through GPS time tags to avoid any synchronization errors. The simulator RF signals are collected and saved using specially configured RF front end connected to a special purpose computer for post processing as will be described later. The collected RF signals are post processed using custom written software that runs under MATLAB® platform and is capable of acquisition and tracking of GPS signals using different tracking algorithms. This software is capable of reading the binary files saved by the front-end utilized and performs GPS signal acquisition for eight channels. As a second step, the software is capable of performing signal tracking using different tracking algorithms such as PLL, FLL, FLL-

assisted – PLL, Kalman filter, and finally, the fuzzy tracking technique developed herein. During tracking, the software is able to resolve the resulting navigation data bits to extract the GPS time required for further integration with IMU data from the simulator or any other inertial software. A custom navigation module is also integrated with the software that is able to read the simulator IMU data and performs a complete mechanization to extract the INS solution. Different GPS/INS integration techniques such as loosely-coupled, tightly-coupled and ultra tightly-coupled integration are also implemented with the different GPS signal tracking schemes.

1.6 Thesis outline

The rest of this thesis is structured in the following way:

Chapter 2 covers the operation theory and architecture of the traditional GPS signal tracking analogue and digital schemes. Phase and frequency tracking are discussed and the benefits of using combined frequency and phase tracking are illustrated. Several parameters and their effects on tracking continuity, accuracy, and thresholds are studied such as tracking loop filter bandwidth, signal strength and integration time. The main tracking error sources and their effects on phase and frequency tracking performance are also discussed. The chapter covers also different approaches that are used for GPS signal tracking using Kalman filter and its advantages and limitations are discussed as well.

Chapter 3 focuses on the usage of fuzzy control as an example of artificial intelligence techniques that can replace conventional GPS signal tracking schemes. An introduction to

fuzzy control systems is introduced. An approach to the design of an innovative GPS signal tracking scheme using fuzzy control as a replacement of a frequency lock loop assisted phase lock loop is also presented. The fuzzy system is designed to be robust against dynamics with minimum tracking noise at the same time and also to avoid conflicting bandwidth tracking requirements during high dynamics in the presence of signal interference.

Chapter 4 introduces an evaluation procedure for the designed fuzzy tracking system. The performance of the proposed tracking scheme is assessed by comparing its tracking measurements with the ones extracted during tracking with other schemes such as PLLs, FLLs and KF-PLLs. Different scenarios that assess the fuzzy system performance in the presence of high dynamics and different signal interference types and levels are presented. Also the effects of changing integration time and pull in frequency are introduced.

Chapter 5 discusses the possible enhancements that can be applied to the fuzzy tracking system described in Chapter 3 using integration with inertial systems. New approach of GPS/INS ultra-tight integration is described. A field experiment that uses real GPS and inertial data is described in details. Improvements gained using this technique regarding tracking robustness and processing time are addressed and discussed.

Chapter 6 is exploring the use of the L2C signal as an example of new data and pilot GNSS signals and the possibility of its usage under the previously described tracking schemes. L2C aiding to L1 signal tracking through a modified design of the new fuzzy tracking scheme is discussed and assessed under the presence signal interference and L1 signal outages. A proposed integrated system that comprises all the above tracking schemes is also introduced.

Chapter 7 concludes the results of this dissertation. The main enhancements and limitations of the proposed GPS signal tracking techniques under signal interference and high dynamics are discussed. Recommendations for further improvements are given.

Chapter Two: GPS Tracking Theory and Limitations

This chapter covers most of the necessary background knowledge for the subsequent chapters. The basic theory of GPS signals tracking using PLLs, FLLs and Kalman filter based PLLs is reviewed. Analog and digital structures are presented. The limitations of these traditional tracking loops in the presence of signal interference and line of sight dynamics are discussed.

2.1 GPS Signal Structure

The GPS Space Vehicles (SVs) transmit the essential navigation signals primarily on two carrier frequencies called L1, the primary frequency, and L2, the secondary frequency. A third frequency L5 was used recently with the last GPS modernization changes (Progri 2006). The carrier frequencies are modulated by spread spectrum codes with unique PRN sequences associated with each SV and by a common navigation data message. All SVs transmit at the same carrier frequencies with minimum interference between channels because of the usage of the Code Division Multiple Access (CDMA) technique. In order to track one SV among several other SVs by the CDMA technique, a GPS receiver must replicate the PRN sequence for the desired SV along with the replica carrier signal, including Doppler effects. Modern GPS signals such as L2C signal and L5 signal carry two multiplexed signals called pilot and data signals. Pilot signals are not modulated by

data message, which enables much longer integration time and which is required for weak signals conditions such as indoor and signal interference cases.

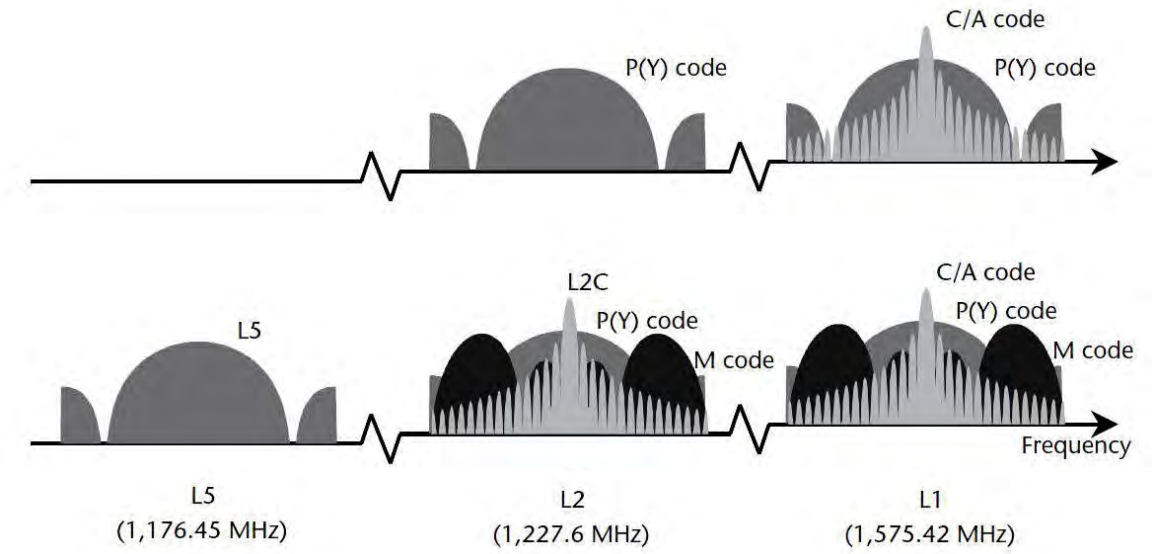

Figure 2-1: Spectrum representation of GPS signals

Figure 2-1 is a spectrum representation of GPS signals (Kaplan & Hegarty 2006) while Table 2-1 summarizes the GPS frequencies along with their original and modernized usage where each composite signal S(t) (in-phase and quadrature-phase) can be described for GPS L1 and L2 frequencies as:

$$S_{L1}(t) = AP(t)D(t)\cos(2\pi f_1 t + \varphi_{o1}) + \sqrt{2}C(t)D(t)\sin(2\pi f_1 t + \varphi_{o1})$$
$$S_{L2}(t) = \frac{A}{\sqrt{2}}P(t)D(t)\cos(2\pi f_2 t + \varphi_{o2}) \quad , \qquad \textbf{(2.1)}$$

where A is the L1 P signal amplitude, *P(t)* and *C(t)* (±1) represent P and C/A code sequences, D (±1) is the navigation message data bit sequence, f_1 and f_2 are the L1 and L2 carrier frequencies, and φ_{o1} and φ_{o2} are the ambiguous L1 and L2 carrier phases .

As one of the main objectives of this work is to study and enhance the performance of the GPS receiver under the effects of signal interference, a description of the received signal power is essential. The free space propagation loss for the distance from the GPS SV to the earth surface is about 184.4 dB, which leads to very weak received signal power. The minimum L1 C/A code signal received power is about -158.5 dBW, whereas the L2 minimum received power is -164.5 dBW (GPS.GOV 1993). These received powers are very low and below the thermal noise floor of a typical receiver, which leads to susceptibility against signal interference.

Table 2-1: GPS Frequencies and Usage

Band	Frequency (MHz)	Phase	Original Usage	Modernized Usage
L1	1575.42	In-Phase (I)	Encrypted Precision, P(Y), code	Encrypted Precision P(Y) code
		Quadrature-Phase (Q)	C/A code	Coarse-acquisition, C/A, code and L1 Civilian code and Military (M) code
L2	1227.60	In-Phase (I)	Encrypted Precision, P(Y), code	Encrypted Precision P(Y) code
		Quadrature-Phase (Q)		L2 Civilian (L2C) code and Military (M) code
L5	1176.45	In-Phase (I)		Safety-of-Life (SoL) Data signal
		Quadrature-Phase (Q)		Safety-of-Life (SoL) Pilot signal

2.2 Carrier and Code Tracking

To extract the required navigation data modulated on the incoming GPS signal, carrier and code tracking loops are required to track the incoming carrier and code signals. Figure 2-2 illustrates typical baseband code and carrier tracking loops for one receiver channel in the closed loop mode of operation. The three complex pairs for "Early (E)", "Prompt (P)", and "Late (L)" of baseband I and Q signals from the digital receiver are passed though "integrate and dump" accumulators, whose duration establishes the Predetection Integration Time (PIT) for the signal. The PIT usually does not exceed 20 ms for a 50-Hz navigation message data bit period for the GPS C/A and P(Y) code signals unless certain techniques are used that allows for longer PIT (Misra & Enge 2004).

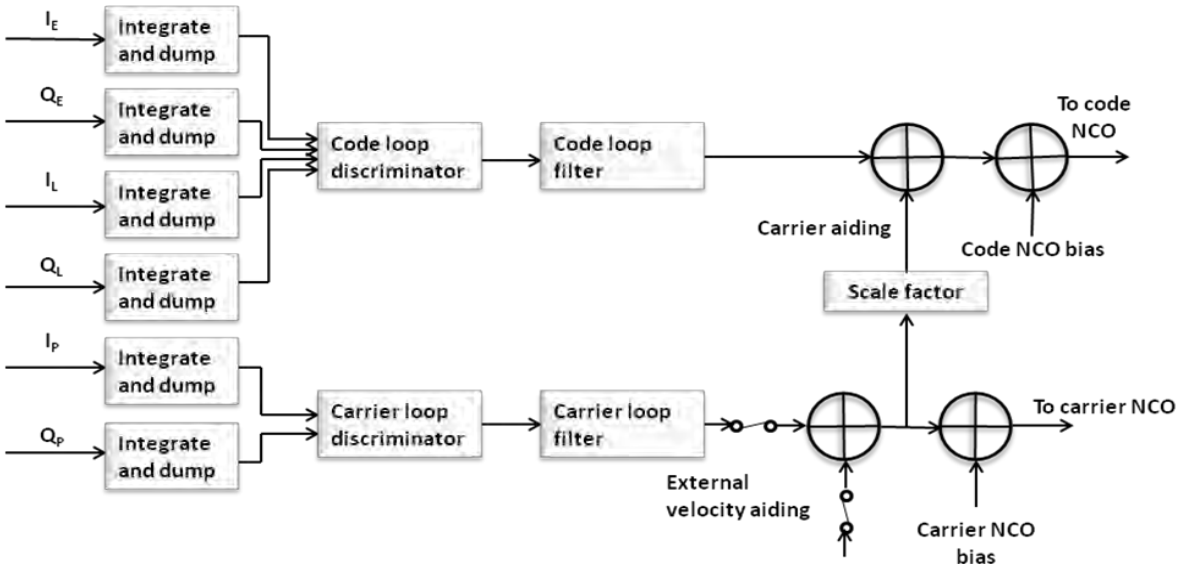

Figure 2-2: Generic Carrier and Code Tracking Loops

Aiding from the carrier tracking loop to the code tracking loop is a typical procedure to remove the LOS dynamic stress from the burden of the latter and hence reduce the code tracking loop bandwidth to minimize the tracking noise. A scale factor is required to map between the carrier frequency and code frequency. The Doppler effect on the signal is inversely proportional to the wave length of the signal. Therefore, for the same relative velocity between the SV and the GPS receiver, the Doppler on the spreading code chip rate is much smaller than the Doppler on the L-band carrier. The Scale Factor (SF) that compensates for this difference in frequency is given by:

$$SF = \frac{R_C}{f_L} \text{ (dimensionless)} , \qquad \textbf{(2.2)}$$

where R_c is the code chipping rate (Hz) and f_L is the carrier frequency (Hz).

External velocity aiding can be applicable also for the carrier tracking loop using external systems such as INS in the same manner as the one described in Equation (2.2). Aiding from carrier tracking loop to the code tracking loop leaves unaided carrier tracking loop to be the weakest link in the tracking procedure. For this reason, the rest of the thesis will be focused on the performance analysis and enhancement techniques for the carrier tracking loop. A carrier tracking loop can be either a PLL or FLL or both in a FLL-assisted-PLL structure (Ward 1998). These loops will be described in details in the following paragraphs.

To extract the modulated navigation data on the GPS signal, an accurate carrier signal tracking system has to be provided. Figure 2-3 presents a block diagram of a GPS

receiver carrier phase tracking loop. The "Integrate and dump", carrier loop discriminator, and the carrier loop filter characterize the receiver carrier phase tracking loop. These three functions determine the two most important performance characteristics of the receiver carrier loop design, namely the carrier phase loop thermal noise error and the maximum LOS dynamic stress threshold. Thresholds and limits will be discussed later in this chapter. As mentioned earlier, the carrier tracking loop is the weakest link in a stand-alone GPS receiver and this is why its thresholds characterize the unaided GPS receiver performance.

The carrier loop discriminator defines the type of tracking loop as a PLL, a Costas PLL (that tolerates the presence of data modulation on the baseband signal), or an FLL. The most commonly used optimal maximum likelihood estimators that characterize the three mentioned discriminators are summarized in Table 2-2 (Kaplan & Hegarty 2006).

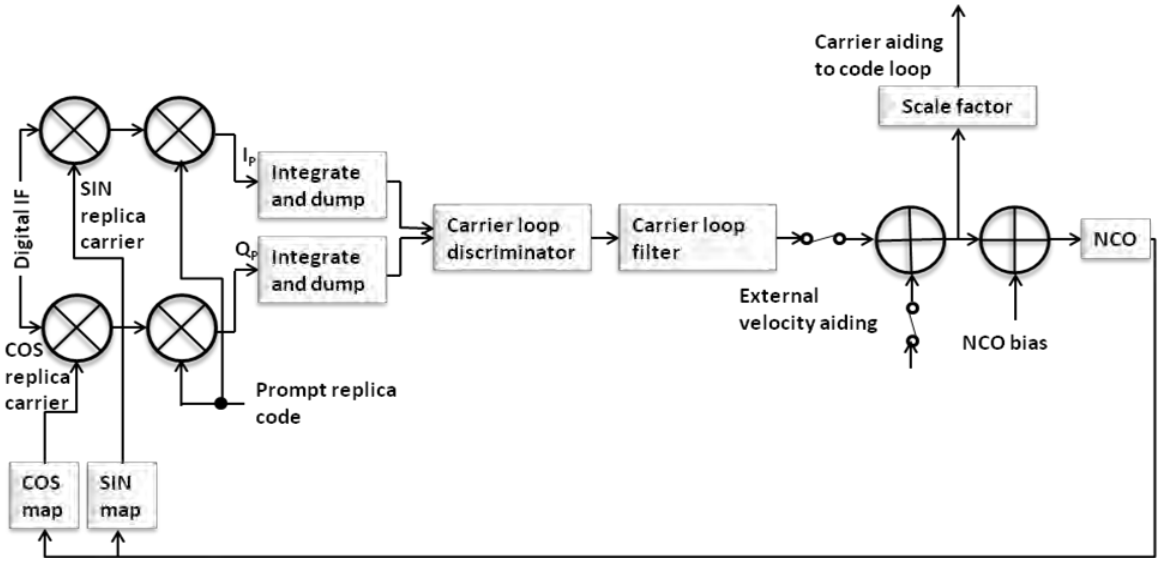

Figure 2-3: Carrier phase tracking loop

Table 2-2: Commonly Used Discriminators

Tracking Loop Type	Discriminator algorithm	Output Error	Characteristics
PLL	$ATAN2(Q_P, I_P)$	Phase error (θ)	Four-quadrant arctangent. Optimal (maximum likelihood estimator) at high and low SNR
Costas PLL	$ATAN(\frac{Q_P}{I_P})$	Phase error (θ)	Two-quadrant arctangent. Optimal (maximum likelihood estimator) at high and low SNR
FLL	$\frac{ATAN2(cross, dot)}{t_2 - t_1}$ $dot = I_{P1} \cdot I_{P2} + Q_{P1} \cdot Q_{P2}$ $cross = I_{P1} \cdot Q_{P2} - I_{P2} \cdot Q_{P1}$	Frequency error $\frac{\theta_2 - \theta_1}{t_2 - t_1}$	Four-quadrant arctangent. Optimal (maximum likelihood estimator) at high and low SNR

The PLL and the Costas PLL are the most accurate, but they are more sensitive to dynamic stress than the FLL. The PLL and Costas loop discriminators produce phase error estimates at their outputs. The FLL discriminator produces a frequency error estimate. Because of this, there is also a difference in the architecture of the loop filter, as described later.

There is a tradeoff between PIT, loop discriminator, and loop filter bandwidth requirements that have to be taken into consideration by the GPS receiver designer during the design of the carrier tracking loop. To tolerate dynamic stress, the PIT should be short, the discriminator should be an FLL, and the carrier loop filter bandwidth should be as wide as possible (Kaplan & Hegarty 2006). However, for the carrier measurements to

be accurate and less noisy, the PIT should be long, the discriminator should be a PLL, and the carrier loop filter noise bandwidth should be narrow. In practice, some compromise must be made to resolve this contradiction.

To acquire the GPS signal in a typical receiver, a multi-hypothesis search of the Doppler and code delay space is done to obtain a rough estimate of these two parameters (Borre et al 2007). A well-designed GPS receiver should start tracking with a short PIT using a wide bandwidth FLL, starting from the obtained signal Doppler and code delay. Because of the data modulation on the carrier, it should then transfer to a Costas PLL, increasing the PIT while also gradually adjusting the carrier tracking loop bandwidth as narrow as the maximum expected dynamics permits, as will be described later. For missile applications, the signal acquisition and tracking are initiated before missile launch. But typically they could be repeated during flight if signal lock is lost due signal interference or high dynamic manoeuvering.

2.3 Filter Design

The most important block in the carrier phase tracking loop is the loop filter. The objective of the loop filter is to reduce noise in order to produce an accurate estimate of the original signal by tuning the Numerically Controlled Oscillator (NCO). The loop filter is a direct implementation of the proportional plus integral (PI) compensator (Golnaraghi & Kuo 2010). The loop filter order and noise bandwidth is a measure of the carrier loop order and bandwidth and also determines the loop filter's response to signal dynamics.

The order of a carrier loop is related to its capability to track different types of signal dynamics. Since a second order PLL is unconditionally stable but suffers from acceleration stress error, high dynamic receivers typically use third order PLLs to provide the desirable characteristic of being able to track an accelerating frequency input. Stability becomes a major concern for higher order loops. The closed-loop system transfer functions along with the corresponding bandwidth are summarized in Table 2-3 (Dierendonck 1996), where ω_n is the natural radian frequency computed from the value of the loop filter bandwidth selected by the designer, N is the filter order and B_n is the loop bandwidth.

Table 2-3: Loop Filter Characteristics

Filter order	**Transfer function** $T_N(s) = \frac{d_1 s^{N-1} + d_2 s^{N-2} + \ldots + d_N}{s^N + d_1 s^{N-1} + d_2 s^{N-2} + \ldots + d_N}$	**Bandwidth** $2B_n = \int_{-\infty}^{+\infty} \lvert T(j2\pi f)\rvert^2 \, df$
N=2	$T_2(s) = \frac{a_2\omega_n s + \omega_n^2}{s^2 + a_2\omega_n s + \omega_n^2}$	$B_n = \frac{d_1^2 + d_2}{4d_1} = \left[\frac{1 + a_2^2}{4a_2}\right]\omega_n$
N=3	$T_3(s) = \frac{b_3\omega_n s^2 + a_3\omega_n^2 s + \omega_n^3}{s^3 + b_3\omega_n s^2 + a_3\omega_n^2 s + \omega_n^3}$	$B_n = \frac{d_1^2 d_2 - d_1 d_3 + d_2^2}{4\left(d_1 d_2 - d_3\right)} = \left[\frac{a_3 b_3^2 + a_3^2 - b_3}{4\left(a_3 b_3 - 1\right)}\right]\omega_n$

The loop filters shown in Table 2-3 can be presented using analog integrators in the Laplace domain as 1/S. The number of the integrators determines the loop filter order and characteristics. An example of a PLL 3rd order loop filter extracted from Table 2-3 is

depicted in Figure 2-4 whereas typical values of multiplier coefficients are introduced in Table 2-4, where ω_{op} is the natural radian frequency of the PLL filter.

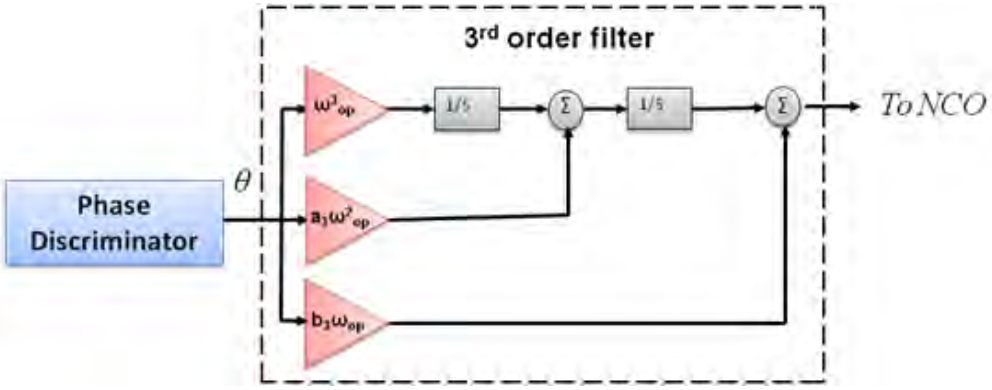

Figure 2-4: PLL 3rd order analog loop filter

Table 2-4: Typical values of 3rd order filter gains

ω_{op}	$a_3\omega_{op}^2$	$b_3\omega_{op}$
$\frac{B_n}{0.7845}$	$1.1\omega_{op}^2$	$2.4\omega_{op}$

For the filter to be digitally represented, an analog to digital transformation for the integrator has to be performed. The digital bilinear z-transform integrator presented in Figure 2-5 linearly interpolates between input samples and more closely approximates the ideal analog integrator (Kaplan & Hegarty 2006). The time interval between each sample T represents a unit delay z^{-1} in the digital integrator.

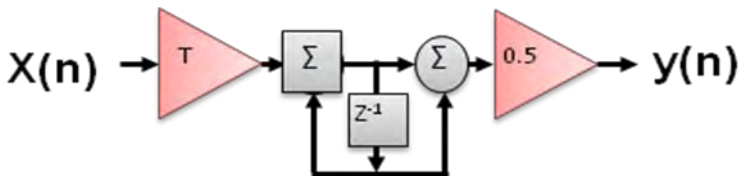

Figure 2-5: Digital bilinear z-transform integrator

To increase the dynamic robustness of the PLL, aiding from FLL is presented in Ward (1998) as an FLL-assisted-PLL structure. This structure is still another configuration that represents a PI compensator with a redundant frequency error input which can help in providing a continuous signal tracking even if phase lock is lost. Figure 2-6 depicts a 3rd order PLL assisted with a 2nd order FLL presented digitally using the bilinear z-transform integrator described above. It can be seen that if the PLL error input is zeroed, the filter becomes a pure FLL. Similarly, if the FLL error input is zeroed, the filter becomes a pure PLL. The lowest noise loop closure process is to close in pure FLL, then apply the error inputs from both discriminators as an FLL-assisted-PLL until phase lock is achieved, then convert to pure PLL until phase lock is lost. However, if the noise bandwidth parameters are chosen correctly, there is very little loss in the ideal carrier tracking threshold performance when both discriminators are continuously operated (Kaplan & Hegarty 2006). Typical values of multiplier coefficients shown in Figure 2-6 are introduced in Table 2-5, where ω_{op} and ω_{of} are the natural radian frequencies of the PLL and FLL filters respectively.

Table 2-5: Typical values of filter gains

ω_{op}	$a_3\omega_{op}^2$	$b_3\omega_{op}$	ω_{of}	$a_2\omega_{of}$
$\frac{B_{np}}{0.7845}$	$1.1\omega_{op}^2$	$2.4\omega_{op}$	$\frac{B_{nf}}{0.53}$	$1.414\omega_{of}$

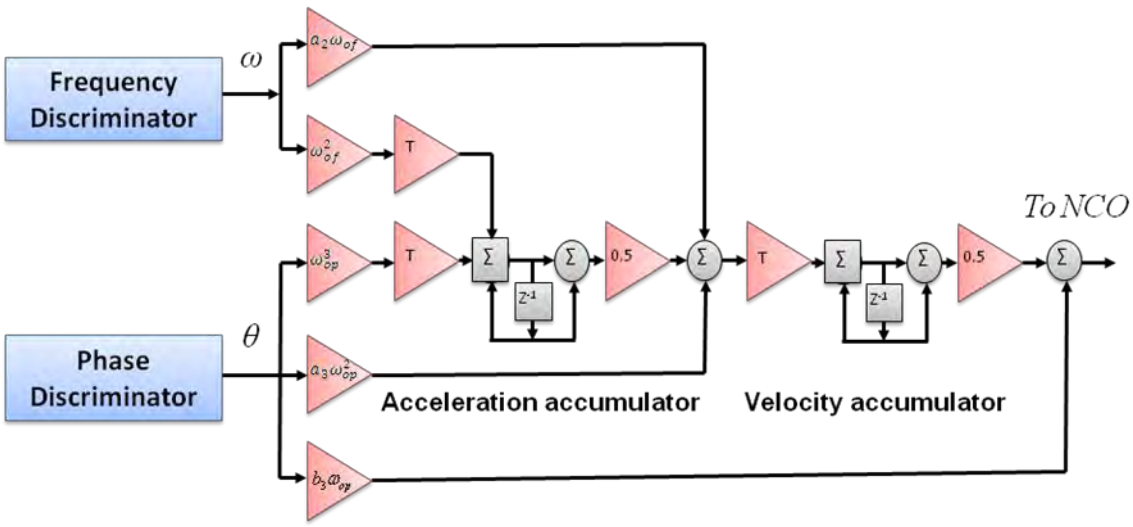

Figure 2-6: Digital FLL-assisted-PLL using bilinear z-transform integrator

2.4 PLL Measurements Error Sources and limitations

Signal tracking continuity is achieved if the phase and frequency measurements errors are not exceeding their thresholds. That is why a clear definition of the dominant error sources has to be provided. The dominant sources of phase error in a GPS receiver PLL are phase jitter and dynamic stress error. The phase jitter (σ_j) is the root sum square of every source of uncorrelated phase errors, such as thermal noise (σ_t) and oscillator noise. Oscillator noise includes vibration-induced jitter (σ_v) and Allan deviation–induced jitter (σ_A).The phase jitter can then be expressed as (Kaplan & Hegarty 2006):

$$\sigma_j = \sqrt{\sigma_t^2 + \sigma_v^2 + \sigma_A^2}\,. \qquad \textbf{(2.3)}$$

A conservative rule of thumb for tracking threshold is that the 3-sigma jitter must not exceed one-fourth of the phase pull-in range of the PLL discriminator. For the case where there is data modulation such as L1 C/A code or L2C M code, the PLL two-quadrant arctangent discriminator must be used and has a phase pull-in range of 180º. Therefore the 3-sigma rule threshold is 45º. Therefore, the PLL rule thresholds are stated as:

$$3\sigma_{PLL} = 3\sigma_j + \theta_e \le 45^o \qquad \textbf{(2.4)}$$

where σ_j is the 1-sigma phase jitter from all error sources except dynamic stress error and θ_e is the dynamic stress error.

Thermal noise and dynamic stress error are the dominant sources of tracking errors especially for the application under consideration where the signal interference and missile high dynamics are directly related to them. For this reason the tracking error analysis is focused on these sources of errors.

2.4.1 Thermal Noise Effect on Tracking Accuracy

Aside from dynamic stress error, PLL thermal noise is treated as the only source of carrier tracking error since the other sources of PLL jitter may be either transient or negligible. The thermal noise jitter for a PLL that uses an arctangent discriminator is computed as follows (Braasch & van Dierendonck 1999, Kaplan & Hegarty 2006):

$$\sigma_t = \frac{360}{2\pi}\sqrt{\frac{B_n}{c/n_0}\left(1+\frac{1}{2Tc/n_0}\right)}\,(\deg), \qquad \textbf{(2.5)}$$

$$\sigma_t = \frac{\lambda_L}{2\pi}\sqrt{\frac{B_n}{c/n_0}\left(1+\frac{1}{2Tc/n_0}\right)}(m), \qquad \textbf{(2.6)}$$

where B_n is the loop bandwidth in (Hz), c/n_0 is the carrier to noise power density expressed as a ratio (Hz) = $10^{\frac{C/N_0}{10}}$ for C/N_0 expressed in dB-Hz, T is the predetection integration time in seconds and λ_L is the ratio between the propagation constant (3×10^8 m/s) and the L-band carrier frequency $\left(1575.42\times10^6 \text{cycles/s}\right)$.

It is clear in Equations (2.5) and (2.6) that the thermal noise jitter is dependent on the loop bandwidth, integration time, and C/N_0. Increasing the bandwidth will increase the noise jitter but will allow more dynamic robustness. At high levels of C/N_0, noise jitter will be smaller, which then allows one to further increase the bandwidth for accommodating the dynamics.

In the presence of signal interference, the C/N_0 value is decreased according to interference level, which again leads to the necessity of bandwidth reduction to decrease its effect. This contradictory relation is depicted in Figure 2-7 and Figure 2-8 at PIT = 1 ms and PIT = 20 ms as the lower and upper boundaries of PIT for a C/A code modulated signal with 50 Hz data message. Increasing PIT leads to noticeable reduction in the thermal noise jitter especially when the C/N_0 is low. Figure 2-9 and Figure 2-10 demonstrates the effect of changing PIT on thermal noise jitter at bandwidths: 1 Hz and 18 Hz, respectively.

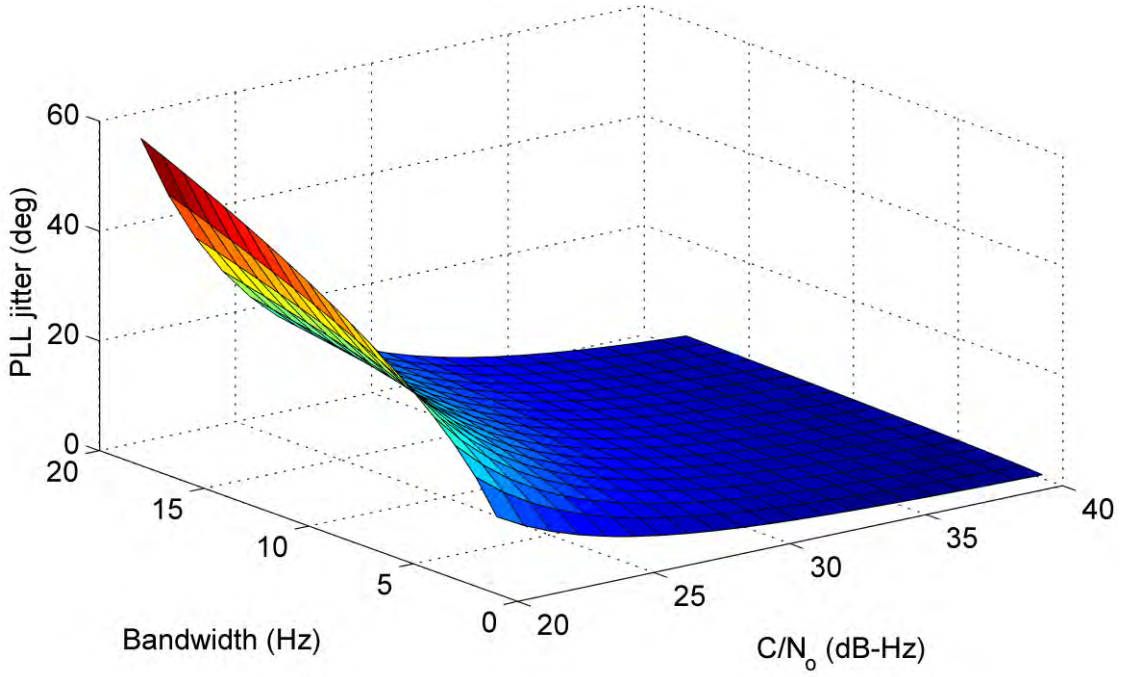

Figure 2-7: PLL thermal noise jitter at PIT = 1 ms

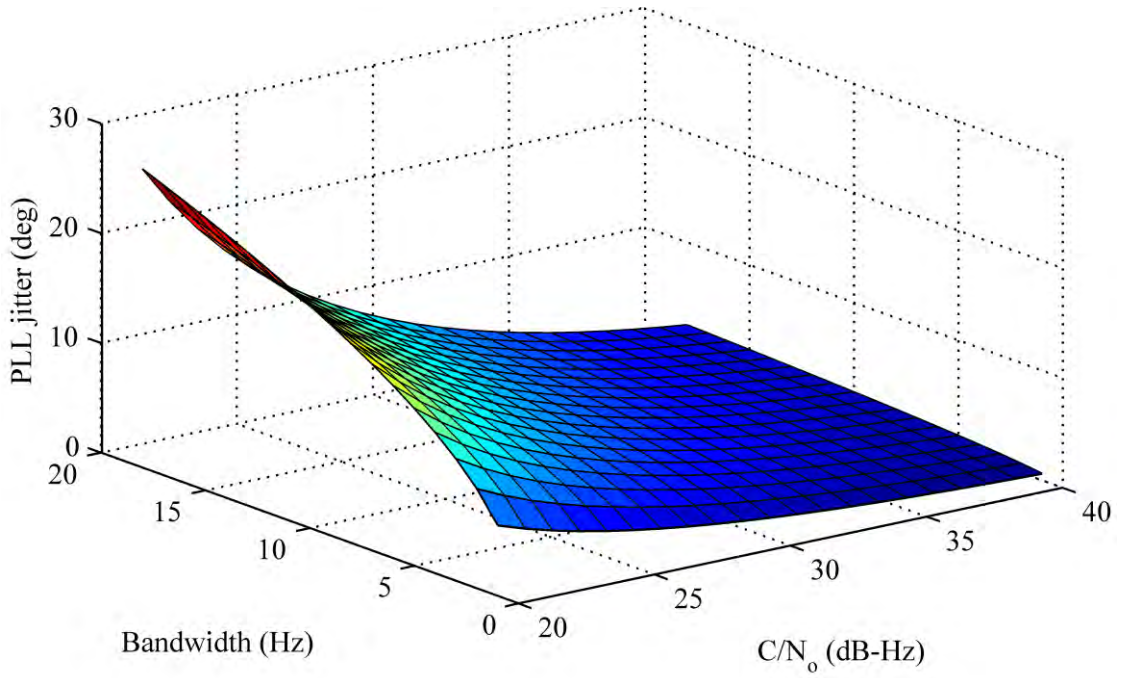

Figure 2-8: PLL thermal noise jitter at PIT = 20 ms

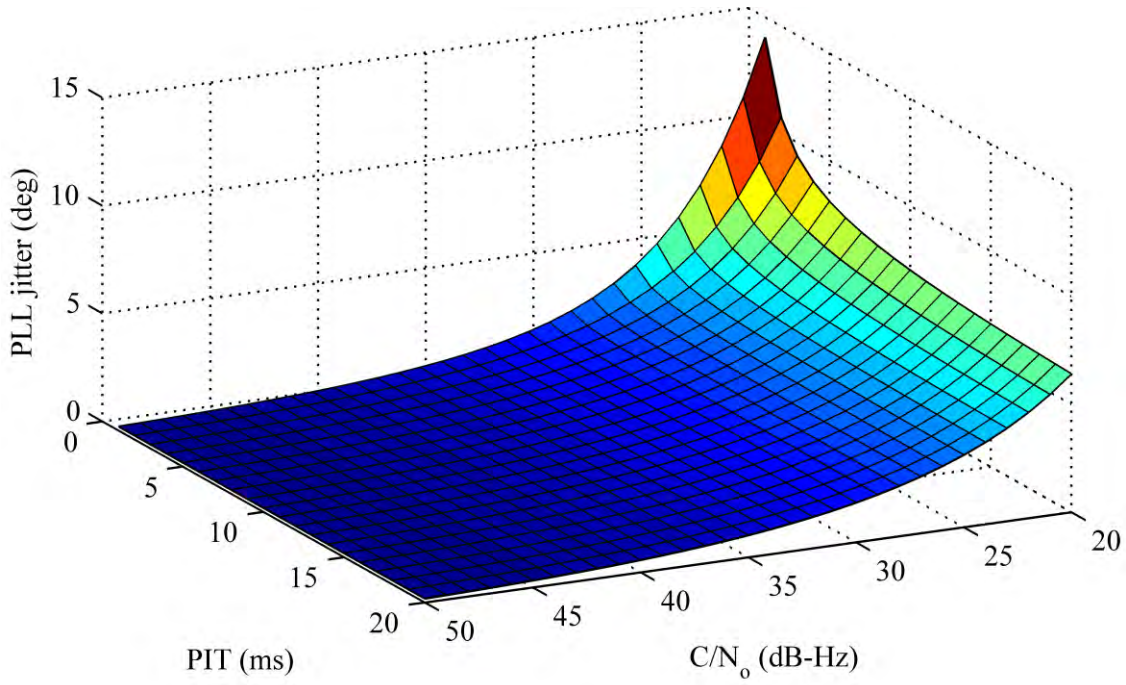

Figure 2-9: PLL thermal noise jitter at BW = 1 Hz

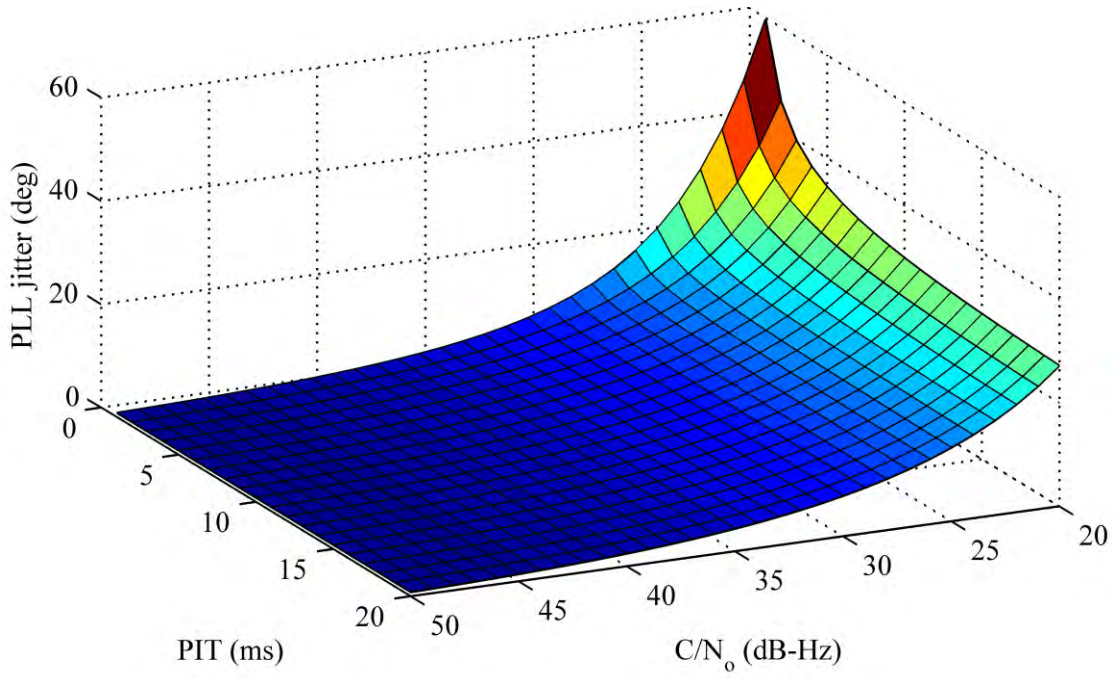

Figure 2-10: PLL thermal noise jitter at BW = 18 Hz

2.4.2 Dynamic Stress Error Effect on Tracking Accuracy

The dynamic stress error is obtained from the steady state error formulas shown in Table 2-6 (Misra & Enge 2004). This error depends on the loop bandwidth and order. The maximum dynamic stress error may be slightly larger than the steady state error if the loop filter response to a step function has overshot, but the steady state error formula is enough. The maximum allowed acceleration stress and jerk stress are calculated for 2nd and 3rd order loops respectively. The transformation from deg/s^2 and deg/s^3 to m/s^2 and m/s^3 are done by dividing by the wavelength of the carrier frequency in deg/m. This factor is calculated for L1 frequency to be $\frac{360(\text{deg})}{0.1903(m)} = 1891.8(\text{deg}/m)$.

Table 2-6: Loop filters dynamic response steady state error

Filter order	Steady state error	Notes
N=2	$\frac{dR^2/dt^2}{\omega_n^2}$	dR^2/dt^2 is maximum LOS acceleration dynamics (deg/s^2)
N=3	$\frac{dR^3/dt^3}{\omega_n^3}$	dR^3/dt^3 is maximum LOS jerk dynamics (deg/s^3)

Figure 2-11 and Figure 2-12 illustrate the relation between the maximum allowed acceleration and jerk stress for 2nd and 3rd order loops respectively. These figures show that for certain phase errors, the dynamic stress capability is increased by the bandwidth increase. Referring to the previous section, this bandwidth increase will cause another increase in the phase tracking jitter and a tradeoff has to be considered. If the maximum phase jitter is considered as stated in Equation (2.4), the maximum allowed jerk stress is

around 30 g/s, which is not enough for missiles applications (Siouris 2004). This is why aiding from FLL is required to increase this threshold as shown in the next section.

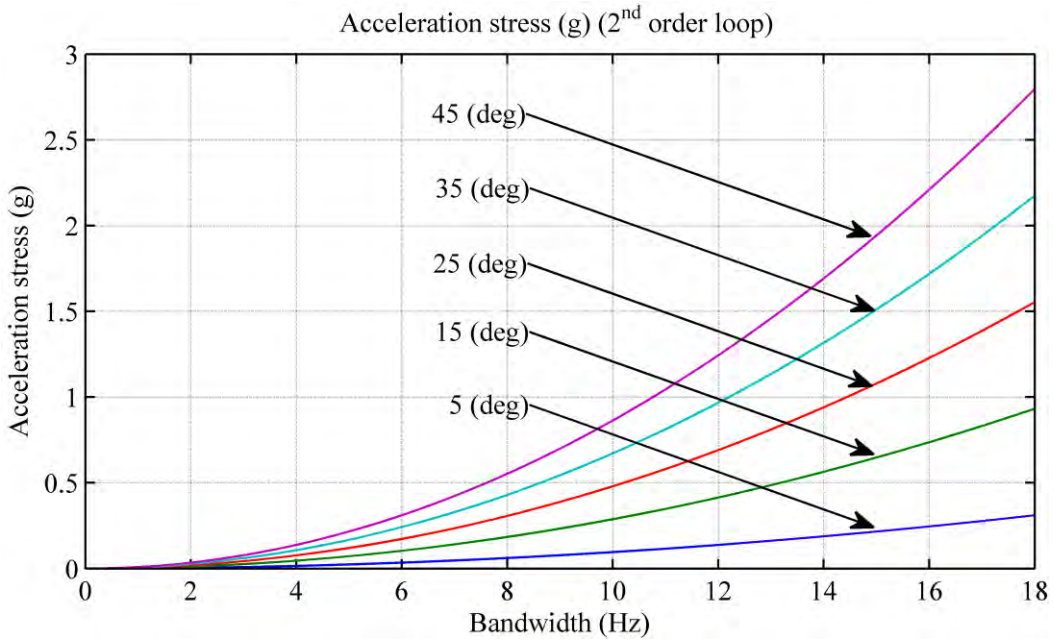

Figure 2-11: Max. acc. stress for 2nd order PLL to maintain certain phase errors

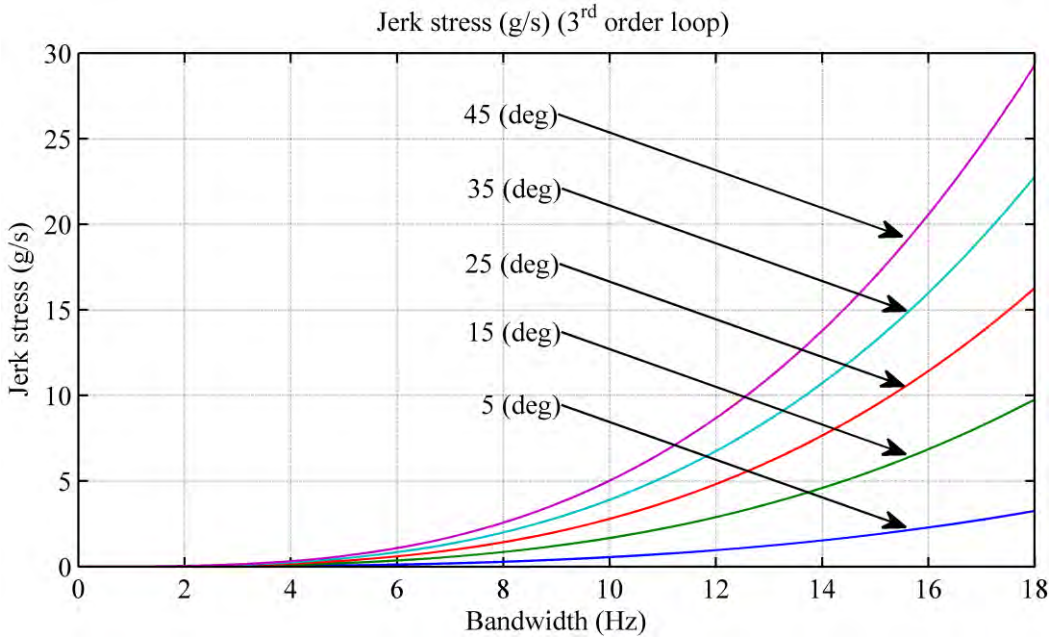

Figure 2-12: Max. Jerk stress for 3rd order PLL to maintain certain phase errors

2.5 FLL Measurements Error Sources and Limitations

The PIT is strongly related to the maximum allowable dynamic stress error when using an FLL. A 3-sigma frequency error as a rule of thumb should not exceed ¼ PIT as follows (Kaplan & Hegarty 2006):

$$3\sigma_{FLL} = 3\sigma_{tFLL} + f_e \le \frac{1}{4} PIT(Hz), \tag{2.7}$$

where σ_{tFLL} is the 1-sigma thermal noise frequency jitter and f_e is the FLL dynamic stress error.

The Frequency Discriminator (FD) described in Table 2-2 uses two consecutive samples to calculate the frequency error. This reduces the maximum PIT for a 50 Hz data modulation as for L1 C/A signal to 10 ms (Kaplan & Hegarty 2006).

The previous rule indicates that by increasing PIT from 1 ms to a maximum of 10 ms to accommodate with FLL, the allowable frequency error threshold is reduced by 90%, which can lead to losing frequency lock if the receiver is subjected to relatively high dynamics.

Figure 2-13 illustrates the relation between the coherent integration time and the maximum allowable frequency error (Hz) due to dynamics, neglecting any other error sources. To sense it in terms of receiver motion, this frequency error (f_e) is related to LOS dynamics through the following equation:

$$f_e = \frac{1}{360\omega_n^N} \frac{d^{N+1}R}{dt^{N+1}}(Hz), \tag{2.8}$$

where N is the loop filter order, ω_n is the natural radian frequency determined from the desired loop filter noise bandwidth and R is the LOS range to the satellite.

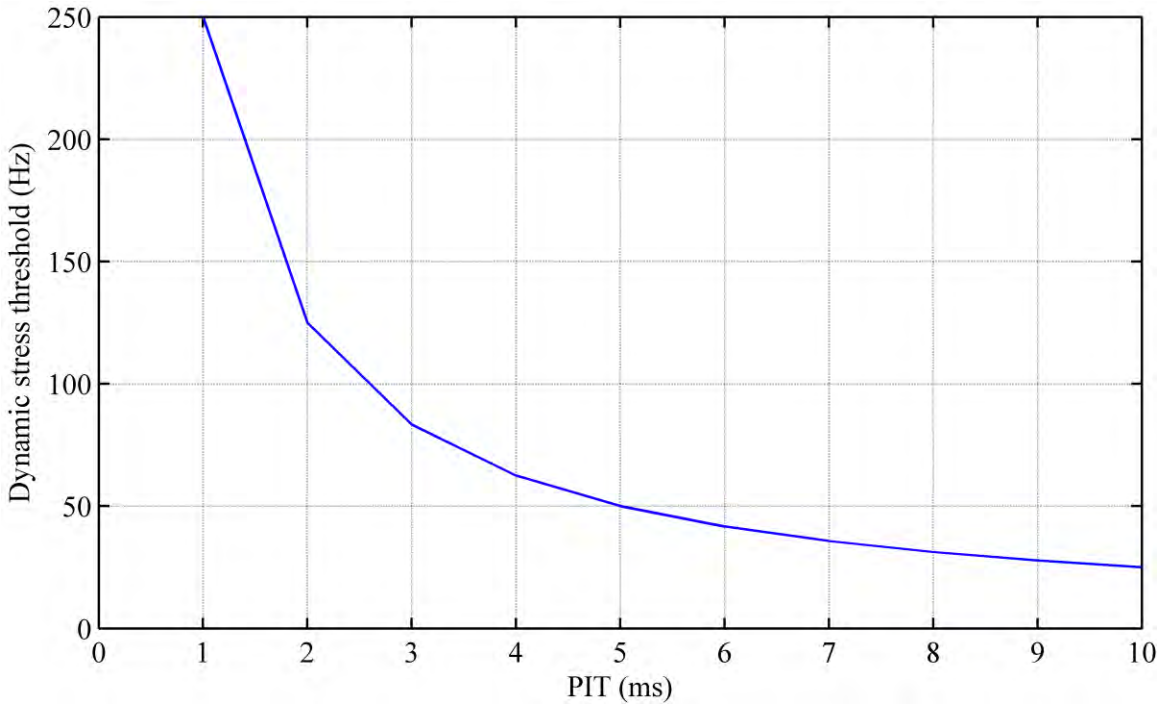

Figure 2-13: Relation between PIT and frequency dynamic stress threshold neglecting any other error source

By knowing the frequency error, the maximum allowable jerk stress can be calculated by using the (deg/m) ratio through the following equation:

$$J = \frac{c\dfrac{d^{N+1}R}{dt^{N+1}}}{(9.81)(360)L1}, \tag{2.9}$$

where J is the jerk stress in g/s, c is the speed of light and $L1$ is the GPS L1 frequency. Figure 2-14 illustrates the relation between PIT and the maximum allowable receiver jerk stress using a second order FLL with a bandwidth of 2 Hz. It can be noticed in this figure

that by increasing PIT from 1 ms to 2 ms, the receiver maximum dynamics is reduced by 50%. If the receiver is to be used on highly dynamic vehicles such as guided missiles or fighters, the frequency tracking loop should have the widest possible bandwidth in addition to a small PIT to accommodate these high dynamics. Figure 2-15 illustrates the relation between PIT and the max allowable receiver jerk stress using a second order FLL with a bandwidth of 10 Hz. It can be seen that by increasing BW, the allowable jerk stress at the same PIT is dramatically increased.

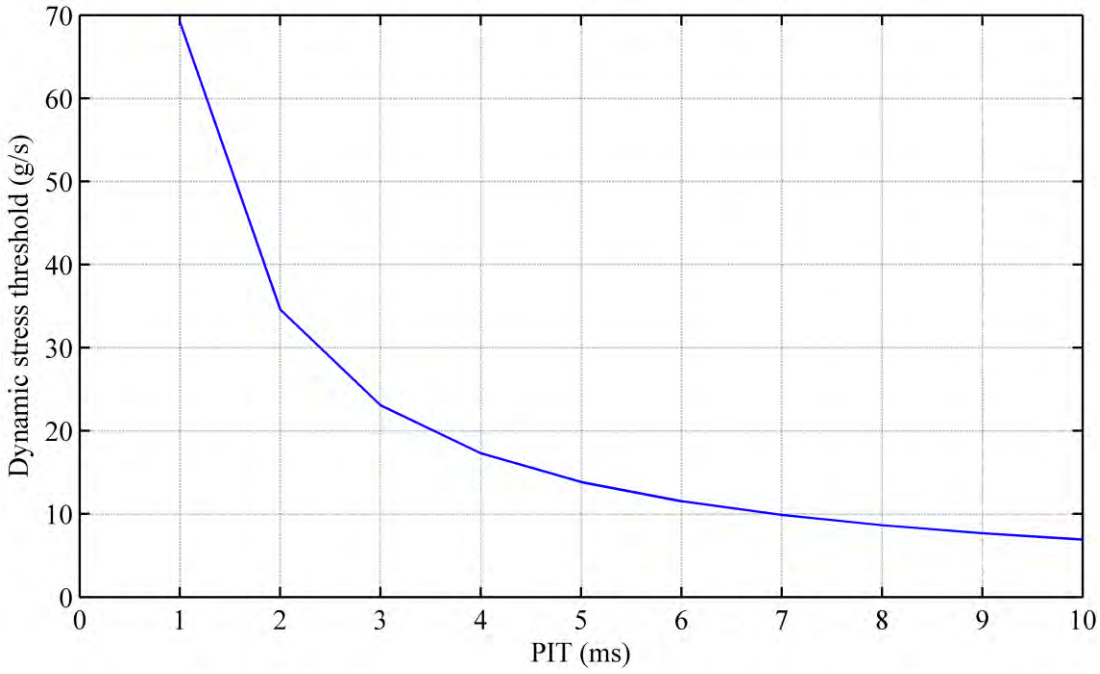

Figure 2-14: Relation between PIT and receiver maximum line of sight jerk dynamics at BW = 2 Hz

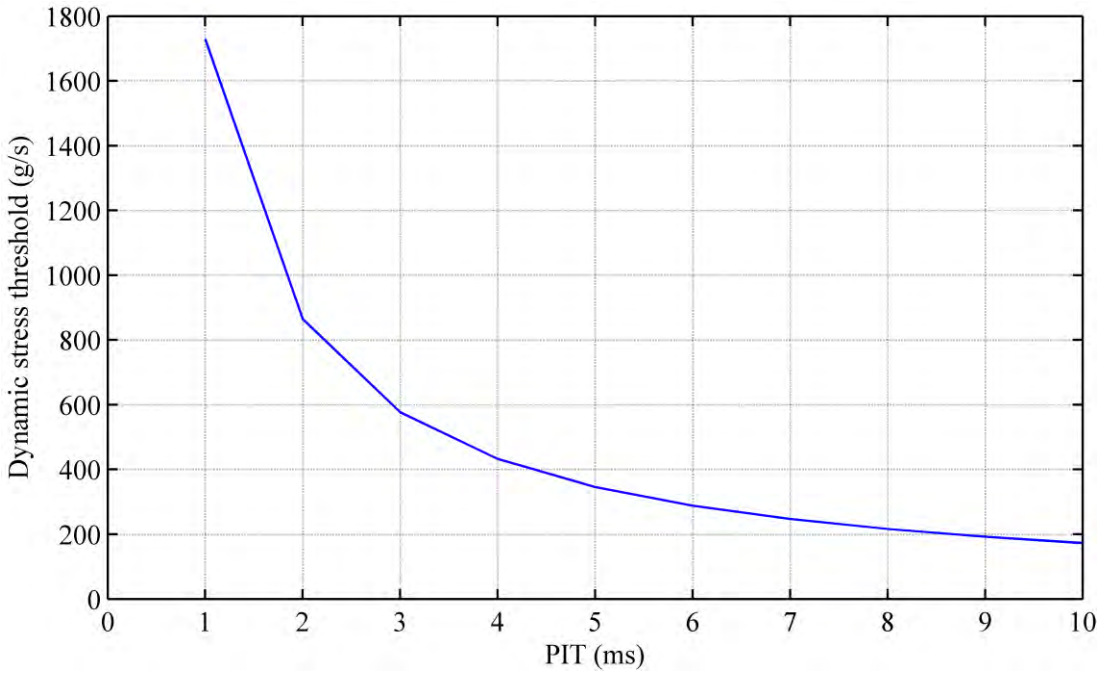

Figure 2-15: Relation between PIT and receiver maximum line of sight jerk dynamics at BW = 10 Hz

As described earlier, increasing the bandwidth to accommodate vehicle dynamics will lead to an increase of the associated frequency jitter. The main component that affects frequency jitter is the thermal frequency jitter. A one sigma thermal frequency jitter (σ_f) can be calculated as (Kaplan & Hegarty 2006):

$$\sigma_f = \frac{1}{2\pi T}\sqrt{\frac{4F.B_n}{c/n_0}\left(1+\frac{1}{Tc/n_0}\right)}\,(Hz) \qquad \textbf{(2.10)}$$

where B_n is the loop bandwidth in (Hz), c/n_0 is the carrier to noise power density expressed as a ratio (Hz), T is the pre-detection integration time in seconds and F is equal to 1 at high c/n_0 and equals 2 near the threshold.

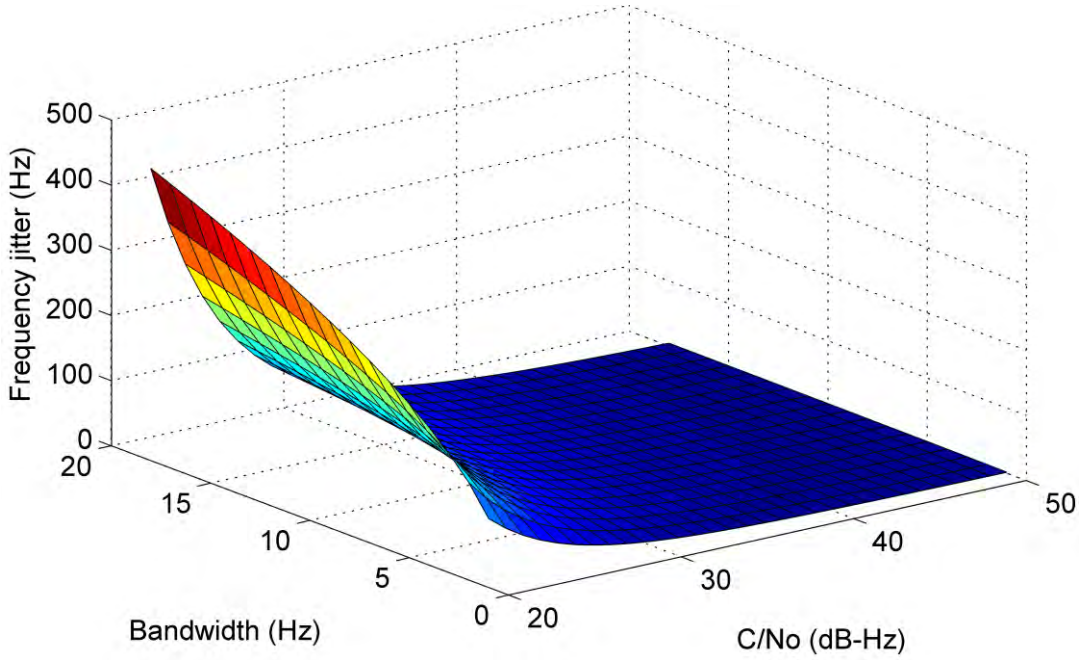

Figure 2-16: Frequency jitter calculated with PIT = 1 ms

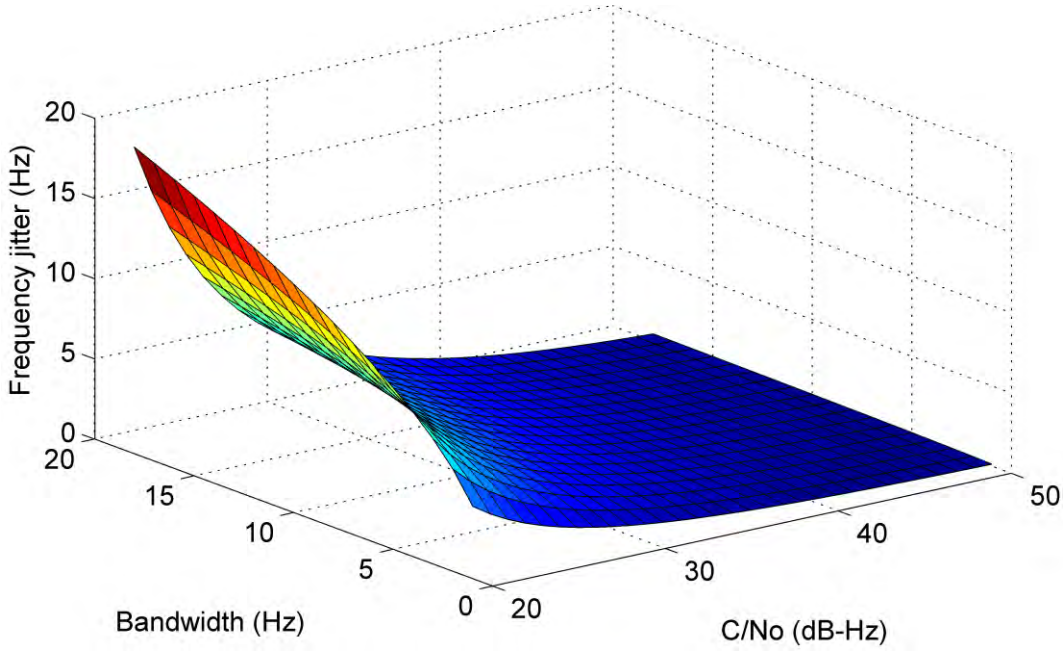

Figure 2-17: Frequency jitter calculated with PIT = 10 ms

Frequency jitter is calculated with C/N_0 and bandwidth for two different PITs, as shown in Figure 2-16 and Figure 2-17 with PIT = 1 ms and 10 ms respectively. It can be seen that frequency jitter is increased while increasing BW, but on the other hand, it is reduced by increasing PIT.

In the previous analysis, it has been shown that increasing PIT is useful for improving the quality of measurements. Increasing PIT will reduce the allowable dynamic stress, which is a serious issue for highly dynamic vehicles under consideration. This problem can be solved through an increase of the tracking loop bandwidth, which will again lead to increasing the tracking jitter level. Consequently the requirements for achieving good quality and robustness are conflicting and a tradeoff has to be considered as illustrated in Figure 2-18.

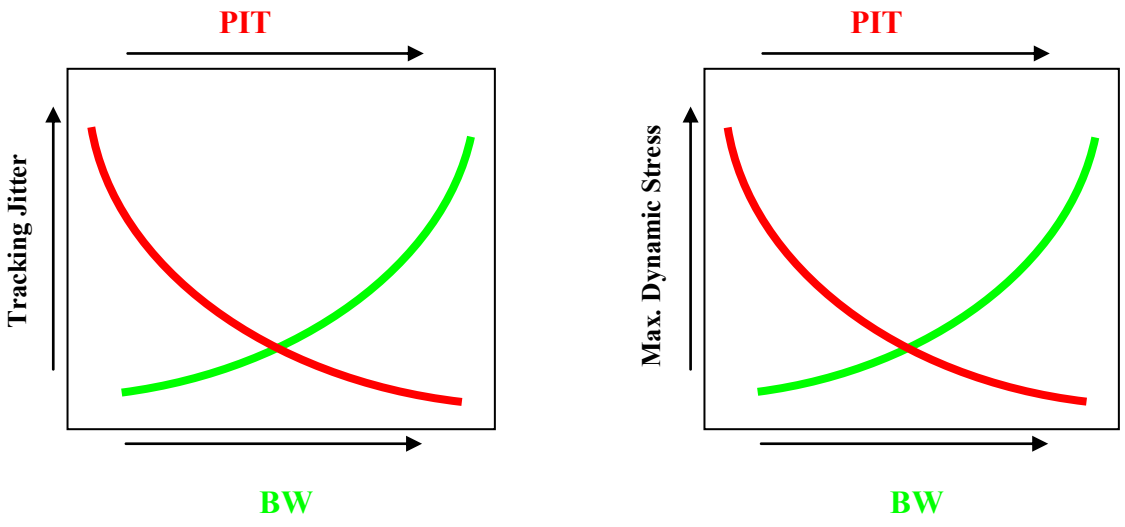

Figure 2-18: Tradeoff of loop bandwidth, PIT, tracking jitter and dynamic stress

2.6 Parameters Used to Describe the Dynamic Performance of Tracking Loop

The tracking loop bandwidth is usually chosen according to the required dynamic performance of the loop, although a minimum value is required to maximize its noise performance. The bandwidth value affects the maximum dynamics thresholds as described earlier in addition to the pull-in capability and the response to the dynamic transients. For this reason the dynamic performance in the rest of the thesis is described by the following characteristics:

1- Tracking continuity robustness in the presence of high dynamics.
2- Maximum pull-in frequency.
3- Transient time response, which can be described by the conversion time required to reach the correct frequency starting from the inaccurate frequency calculated through the acquisition process.

2.6.1 Tracking Robustness

Tracking continuity robustness is related to the dynamic thresholds described earlier and is not repeated. Loop filter order and bandwidth are the two main parameters that control these thresholds. Because the focus of this work is on missile applications, which perform relatively high dynamics, all the performance analyses presented in the rest of the thesis are compared to 3rd order PLLs. Both wide and narrow bandwidths are used for noise performance comparisons in addition to FLL-assisted-PLL with narrow bandwidth for

noise reduction and dynamic threshold increase. Adaptive bandwidth PLLs solutions are inherently studied by exploring the performance of narrow and wide bandwidth PLLs.

2.6.2 Pull-in Frequency

Frequency uncertainty during signal acquisition is bounded by the maximum Doppler frequency due to satellite and receiver motions plus or minus the incoming GPS signal frequency as well as the frequency offset of the receiver clock oscillator. During acquisition, this range is divided into frequency bins and the test for signal existence is applied for each bin. The smaller the frequency bin, the more accurate is the acquired signal. If the pull-in frequency range is wide, a larger error in the estimated incoming frequency is allowed and hence wider frequency bins, which ensures faster acquisition. A detailed performance assessment regarding this point will be included in the context of the thesis in later chapters that will include a comparison between different bandwidths PLLs and FLL-assisted-PLLs and new innovative techniques.

2.6.3 Transient Time Response

Starting from the filter transfer functions and values presented in Table 2-3 and Table 2-4, the step response performance of the loop filter can be calculated. Settling time and rise time are the main characteristics that can be extracted from this response. As mentioned earlier, wider bandwidths ensure faster response. Third order loop filter step response for four different bandwidths are illustrated in Figure 2-19. It can be seen that

by increasing the bandwidth from 3 Hz to 18 Hz, the settling time is almost reduced by 80%. The rise time is also calculated for different bandwidths and this relation is presented in Figure 2-20, where it can be seen that the relation is logarithmically linear. The rise time is related to the convergence time required by the tracking loop to converge to the correct frequency starting from the erroneous acquisition frequency, which has to be within the capture range. An example of this performance is illustrated in Figure 2-21, where the acquisition frequency is shifted by 40 Hz. In this example two PLLs with bandwidths of 14 Hz and 4 Hz are used. The time taken for PLL to converge to the correct frequency for the 4 Hz PLL is much larger than the PLL 14 Hz, which is consistent with the previous analysis.

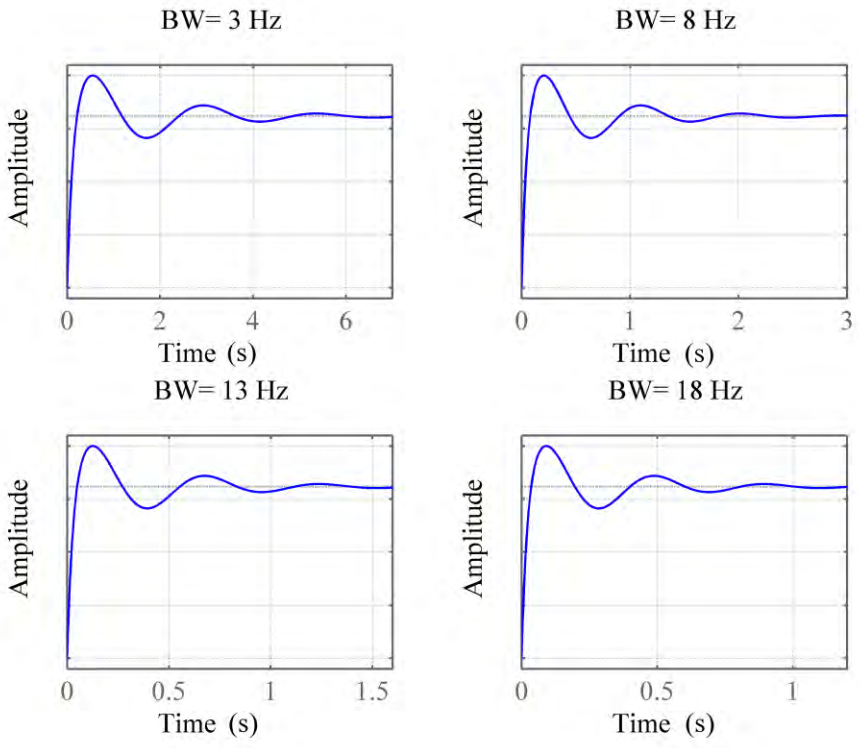

Figure 2-19: 3rd order loop filter step response for four bandwidths

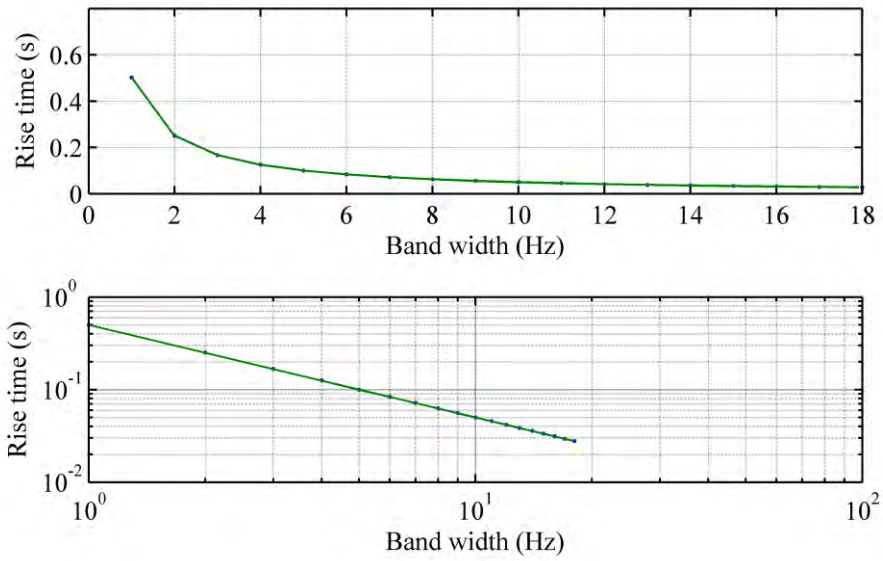

Figure 2-20: Relationship between bandwidth and rise time

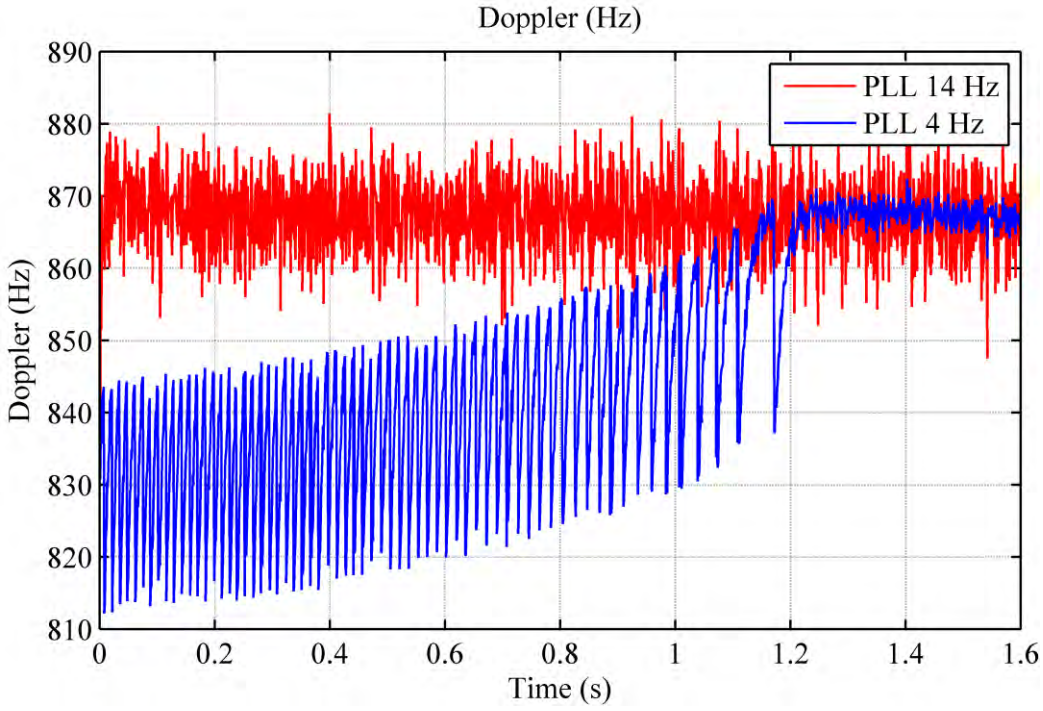

Figure 2-21: Estimated Doppler calculated for wide and narrow bandwidths with initial frequency error of 40 Hz

2.7 Interference Effect on GPS Signal Tracking

RF interference can result in degraded navigation accuracy or complete loss of receiver tracking. The effect of RF interference on code correlation and loop filtering is to reduce the C/N_0 for all the incoming signals. The receiver can lose lock if the effective C/N_0 is reduced under the tracking threshold.

To analyze the RF interference effect, the unjammed C/N_0 has to be first calculated. C/N_0 at baseband can be calculated as

$$C/N_0 = S_r + G_a - 10\log(kT_o) - N_f - L(dB-Hz) \quad \textbf{(2.11)}$$

where S_r is the received GPS signal power (dBW), G_a is the antenna gain (dBic), k is the Boltzmann's constant, T_o is the thermal noise reference temperature (K), N_f is the noise figure of the receiver including antenna and cable losses (dB), and L is the implementation loss.

The level to which the unjammed C/N_0 is reduced by RF interference is called the equivalent C/N_0 or $(C/N_0)_{eq}$, which can be calculated as (Kaplan & Hegarty 2006)

$$\left(C/N_0\right)_{eq} = -10\log\left[10^{-\frac{C/N_0}{10}} + \frac{10^{\frac{J/S}{10}}}{QR_c}\right](dB-Hz) \quad \textbf{(2.12)}$$

where R_c is the PRN code chipping rate, Q is a dimensionless spread spectrum processing gain adjustment factor (different for each interference type), and J/S is the jammer- to- signal power ratio (dB).

Equation (2.12) can be rearranged to calculate J/S as

$$J/S = 10\log\left[QR_c\left(10^{\frac{-(C/N_0)_{eq}}{10}} - 10^{\frac{-C/N_0}{10}}\right)\right](dB). \quad \textbf{(2.13)}$$

Equation (2.13) can be used for theoretical calculations of J/S, however for practical cases previous knowledge of interference type has to be known to substitute for the spread spectrum processing again adjustment factor, and different techniques for interference warning have to be implemented.

2.8 GPS Signal Tracking Using Kalman Filter Based PLLs

This section briefly introduces some KF approaches that are practically used as a replacement for the standard PLLs and FLLs described earlier in this chapter.

2.8.1 Introduction to Kalman Filter

KF based tracking systems are widely used for aviation and military applications. A perfectly tuned KF used for GPS signal tracking is much more robust than any standard tracking algorithm such as PLLs and FLLs. The KF designer faces several challenging tasks such as designing the dynamic model and a correct description of the noise matrices, which are related to the measurements and process.

KF estimates its process states using a form of feedback control by estimating the process state and then obtaining feedback in the form of noisy measurements. As such, the KF equations are categorized into two sets described as time update equations and measurement update equations. The time update equations are responsible for projecting

forward in time the current state and error covariance estimates to obtain the a priori estimates for the next time step. The measurement update equations are responsible for the feedback by incorporating a new measurement into the a priori estimate to obtain an improved a posteriori estimate.

KF equations for time and measurement updates can be written as (Grewal & Andrews 2008):

$$X_{k+1}^{-} = \Phi_{k,k+1} X_k^{+} + G w_k , \tag{2.14}$$

$$P_{k+1}^{-} = \Phi_{k,k+1} P_k^{+} \Phi_{k,k+1}^{T} + Q , \tag{2.15}$$

$$K_k = P_k^{-} H^T (H P_k^{-} H^T + R)^{-1} , \tag{2.16}$$

$$X_k^{+} = X_k^{-} + K_k (Z_k - H X_k^{-}) , \tag{2.17}$$

$$P_k = (I - K_k H) P_k^{-} , \tag{2.18}$$

where X represents the state vector, Φ represents the transition matrix, P is the error covariance matrix, R and Q are the measurement and process noise covariance matrices, K is the Kalman gain, Z is update measurements, and H is the observation model, which maps the true state space into the observed space. The negative sign (-) denotes prediction based on model dynamics only, where as the positive sign (+) denotes correction accounting for the measurements.

The first task during the measurement update is to compute the Kalman gain, K. The next step is to actually measure the designated state data input, and then to generate an a

posteriori state estimate by incorporating the measurement as in Equation (2.17). The final step is to obtain an a posteriori error covariance estimate. After each state prediction and measurement update pair, the process is repeated with the previous a posteriori estimates used to project or predict the new a priori estimates. This process is illustrated in Figure 2-22 and Figure 2-23 (Brown & Hwang 1997).

In the actual implementation of the filter, the measurement noise covariance R is usually measured prior to operation of the filter. The determination of the process noise covariance Q is generally more difficult because practically there is no direct observation of the process during estimation.

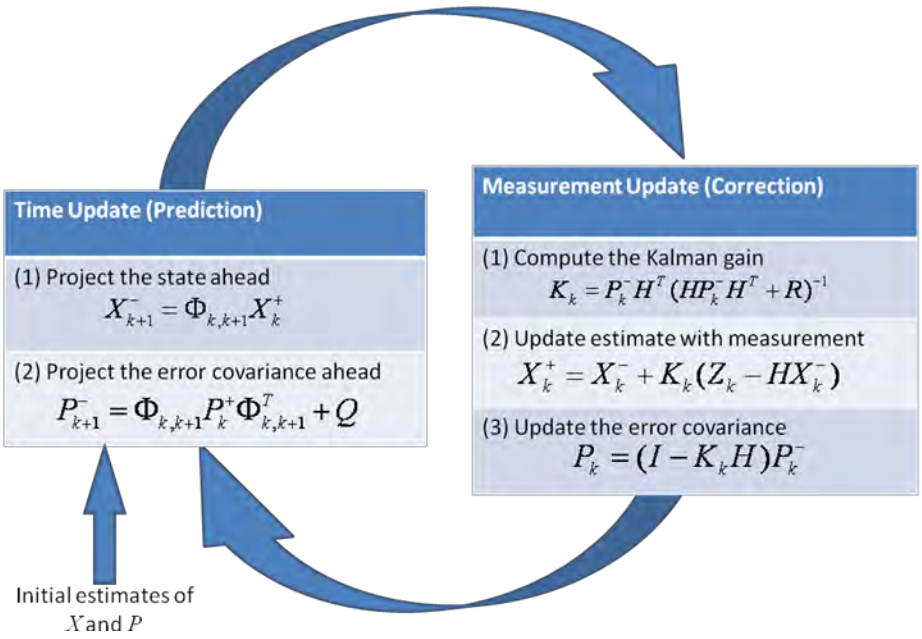

Figure 2-22: Kalman filter process

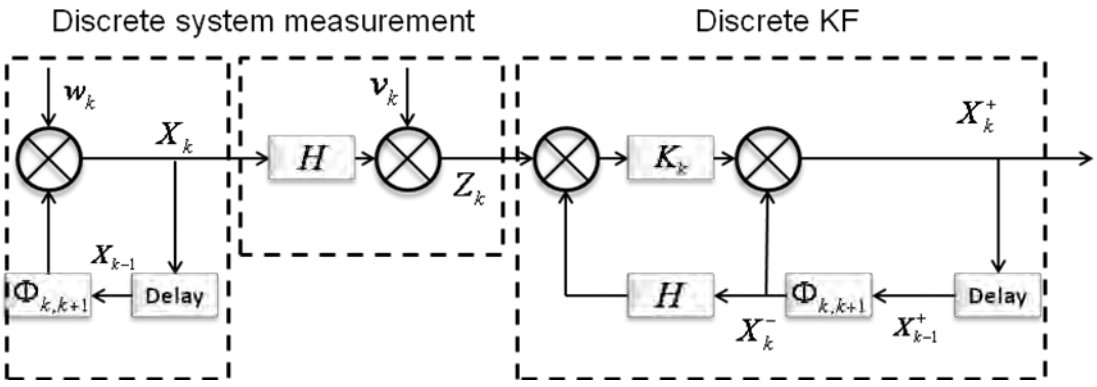

Figure 2-23: Block diagram of a system, a measurement model, and a discrete Kalman Filter

2.8.2 Kalman Filter Based PLLs

Kalman filter processes are utilized in many different ways in the context of GPS signal tracking. Different algorithms are proposed to design a Kalman filter based PLLs such as what is presented in Pisiaki (2001), Petovello & Lachappelle (2006) and Kazemi (2010). In these algorithms, KF can be used to replace the PLL filter or both PLL discriminator and filter. The first approach will be briefly described here because its update process is the closest to what is used in the innovative schemes described later in the next chapters. However, all different approaches are using almost the same construction with slight changes.

The carrier phase dynamics model takes the form of a discrete-time triple integrator driven by discrete-time white noise as

$$\begin{bmatrix}\theta_{k+1}\\ \omega_{k+1}\\ \alpha_{k+1}\end{bmatrix}=\begin{bmatrix}0 & \Delta t_k & \frac{\Delta t_k^2}{2}\\ 0 & 1 & \Delta t_k\\ 0 & 0 & 1\end{bmatrix}\begin{bmatrix}\theta_k\\ \omega_k\\ \alpha_k\end{bmatrix}-\begin{bmatrix}\Delta t_k\\ 0\\ 0\end{bmatrix}\omega_{NCO_k}+\begin{bmatrix}1 & 0 & 0\\ 0 & 1 & 0\\ 0 & 0 & 1\end{bmatrix}w_k \qquad \textbf{(2.19)}$$

where θ_k is the difference between the true carrier phase and the phase of the PLL's NCO, ω_k is the carrier Doppler shift, α_k is the rate of change of carrier Doppler shift, and $\Delta t_k = t_{k+1} - t_k$ is the accumulation interval.

The 3×1 vector w_k is the process disturbance vector and is a combination of three terms. One models a random walk acceleration of the LOS vector to the GPS satellite and the other two model the effects of receiver clock phase random walk and frequency random walk. The w_k covariance has the following statistics (Psiaki 2001, Psiaki & Jung 2002):

$$E\left\{w_k w_k^T\right\}=$$
$$q_{LOS}\begin{bmatrix}\Delta t_k^5/20 & \Delta t_k^4/8 & \Delta t_k^3/6\\ \Delta t_k^4/8 & \Delta t_k^3/3 & \Delta t_k^2/2\\ \Delta t_k^3/6 & \Delta t_k^2/2 & \Delta t_k\end{bmatrix}$$
$$+S_g\omega_{L1}^2\begin{bmatrix}\Delta t_k^3/3 & \Delta t_k^2/2 & 0\\ \Delta t_k^2/2 & \Delta t_k & 0\\ 0 & 0 & 0\end{bmatrix}+S_f\omega_{L1}^2\begin{bmatrix}\Delta t_k & 0 & 0\\ 0 & 0 & 0\\ 0 & 0 & 0\end{bmatrix} \qquad \textbf{(2.20)}$$

where q_{LOS} can be determined depending on the dynamics. S_g is the receiver clock's frequency random walk spectral density function amplitude, S_f is the white frequency

noise spectral density function amplitude, and ω_{L1} is the nominal L1 carrier frequency. S_g and S_f can be calculated using the key Allan variance parameters h_0, h_{-2} used to describe clock drift according to the following formulas (Dierendonck et al 1984):

$$S_f = \frac{h_0}{2} \tag{2.21}$$

$$S_g = \frac{2}{3}\pi^2 h_{-2}\,. \tag{2.22}$$

Typical Allan variance parameters for various clocks are listed in Table 2-7 (Brown & Hwang 1997).

Table 2-7: Typical power spectral density coefficients for various timing standards

Clock type	h_0	h_{-1}	h_{-2}
Crystal	2×10^{-19}	7×10^{-21}	2×10^{-20}
Ovenized Crystal	8×10^{-20}	2×10^{-21}	4×10^{-23}
Rubidium	2×10^{-20}	7×10^{-24}	40×10^{-29}

The Kalman filter finishes its operations for the interval by applying a measurement update. This update is based on the accumulations I_{k+1} and Q_{k+1} signals, which is computed by the receiver's baseband digital processor.

In addition to a carrier NCO and a baseband mixer, the baseband processor uses a code chipping rate from a DLL as the input to its code NCO, which produces the replica PRN

code that the processor uses to wipe the code off of the received signal before computing its accumulations as described earlier in section(2.2). This analysis presumes that the DLL and the code NCO perform PRN code removal with a negligible error. The accumulations I_{k+1} and Q_{k+1} are used in the Phase Discriminator (PD) presented in Table 2-2 in order to compute the phase error measurement. The Kalman filter measurement update uses an a priori estimate of what the measurement would have been if the state estimates were correct. This estimate takes the following form:

$$\bar{y}_{k+1} = \begin{bmatrix} 1 & \frac{\Delta t_k}{2} & \frac{\Delta t_k^2}{6} \end{bmatrix} \begin{bmatrix} \theta_k \\ \omega_k \\ \alpha_k \end{bmatrix} - \frac{\Delta t_k}{2} \omega_{NCO_k} + v_{k+1}, \qquad \textbf{(2.23)}$$

Where v_{k+1} is the measurement noise defined as Gaussian white noise sequence with covariance matrix R.

The filter innovation is completed by computing the error between the phase measurement and the estimated one according to Equation (2.23).

The state estimates are used at the end to compute the NCO frequency ω_{NCO_k} for the next iteration. The model that combines these estimates is arbitrary chosen. The NCO frequency must not differ from the true Doppler shift by a large amount to cause aliasing or even to cause significant power loss in the accumulations. The NCO feedback control law used in this work is (Psiaki et al 2007)

$$\omega_{NCO_{k+1}} = \begin{array}{l} \dfrac{1}{\Delta t_{k+1}}\left\{(1-\eta)^2(\theta_k-\theta_{desired})+(1-2\eta)\Delta t_k\left(\omega_k-\omega_{NCO_k}\right)-\eta\Delta t_k^2\alpha_k\right\} \\ +\omega_k+\dfrac{\left(\Delta t_k+\Delta t_{k+1}\right)^2}{2\Delta t_{k+1}}\alpha_k \end{array}, \quad \textbf{(2.24)}$$

where η is a feedback tuning parameter and $\theta_{desired}$ is the desired steady-state value of the phase error θ_k as a point of reference.

A KF based PLL structure, as a modified version of the standard PLL shown in Figure 2-3, is shown in Figure 2-24.

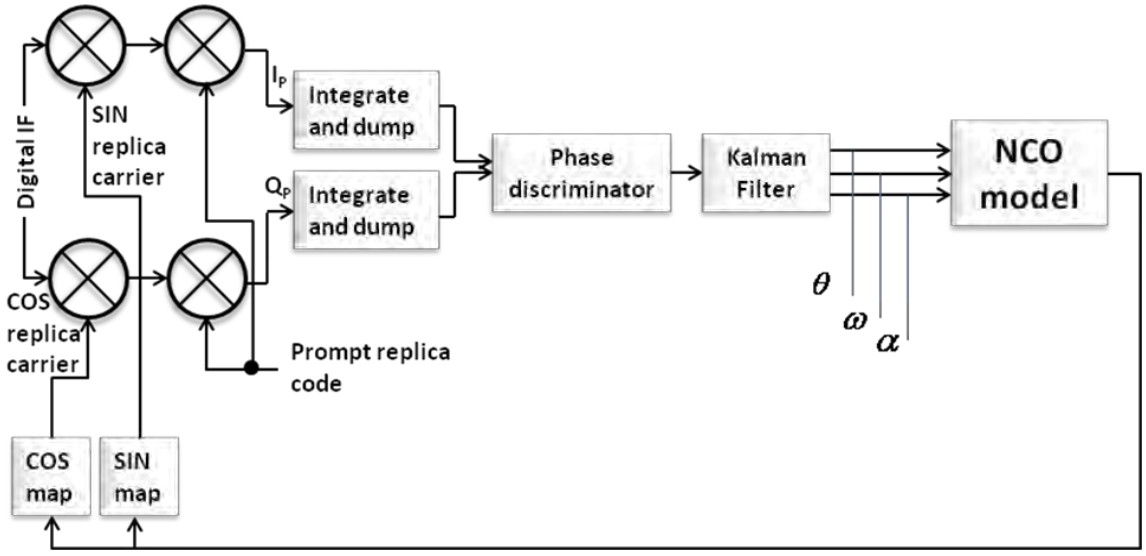

Figure 2-24: Kalman filter based PLL

2.9 Summary

Necessary background knowledge for the GPS carrier signal tracking loop operation was covered in this chapter. Digital designs of PLL and FLL-assisted-PLL have been

presented with the focus on the filter design. Dynamic and noise performance has been presented with focus on the effect of different parameters such as bandwidth, pre-detection integration time, and C/N_0. Parameters that characterize GPS dynamic performance have been also discussed. RF interference effect on the effective C/N_0 has also been presented.

A brief introduction to Kalman filtering and approaches to Kalman filter PLLs have also been given for later comparisons with new innovative approaches.

Chapter Three: Design of Fuzzy Tracking System

This chapter covers most of the necessary background knowledge for the fuzzy logic control, definition of fuzzy sets and different parameters related to Fuzzy Logic Controller (FLC) design. An approach of a new innovative fuzzy based PLL is described.

3.1 Introduction

The concept of fuzzy logic approximates the human reasoning performed by computers. It was first presented by Lotfi Zadeh (1965), who is known as the father of fuzzy theory. Zadeh contends that human thinking does not embrace strict definitions, but classes of definitions in which the transition from state to another is gradual rather than sudden. The state of a variable is defined by a membership, whose degree is specified by a number between "1", a full membership, and "0", non membership. The fuzzy logic approach has the following three distinguishing features.

1. It uses linguistic variables in place of, or in addition to, numerical values.
2. Simple relations between the variables are characterized by conditional fuzzy statements.
3. Complete relations are characterized by fuzzy algorithms.

The theoretical foundation of fuzzy logic is actually quite precise and mathematical (Kosko 1992). The source of imprecision is not in the theory but in the way the data is described. The data can be expressed vaguely, such as **high** temperature, **medium**

pressure and take on linguistic quantifiers, such as **very high**. This information is then combined and processed to produce a result that can be either vague or precise. Fuzzy logic gets its name from the fuzzy sets, which are the building blocks of the fuzzy logic system. These fuzzy sets differ from classical or crisp sets in that they allow for partial degrees of Membership Function (MF). A fuzzy set is defined by the following three principal features, as shown in Figure 3-1:

1. the domain or range of values over which the fuzzy set is valid (the x-axis),
2. the degree of membership axis (the y-axis),
3. the fuzzy set function, which maps the domain to the degree of membership.

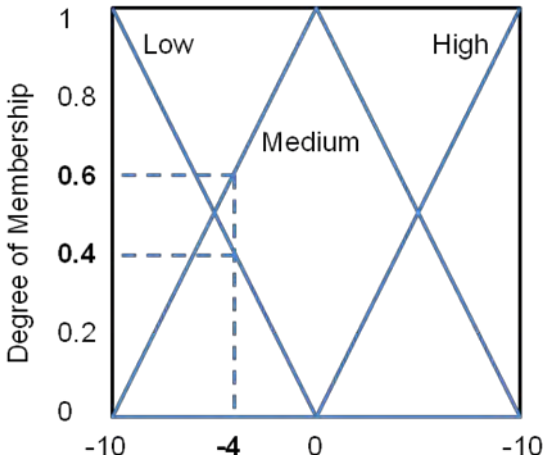

Figure 3-1: Fuzzy membership functions

The fuzzy membership function is a measure of the degree of occurrence of the object with its definition. So, if a value from the domain is known then the membership in the fuzzy set can be determined. For example from Figure 3-1, a discrete value of -4 has a membership or $\mu = 0.4$ in the fuzzy set "low" and membership or $\mu = 0.6$ in the fuzzy set

"Medium". Fuzzy logic involves gradual decision making. It attempts to model the human thought processes or the soft decisions that occur in these processes. Often the fuzzy membership values processes are combined with membership values from other fuzzy states, through union, intersection and complementation operators, to produce a composite truth value (Bourke 1995). The fuzzy inference or implication has a mathematical basis so that a fuzzy model can provide the same kind of discrete or deterministic result that is obtained from conventional knowledge based systems. The operations of transforming discrete values to linguistic variables and vice versa are called Fuzzification and Defuzzification respectively. Using a priori knowledge of the problem, the fuzzy system designer is able to choose the appropriate membership functions and construct sufficient rules to fulfill the correct operation. An illustration of a complete fuzzy inference process is shown in Figure 3-2.

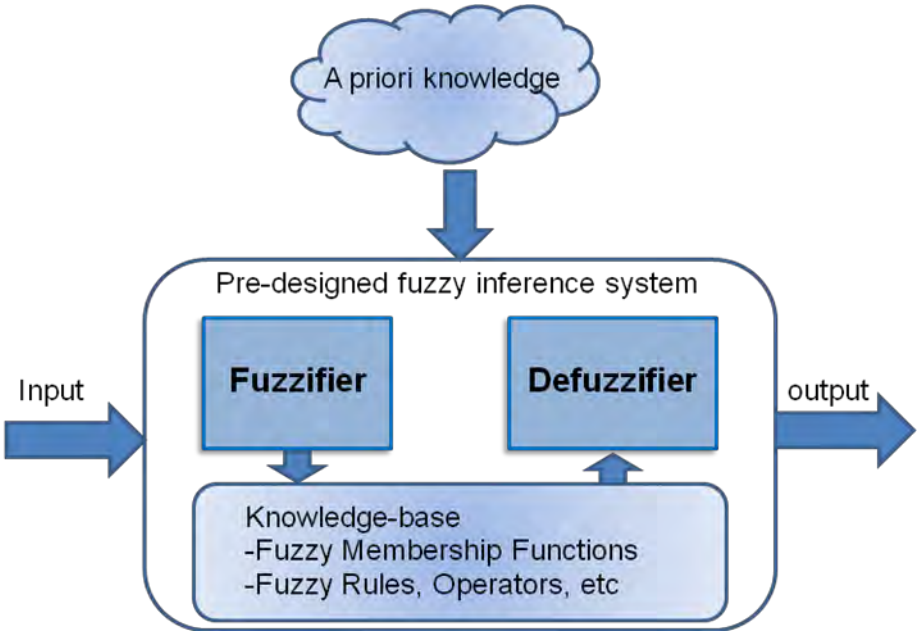

Figure 3-2: Fuzzy inference process

3.1.1 Fuzzy Sets

In classical set theory, the membership of elements in relation to a set is assessed in binary terms according to a crisp condition. In that sense, the element either belongs or does not belong to the set. If X represents a fundamental set and x are the elements of this fundamental set to be assessed and assigned to a subset A of X, classical sets can be described by a characteristic function $m_A(x)$ such as

$$m_A(x) = \begin{cases} 1, x \in A \\ 0, x \notin A \end{cases} \rightarrow m_A(x) \in \{0,1\}. \quad \textbf{(3.1)}$$

As a further development of classical set theory, fuzzy set theory permits the gradual assessment of the membership of elements in relation to a set; this is described with the aid of a membership function. A fuzzy set is defined as follows. If X represents a fundamental set and x are the elements of this fundamental set to be assessed according to an uncertain proposition and assigned to a subset A of X, the set $\tilde{A} = \{(x, \mu_{\tilde{A}}(x)) | x \in X\}$ is referred to as the uncertain set or fuzzy set on X.

$\mu_{\tilde{A}}(x)$ is the membership function of the fuzzy set and may be continuous, or the set contains only discrete elements assessed by membership values such as $\mu_{\tilde{A}}(x) \in [0,1]$. A comparison between crisp and fuzzy sets is shown in Figure 3-3.

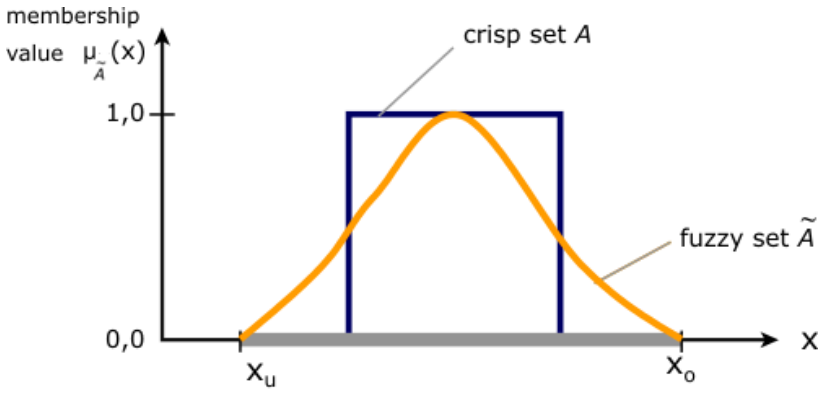

Figure 3-3: Crisp and fuzzy sets

There are different types of MFs. The most commonly used MFs are summarized in Table 3-1 and an illustration of these types is depicted in Figure 3-4.

Table 3-1: Commonly used membership functions

	MF type	Characterization
1	Trapezoidal	Four points
2	Gaussian	Mean – Standard Deviation (SD)
3	Triangular	Three points
4	Singleton	One point and degree

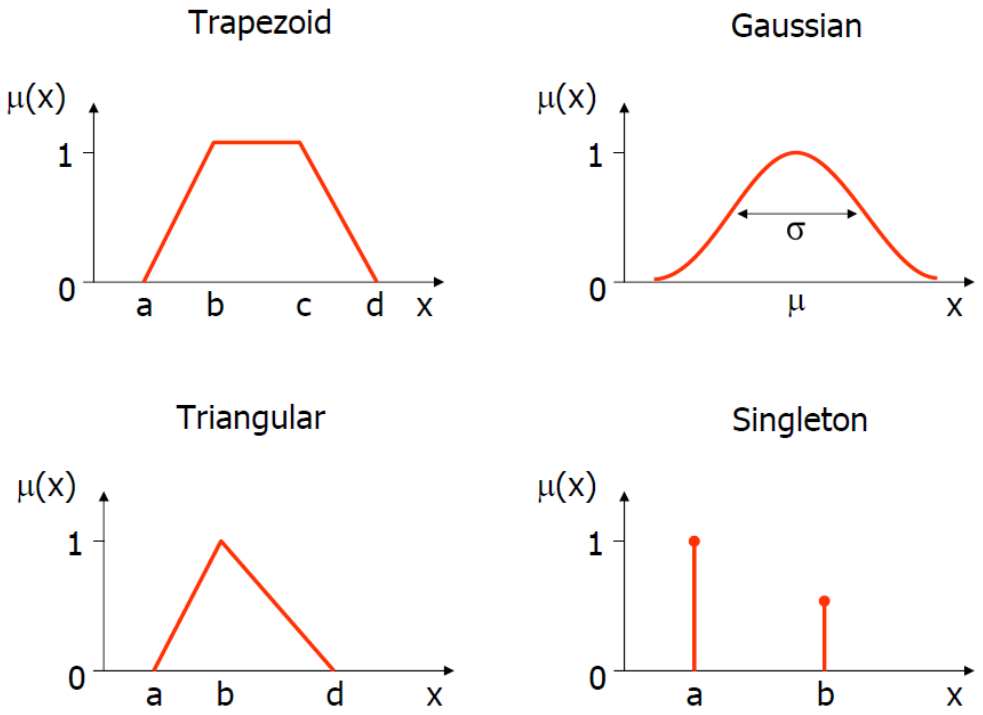

Figure 3-4: Commonly used membership functions

Every type of membership function has its advantages and disadvantages. For instance, the triangular membership function is very easy to implement and fast to calculate on real time based systems. However, it is very difficult for triangles to adjust adaptively using statistical methods in on/off-line learning schemes towards better system performance due to their discontinuity in their mathematical form. In the context of control systems, obviously the priority of the system often lies on the speed of real-time system performance in most industrial control systems. Thus the triangle type membership function has been employed widely in control engineering. MFs modeled with Gaussian functions require more time to calculate their output, but being a naturally distributed statistical model, they better describe the gathered data. Indeed the exponential term in

Gaussian functions allows the adaptive mechanism to better adjust them with the statistical learning functions. This property of Gaussian basis functions provides higher accuracy and more flexibility to model non-linear systems.

3.1.2 Construction of a Fuzzy Inference System (FIS)

In the field of artificial intelligence (AI), there are various ways to represent knowledge of complex or fuzzy systems. The most common way to represent human knowledge in these systems is to cast the knowledge into natural language expressions of the type IF-THEN "rule-based" form. It typically expresses an inference such that if a fact (premise, hypothesis, or antecedent) is known, then another fact called a conclusion (consequent) is derived. This form of knowledge representation is quite appropriate in the context of linguistics because it expresses human empirical and heuristic knowledge in a language of communication. Fuzzy rules are also described as Fuzzy Associative Memories (FAMs) that map the input fuzzy sets to the output fuzzy sets.

The rule-based system is distinguished from classical expert systems in the sense that the rules comprising a rule-based system might be driven from sources other than human experts and, in this context, is distinguished from expert systems. The work presented later in this thesis is based on the fuzzy rule-based systems (of which expert systems could be seen as a subset) because of their prevalence and popularity in the literature, and their wide use in engineering practice.

Most rule-based systems involve more than one rule. The process of obtaining the overall consequent (conclusion) from the individual consequents, outputted by each rule, is known as the aggregation of rules. Depending on the context, the two following basic aggregation operations, intersection or union, can be chosen for determining an aggregation strategy.

(i) Conjunctive system of rules:

In the case of a system of rules that have to be jointly satisfied, the rules are connected by "and" connectives. In this case the aggregated output (consequent) y is found by the fuzzy intersection of all individual rule consequents y^i, where i = 1, 2, . . . , r, as follows:

$$y = y^1 \quad and \quad y^2 \quad and....and \quad y^r \tag{3.2}$$

or

$$y = y^1 \cap y^2 \cap ....y^r, \tag{3.3}$$

which is defined by the membership function

$$\mu_y(y) = \min\left(\mu_{y^1}(y), \mu_{y^2}(y), ...\mu_{y^r}(y)\right) \quad for \quad y \in Y \tag{3.4}$$

where minimum function defines the intersection of the overlapping membership functions.

(ii) Disjunctive system of rules:

For the case of a disjunctive system of rules where the satisfaction of at least one rule is required, the rules are connected by the "or" connectives. In this case, the aggregated output is found by the fuzzy union of all individual rule contributions as:

$$y = y^1 \quad or \quad y^2 \quad or....or \quad y^r \tag{3.5}$$

or

$$y = y^1 \cup y^2 \cup ....y^r, \tag{3.6}$$

which is defined by the membership function

$$\mu_y(y) = \max\left(\mu_{y^1}(y), \mu_{y^2}(y), ...\mu_{y^r}(y)\right) \quad for \quad y \in Y \tag{3.7}$$

where maximum function is chosen because it defines the union of the overlapping membership functions.

After rules aggregation, the result has to be defuzzified if a crisp output is required. Defuzzification is the mathematical process whereby a fuzzy membership function is reduced to a single scalar quantity that best summarizes the function, if a single scalar value is needed. Of the various methods of defuzzification, the centroid or centre-average method is intuitive since it represents the center of gravity of the area defined by the membership function.

The output Z is obtained as

$$Z = \frac{\sum_{i=1}^{n} y_i u(y_i)}{\sum_{i=1}^{n} u(y_i)} \tag{3.8}$$

where n is the number of fuzzy output sets, y_i is the numerical value of the i^{th} output membership function, and $u(y_i)$ represents its membership value at the i^{th} quantization level.

A graphical representation of the defuzzification process using centroid or centre-average method is shown in Figure 3-5.

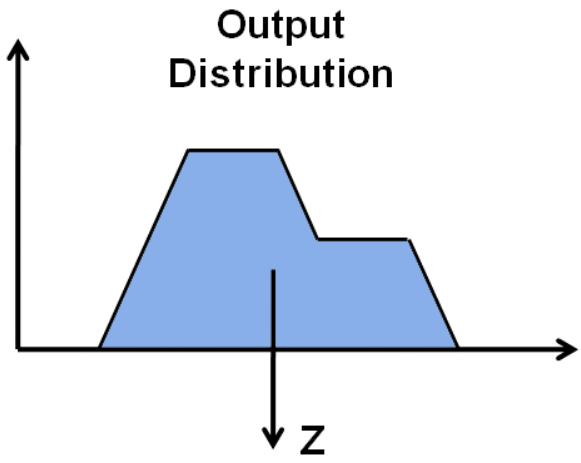

Figure 3-5: Defuzzification using centroid or centre-average method

The previously explained inference system is described in literature as a Mamdani type fuzzy inference system (FIS) which is the most common type of FIS (Knapp 2004). Finally this FIS operation can be summarized in six steps as follows:

1. Determining a set of fuzzy rules.
2. Fuzzifying the inputs using the input membership functions.
3. Combining the fuzzified inputs according to the fuzzy rules to establish the rule strength.
4. Finding the consequence of the rule by combining the rule strength and the output membership function.
5. Combining the consequences to get an output distribution.

6. Defuzzifying the output distribution (this step is only used if a crisp output (class) is needed).

An example of two inputs x and y conducting to one z fuzzy system output using triangular MFs for inputs and output is graphically represented in Figure 3-6. The rules are conjunctively satisfied and hence the minimum of the intersection operator is used as described in Equation (3.4). The output distribution is obtained by combining the consequence of each rule and finally the crisp output is obtained by applying Equation (3.8) as depicted in Figure 3-5. In this example, input *x* is simultaneously covered by MFs *mx1* and *mx2*. Input *y* is also simultaneously covered by MFs *my1* and *my2*. If there are connecting rules that map both inputs to outputs it will be written as follows.

$$\begin{array}{l} if\,(x = mx1)\ and\ (y = mx1)\ then\ (z = mz1) \\ if\,(x = mx2)\ and\ (y = mx2)\ then\ (z = mz2) \end{array}, \qquad \textbf{(3.9)}$$

where *mx1* and *mx2* are the corresponding MFs for input *x*, *my1* and *my2* are the corresponding MFs for input *y*, and *mz1* and *mz2* are the corresponding MFs for output *z*. As a Mamdani type FIS, the "and" operation is defined by "min" function as it has been seen in Equation (3.4). This operation specifies the rule strength for the corresponding output MF. After specifying which output MFs are triggered and by which level, the output is calculated by combining all the outputs using the union (max) operation and calculating the centroid of the resultant figure.

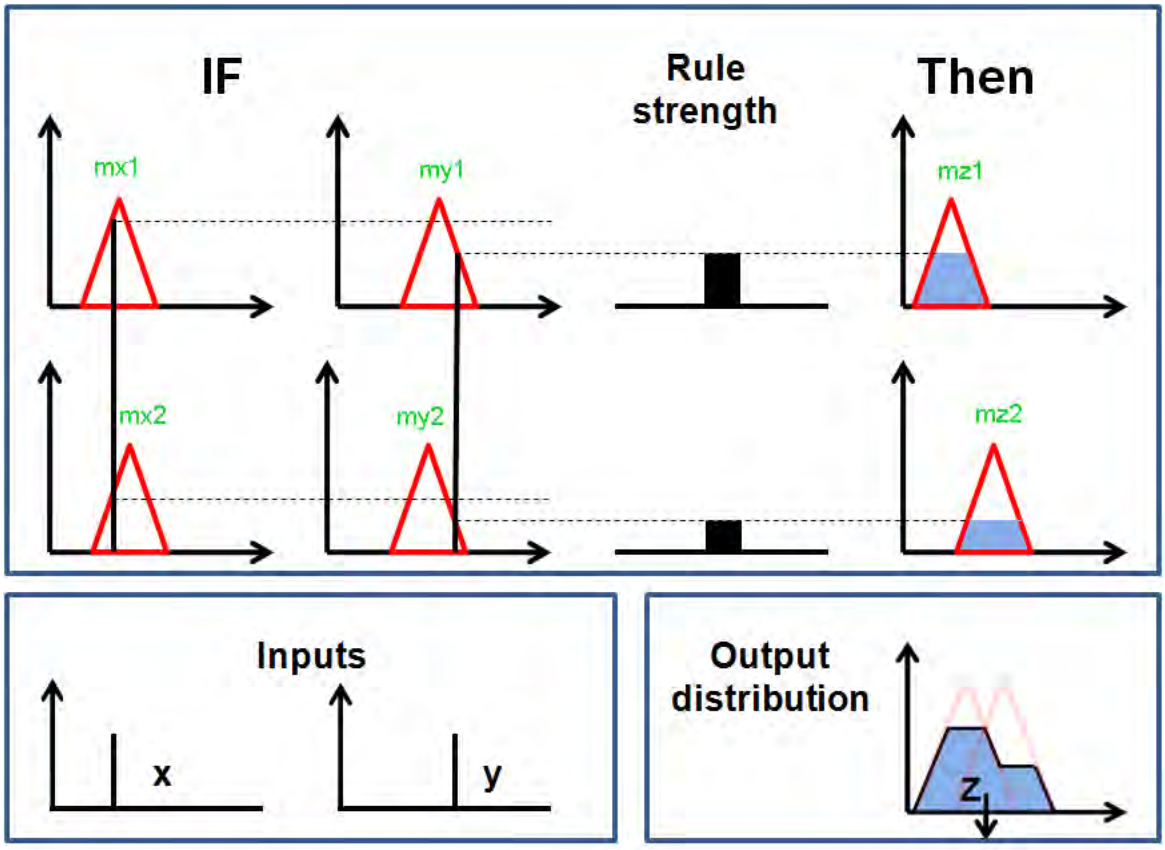

Figure 3-6: An example of two input-one output Mamdani FIS

3.1.3 Relation Between Fuzzy and Probability

Fuzzy logic is different but related to probability. Probability describes event occurrence, i.e. if it does or if it does not occur. Fuzzy logic measures the degree to which an event occurs, not if it has occurred. Both fuzziness and probability describe their numerical uncertainties with numbers in the unit interval [0, 1]. They also both combine their sets and propositions through the De Morgans laws of associativity, commutativity and distributivity as well. Probability theory and set theory require that:

$$A \bigcap \bar{A} = \phi \tag{3.10}$$

where ϕ is the empty or null set and $\bar{A}$ is the complement of the set A.

Fuzzy set theory begins with the opposite axiom:

$$A \bigcap \bar{A} \neq \phi . \tag{3.11}$$

The bivalent nature of Equation (3.10) results in numerous contradictions if statement S and its opposite $\bar{S}$ have the same truth value, namely t(S). An example is given by a card which has "The sentence on the other side is true" written on one of its sides, and "The sentence on the other side is false" written on the other side. Analytically, this can be stated as:

$$\begin{aligned} \mathrm{t}(S) &= t(\bar{S}) \\ &= t(1-S) . \\ &= 1 - t(S) \end{aligned} \tag{3.12}$$

Furthermore if $\mathrm{t}(S)$ equals one as in classical set theory, then

$$\begin{aligned} \mathrm{t}(S) &= 1 - t(S) \\ 1 &= 0 \end{aligned} . \tag{3.13}$$

Equation (3.13) gives a contradiction. Fuzzy logic can solve this problem by assigning a degree to $\mathrm{t}(S)$ instead of only "1" or "0". For example, if $\mathrm{t}(S)$ equals 0.5, the paradox is reduced to half truths.

Probability measures relate to fuzzy sets through the use of membership functions. The associated membership function of a fuzzy set can be interpreted as a likelihood function of X for a fixed set S. This relationship is true because the process of defining a

membership function is subjective in nature, reflecting the designer experience regarding the level of membership in the set S. Furthermore, because membership functions are merely non-negative, they can serve as likelihoods. Then for a given probability-based prior distribution, the membership functions, as likelihoods, can be combined with that prior through Bayes' theorem and produce a probability-based posterior.

3.2 Design of a GPS Signal Fuzzy Tracking System

3.2.1 Introduction to PLL Fuzzy Tracking

Most physical processes are nonlinear in nature. The use of linear approximations and models is due to the fact that linear systems are simple, understandable, and can provide acceptable approximations of the actual processes. Unfortunately, most tracking problems are complex and their linear approximation does not provide sufficient insight on the system in all the environmental conditions (Ross et al 2002).

Standard tracking loops are obtained by solving an optimization problem where the noise characteristics and the order of the signal dynamics are known. Tracking loops strongly rely on the knowledge of the operating conditions and their adherence to the model adopted for the loop design. Model imperfections can lead to a catastrophic reduction in the system performance and this lack of robustness is a problem common to adaptive bandwidth and Kalman filter based algorithms. To overcome the problem of model uncertainties, an approach based on a linguistic description of the system can be

preferable. In that sense, fuzzy control systems provide the sufficient tools for designing a robust alternative to standard loop filter.

A few researchers have tried to use fuzzy techniques for PLL design. For example, Simon & El-Sherief (1994) have proposed a fuzzy PLL estimation filter for missile navigation. The tracking model used needed a priori known specific trajectory to train the fuzzy PLL architecture, and thus it was not a suitable method for practical receiver design. Unglaub & Tsang (1999) have used a FLC to tune the PLL filter bandwidth according to phase error dynamics using information from the PD output and its rate of change. Mao et al (2004) used the PD and FD outputs as inputs to an FLC, which produces an error driving the loop filter. In all these previous cases, FLCs were used in parallel with a classic PLL architecture and is based on controlling the inputs or changing bandwidth of the existing filter. These approaches may enhance the performance of the standard PLLs but all the limitations described in Chapter 2 still apply.

In the work presented in this thesis, a different approach is used. More specifically, a pure FLC is used to directly tune the NCO frequency and track the incoming signal carrier frequency and phase. A new filter is designed based on fuzzy concepts and replaces the traditional FLL-assisted-PLL filter, and hence all the limitations related to the traditional filter and described earlier are not applicable and new assessments for the proposed system have to be performed. Significant improvements are achieved as will be seen in the following chapters.

The new system uses the noisy PD and FD outputs and directly produces a control signal that represents the frequency change required by the NCO to maintain phase lock. The

structure of the proposed design is illustrated in Figure 3-7 where the standard loop filter is replaced by the proposed Fuzzy Frequency Phase Lock Loop (FFPLL) controller.

The FFPLL fuzzy controller belongs to binary input-output FAMs (BIOFAMs) systems, which are the most widely used fuzzy systems (Kosko 1992). BIOFAMs map system state-variables to control, classification, or other output data. There are two input fuzzy variables and one control fuzzy variable. The first state variable is the phase error from the PD output. The second state variable is the frequency error from the FD output. The control fuzzy variable is the required tuning frequency of the NCO to generate an exact replica of the incoming signal. The real line R is the universe of discourse of the three fuzzy variables. However, in practice it is restricted to the discriminators output domains and to small interval domains for the output chosen by the designer according to previous experience.

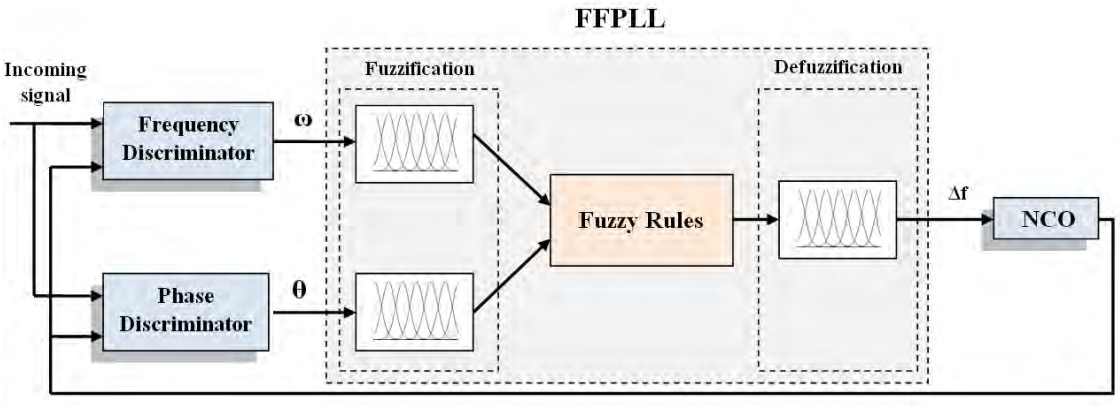

Figure 3-7: FFPLL filter construction

The choice of input and output fuzzy MFs in addition to the connecting fuzzy rules is a challenging task and requires a previous designer experience of the original FLL-

assisted-PLL filter design and the input-output behavior in different conditions. For this reason a huge number of scenarios that include signal tracking and different tracking parameters such as different signal qualities, interference power, dynamics level, loop order, or bandwidth are generated and monitored. The primary equipment used for generating these scenarios for GPS signals , is a GPS GSS7700 hardware simulator (Spirent 2006). The current hardware configuration is capable of producing GPS signals at the L1, L2 and L5 frequencies in addition to adjustable additive interference through two separate signal generators. Several custom scenarios representing typical missile dynamics in space have been designed and tested. The RF signals are collected through an National Instruments (NI) PXI 5661 front-end (NationalInstruments 2006) after passing through an external LNA using a sampling frequency of f_s = 10 MHz and intermediate frequency f_{IF} = 0.42 MHz, and finally saved for post-processing. A software GPS receiver under a MATLAB® platform is implemented and used. Figure 3-8 shows the hardware configuration used for generating and collecting GPS signals.

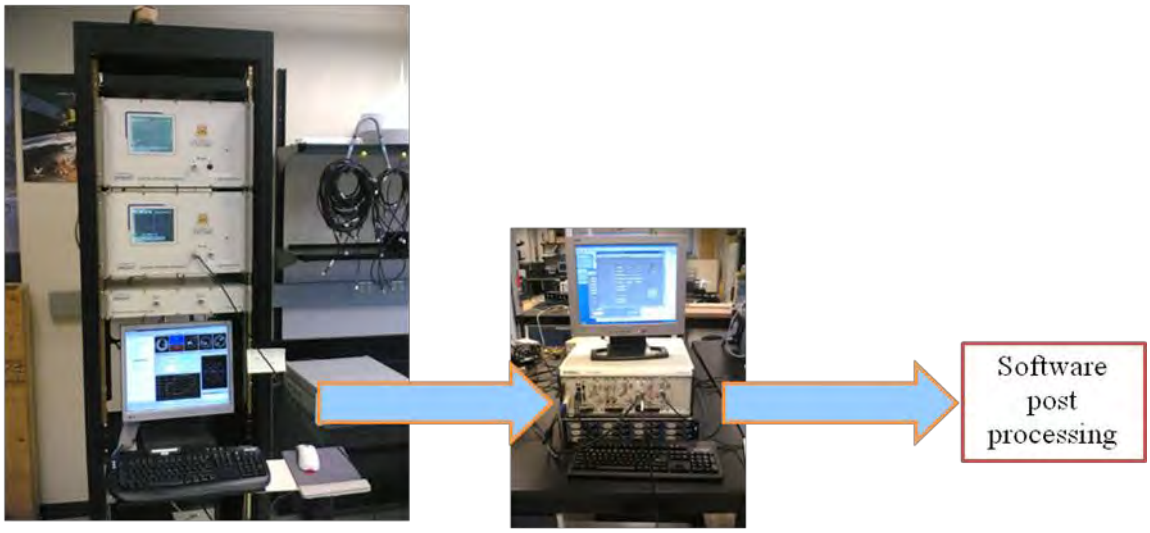

Figure 3-8: Hardware configuration used for GPS signal generation and testing

The next subsections include inputs definition and an investigation of the input-output relation of the standard FLL-assisted-PLL filter in order to gain the sufficient experience necessary to design the fuzzy MFs and rules.

3.2.2 Membership Functions Design

The fuzzy frequency/phase tracking system is designed to rapidly recover the signal frequency in the presence of large frequency errors, i.e. after acquisition/reacquisition, and to behave as a PLL, with precise phase recovery, in the case of small frequency errors. The fuzziness of the system inputs is mainly due to the low power of GPS signals with respect to thermal noise, which is the main source of phase/frequency jitter (Kaplan & Hegarty 2006). Noise distribution then plays a major role in the system design. This is

why an a priori knowledge of expected signal parameters like noise variance or C/N_0 is essential. This knowledge can be achieved during signal acquisition or in the first stages of signal tracking. For example, a signal with a C/N_0 equals to 39 dB-Hz, in static conditions and in an interference free environment, is characterized by a PD output with a distribution approximately Gaussian as shown in Figure 3-9. The variance of this signal can be theoretically calculated as (Crosta & Alenia 2009)

$$\sigma_\theta^2 = \frac{1}{2Tc/n_0}\left(1+\frac{1}{2Tc/n_0}\right) \quad \textbf{(3.14)}$$

where σ_θ^2 is the variance of the dot-product discriminator, which also suits well the arctangent discriminator used in this research, T (s) is the predetection integration time and c/n_0 carrier to noise power expressed as a ratio (Hz).

Figure 3-9 shows the time domain representation for the PD output during the tracking of the incoming signal received from PRN 5 using a 4 Hz 3rd order PLL with a 1 ms coherent integration time. Figure 3-9 also shows its histogram with the Gaussian function approximation. In this case, the corresponding Gaussian Probability Density Function (PDF) covers the signal expected values in standard tracking conditions at a certain C/N_0 level. It can be linguistically described as "Zero" state when it is compared with the ideal PD output.

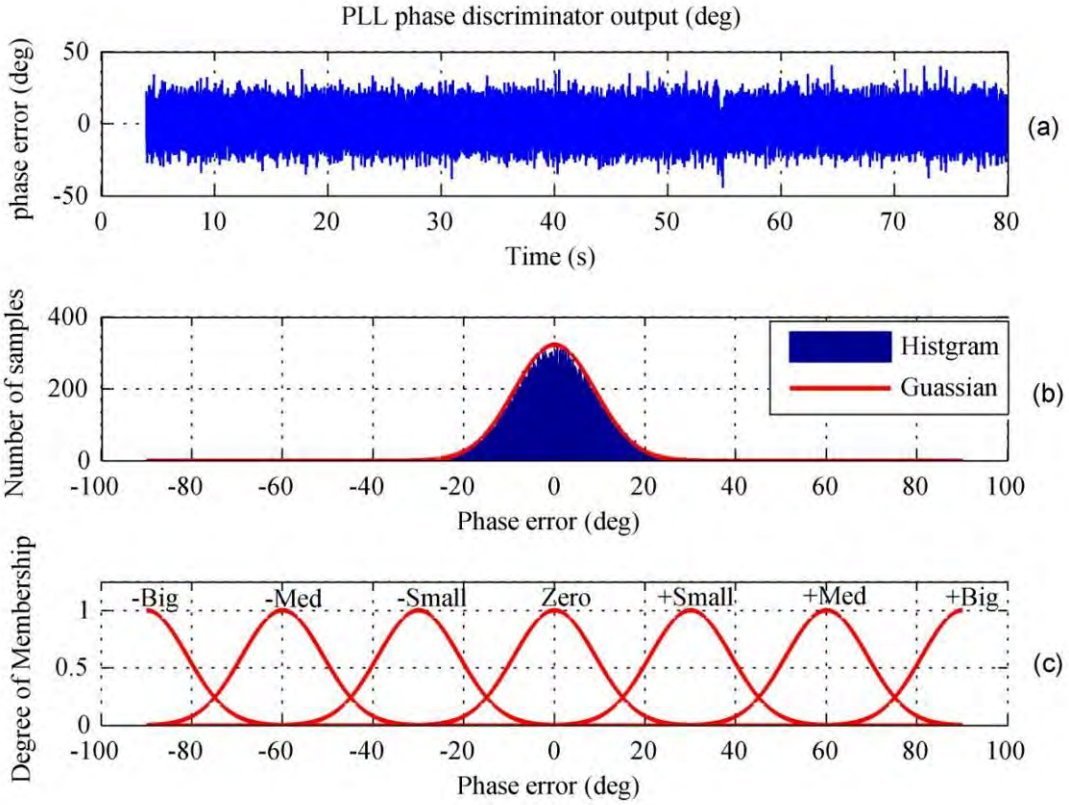

Figure 3-9: (a)Time domain representation of a PLL PD output, (b) histogram and Gaussian approximation and (c) an example of mapping between PDF and MF

The mean and standard deviation, which are the two main parameters that governs the Gaussian distribution function, are directly related to the signal dynamics and signal quality, respectively. Receiver dynamics can cause phase tracking error and hence, the distribution mean will be shifted from zero. On the other hand, the changes in the signal quality or PIT will result in changes in the standard deviation as previously described in Equation (3.14). An appropriate mapping between the signal PDF and fuzzy MFs can be made. In this case the probability of occurrence, which is described by the PDF, will be

replaced by a degree of occurrence sensed by a number of overlapped Gaussian MFs, as depicted in Figure 3-9.

Using the above approach, both phase and frequency error inputs, in addition to the NCO tuning frequency output domains, are clustered into several overlapping Gaussian fuzzy sets, each of them describing a certain linguistic definition of input or output value (for example: Big, Medium, Small, Zero…etc). The number of MFs adopted for the fuzzy controller is given in Table 3-2 and the connecting relations are described later.

Table 3-2: Distribution of fuzzy membership functions

Type	Fuzzy Variable	Number of MFs
Input(1)	Phase	9
Input(2)	Frequency	9
output	Tuning frequency	11

The number of fuzzy sets associated with each fuzzy variable is a design parameter selected according to the required tracking accuracy. How much these contiguous sets should overlap is also a design issue depending on the problem at hand: too much overlap blurs the distinction between the fuzzy set values, whereas too little overlap can produce excessive overshoot and undershoot. Empirical results show that an overlapping of about 25% is ideal to avoid rules blurring or excessive over/undershoots (Kosko 1992).

A defuzzification process is utilized to determine a crisp value according to the fuzzy output from the inference mechanism. The centre-average method (Chen & Pham 2001) or Fuzzy centroid described earlier, which calculates the centre of the area of the inference mechanism output possibility distribution, is used as a defuzzification strategy in FFPLL.

The chosen Gaussian MFs for the phase, the frequency and NCO tuning frequency are shown in Figure 3-10, Figure 3-11 and Figure 3-12, respectively, where they are defined as

(N)(P)B	:	±Big
(N)(P)MB	:	±Medium Big
(N)(P)M	:	±Medium
(N)(P)SM	:	±Small Medium
(N)(P)S	:	±Small
Ze	:	Zero

It is noted that the variance of each Gaussian function can be changed according to signal to noise level, as described earlier. Online adaptation can be performed and will be described in the next section.

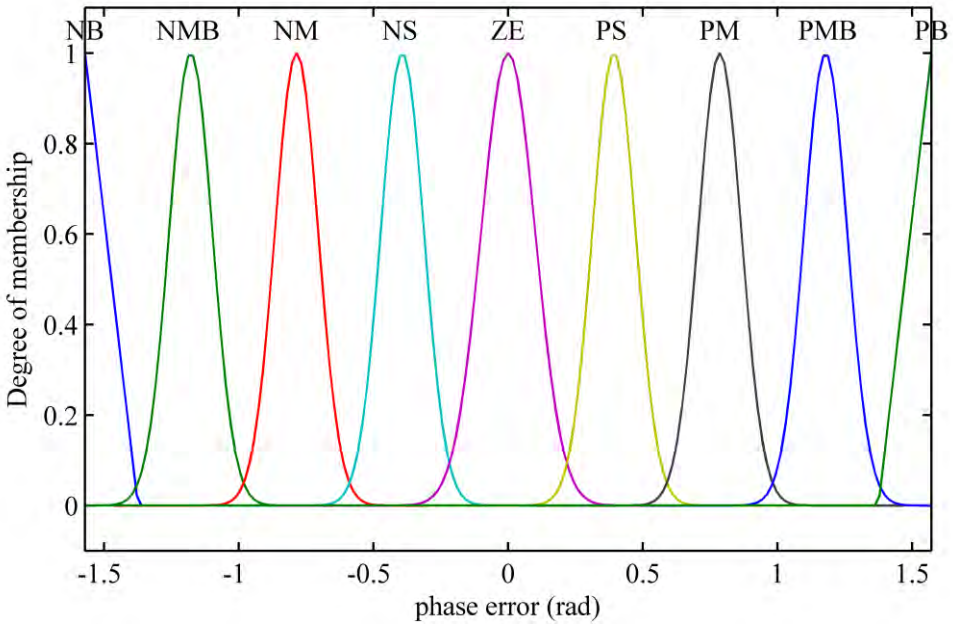

Figure 3-10: Phase membership functions

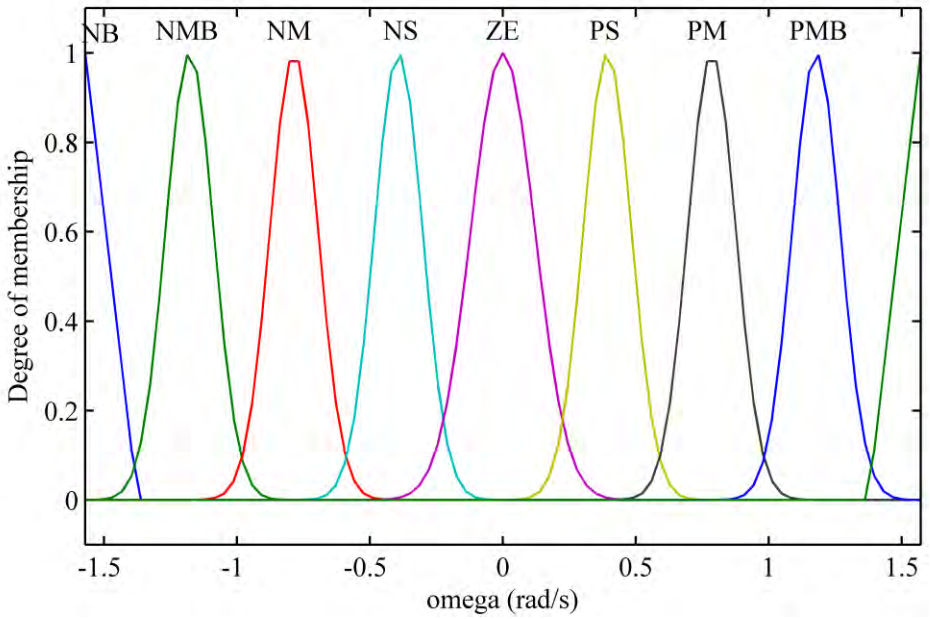

Figure 3-11: Frequency membership functions

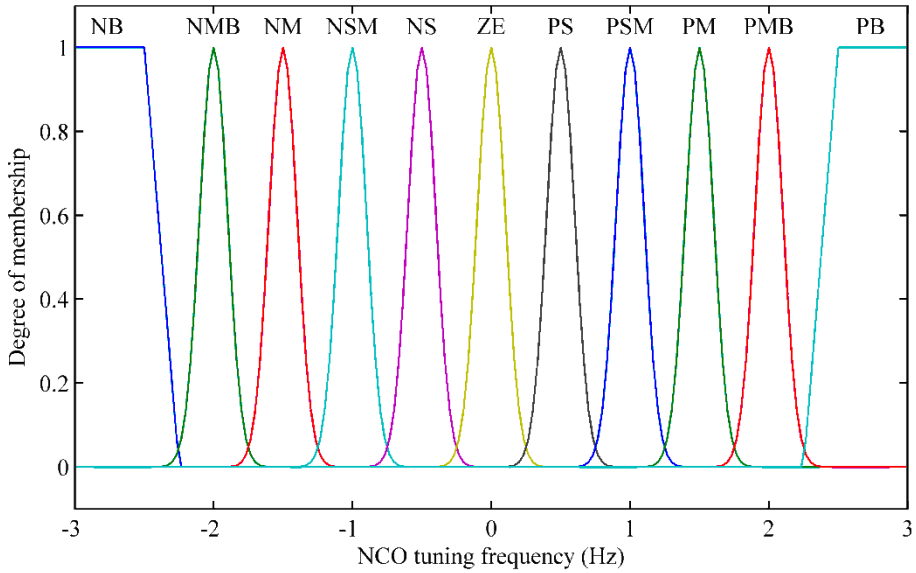

Figure 3-12: NCO tuning frequency membership functions

3.2.3 Fuzzy Rules Design

In order to write the input-output connecting rules, the input-output relation and its behaviour during standard PLL, tracking itself has to be studied.

Phase tracking is a challenging task. An ideal frequency tracking always needs a continuous tuning to track the phase. An example of phase tracking concept is shown in Figure 3-13. Signals A and B are exactly at the same frequency but different in phase. If signal B is the replica signal, a continuous frequency increase and decrease (tuning) has to be performed to adjust the phase.

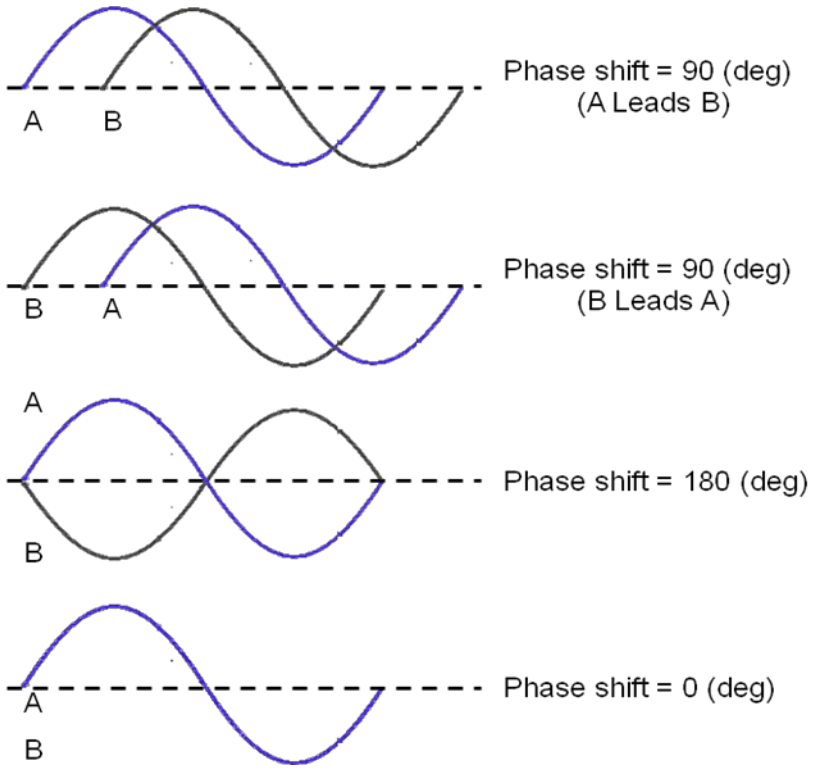

Figure 3-13: Illustration of signal phase tracking

To gain the sufficient experience required to design a replacement of the PLL filter using fuzzy control, the relation between the phase tuning frequency and the PD output has to be studied.

Under normal tracking conditions, filter input, which is the PD output, is a zero mean signal contaminated by Gaussian noise, whose standard deviation can be theoretically calculated in a standard PLL structure according to Equation (3.14).

Filter output is the control signal that is required to tune the NCO to continuously produce an exact replica (in frequency and phase) of the incoming signal carrier. Because of the filter input noise, its output will be contaminated with corresponding noise and so

will the generated carrier replica. This error in frequency will be reflected on the generated carrier phase and phase error will occur. Indeed continuous fine tuning of the NCO output has to be performed.

The filter output, which is the NCO course tuning frequency, is modulated by high frequency noise component correlated with the discriminator output noise. The course frequency component reflects the large and slow frequency variations, which are related to the signal Doppler and therefore correlated with the satellite-receiver LOS dynamics. High frequency noise modulated on this signal is related to the incoming signal C/N_0 as well as the filter bandwidth. This noise affects the carrier replica generated by the NCO, and any small frequency changes required to tune the NCO output for perfect phase tracking (fine tuning) will be obscured by this noise.

The relation between the PLL filter input and output can then be tested by studying the noise effect on the filter output. To do so, a simple experiment is used where the test configuration described earlier is used to produce a large number of scenarios. All the scenarios have been processed, and the recorded GPS signals are tracked using a standard PLL with a varying filter bandwidth ranging from 2 Hz to 18 Hz. The choice of the upper bound is justified by the maximum bandwidth that can be used for stable tracking as described in (Kaplan & Hegarty 2006). The filter output is then passed through a high pass filter (HPF) to decouple the course tuning frequency (low frequency) from the fine tuning and noise components. Because it is hard to exactly define the HPF parameters or range, it is possible to simulate its function by subtracting the noisy filter output extracted

during signal tracking from the exact filter output, calculated from exact Doppler which can be saved by the simulator software.

To illustrate this idea, one of the scenarios is detailed herein. In this scenario, the receiver is at rest for the first 50 seconds followed by a manoeuvring action as illustrated in Figure 3-14. The dynamic profile, which includes the absolute values of velocity, acceleration and jerk is shown in Figure 3-15. Tracking is performed in this scenario using a 14 Hz PLL. The estimated Doppler of PRN 5 during tracking is shown in Figure 3-16 where the effect of the manoeuvre on the calculated Doppler can be easily noticed after 50 seconds.

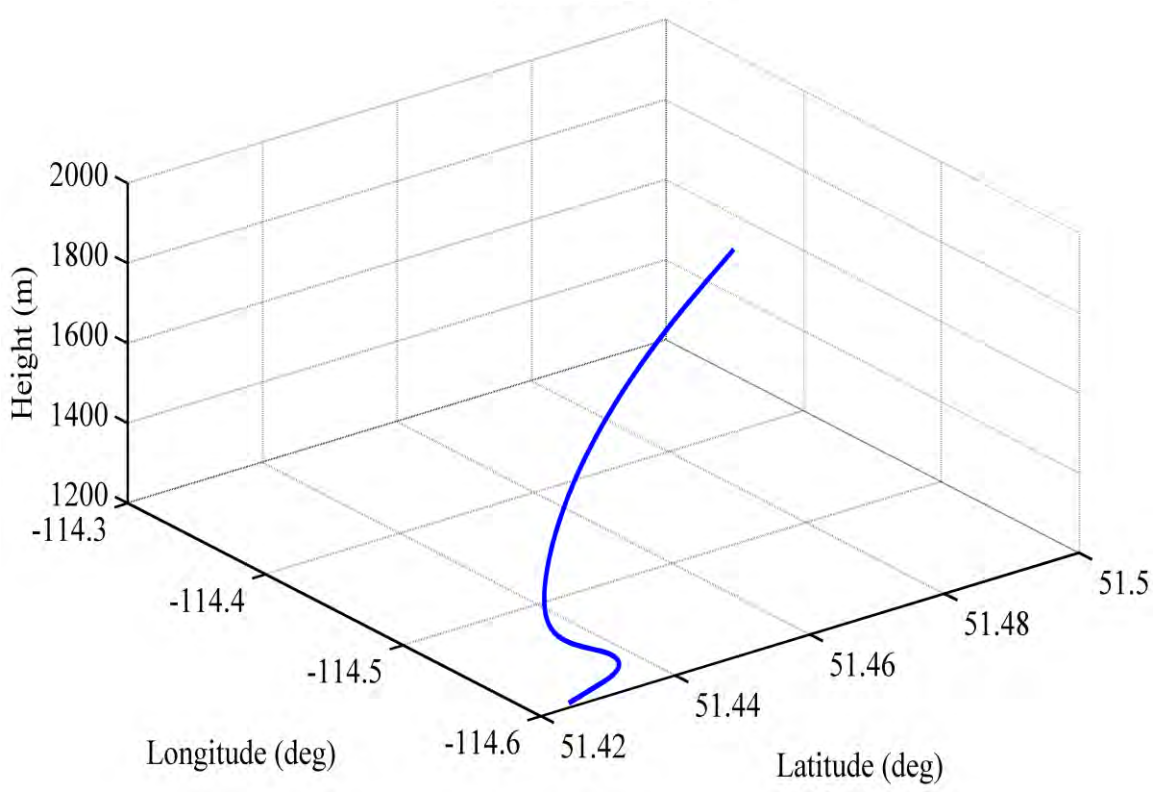

Figure 3-14: Receiver motion and manoeuvre

The exact filter output calculated from the scenario profile from the simulator (shown in Figure 3-17 (b)) is subtracted from the processing filter output (Figure 3-17 (a)) and the result δf is shown in Figure 3-17 (c). The PD output (θ) is a zero mean Gaussian signal and its standard deviation depends on the signal C/N_0 as described in Equation (3.14). The PD output during PRN 5 tracking is illustrated in Figure 3-18.

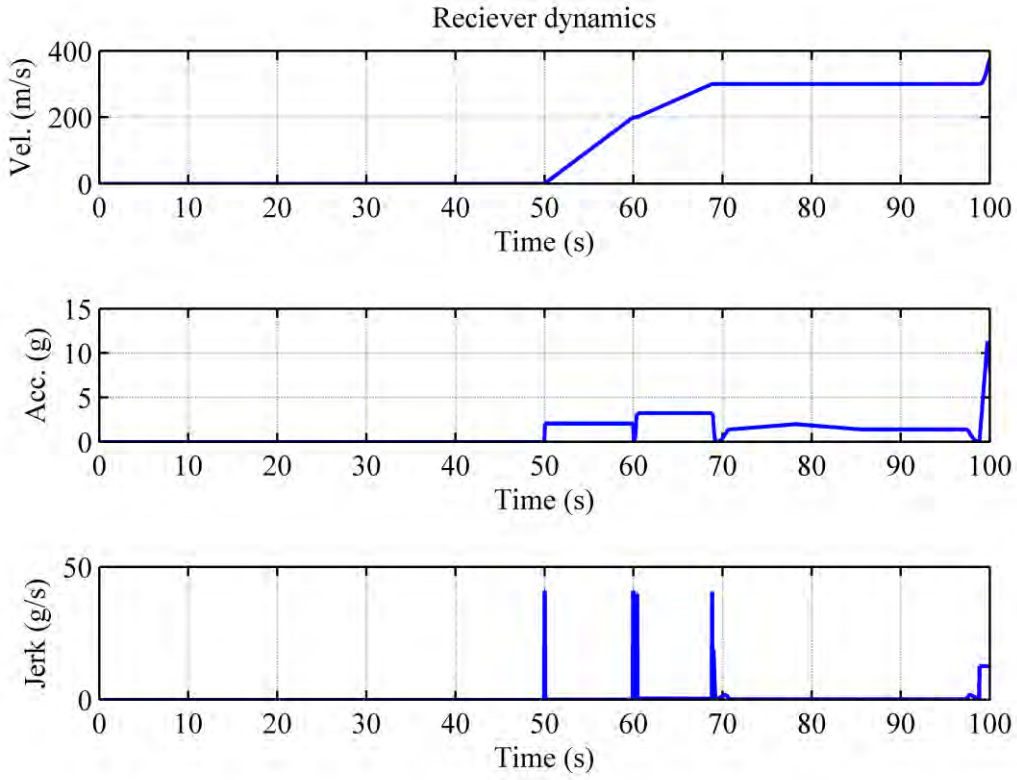

Figure 3-15: Receiver dynamic profile

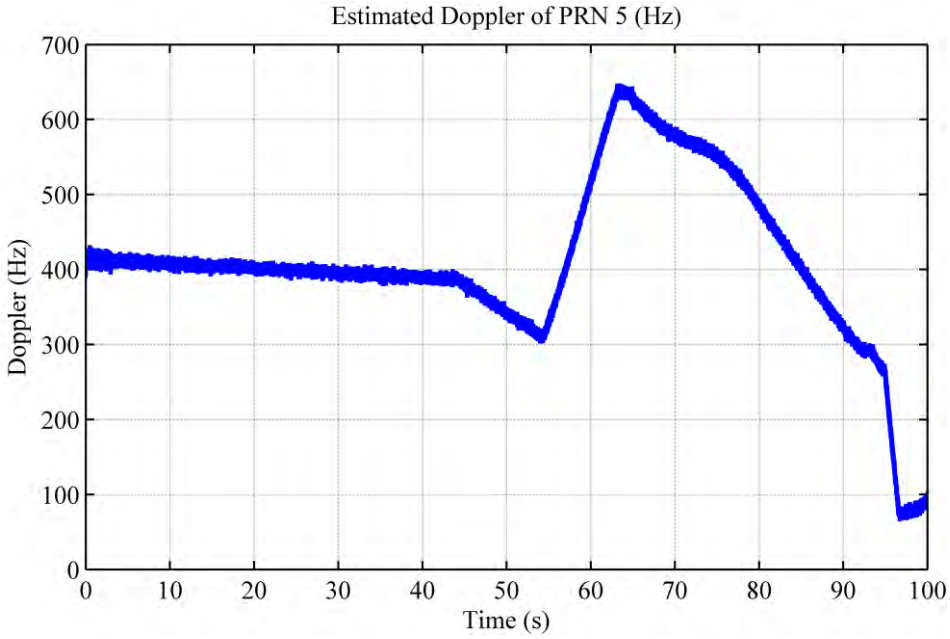

Figure 3-16: Estimated Doppler during tracking of PRN 5

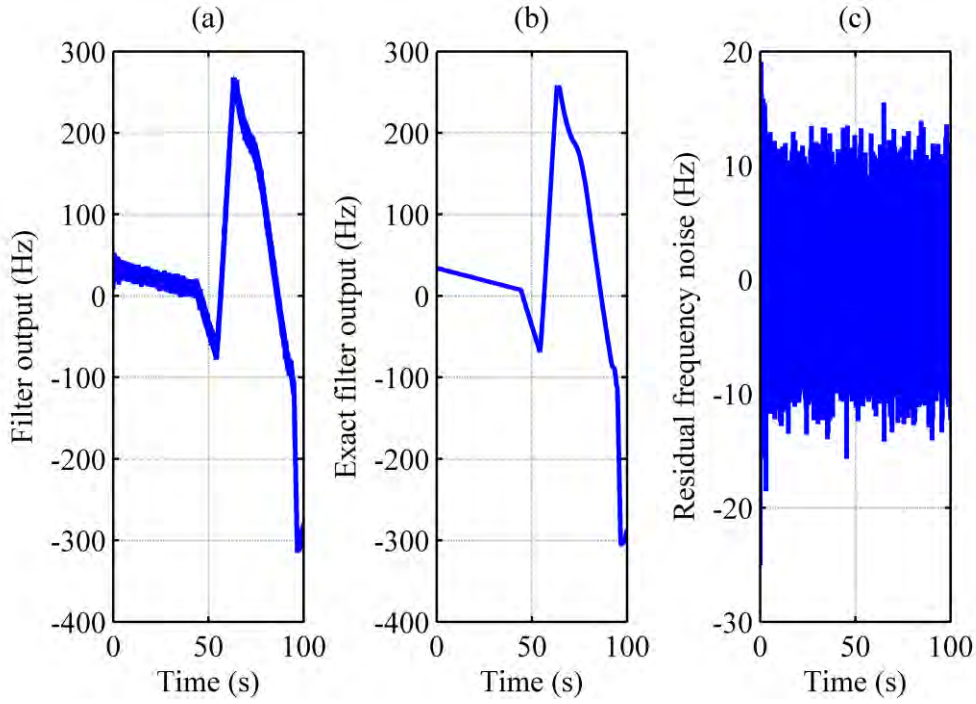

Figure 3-17: (a) Processed filter output (b) Reference filter output (c) Residual noise δf [(a)-(b)]

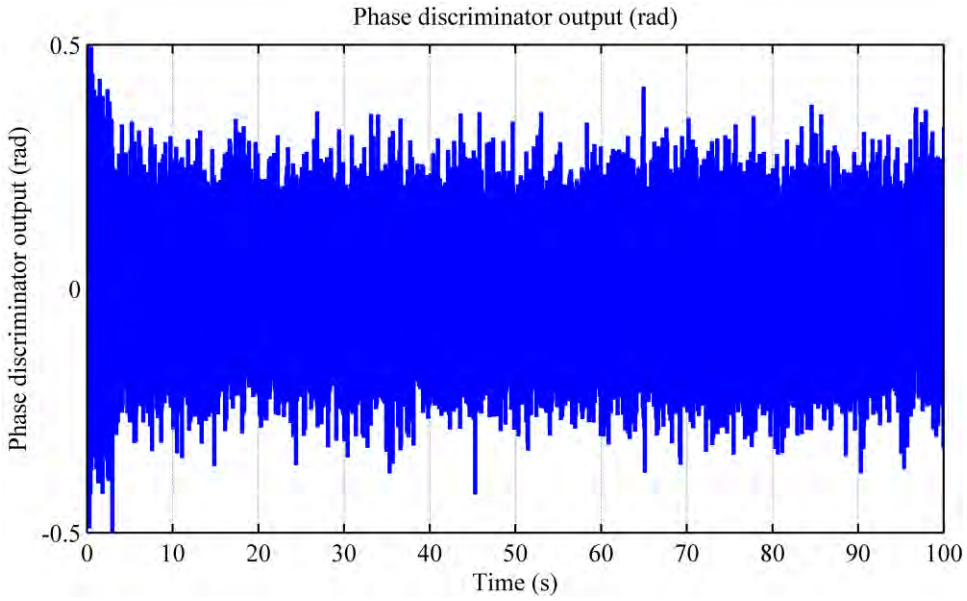

Figure 3-18: PD output

After noise calculation, the relation between δf and θ is calculated and fitted as a linear function as can be seen in Figure 3-19. The fitted line slope is dependent on BW and can be defined as the filter noise gain. The same relation is calculated for the same scenario but for different bandwidths ranging from 2 Hz to 18 Hz. Figure 3-20 shows the θ-δf relation for different selected BWs. The relation between the BWs and calculated noise gains is also fitted as a linear function as shown in Figure 3-21. The θ-δf relation can then be formulated, as follows and further used to estimate the corresponding fuzzy BW:

$$\delta f = (2.7BW - 0.42)\theta . \qquad \textbf{(3.15)}$$

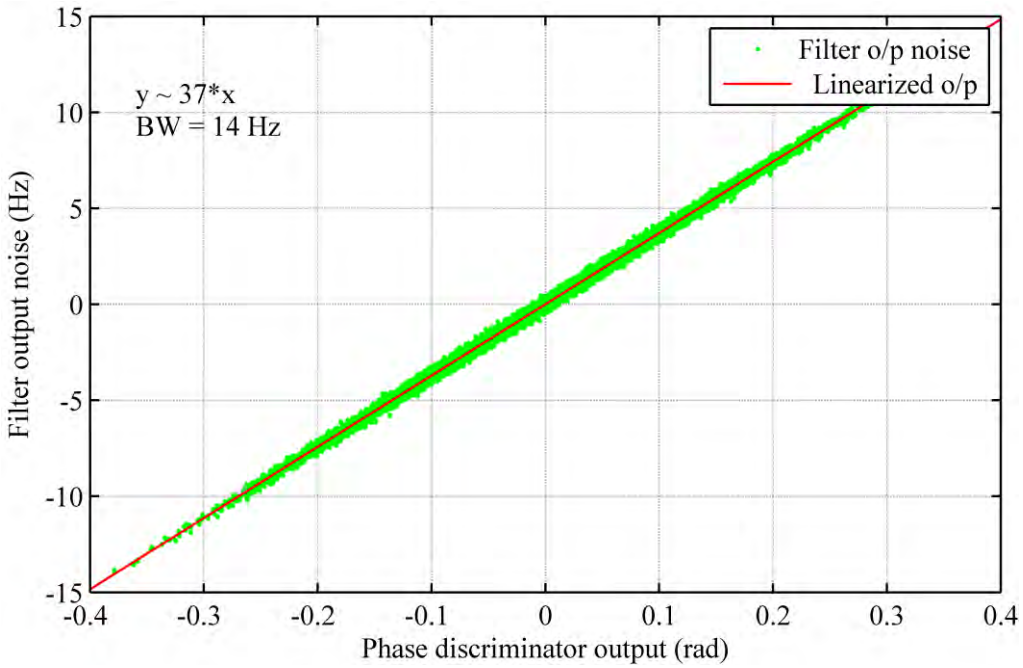

Figure 3-19: Relation between PD output and NCO phase tuning frequency at BW =14 Hz

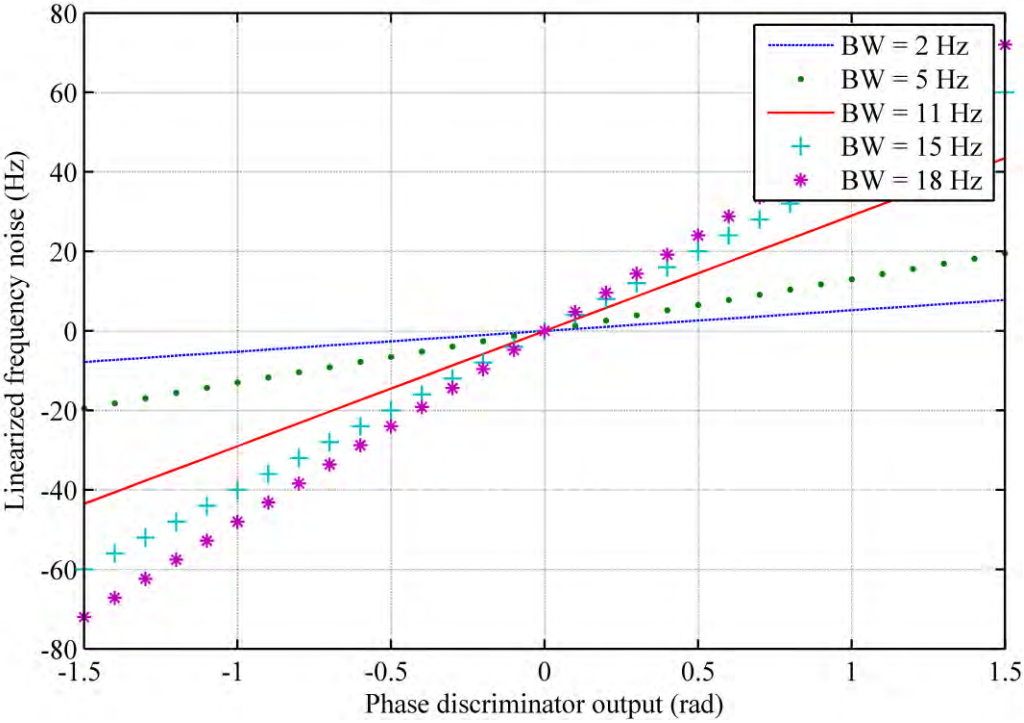

Figure 3-20: Relation between θ and δf at different BWs

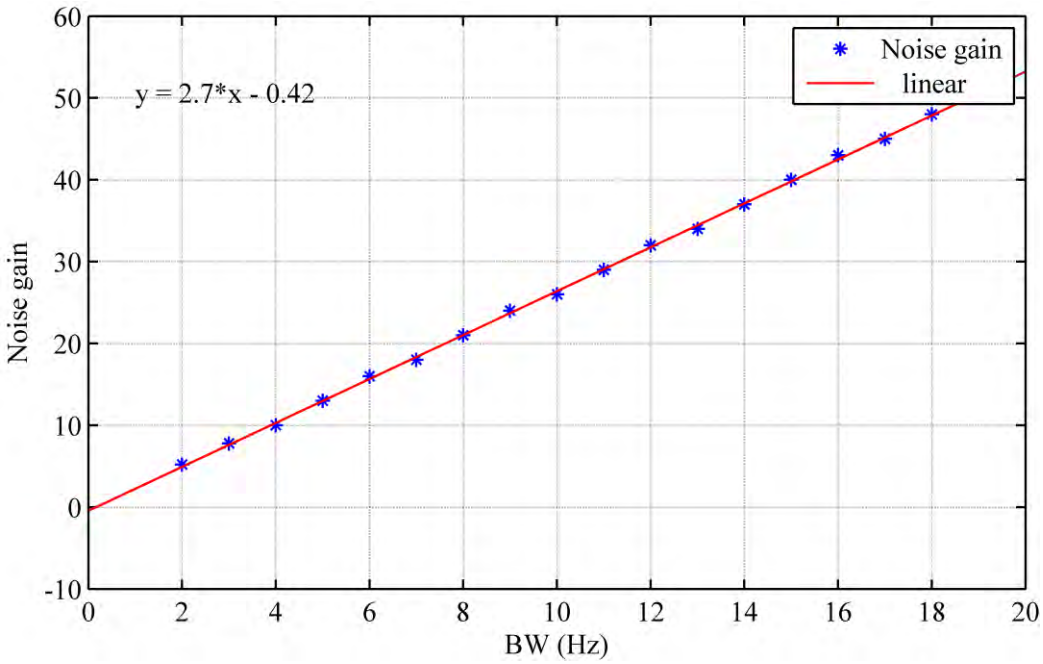

Figure 3-21: Linear relation between BW and PLL filter noise gain

By gaining the sufficient experience and knowledge of the traditional PLL behaviour in order to achieve good phase tracking performance, the design of a fuzzy tracking system that can provide better performance is now possible.

A good phase tracking performance can be achieved by obtaining a piecewise-linear θ-δf relation. For example if the phase error is within certain limits, it is sufficient for BW to be narrow. If θ is high due to any error, BW could be increased to rapidly recover this error. A θ-δf relation can be then described as a linear relationship with different slopes according to the phase error, which translates the same idea as of that of an adaptive BW filter. To show this approach, an example is illustrated in Figure 3-22 where PLL of BW of 4 Hz is used when θ is between -0.5 and 0.5 rad and 14 Hz is outside this range.

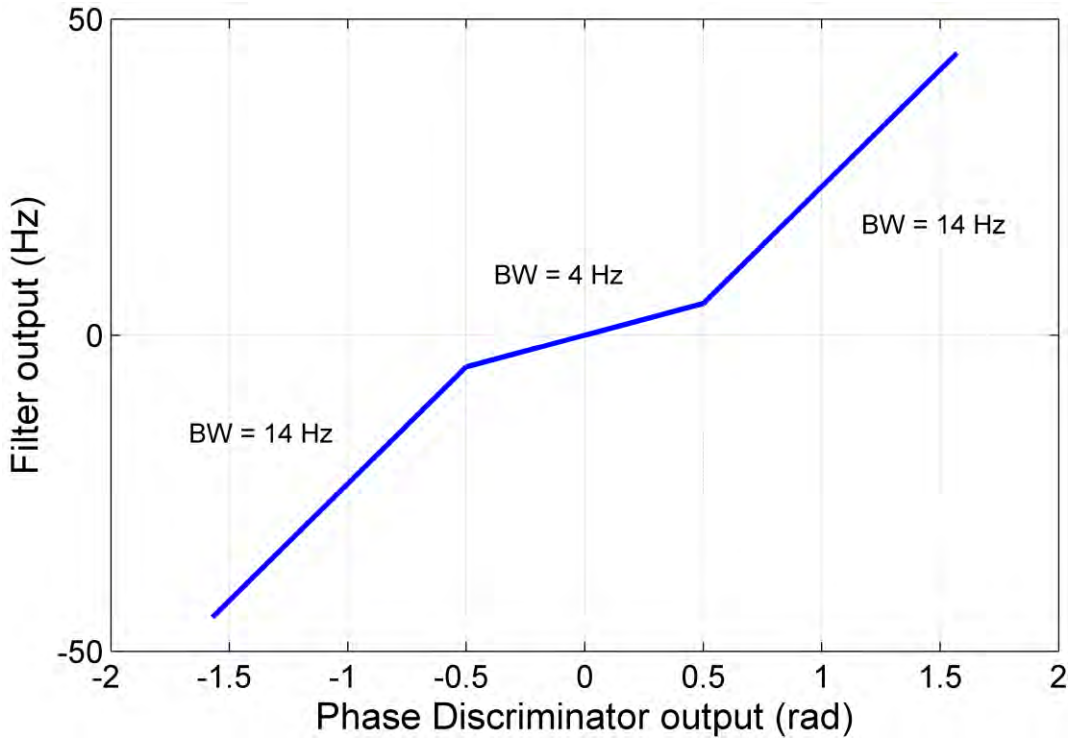

Figure 3-22: θ-δf linear relation at different Bandwidths

In a fuzzy control design, the designer has the complete ability to change the system performance by simply change the location and distribution of the fuzzy sets.

FAM rules are triples, such as: (Ze, -M, -SM). They describe how to modify the control variable for observed values of discriminators outputs. A FAM rule associates the PD fuzzy-set value with the FD fuzzy-set value and the required NCO tuning frequency fuzzy-set value. Hence the triple can be interpreted as the following set-level implication:

IF *the frequency error is* ***Zero***

AND *phase error is* ***negative*** *but* ***Medium***

Then *the required NCO tuning frequency is* ***negative*** *but* ***Small Medium*****.**

In general, the fuzzy rules relating all the linguistic variables can be expressed then as

$$R_i : \text{if } \theta = A_1^i \ \& \ \omega = A_2^i \text{ then } \Delta f = B^i \text{ for } i = \{1, \cdots, 81\} \quad \textbf{(3.16)}$$

where θ, ω, and Δf are linguistic variables and A_1^i, A_2^i and B^i are linguistic labels (or fuzzy sets) characterized by a MF.

Nine fuzzy MFs for each input means that 81 rules have to be processed in parallel. These fuzzy rules, which provide the human knowledge base of the controller gained from the previous analysis, are given in Table 3-3.

The FAMs are designed to act like an FLL for fast frequency tracking recovery in case of large frequency errors indicated by the FD. This can be seen in Table 3-3 in all the rules except when the frequency error is covered by the zero MF. In this case, it starts to look for the phase error, which is indicated by the PD for accurate phase tracking, and extracts the required data message. The Gaussian input membership functions means are chosen so that the input universe of discourse is clustered and covered by the nine functions. The variance of each Gaussian function is chosen according to the signal quality as described earlier. The corresponding output is chosen to resemble the adaptive BW tuning PLL as shown in Figure 3-22. The Gaussian output MFs is tuned to provide the required phase tuning frequency regardless of the input noise.

Table 3-3: Fuzzy rules

ω ↓ θ →	-B	-MB	-M	-S	Ze	+S	+M	+MB	+B
-B	+B	+B	+B	+B	+B	+B	+B	+B	+B
-MB	+MB	+MB	+MB	+MB	+MB	+MB	+MB	+MB	+MB
-M	+M	+M	+M	+M	+M	+M	+M	+M	+M
-S	+SM	+SM	+SM	+SM	+SM	+SM	+SM	+SM	+SM
Ze	-MB	-M	-SM	-S	Ze	+S	+SM	+M	+MB
+S	-SM	-SM	-SM	-SM	-SM	-SM	-SM	-SM	-SM
+M	-M	-M	-M	-M	-M	-M	-M	-M	-M
+MB	-MB	-MB	-MB	-MB	-MB	-MB	-MB	-MB	-MB
+B	-B	-B	-B	-B	-B	-B	-B	-B	-B

The set of all possible input-output pairs defines a FAM surface in the input-output product space, in this case in R^3 , is illustrated in Figure 3-23.

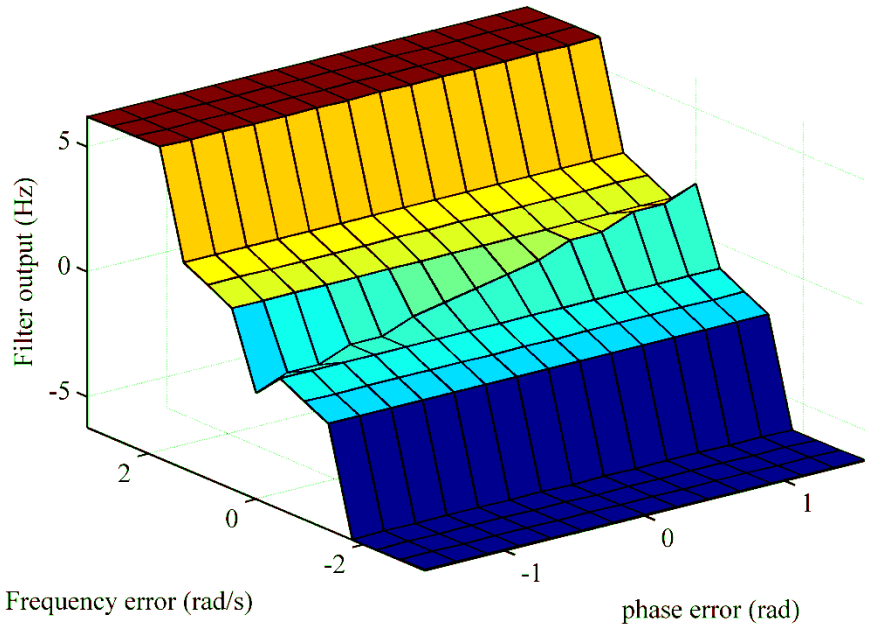

Figure 3-23: Fuzzy control surface

The same scenario as the one used before is used again to examine the relation between the PD output and filter output during fuzzy tracking. Using the FAM rules provided in Table 3-3, it is possible to derive a partial linear relationship, which indicates a variable noise gain as shown in Figure 3-24. A corresponding bandwidth can be calculated using Equation (3.15). In Figure 3-24, it can be seen that the line slope is small and hence the bandwidth is narrow (~ 0.6 Hz) in the range [-0.15, 0.15] radians, which guarantees a reduced noise performance. Out of this range, the bandwidth is increased to guarantee a rapid recovery of the phase tracking.

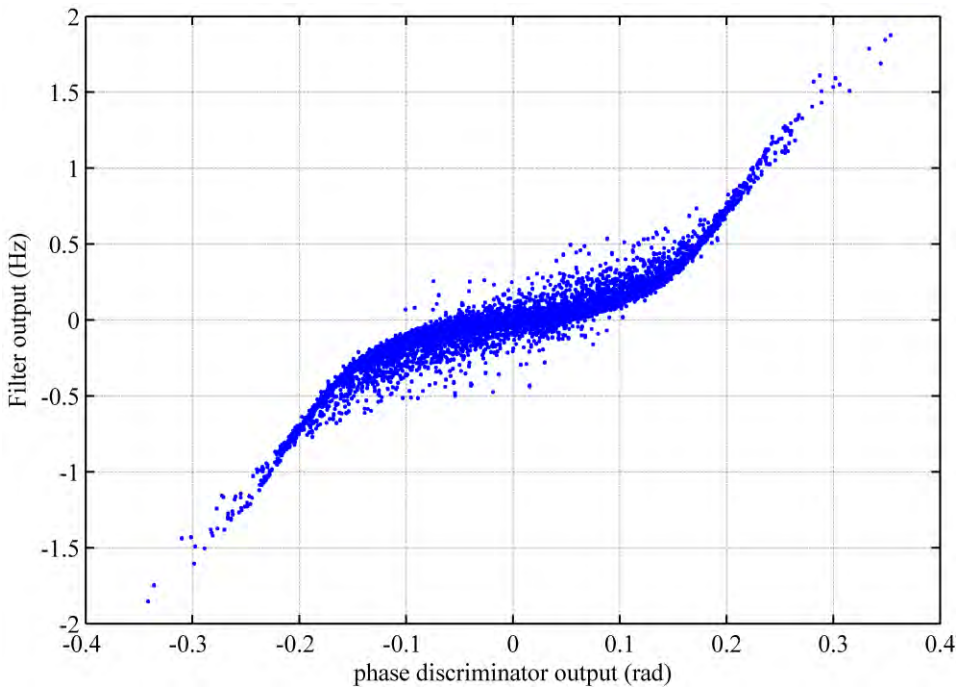

Figure 3-24: Relation between PD output and NCO phase tuning frequency using fuzzy filter

3.2.4 Interference Effects and Online Adaptation

As shown in Equation (3.14), higher C/N_0 values insure a small noise standard deviation and hence accurate and stable tracking. Increasing signal interference level will lead to a decrease of the C/N_0 level.

Interference signal power usually changes according to the receiver manoeuvre by approaching or moving away from a jammer, jammer motion, or to the jammer power changes. These changes affect the effective C/N_0 on the receiver side. The analogy between Gaussian noise distribution and fuzzy MFs shown in Figure 3-9 still holds but a continuous change of the MF parameters, particularly the standard deviation, is required to cope with the C/N_0 variations. An illustration of how phase error input MF changes with time and effect of increased interference level is shown in Figure 3-25.

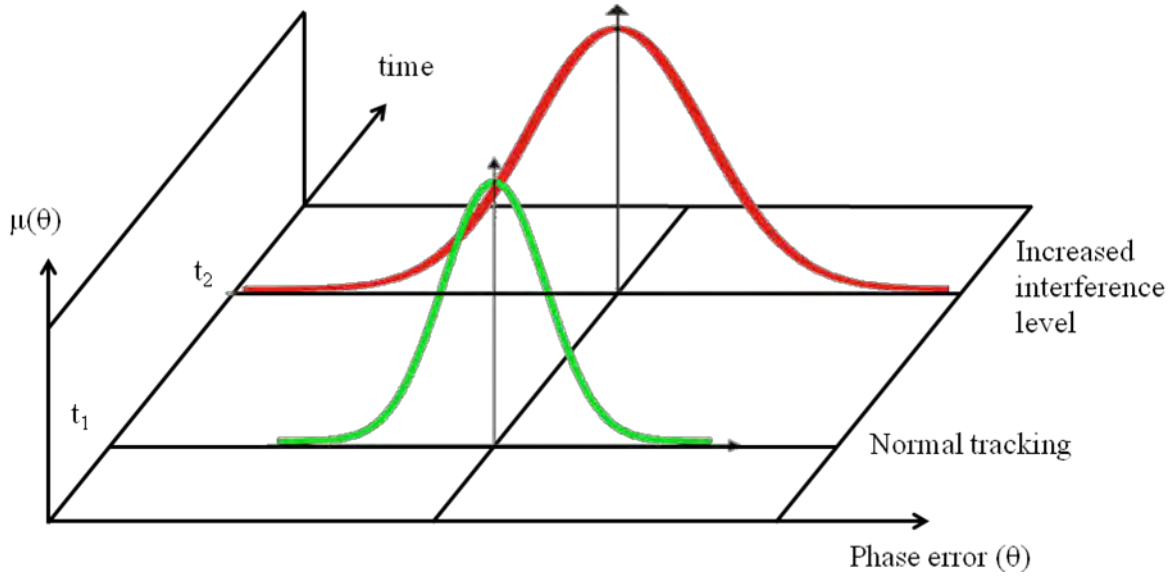

Figure 3-25: Phase input MF change with time and effect of increased interference level

For online adaptation of the MFs, the noise standard deviation associated with the PD and FD outputs has to be continuously estimated. This can be done using past samples from the PD and FD. Small analysis windows, used for collecting past PD and FD samples, should be used in order to properly follow rapid changes due to the interfering signal. A trade off between sensitivity and accuracy has to be taken into consideration. A small analysis window with a width of 1 s is found to be enough for good sensitivity at high dynamics (Kamel et al 2011a). However, although it maybe not long enough to provide accurate information about PD and FD output standard deviations specially at low levels of C/N_0 but still it can provide some information about the noise trend and whether it is increasing or decreasing to increase the chance of describing the signal by its actual MF. Figure 3-26 shows the modified FFPLL system with the standard deviation estimation. This information is used for the online adaptation of the Gaussian fuzzy MFs.

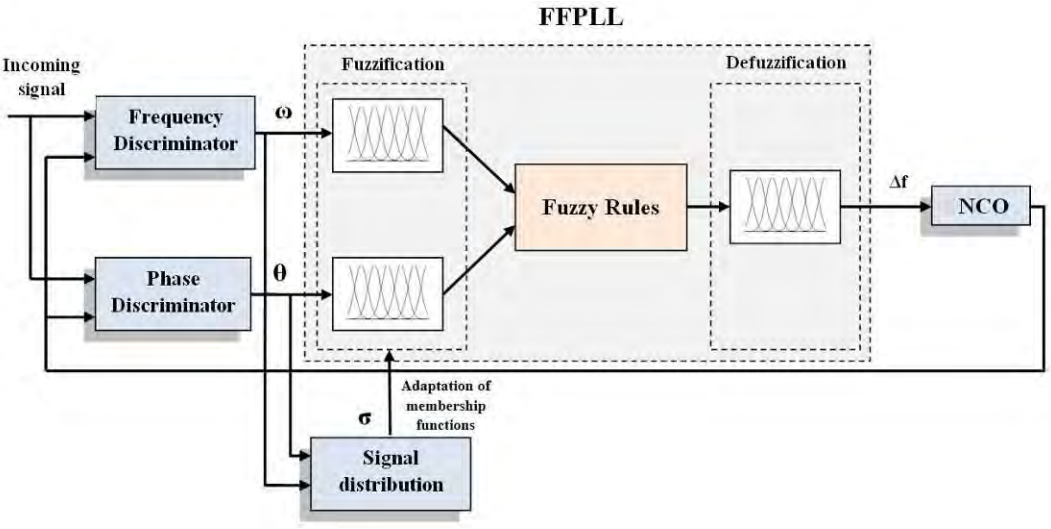

Figure 3-26: Modified FFPLL with estimation of PD and FD output standard deviation for MF online adaptation

3.3 Summary

In this chapter, an introduction to the general concepts of fuzzy control theory has been presented. The second section involved the description of the new innovative fuzzy tracking system that replaces the traditional FLL-assisted-PLL filter with the new FFPLL filter. The approaches used to design the input and output membership functions in addition to the connecting fuzzy rules are described. It was shown that by defining the fuzzy rules, the performance of the filter output can correspond to a standard filter with different or adaptive bandwidths for controlling the noise amount and dynamic performance of the filter.

Chapter Four: Performance Assessment of FFPLL

A performance assessment of the proposed FFPLL is conducted in this chapter. Since the goal of the research focuses on enhancing the tracking loop performance in the presence of high dynamics and signal interference, which is not practical to test using live GPS, the hardware GPS simulator introduced in Chapter 3 and related hardware setup is used herein.

4.1 Introduction

In order to assess the performance of the proposed tracking algorithm under interference and dynamic effects, five main categories of assessment tests have been designed. The first category is designed to test the effects of dynamics. Scenarios with a GPS receiver mounted on a missile have been simulated with high dynamics including high levels of accelerations and jerks (Kamel 2010). The second category is designed to test interference effects with a static receiver and a gradually increasing interference level (Kamel et al 2011a). Interference and high dynamic effects are examined together in the third category, in which some scenarios of a missile that manoeuvres near an interference source are designed (Kamel et al 2011a, Kamel et al 2011b). Because of the contradictory relationship between the coherent integration time and the signal to noise ratio with the dynamic capabilities, the fourth category is designed to show the effect of changing the coherent integration time during tracking. The fifth and last category deals with the

empirical calculation of the maximum pull in frequency which is the maximum frequency error that can be injected into the carrier tracking loop to start a successful signal tracking. Pull in frequencies for different tracking algorithms are calculated and compared.

Sample results for each test category, including a description of the scenario design and results analysis, are presented in the following paragraphs. Table 4-1 summarizes the tests categories used for the assessment.

Table 4-1: Summary of tests types

Category number	Tested Parameters
1	Dynamics
2	Interference
3	Interference + Dynamics
4	Coherent integration time
5	Pull in frequency

GPS RF samples are post-processed and tracked using different tracking algorithms for comparison purposes. These algorithms are summarized in Table 4-2. First three algorithms are based on standard tracking schemes using PLL and FLL. PLLs with wide and narrow bandwidths, namely 14 Hz and 4 Hz, are used to show the effect of increasing bandwidth to cope with the effect of dynamics on the interference resistance. A narrow bandwidth PLL with BW= 4 Hz assisted with a 3 Hz FLL to increase its dynamic performance is also used. The fourth algorithm is based on the usage of a Kalman filter

tracking described earlier in Chapter 2 and is included as a practical tracking algorithm, which is usually used for military applications. Finally the new FFPLL is used.

Table 4-2: Algorithms used for comparative analysis of GPS tracking loops

	Name	Standard Tracking Loop	Kalman Filter Based	Fuzzy Logic
1	PLL (14 Hz)	X		
2	PLL (4 Hz)	X		
3	FLL (3 Hz)-assisted-PLL (4 Hz)	X		
4	KF		X	
5	FFPLL			X

The KF is tuned offline by knowing the measurements and processing statistics in post processing. However, it can be assumed that for missile applications these statistics can be properly estimated for online tuning of the Kalman filter. A temperature-compensated crystal oscillator (TCXO) is modeled and used. Referring to Equation (2.20), the process noise matrix characteristics are defined by the receiver clock's frequency random walk spectral density function amplitude S_g and the white frequency noise spectral density function amplitude S_f, where $S_f = 5\times10^{-21}$ s and $S_g = 5.9\times10^{-20}$ /s, which yields a minimum root Allan variance of 1.4×10^{-10} at $t_{min} = 0.5$ s. Another value that has been used is $q_{LOS} = 0.5$ rad^2/sec^5, which provides an extreme test condition for the tracking Kalman filter as used in (Psiaki & Jung 2002).

As mentioned earlier in Chapter 1, GPS navigation systems used in missiles rarely depend on standalone GPS as a sole mean for providing positioning information but

rather they are usually integrated with INS to improve overall system robustness and increase immunity against interference. To get mutual benefits ultra-tight integration is usually used. One of the parameters needed from GPS to update INS navigation processing in this technique is the signal Doppler measurements. For this reason the results analysis is focused more on the Doppler estimation performance using FFPLL. For short range missile applications, the flight time is usually short and GPS satellite data is not strictly needed since the data collected at the launching time can be used to determine the satellite position. However, for long range missiles this data is definitely required as the satellite sky view changes from place to place which can be on the other side of the globe. Phase tracking then is essential to extract this data. A good phase tracking performance results in a reliable or robust extraction of the navigation data bits.

The performance of each algorithm is evaluated by assessing the continuity of tracking during high dynamics, i.e. the ability of the receiver to maintain lock, and the noise standard deviation of the estimated Doppler. Phase tracking is also assessed by using the Phase Lock Indicator (PLI) described in (Dierendonck 1996).

The criteria for assessing the proposed tracking scheme are the following:

- tracking robustness under different dynamic conditions,
- tracking quality by measuring noise distribution modulated on the estimated carrier Doppler,
- ability to reduce signal interference effects on estimated Doppler,
- phase tracking performance indicated by the PLI and
- signal reacquisition ability and time.

4.2 High Dynamics and Bandwidth Effects on Tracking Accuracy

The first category of tests aims at investigating tracking performance under very high dynamic conditions. Different simulation scenarios for a manoeuvring missile have been built and used for the analysis. One of the scenarios considered is reported herein.

4.2.1 Scenario Design

The dynamic profile of the scenario considered for this test is shown in Figure **4-1**. This figure contains three plots showing the time evolution of the total velocity, acceleration and jerk, respectively.

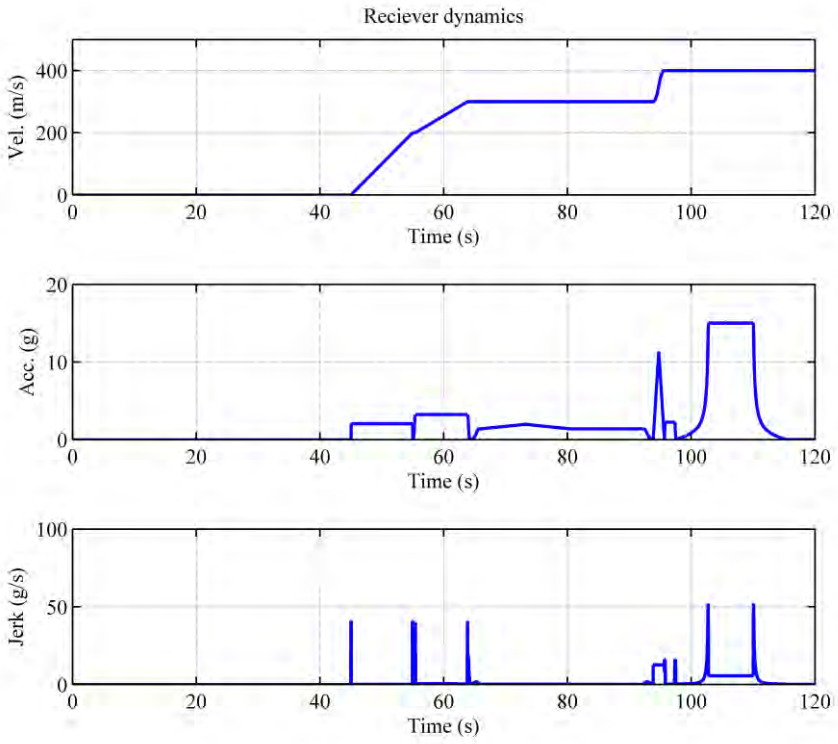

Figure 4-1: Receiver dynamics profile

The scenario comprises first a static period of around 50 seconds and then the total missile velocity is increased gradually to reach 450 m/s while performing sharp manoeuvres that reach up to 15 g. The manoeuvres are also associated with high and sudden jerks that reach up to 50 g/s. A 3D plot that shows the missile motion in space is depicted in Figure 4-2. The five tracking schemes are used for GPS signal tracking, as described earlier.

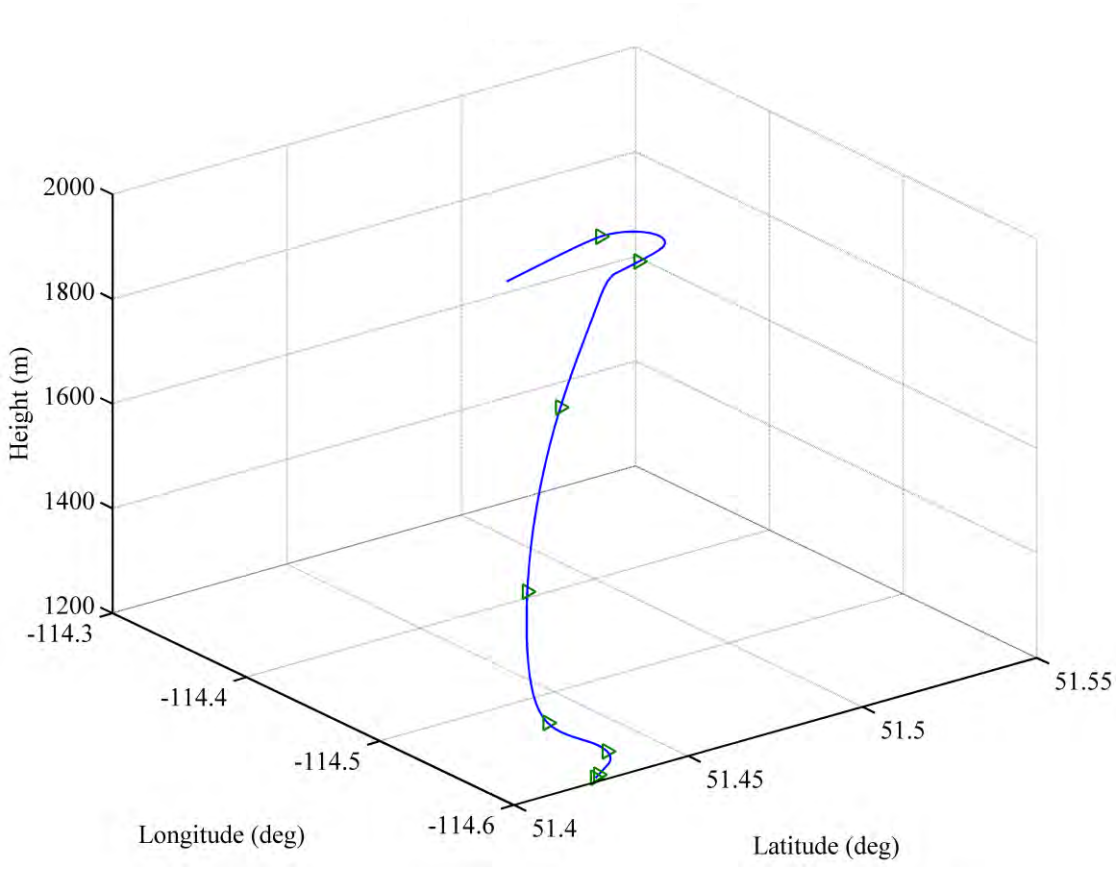

Figure 4-2: Receiver 3D motion plot

4.2.2 Tracking Results

Tracking results show that, while using a wide bandwidth is preferable to track high levels of dynamics, it is not advantageous in terms of noise variance. On the contrary, narrow band PLL loses lock when applied to high dynamic signal but it provides a very good noise cancellation level. The use of a narrow bandwidth PLL assisted with FLL provided a slight improvement in the dynamic robustness but with more noisy performance for the same stand alone PLL bandwidth. The KF based algorithm is tuned to be robust in the presence of high dynamics with minimum noise level which comprises the benefits from wide and narrow bandwidth PLLs as long as the noise characteristics is correct and modeled correctly. Tracking using FFPLL shows better performance in terms of continuity and noise cancellation as it is able to track the high dynamic signals while giving a reduced jitter level which is comparable to a well tuned KF based tracking.

Figure 4-3 illustrates the Doppler tracking performance for four different satellites, namely PRNs 24, 23, 3 and 9, using the five different tracking schemes, with an increase of the coherent integration time to 2 ms after 4 seconds of tracking. It can be seen that the receiver dynamics affect differently the tracking performance of each scheme according to the receiver's velocity projected along the line of sight unit vector between the receiver and satellite. Clearly from Figure 4-3, only the wide bandwidth PLL, KF, and FFPLL schemes are able to provide continuous tracking during the whole scenario. Indeed tracking schemes using a narrow bandwidth PLL, even assisted with FLL, are not able to

provide continuous tracking and failed at the point of loosing lock, which is marked with a black circle.

The first 10 seconds of the considered scenario and same satellite are further analyzed in Figure 4-4 and detailed for PRN 24 in Figure 4-5, from which two important characteristics of tracking algorithms can be analyzed. These characteristics are the variations in the Doppler estimates and system transient response to dynamic changes.

To speed up the acquisition procedure, the frequency bins used to find the right frequency are usually chosen to be large, which is the case here with the frequency bin size equals to 500 Hz. This explains why tracking will always start with a significant frequency error. The maximum permitted frequency error, which allows the tracking loop to converge and start tracking, is called the pull in frequency and is discussed in the last section of this chapter. Convergence speed of a tracking loop to the right frequency is a very critical issue, especially when a vehicle moves with high velocities. It can be seen in Figure 4-4 that using a narrow PLL bandwidth, convergence is very slow when compared with the other schemes. Assisting the tracking scheme with FLL provides better performance in terms of convergence speed but still wide bandwidth PLL, KF, and FFPLL schemes are superior. The times required by the five tracking schemes to converge to the four considered PRNs Dopplers values (settling time) are summarized in Table 4-3, where it can be seen that PLL 14 Hz tracking provides the fastest performance.

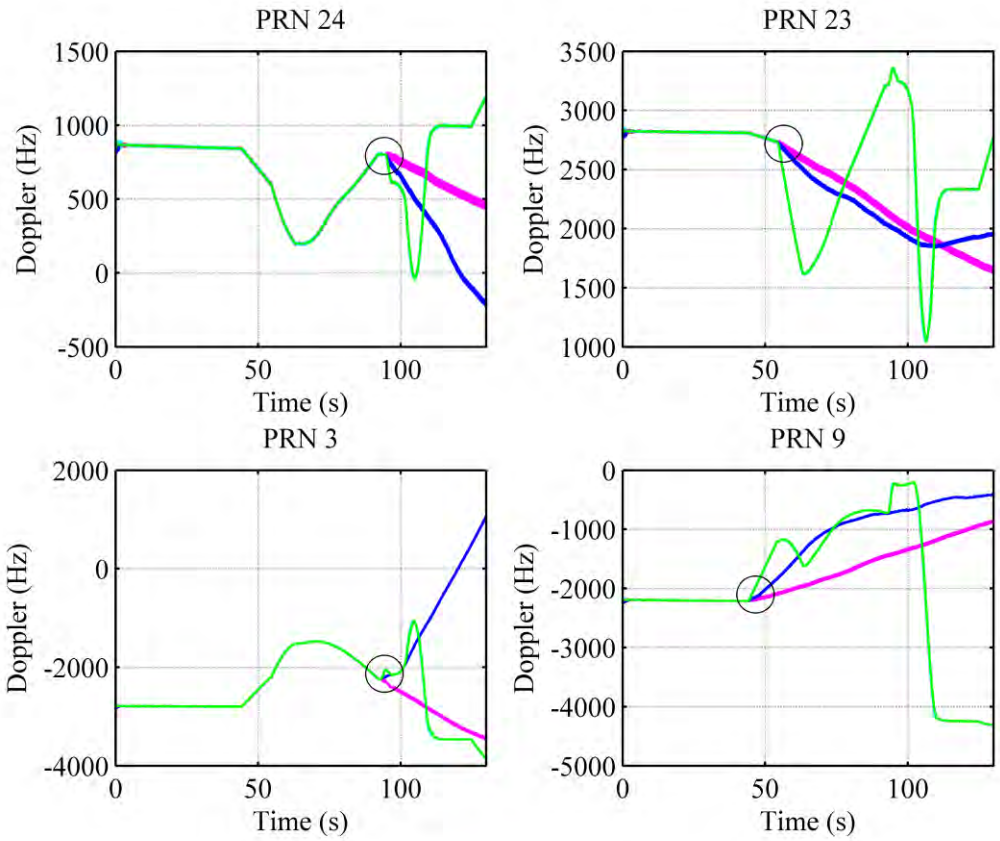

Legend: **PLL 14 Hz** – **KF** – **PLL/FLL 4/3 Hz** – **PLL 4 Hz** - **FFPLL**

Figure 4-3: Tracking performance for five different schemes and four different signals

Table 4-3: Doppler convergence times using different algorithms

	PRN 24	PRN 23	PRN 3	PRN 9
PLL 14 Hz	0.016	0.017	0.009	0.014
PLL 4 Hz	1.221	1.646	1.037	1.534
FLL/PLL 3/4 Hz	0.351	0.47	0.29	0.471
KF	0.22	0.25	0.68	0.24
FFPLL	0.158	0.178	0.113	0.209

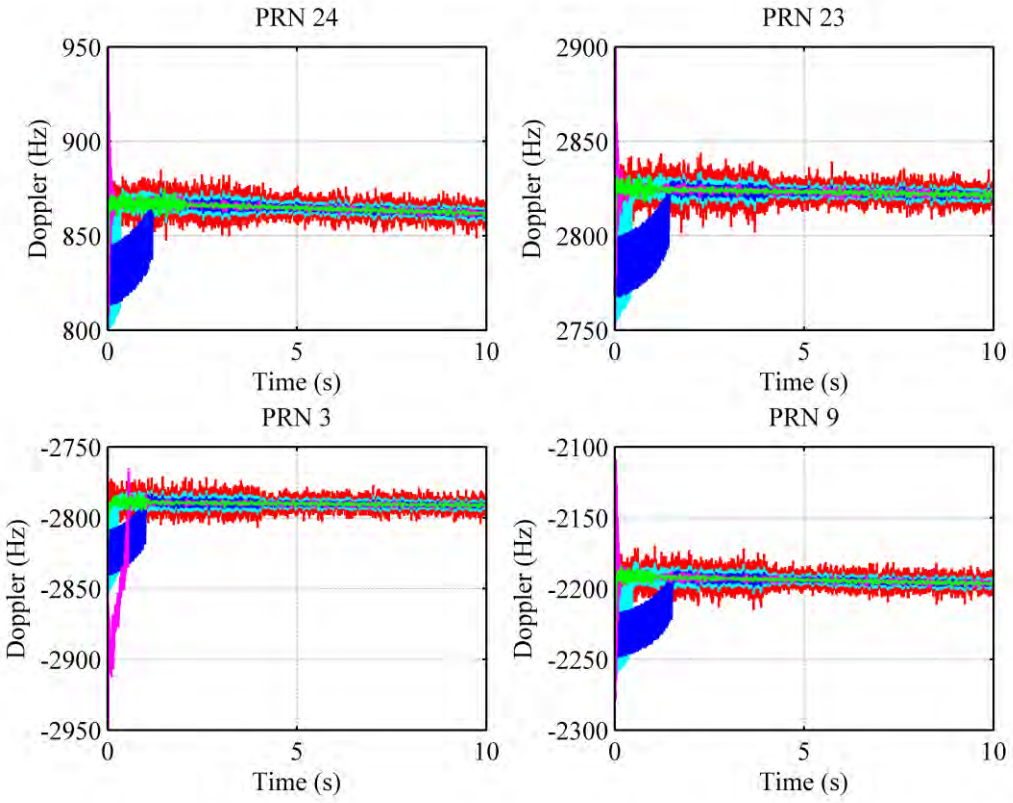

Legend: **PLL 14 Hz** – **KF** – **PLL/FLL 4/3 Hz** – **PLL 4 Hz** - **FFPLL**

Figure 4-4: Tracking performance in terms of Doppler estimates for five different schemes in four tracking channels (zoomed)

Convergence speed doesn't only affect the tracking of the right frequency but also the tracking of the right signal phase and hence obtaining the required navigation data bits through correlation. Figure 4-6 illustrates the first second of the PLI while Figure 4-7 illustrates the first second of the in phase prompt correlator for PRN 24 using the tracking schemes selected. It can be seen that phase lock and hence navigation bits are obtained much faster in case of the 14 Hz bandwidth PLL, KF and FFPLL, which gives the fastest convergence speed to the correct signal phase.

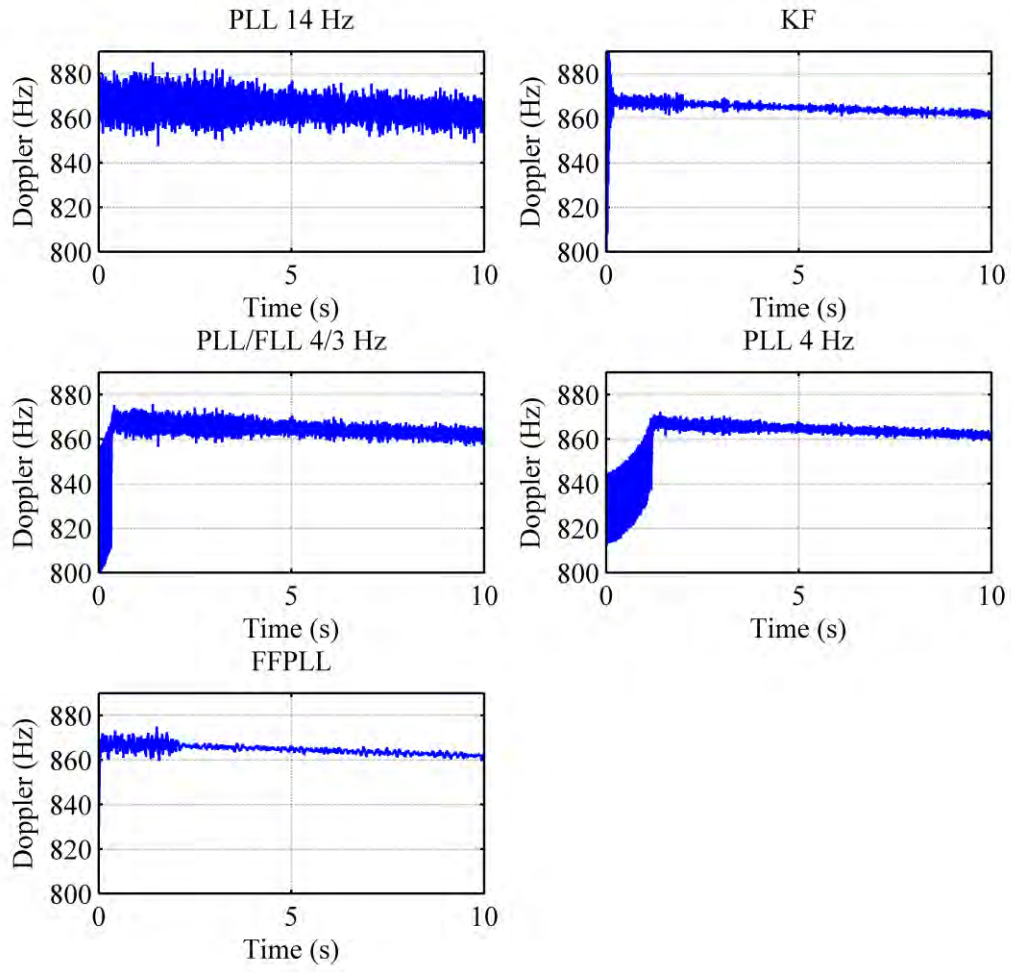

Figure 4-5: Tracking performance in terms of Doppler estimates for five different schemes for PRN 24 (zoomed)

To study the differences between the five tracking schemes in terms of tracking jitter, the standard deviations of the estimated Doppler frequencies are calculated continuously along the whole scenario using a 10 milliseconds moving window as shown in Figure 4-8. The average of the standard deviations for the five methods are calculated and shown

in Figure 4-9. It is clear that the proposed fuzzy tracking system is superior in terms of noise reduction.

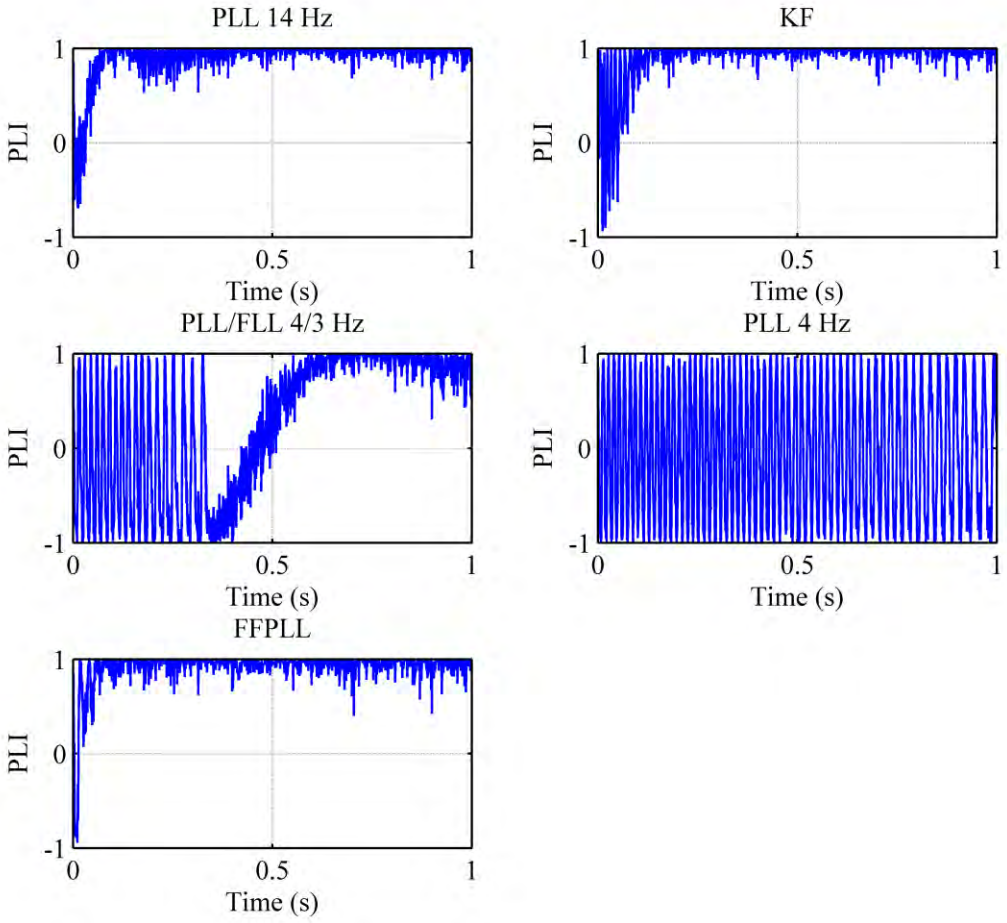

Figure 4-6: PLI calculated using five different tracking schemes for PRN 24

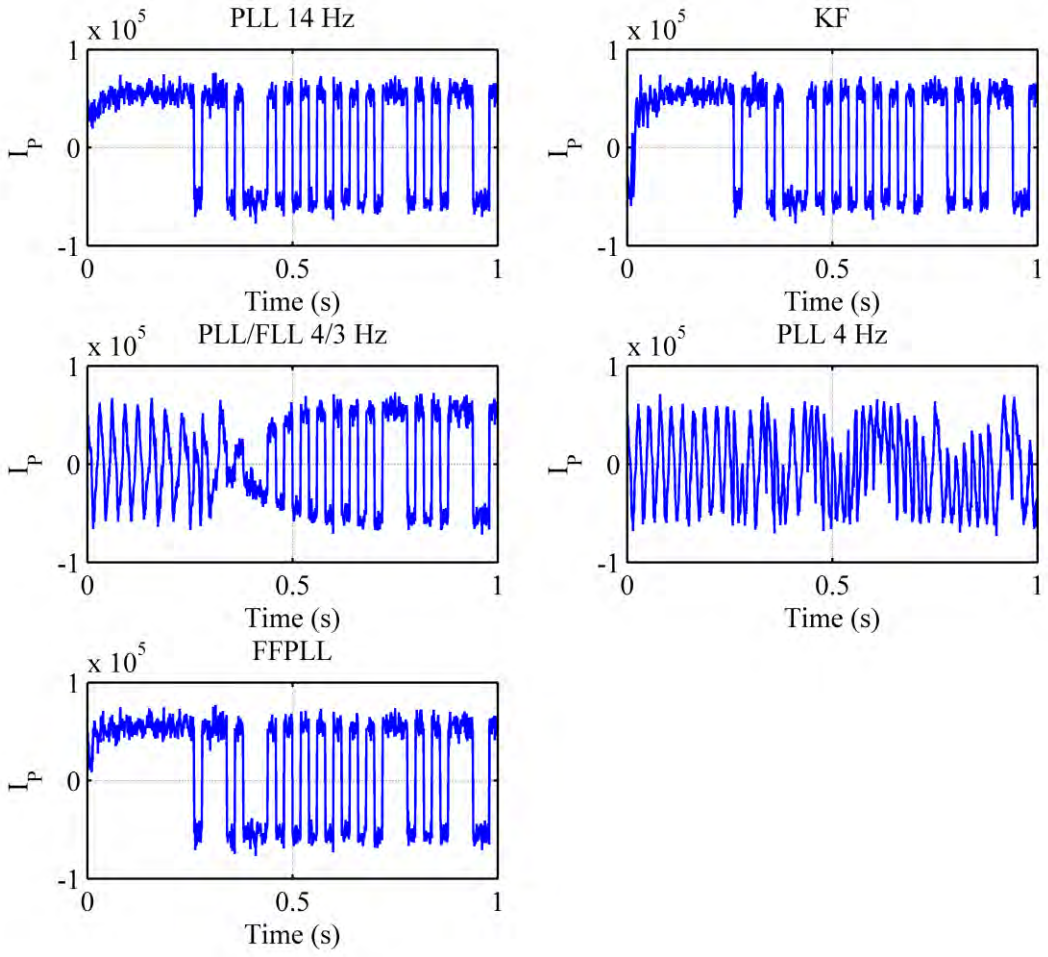

Figure 4-7 Navigation data bits obtained using five different tracking schemes for PRN 24

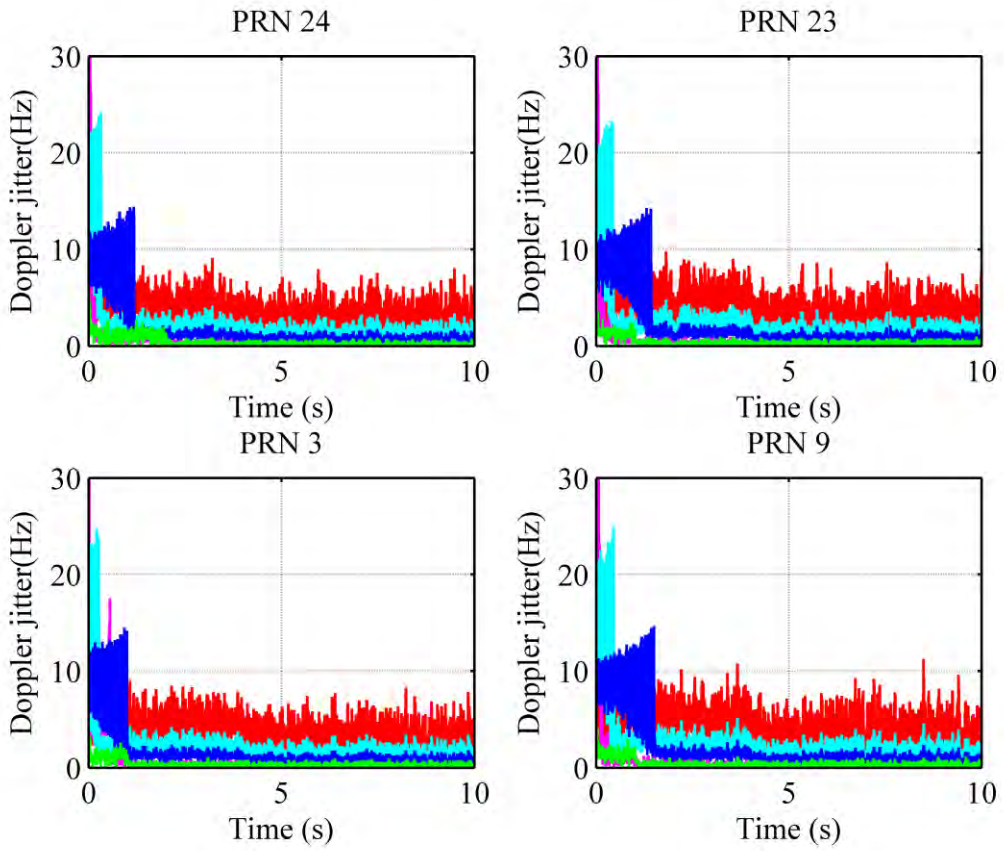

Legend: **PLL 14 Hz** – **KF** – **PLL/FLL 4/3 Hz** – **PLL 4 Hz** - **FFPLL**

Figure 4-8: Doppler standard deviation calculated continuously using a 10 ms moving window

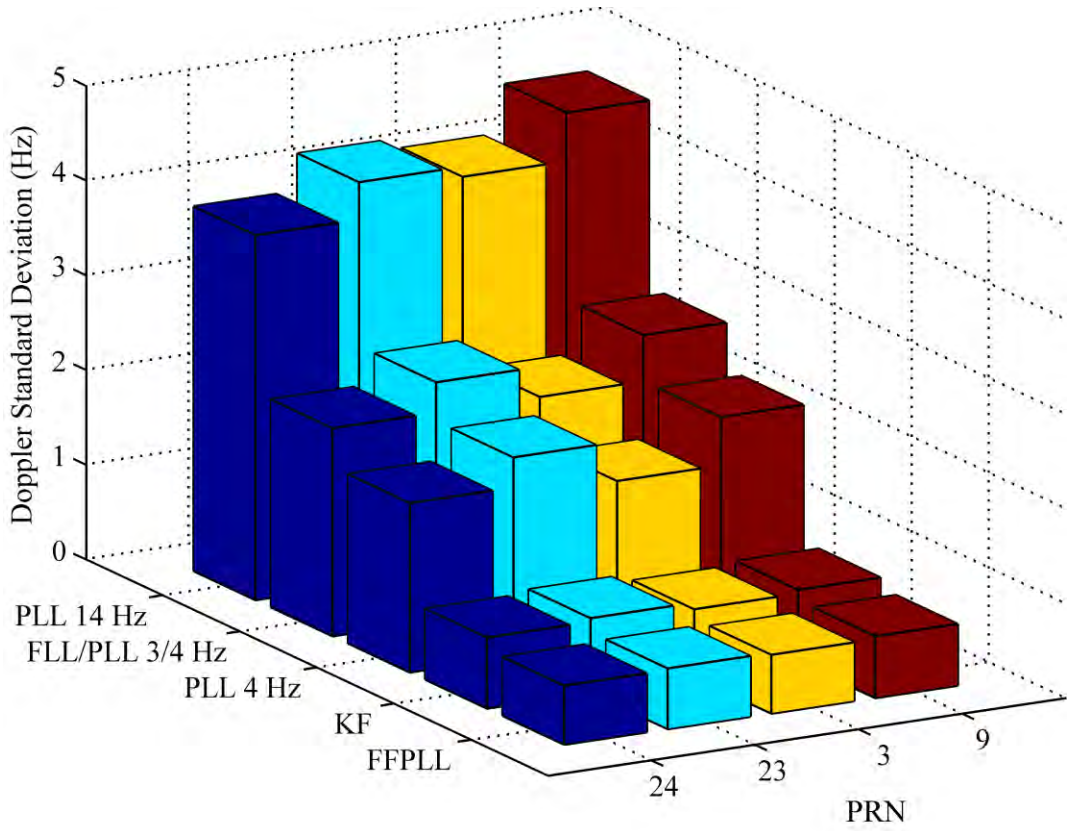

Figure 4-9: Average Doppler standard deviation for five tracking schemes for the four considered satellites

4.2.3 Interference Effect on Tracking Accuracy

The second test category involves studying the effect of interference on GPS signal tracking capability and accuracy. For this reason custom designed scenarios using a static GPS receiver with gradually increasing the interference level have been investigated. The interference signal generator, connected to the Spirent GSS7700 GPS hardware simulator, is capable of generating different types of interference. The performance of carrier tracking depends on the signal quality at the output of each correlator and hence

the output of the discriminators in the receiver. Usually, the GPS receiver is able to minimize the effects of wide band interference defined previously in Chapter 1 thanks to the code correlation procedure utilized in this type of communication systems (Parkinson & Spilker 1996). However, a wide band jammer generating an interference signal with the same modulation frequency or with a duplicated PRN code could result in a spoofer, which is usually taken care of using specific techniques in military applications. These techniques are outside the scope of this research. On the other hand, narrow band interference can seriously affect the signal tracking operation and reduce the effective C/N_0 below the tracking threshold (Phocas et al 2004). For these reasons, generated interference signal is chosen to be a narrow band interference signal with different powers, particularly ranging from 10 dB to 60 dB higher than the GPS signal power. Three types of narrow band interference signals are generated and used for the assessment:

1. CW interference centered at the GPS L1 carrier frequency,
2. Swept CW sweeping from L1-2 MHz to L1+2 MHz,
3. Sinusoidal FM modulation interference (FMI) centered at the GPS L1 carrier frequency.

For comparison purposes, the same satellite configuration is applied to all tests. The tracking performance test is applied to all satellites in view. However, only the results of one of them, namely PRN 23, are chosen because its signal power is high enough to sustain tracking at a higher interference level due to its location in the sky as it can be seen in Figure 4-10. Though, it has to be stated that the tracking performance of the rest

of the satellites is comparable. Figure 4-10 shows the sky plot of the satellites in view during for this experiment.

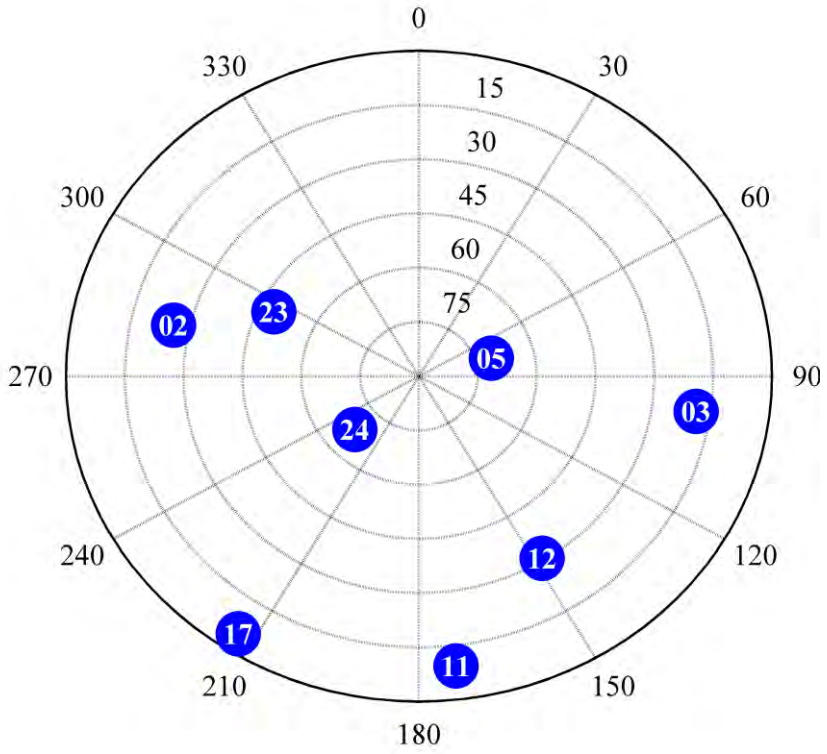

Figure 4-10: Sky plot of the GPS satellites in view during experiment

The interference signal is combined with the generated GPS L1 signal and collected by an NI front-end for post processing. Figure 4-11 shows the increasing interference effect on the signal quality, particularly the signal C/N_0 where N_0 is referring to the Gaussian noise plus interference in this case. C/N_0 is estimated during FFPLL tracking and computed from the correlator outputs using a Narrow-Band/ Wide-Band power estimator (Dierendonck 1996). The jamming to signal (J/S) interference power is gradually increased every 10 seconds in steps of 10 dB, each starting from 0 dB higher than the GPS L1 power or in other words starting being equal to GPS L1 power.

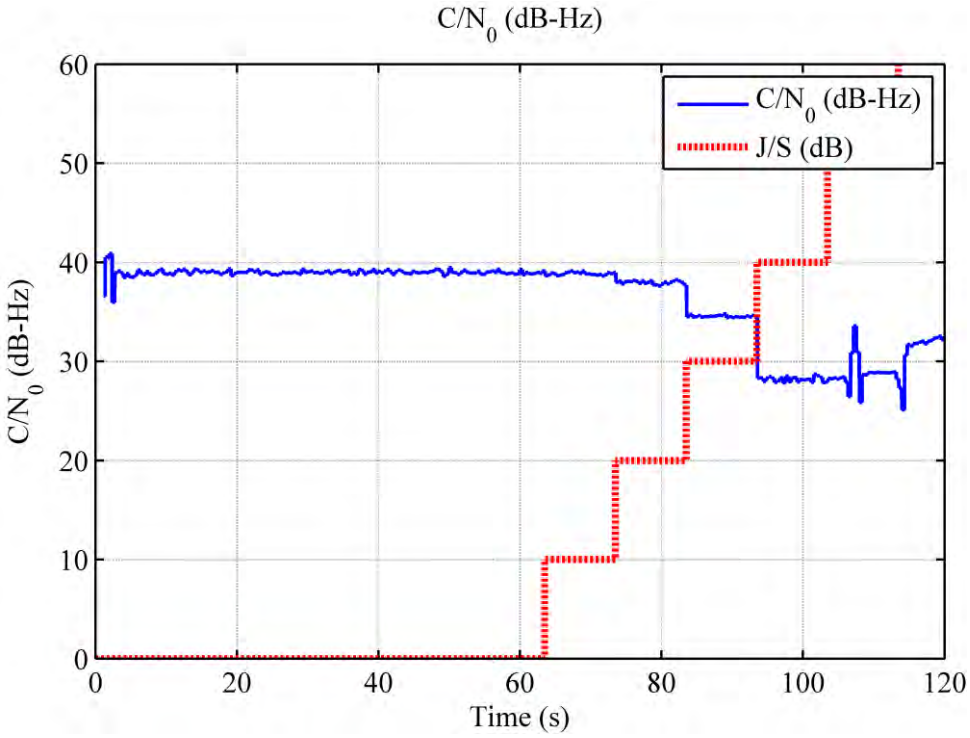

Figure 4-11: Effect of increasing J/S on C/N_0 level changes for PRN 23

After reaching an interference power of about 40 dB higher than the GPS power, none of the tracking algorithms is able to track the signal and hence 40 dB is considered the maximum jamming tracking threshold, which is consistent with the results obtained in (Lewis 2003) . Lower elevation satellites lose lock at lower interference levels. This is noticed for PRN 11 and PRN 17 as they have lost lock at J/S = 30 dB. The changes in the C/N_0 level due to the increasing interference level affect the discriminators output standard deviation and hence the standard deviation of the corresponding fuzzy MF is changed accordingly as depicted in Figure 4-12.

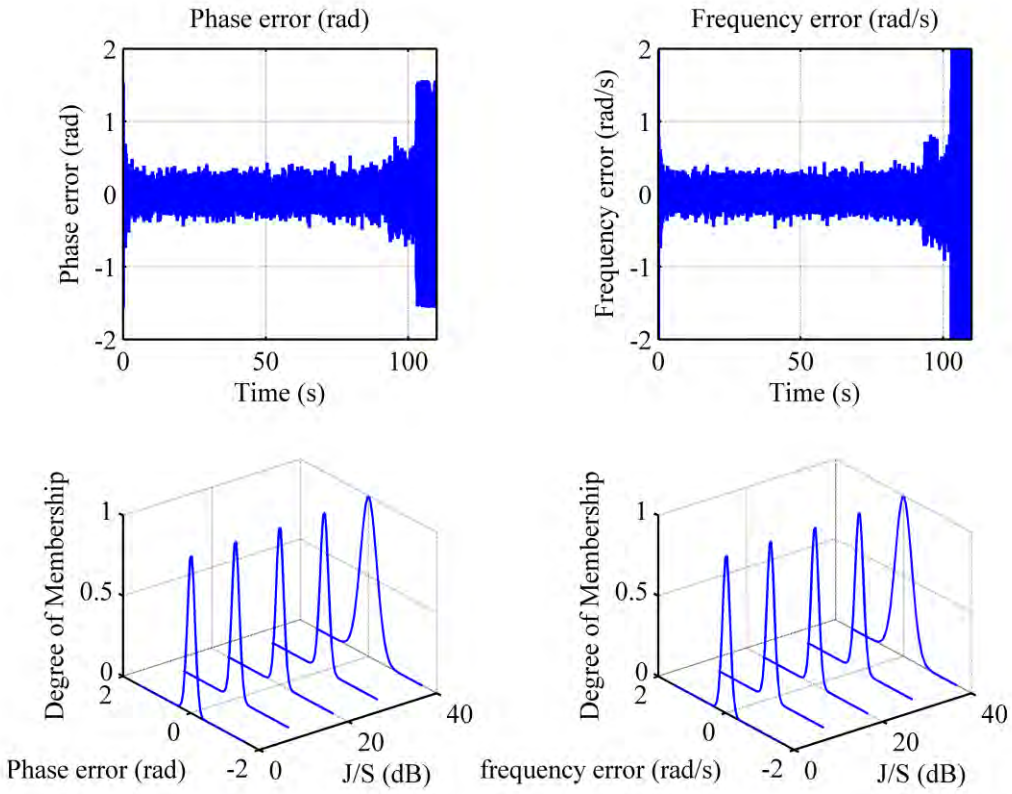

Figure 4-12: PD and FD outputs and the corresponding zero mean Gaussian MF

Figure 4-13 shows the estimated Doppler average standard deviations for PRN 23 using the five tracking schemes described earlier at different interference levels during CWI. It can be observed that the FFPLL scheme is superior to the other tracking schemes in terms of Doppler tracking jitter and hence tracking accuracy. The changes in C/N_0 level due to the increasing interference level affect the discriminators output noise level as described in Chapter 2 and hence the estimated Doppler noise. These effects are clearly visible in Figure 4-13. On the contrary, these changes are almost absorbed by the adaptive FFPLL, and hence the C/N_0 changes have a minimum effect on its estimated Doppler noise.

Figure 4-14 and Figure 4-15 show the estimated Doppler average standard deviation for PRN 23 using the five tracking schemes during SCWI and FMI, respectively. It can be seen that the same superior performance of FFPLL can be achieved during SCWI and FMI.

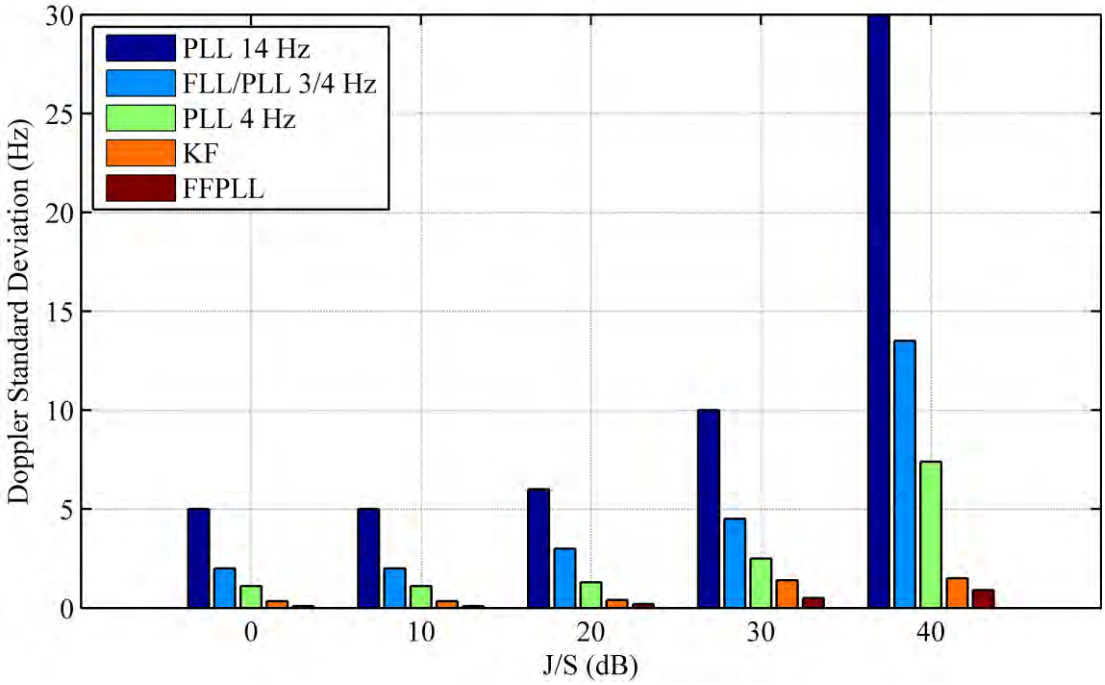

Figure 4-13: Doppler average standard deviations calculated for PRN 23 using five tracking configurations during CWI

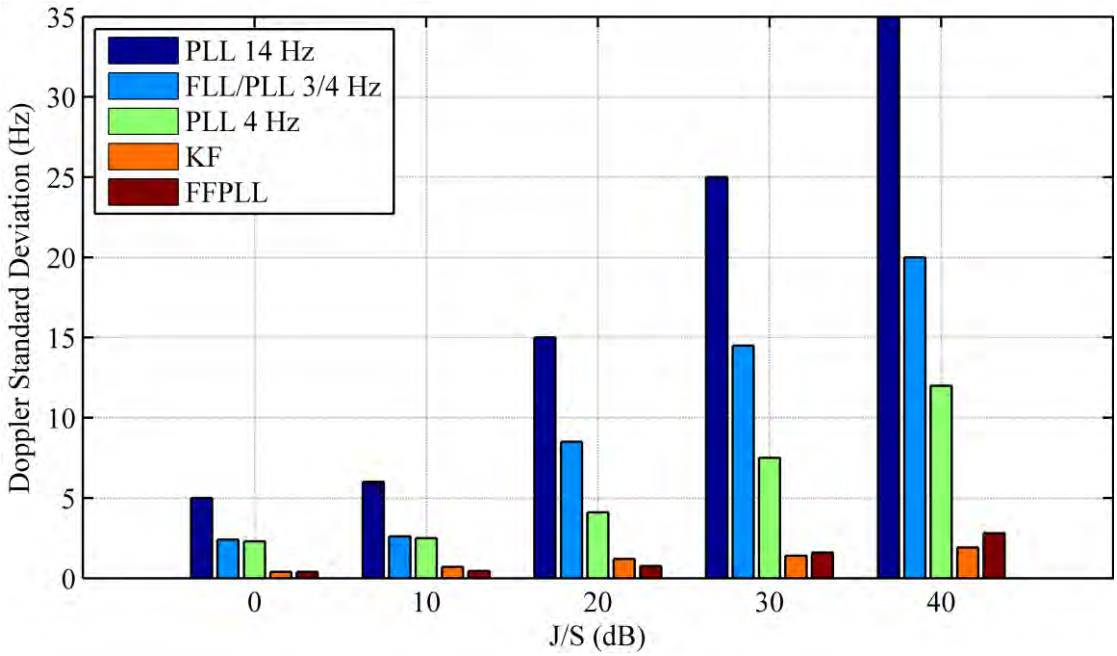

Figure 4-14: Doppler average standard deviations calculated for PRN 23 using five tracking configurations during SCWI

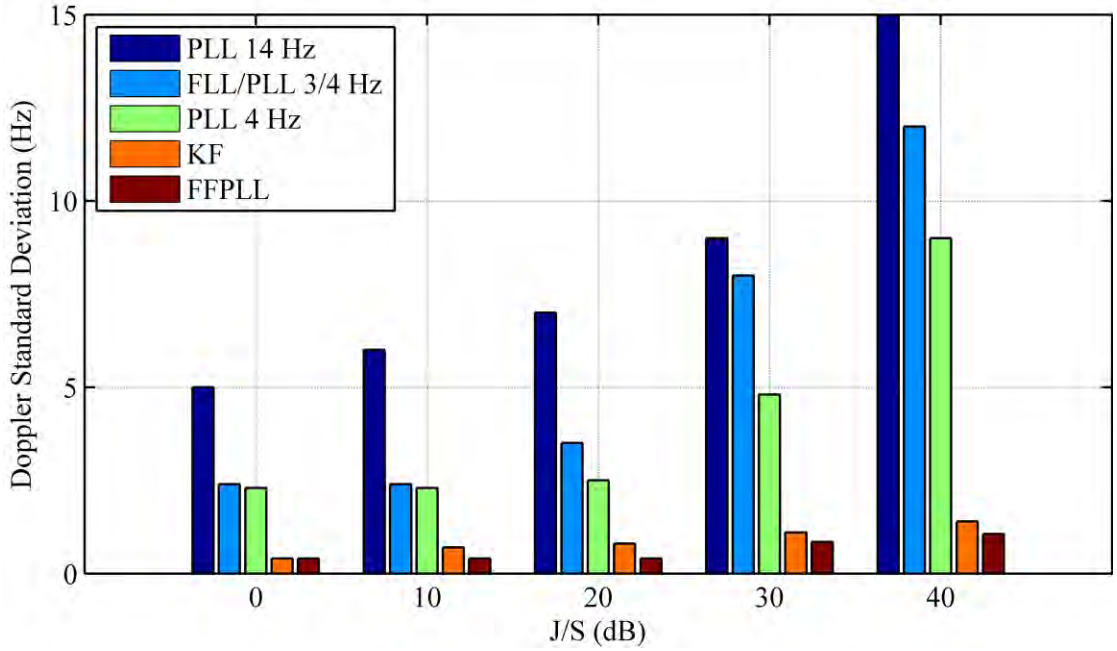

Figure 4-15: Doppler average standard deviation calculated for PRN 23 using five tracking configurations during FM interference

Phase tracking performance is also investigated using a PLI as described previously. Figure 4-16 shows the PLI calculated for PRN 23 using the five tracking algorithms during CWI scenario. It can be seen that the FFPLL gives a comparable performance to KF and a 14 Hz bandwidth PLL at low J/S levels. At the same time, at high levels of J/S, FFPLL gives a better phase tracking performance comparable to narrow bandwidth PLL.

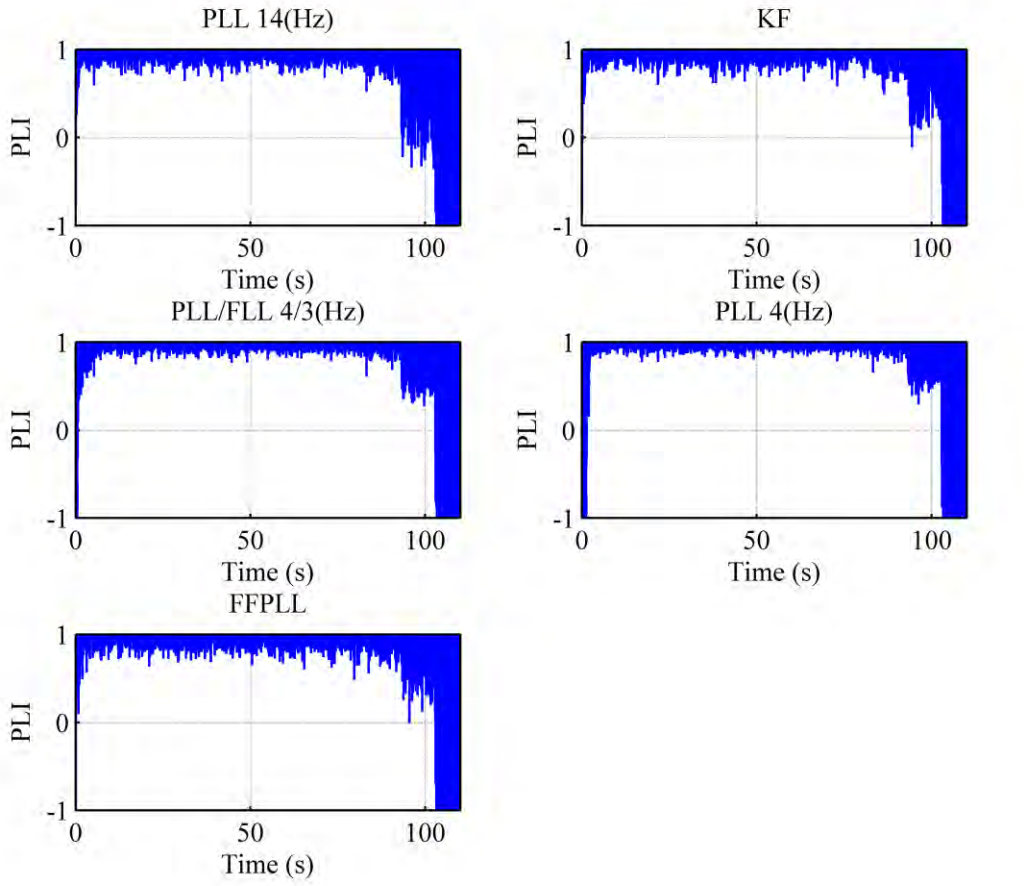

Figure 4-16: Phase Lock Indicator calculated for the five tracking algorithms used for PRN 23

4.3 Combined Interference and High Dynamics Scenarios

The third test category assesses the system performance under CW interference and high dynamics. The scenario considered here comprises the effect of missile manoeuvres near an interference source. During this manoeuvre, the GPS signal C/N_0 changes with the distance from the interference source. The missile velocity in this scenario is increased to reach 300 m/s, performing hard manoeuvres with acceleration up to 8 g and jerks up to 50 g/s. The dynamic profile of this scenario is illustrated in Figure **4-17**.

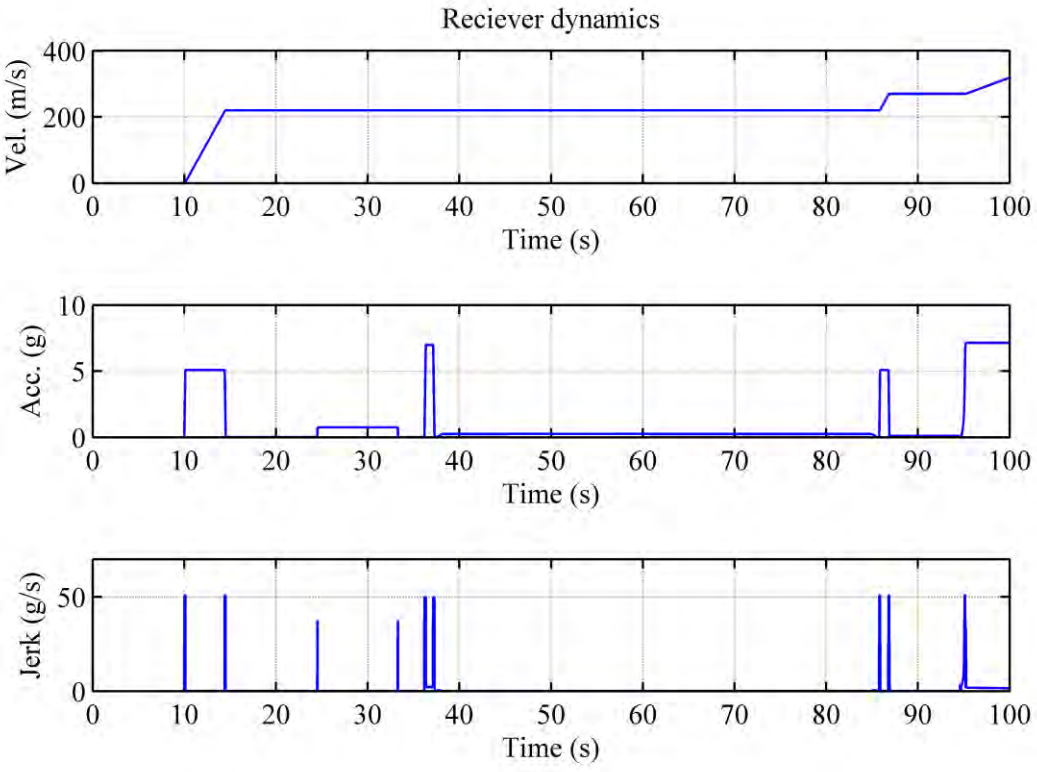

Figure 4-17: Receiver dynamics profile

The same scenario is repeated five times with different CW interference powers. Due to missile high dynamics, narrow bandwidth PLL or FLL-assisted-PLL was not able to provide continuous signal tracking and loss of lock occurred, which is consistent with the results obtained in Section 4.2.2. For this reason, only a 14 Hz bandwidth PLL, KF and FFPLL are considered for further analysis. The interference powers generated are 20, 30, 40, 45 and 50 dB, respectively, above normal GPS signal power.

Figure **4-18** shows the 3D plot of the missile's trajectory and its manoeuvres near the jammer, while Figure **4-19** shows the effect of these manoeuvres on the signal C/N_0 for PRN 3 when a 40 dB interference signal is applied. C/N_0 increases and decreases according to the separation from the interference source.

Tracking results show the ability of continuous tracking under interference level up to 40 dB higher than the GPS signal for both PLL 14 Hz and FFPLL. Higher levels of interference lead to tracking loss. FFPLL is able to recover tracking mode and retrieve the signal phase when interference effects are reduced due to missile manoeuvres around the jamming source whereas the wideband PLL nor KF are not able to retrieve back the signal phase in these high dynamics conditions. This conclusion is elaborated in more details in the next chapter.

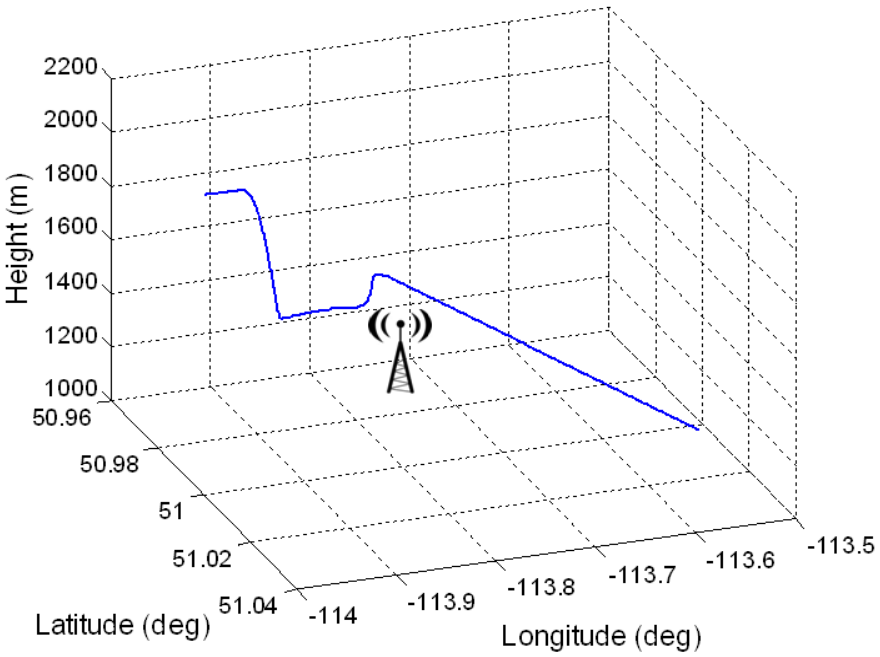

Figure 4-18: 3D plot of the missile manoeuvres near an interference source

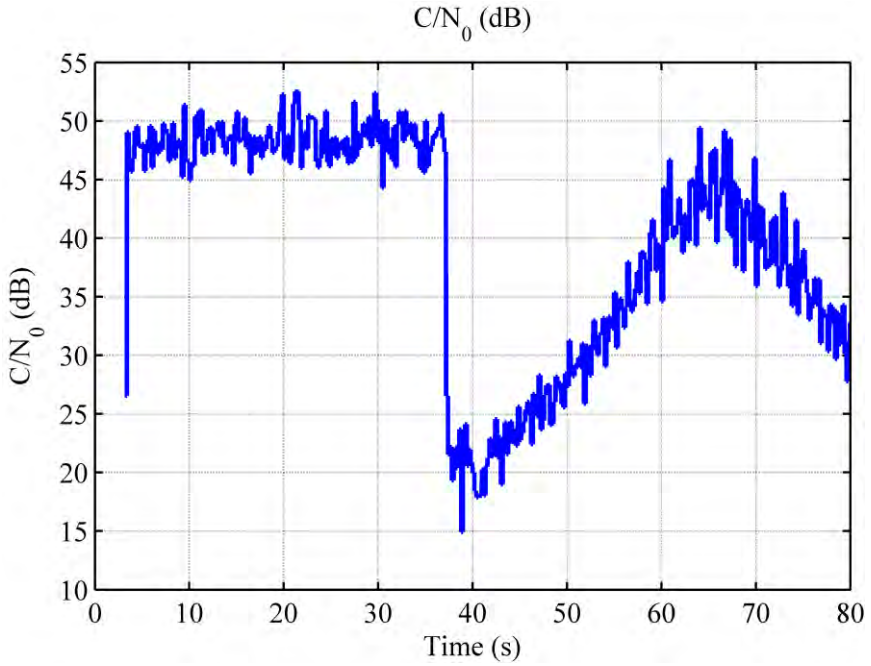

Figure 4-19: C/N_0 evaluated as a function of time for PRN 3 during manoeuvres around an interference source

Figure **4-20** and Figure **4-21** show the effect of adding a 40 dB interference signal on PRN 3 estimated Doppler and Doppler standard deviations respectively, using PLL 14 Hz, KF and FFPLL. Tracking continuity is achieved using the three algorithms but interference signal greatly affects PLL tracking accuracy whereas comparable and much better accuracies are obtained using KF and FFPLL in both interference and interference free conditions.

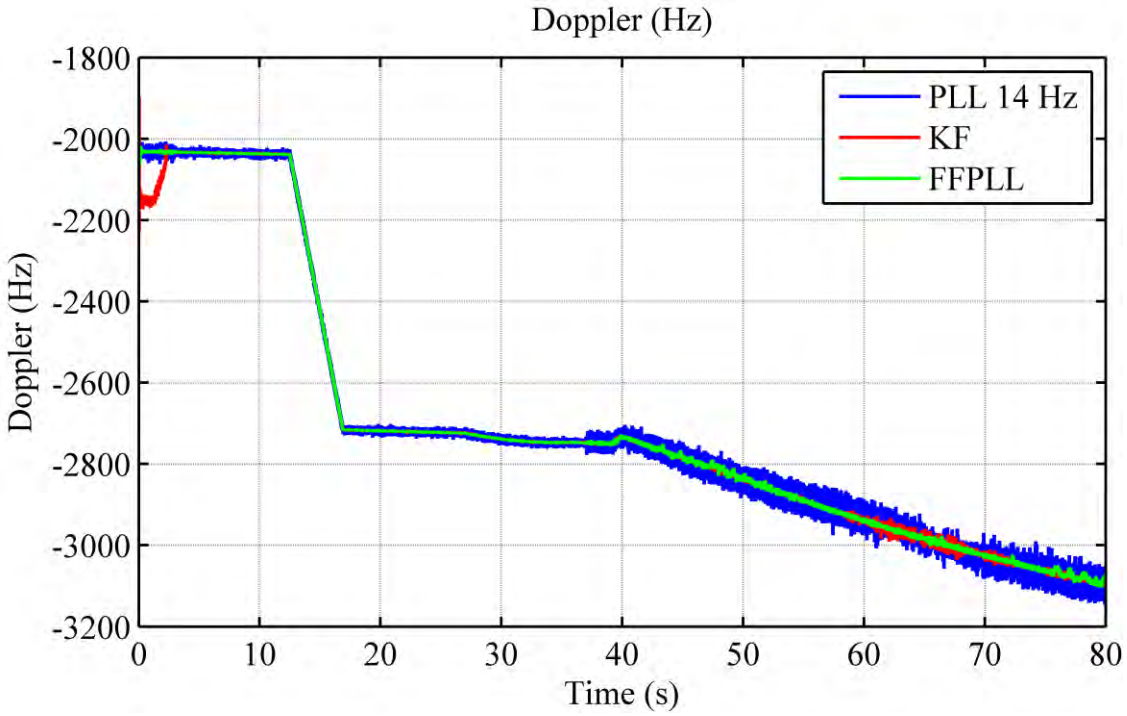

Figure 4-20: Estimated Doppler calculated for PRN 3 using KF, PLL 14 Hz and FFPLL at J/S = 40 dB

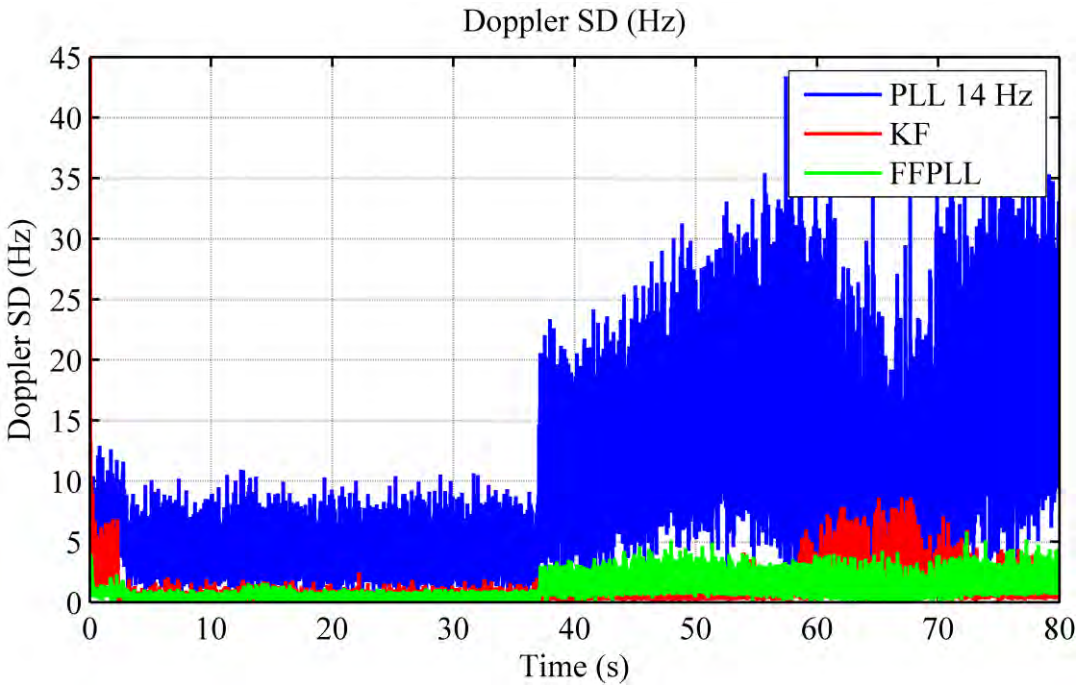

Figure 4-21: Estimated Doppler standard deviations calculated for PRN 3 using KF, PLL 14 Hz and FFPLL at J/S = 40 dB

4.4 Effect of Predetection Integration Time on Tracking Robustness and Continuity

This section discusses another important parameter that affects the tracking robustness and accuracy. This parameter is the PIT, which has contradicting effects regarding the ability of tracking high dynamics and the measurement accuracy as will be seen in the following subsections.

4.4.1 Effect of Integration Time on Estimated Doppler Jitter

FFPLL output is dependent on the PD and FD outputs, which are strongly related to the signal C/N_0 and PIT, as detailed before in Chapter 2. Increasing the PIT will reduce the

PD output noise standard deviation, which will in turn enhance the estimated Doppler quality. FFPLL is designed to have an adaptive input membership function distribution. This adaptation is originally initiated to mitigate the interference effect on the tracking quality but it also deals with the variations in discriminator outputs due to PIT changes. The tracking quality is assessed by the amount of noise measured on the estimated Doppler.

To study the effect of changing PIT on the estimated Doppler quality as theoretically mentioned before in Chapter 2, the GPS signal is collected and sampled in a static scenario. The collected signal is post-processed using standard PLL with a BW = 18 Hz and FFPLL. The estimated Doppler noise standard deviation is calculated and compared to the theoretical values calculated at the same C/N_0. Consistency of the results is achieved, as it can be observed in Figure **4-22**. In this figure, it can be seen that by increasing PIT from 1 ms to 10 ms, the noise is reduced by around 90%.

FFPLL also is used to track the collected signal using different PITs and the estimated Doppler standard deviation is calculated and depicted in Figure **4-23**. Two main advantages were found. The first one is that the estimated Doppler standard deviation is much less than the one calculated using standard PLL at the same PIT which was noticed during the preceding experiments. The second benefit is the tracking quality enhancement in Doppler estimation gained by increasing PIT from 4 ms to 10 ms. In this case, the Doppler noise is reduced by around 40%, which can be compared to 85% reduction in the case of the standard PLL. This means that by using small PIT values with FFPLL,

approximately the same noise level can be reached as if large PIT values are used. Consequently a larger dynamic margin with this small PIT is achieved.

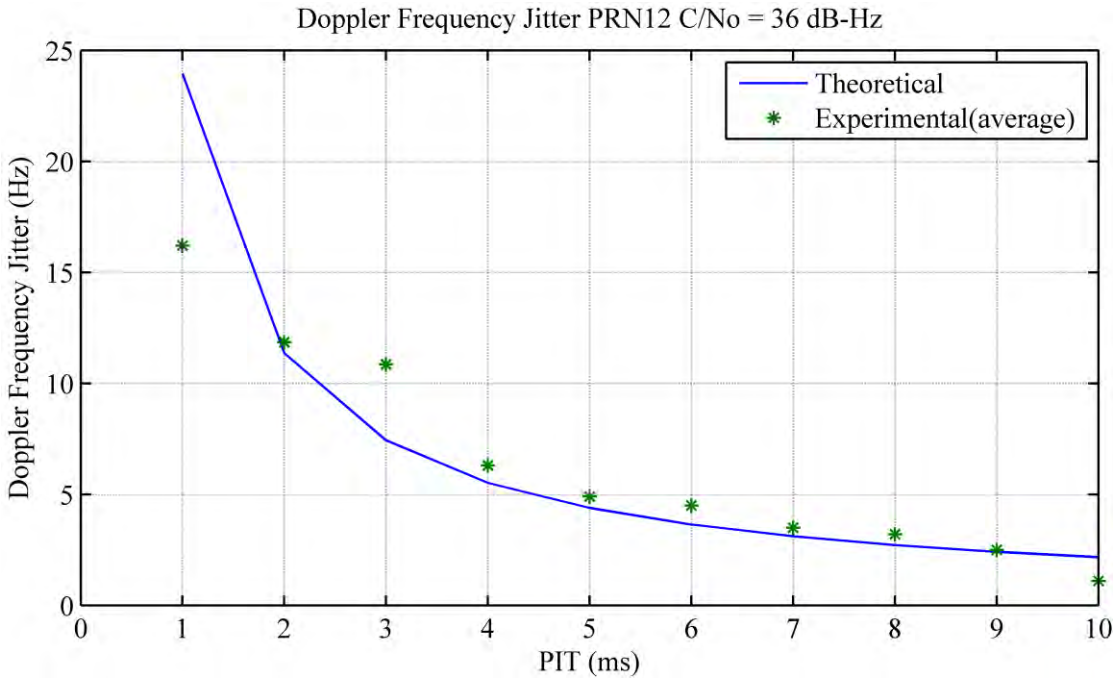

Figure 4-22: Doppler frequency jitter calculated for different integration times using PLL with BW = 18 Hz

For illustration purposes, the estimated Doppler of PRN 12 at different PITs using a FFPLL is shown in Figure **4-24**, and a comparison between the estimated Doppler of PRN 12 while increasing PITs up to 4 ms using PLL 18 Hz and FFPLL is shown in Figure **4-25**.

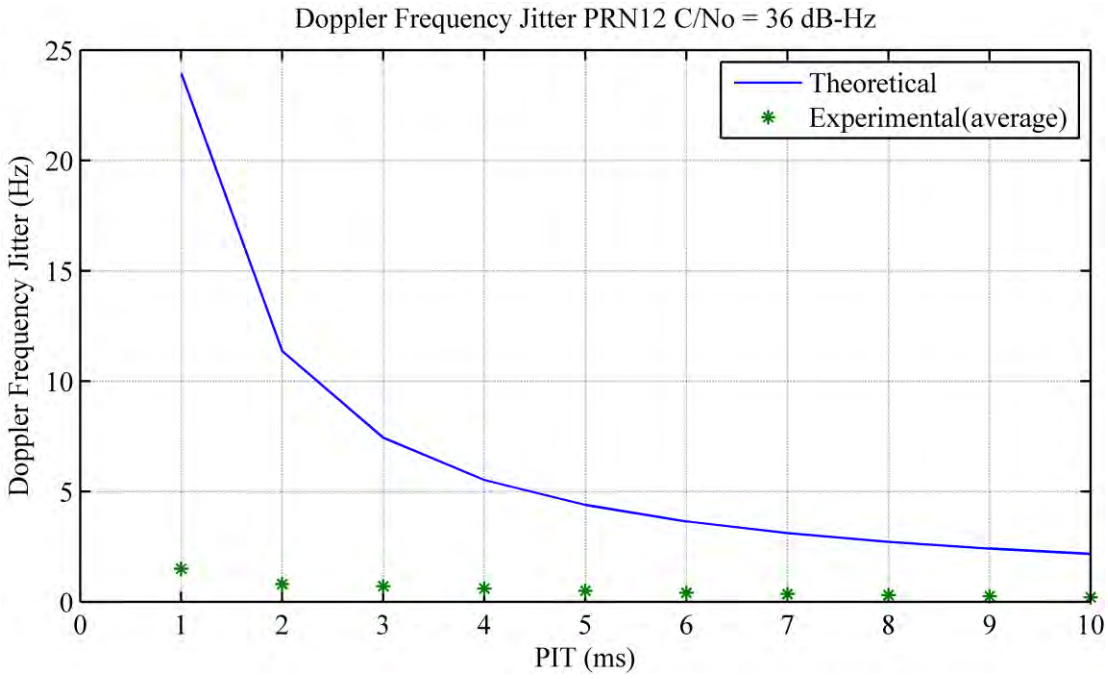

Figure 4-23: Doppler frequency jitter calculated for different integration times using FFPLL

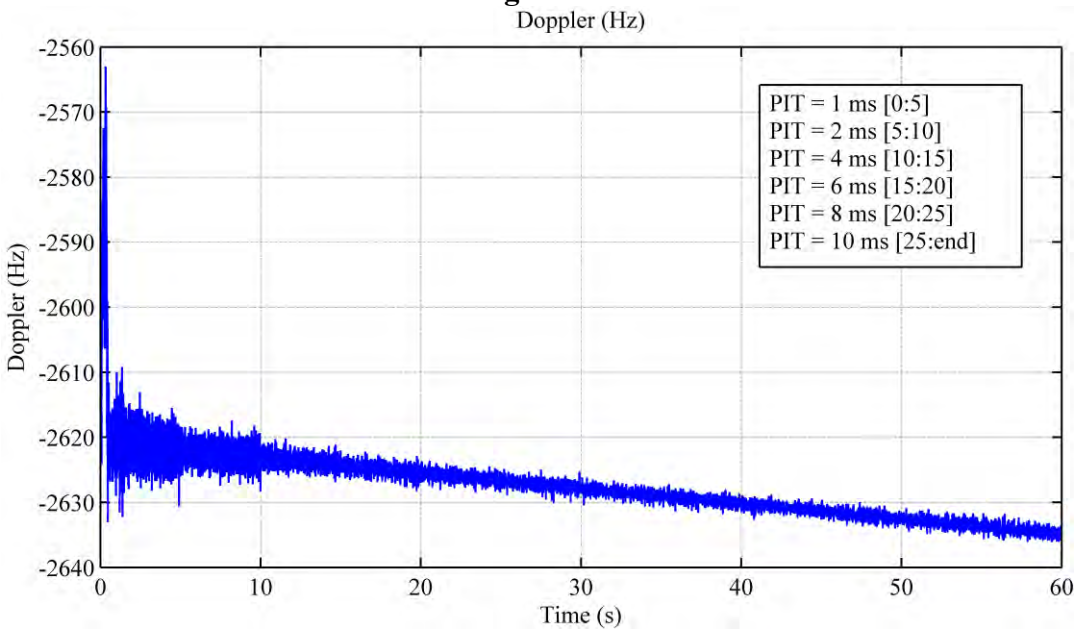

Figure 4-24: FFPLL Doppler calculated for PRN 12 using different integration times

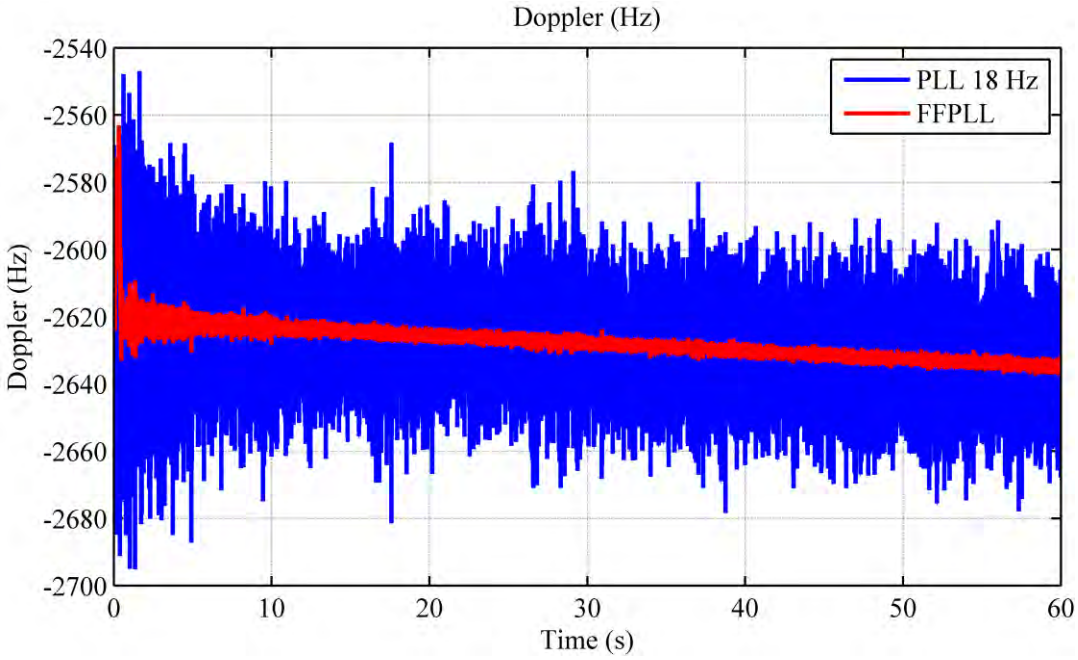

Figure 4-25: Doppler calculated for PRN 12 using PLL 18 Hz and FFPLL at gradually increasing integration times up to 4 ms after 15 s

4.4.2 Effect of Integration Time on Dynamic Robustness

Dynamic robustness in this context is the ability of the tracking loop to maintain tracking under different dynamic conditions and to retrieve it without going back to the acquisition stage if the loss is due to external effects such as signal interference or temporary outages. The SPIRENT GS7700 hardware simulator is used to simulate some scenarios with missile manoeuvres. The selected scenario corresponds to a manoeuvring missile that performs increasing level of normal accelerations. The missile speed is increased up to 200 m/s with a 2 g's linear acceleration, then followed by six turns, performing 3, 5, 7, 9, 13 and 15 g's of normal acceleration sequentially. Figure **4-26**

illustrates the 2D missile trajectory while Figure **4-27** shows the missile velocities, accelerations and jerks respectively.

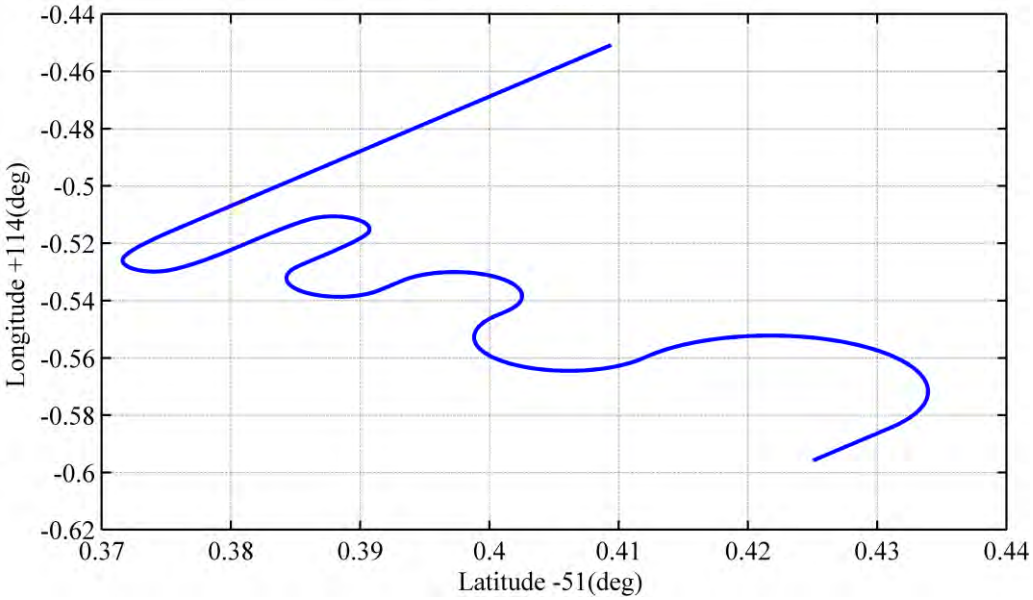

Figure 4-26: Missile manoeuvring trajectory

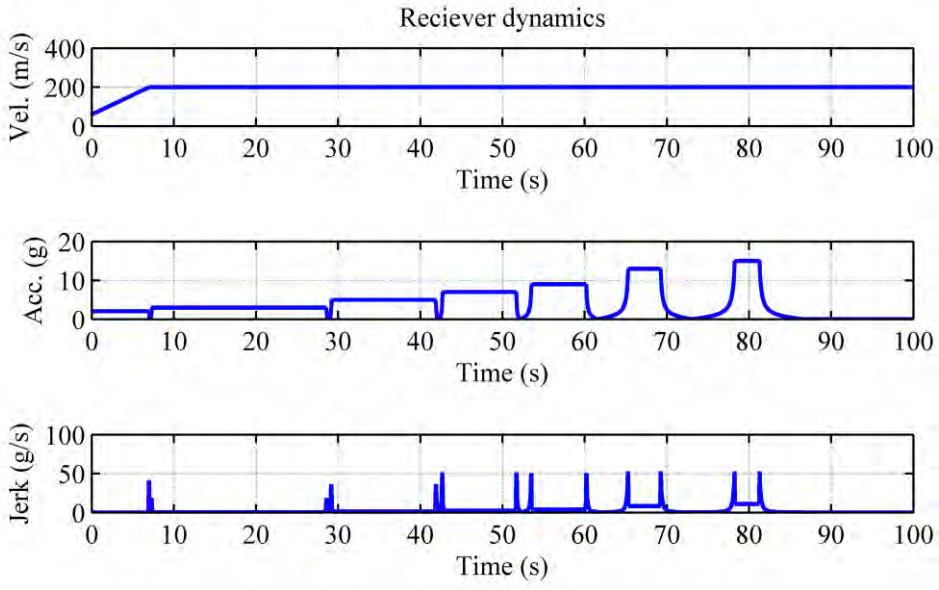

Figure 4-27: Missile dynamics profile

The collected signal is processed using FFPLL and standard PLL with different bandwidths and PITs. A standard PLL with minimum bandwidth of 10 Hz and PIT of 1 ms is empirically found to be sufficient to provide continuous signal tracking through the whole scenario. While increasing the PIT to 5 ms with the same bandwidth, signal tracking gets lost at the 13 g's manoeuvre. In addition, phase tracking is temporary lost at lower acceleration levels. FFPLL tracking provided continuous signal tracking at the same PIT with a smaller noise level than the corresponding standard PLL. Figure 4-28 shows the estimated Doppler calculated for PRN 23 using a PLL with a BW = 10 Hz and PIT = 1, 5 ms, respectively, and a FFPLL with PIT = 5 ms. Previous results can easily be observed.

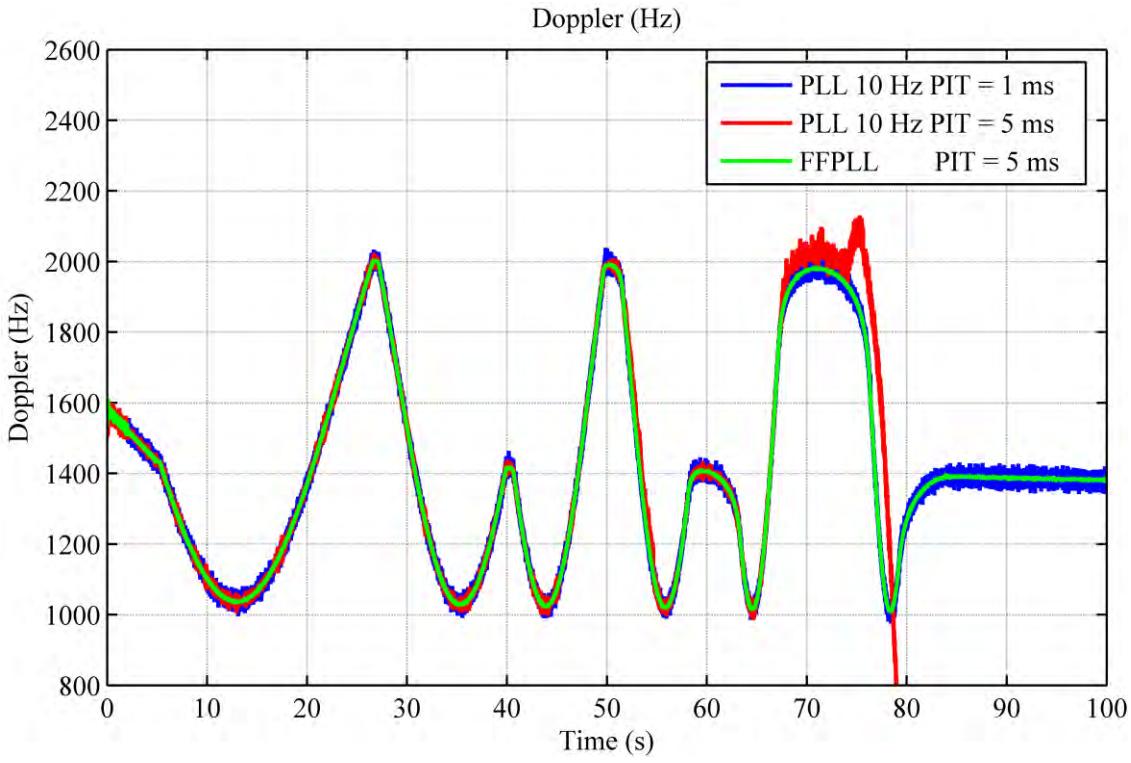

Figure 4-28: Doppler calculated for PRN 23 using PLL with BW = 10 Hz and PIT = 1 and 5 ms and FFPLL with PIT = 5 ms

4.5 Pull-in Frequency Calculation

All modern GPS receivers use a multi-hypothesis search over Doppler and code delay. Different to code search done by correlation, a Doppler search allows for lower resolution search by using wider frequency steps. Hence, Doppler frequency is acquired with a significant frequency error. The pull-in frequency is the maximum allowed frequency error (MAFE) for the carrier tracking loop to start successful tracking or in other words, it is the maximum frequency difference between the local oscillator and the reference frequency of the carrier tracking loop over which the local oscillator can be locked. With standard PLLs or FLLs, the pull-in range is affected by the PIT and the MAFE sensed by the discriminator used. The pull-in range and time are also related to the loop filter parameters such as loop transfer function natural frequency (Razavi 1996) and hence to the filter bandwidth as seen previously in Chapter 2. As the effective bandwidth is narrowed, the pull-in range becomes smaller and the pull-in time becomes larger (Antonio 2011). If the local replica of the signal is too far off from the desired frequency, lock will not occur. Frequency uncertainty during signal acquisition is bounded by the maximum Doppler frequency due to satellite and receiver motions plus/minus the incoming GPS signal frequency. During acquisition, this range is divided into frequency bins and the test for signal existence is applied for each bin. The smaller the frequency bin, the more effective the acquired signal is. If the pull-in frequency range is wide, a larger error in the estimated incoming frequency is allowed and hence wider frequency bins, which ensures faster acquisition.

To empirically calculate the pull-in frequency, a frequency error was intentionally added to the acquired frequency. This frequency error is increased in small steps until tracking is not possible. This experiment is applied to the acquired signal to test the previously described five tracking algorithms and results are recorded. Results for PRN 24 are shown below.

Using a circular correlation technique and Doppler bin size equals to 500 Hz with a 20 ms non-coherent integration, the incoming signal frequency is estimated with an error within the used bin size. Figure 4-29 shows the 3D plot of acquisition results in the frequency and code domains using an intermediate frequency of 0.42 MHz for PRN 24. In this case, the estimated Doppler is 828 Hz, which corresponds to an error of about 40 Hz from the reference Doppler specified by the simulator.

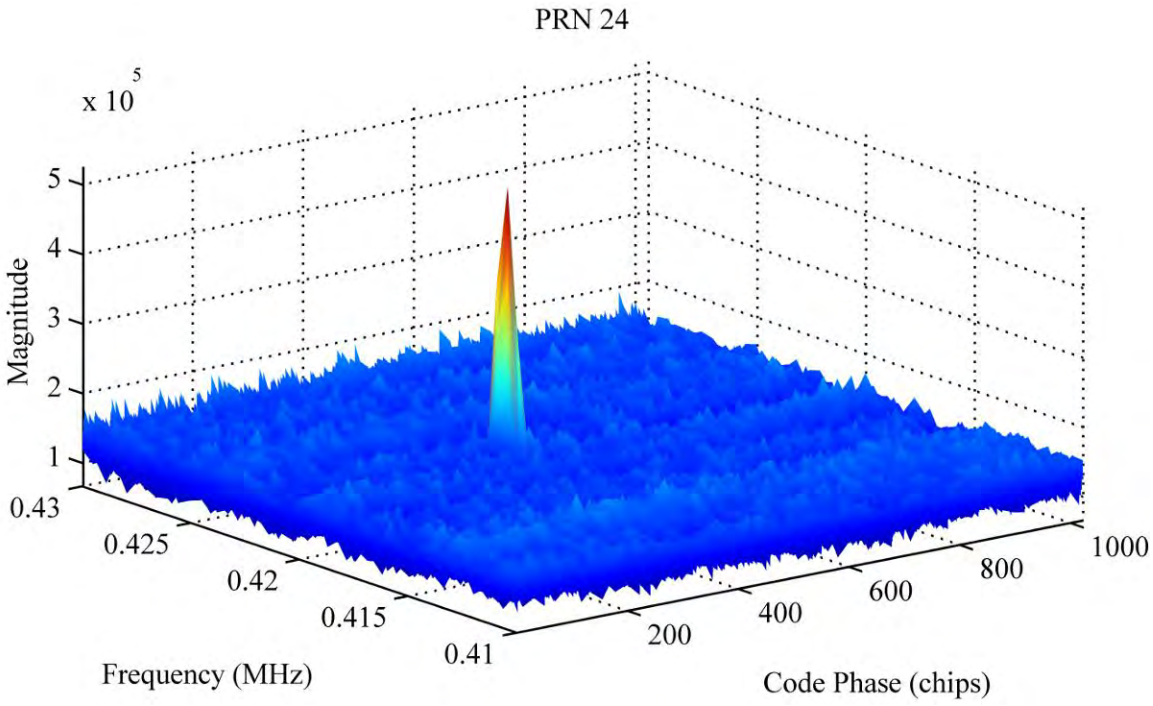

Figure 4-29: PRN 24 acquisition results

By intentionally increasing the acquired frequency error and applying signal tracking using the five tracking algorithms, three parameters are observed:

1. maximum allowed frequency error (MAFE),
2. Doppler convergence time starting from MAFE,
3. phase convergence time starting from MAFE.

Globally the FFPLL results show superior performance for all three parameters. KF almost provides the same MAFE but with longer convergence times. Wide and narrow bandwidth PLLs and FLL-assisted-PLLs give a lower performance level according to their bandwidths. Figure 4-30 shows six seconds of PRN 24 estimated Doppler tracking starting from the MAFE of each algorithm used. It can be seen that the FFPLL provides the widest frequency error range in addition to the fastest convergence time.

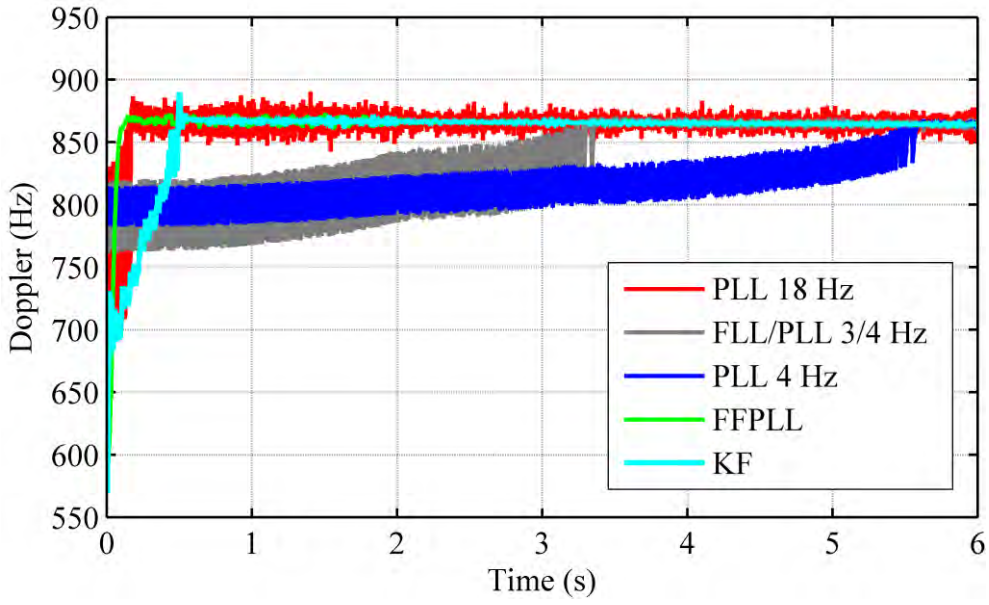

Figure 4-30: Estimated Doppler for PRN 24 starting from the maximum pull in frequency error for different tracking schemes

The 250 Hz pull-in frequency range calculated for KF and FFPLL as seen in Figure 4-31 corresponds to the maximum frequency error sensed by the ATAN2 frequency discriminator presented in Chapter 2 with PIT= 2 ms (Kaplan & Hegarty 2006). The resulting average MAFEs and convergence times calculated for eight visible satellites are depicted in Figure 4-31.

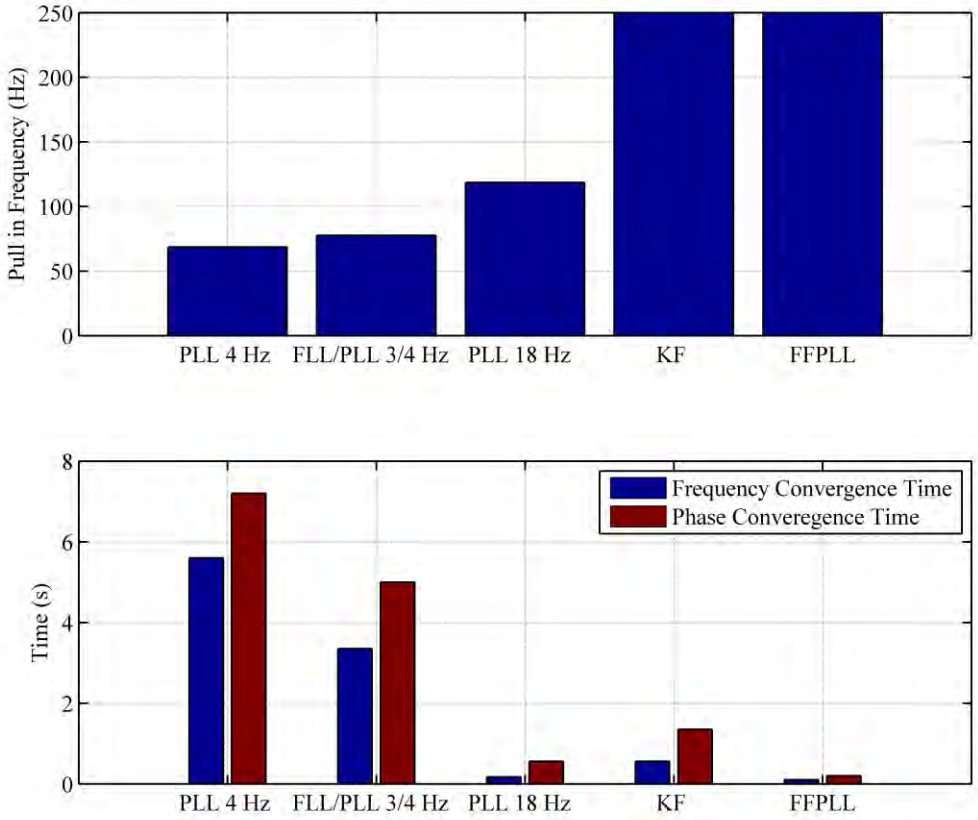

Figure 4-31: *up:* Pull in frequency – *down:* frequency and phase convergence time

4.6 Summary

In this chapter the fuzzy tracking system has been tested and compared to other tracking techniques. The new system solves the contradiction between receiver bandwidth requirements using classical tracking techniques for either noise reduction or dynamics tracking. It shows better performance in both cases since it performs as a narrow bandwidth tracking system in term of noise reduction, and a wide bandwidth tracking system in term of dynamic response.

Using a GPS hardware simulator, numerous scenarios were generated involving missile high dynamic motion in addition to signal interference at different levels. Four points of assessment were taken into consideration while evaluating the new system tracking performance. These points are tracking continuity, noise reduction, immunity against interference and signal tracking recovery. The proposed fuzzy tracking algorithm FFPLL provided tracking robustness in the presence of very high dynamics and signal interference up to 40 dB higher than the GPS L1 power. In addition, the noise level calculated from the estimated Doppler was very small, which is equivalent to results obtained using a very narrow PLL bandwidth under normal conditions. During high dynamics, tracking continuity was achieved using FFPLL whose dynamic performance is comparable to the performance of a wide band PLL or KF. Also signal tracking recovery was achieved if the interference power, which is causing signal tracking denial, was reduced or turned off. Effect of integration time on the dynamic performance and noise level was also discussed. FFPLL test results showed that such a loop can sustain a higher

level of dynamics at longer integration times while providing a superior noise level cancellation at shorter integration times. An intermediate value of 4 ms integration time was empirically found to be the optimum integration time value for a robust and less noisy performance.

The pull-in frequency range has been also calculated for FFPLL and compared with other tracking techniques. A wider pull-in range associated with fastest convergence time was achieved using the FFPLL.

Chapter Five: Design and Testing of an INS Assisted FFPLL

Through the assessment of Fuzzy Logic based phase/frequency lock loops algorithms conducted in the previous chapter, better performance in terms of dynamic robustness and associated Doppler noise as compared with a standard PLL and KF have been observed. However it could be further improved using onboard inertial navigation signals that are commonly available in missiles or aircraft. Fuzzy control systems have been used for many years in the context of inertial control systems used in missile autopilots. A novel aspect is to use the combined Inertial/ Fuzzy systems for GPS robust signal tracking. Therefore, a novel inertial assisted Fuzzy logic based Frequency Lock Loop has been developed and is presented herein.

5.1 INS Assisted FFPLL Design

Inertial sensors are usually used for navigation and guidance purposes for military vehicles such as missiles. They are usually used to provide aiding to GPS navigation and help to bridge its outages.

As has been seen in Chapter 4, using the designed FFPLL for GPS signal tracking requires the triggering of 81 fuzzy rules in parallel. This number of parallel operations can be considered a large computational load especially when real time signal tracking is required. Taking advantage of the existence of inertial sensors, a real benefit can be taken by using inertial aiding to reduce the fuzzy computational load as shown in this chapter.

5.1.1 Calculating INS Doppler

Coupling GPS and INS signals provides a good solution for improving guidance of high-rate manoeuvring platforms. The concept links GPS and INS to allow aiding. Aiding as it was previously shown in Chapter 1 can be performed in several ways. GPS can be used to periodically update the INS to establish minimum bias errors. The INS can improve tracking and reacquisition time by providing a reference signal to the GPS receiver tracking loops. GPS and inertial signals are usually coupled using Kalman filtering techniques to fuse navigation information and handle short GPS outages, signal interferences or intentional jamming (Farrell 2008). The levels of performance achieved depend on the grade of the IMU and satellite visibility. They are driven by the required accuracy or missile-target miss-distance. Although IMU quality is less important for many ultra-tight integration cases (LI et al 2010b), it is still important for missile applications where GPS jamming is very likely to happen. In addition, its cost is insignificant as compared to that of the missile cost. Coupling becomes necessary on missile systems and projectiles in order to mitigate the effects of extreme dynamics, rapidly changing GPS visibility and jamming.

Based on different data fusion strategies, GPS/INS integrated systems can be classified into three types as mentioned before in Chapter 1 (Groves 2008):

1. loosely coupled GPS/INS,
2. tightly coupled GPS/INS and
3. ultra-tight GPS/INS integration.

As the main objective of the proposed research is to aid the GPS tracking loop with IMU data, the chosen coupling scheme corresponds to an ultra-tight integration architecture. This combines the GPS signal tracking functions, the IMU data and the integration filter into a single estimation algorithm. In this algorithm, the INS measurements are fed back to the receiver for decreasing GPS signal tracking errors and enhancing the final GPS positioning performance. It can also help in directly pulling back the tracking loop to the tracking mode without passing through an acquisition step if signal lock is lost due to interference or very high dynamics (Li et al 2010a). Referring to Chapter 2, a modified version of the carrier tracking loop using INS Doppler aiding is shown in Figure 5-1.

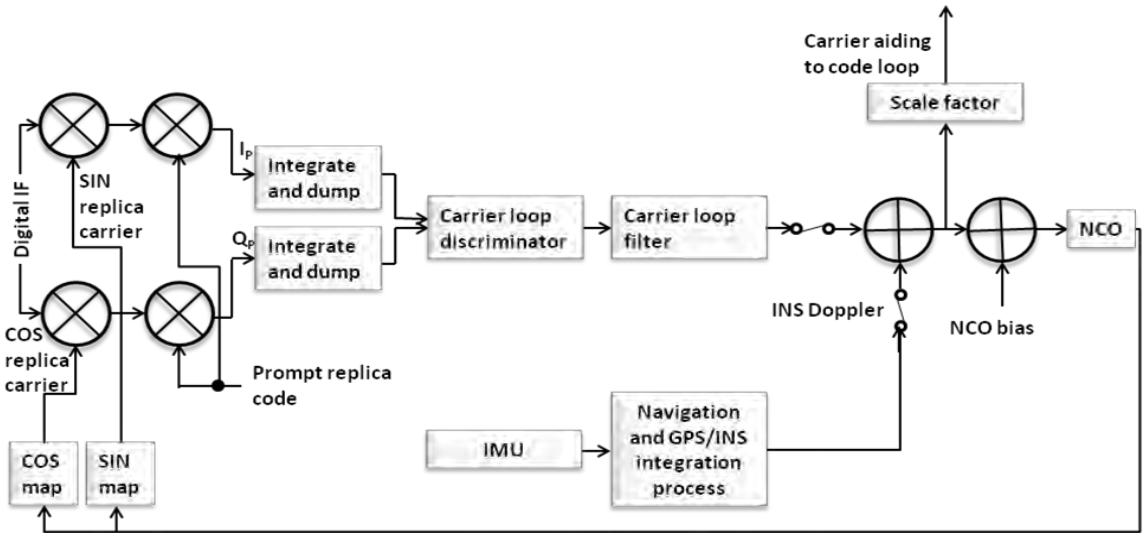

Figure 5-1: Standard carrier tracking loop using INS Doppler aiding

An IMU is comprised of a number of angular rate sensors (gyroscopes) and acceleration sensors (accelerometers). When an IMU is supplied by a navigation processor, it is called an INS. INS for autonomous navigation purposes has been widely used for decades. New technologies made it suitable to replace the huge size of old mechanical sensors with

very small and cheap MEMS. For missile applications, the IMU cost is negligible with regards to the system cost and hence high quality tactical and navigational grade sensors are usually used. Most of the errors accompanied with these types of IMUs measurements such as bias, drift, and scaling factor can be well defined, characterized and mitigated through the navigation processing. However, errors such as thermal noise and clock drift are hardly reduced and can cause large deviations from the correct navigation solution in a very small period of time.

Inertial measurements from gyros and accelerometers are used through a series of integrations, coordinate transformations, and compensations to drive a navigation solution that can be well understood by a navigator on earth and is defined by easting and northing coordinate frames. This process is known in literature as "strap-down mechanization process" and can be illustrated in blocks as shown in Figure 5-2 (Titterton & Weston 2004).

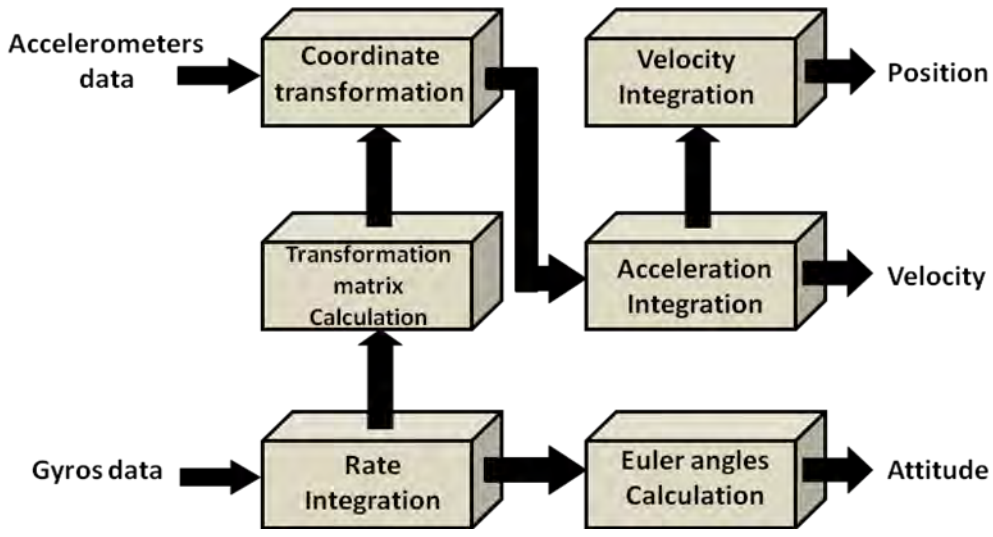

Figure 5-2: Strap-down mechanization blocks

By setting the initial position, IMU measurements can be translated into sequence of positions and velocities estimated upon their previously determined values and that is the definition of a dead reckoning system.

The INS data of interest to assist the tracking loops consists of inertial Doppler. Doppler data is extracted using inertial velocities and the relative positions between the INS and the GPS satellites as shown in the following paragraphs.

Using ephemeris data calculated with the incoming data bits extracted during the signal tracking phase, the satellite positions and velocities are calculated in the Earth-Centered, Earth-Fixed (ECEF) coordinates frame. This information is then combined with the calculated ECEF navigation coordinates using INS only in a strapdown integration scheme to estimate the associated Doppler through the steps described below.

Firstly, the LOS between the kth satellite and the INS processed location is calculated as

$$\begin{aligned} \mathbf{e}_k &= \frac{1}{r_k}\left(\mathbf{x}_{INS} - \mathbf{x}_{s_k}\right) \\ r_k &= \sqrt{\left(\mathbf{x}_{INS} - \mathbf{x}_{s_k}\right)^T \left(\mathbf{x}_{INS} - \mathbf{x}_{s_k}\right)} \end{aligned} \tag{5.1}$$

where r_k is the distance between the kth satellite and the INS coordinates. $\mathbf{e}_k$ is the unit vector of the LOS between the kth satellite and the INS position. $\mathbf{x}_{INS}$ represents the INS coordinates in the ECEF. $\mathbf{x}_{sk}$ represents the kth satellite position in ECEF.

Secondly, the INS Doppler ($f_{d\text{-}INS}$) is derived from Equation (5.1) using

$$\mathrm{f}_{\text{d-INS,k}} = \frac{1}{\lambda_{L1}} \mathbf{e}_k^T \left(\mathbf{v}_{INS} - \mathbf{v}_{s_k}\right) \tag{5.2}$$

where $\mathbf{v}_{INS}$ and $\mathbf{v}_{s_k}$ are the INS velocity and the kth satellite velocity in the ECEF, respectively. λ_{L1} is the GPS L1 frequency wavelength.

Using the INS estimated Doppler, the INS carrier frequency can be easily calculated and used as a reference in the GPS signal tracking loop. FD in this case can be removed and only PD is used for tracking frequency errors and ensuring accurate phase tuning.

5.1.2 Design of Reduced FFPLL Using INS Assistance

The use of INS estimated Doppler reduces the complexity of FFPLL by using only the PD output and the INS Doppler ($f_{d\text{-}INS}$) for tuning the frequency. The INS Doppler is added to the IF frequency (f_{IF}), and then the NCO generated carrier frequency ($f_{c\text{-}NCO}$) is subtracted from it. The resulting frequency corresponds to a frequency correction signal ($\Delta f_{correction}$) that is used to adjust the NCO tuning frequency (Δf). Therefore only nine fuzzy rules corresponding to the phase input, instead of the 81 in FFPLL original design, are used for the input fuzzy sets. The complete INS assisted FFPLL is shown in Figure 5-3.

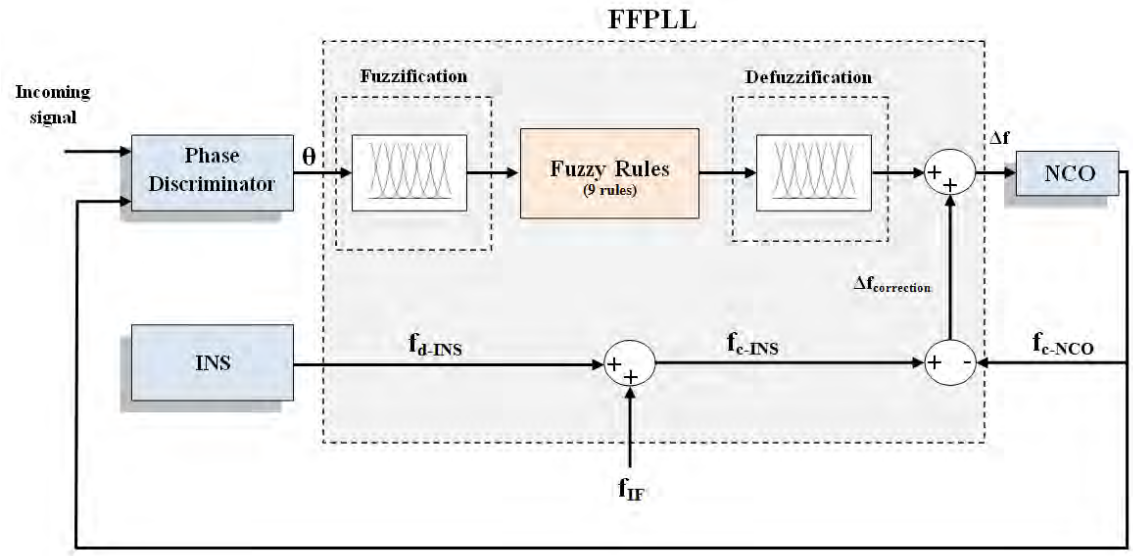

Figure 5-3: INS assisted FFPLL

5.2 Test Description

The main test to assess the proposed INS-assisted FFPLL was conducted using real GPS signals, which were processed with real IMU data processing and a GPS jammer. However, because it is very hard to conduct a test that includes missile level dynamics to be consistent with the scope of the research, simulated GPS and IMU signals are first used with high dynamics to assess the validity of the proposed algorithm.

5.2.1 Simulator Tests

The proposed algorithm was first tested using the previously described GPS hardware simulator. The simulator is capable of providing IMU like measurements with a controllable output rate and perfectly synchronized with the GPS RF signals. According

to the type of application adopted in this work, the tactical grade Litton LN-200 IMU has been simulated and used. The error characteristics of this IMU are shown in Table 5-1.

Table 5-1: Error characteristics of Litton LN-200 IMU

1-σ Error Sources	Gyro bias	Gyro scale factor	Gyro mis-alignment	Gyro g-drift	Gyro g2-drift	Gyro random walk	Accel. bias	Accel. scale factor	Accel. mis-alignment	Accel. random walk
Units	deg/hr	ppm	mrad	deg/hr/g	deg/hr/g2	deg/√hr	mg	ppm	mrad	m/s/√hr
	0.35	100	0.1	0.5	0.05	0.07	0.05	300	0.1	0.03

Although it is proposed to perform a complete GPS/INS ultra-tight integration, RF signal processing is developed up to the level of signal tracking and solving the navigation data bits to obtain the GPS time for synchronization purposes. IMU simulated measurements are processed to calculate the INS solution through the strap-down mechanization process shown in Figure 5-2. To get close to the ultra-tight integration objective, the IMU and GPS simulated data are tightly integrated through an extended Kalman filter (EKF) (El-Sheimy 2007) to provide a corrected estimate of the INS solution. The corresponding INS Doppler is estimated as per equations (5.1) and (5.2) using the GPS satellite positions and velocities provided by the simulator. As a final step, the calculated INS Doppler is used separately to aid the RF signal tracking process through FFPLL. This approach is clearly illustrated in Figure 5-4 as a modified version of the ultra-tight integration scheme introduced earlier in Chapter 1.

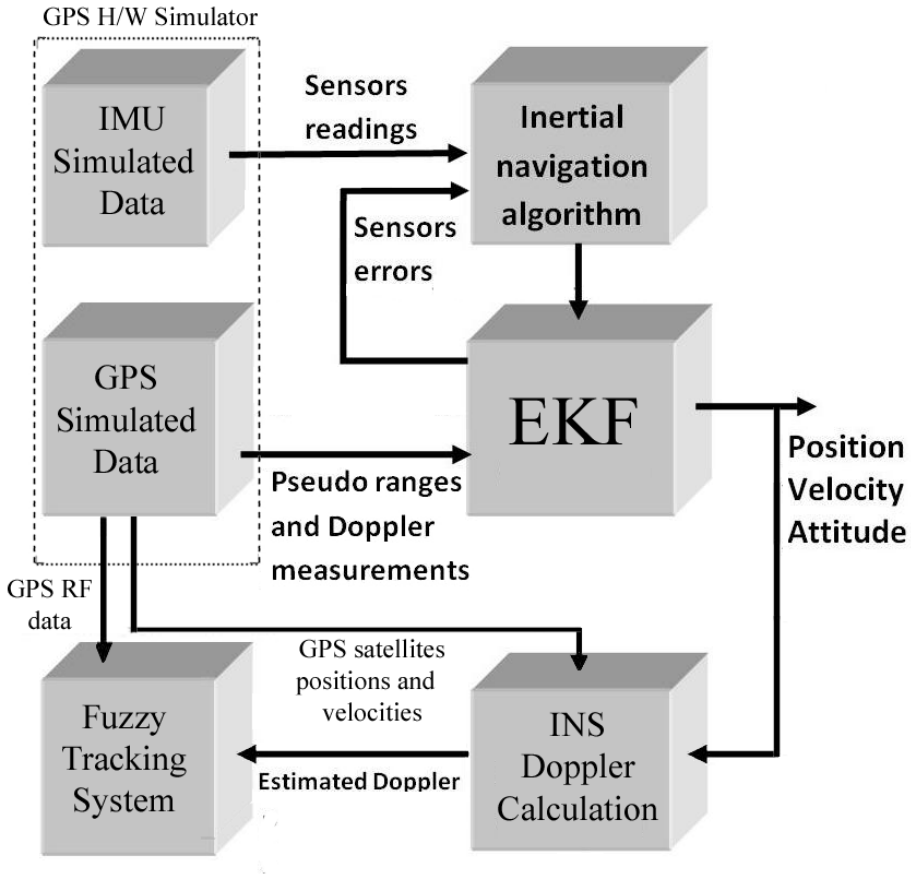

Figure 5-4: Process used to calculate INS Doppler to aid FFPLL

For illustration purposes, the scenario for missile manoeuvre explained in Section 4.3 is used herein. A CW jammer producing J/S = 45 dB of jamming signal is used in this scenario. Estimated C/N_0 changes as the missile performs an evasive manoeuvre to escape this jamming are shown in Figure 5-5. As shown previously in Chapter 4, the FFPLL is capable of maintaining signal lock regardless of the missile dynamics or if low or moderate interference levels are applied. Using very accurate Doppler estimates from a tactical grade IMU will help to provide continuous signal tracking even if a high level of interference is applied. When tracking is switched from FFPLL to INS-assisted-FFPLL,

course frequency tracking is totally dependent on INS provided Doppler and hence, the fuzzy processor is responsible only for frequency fine tuning and for providing phase tracking. Using a one input fuzzy processor reduces its complexity and the number of fuzzy rules processed in parallel. Consequently the computational load gets reduced as will be described later.

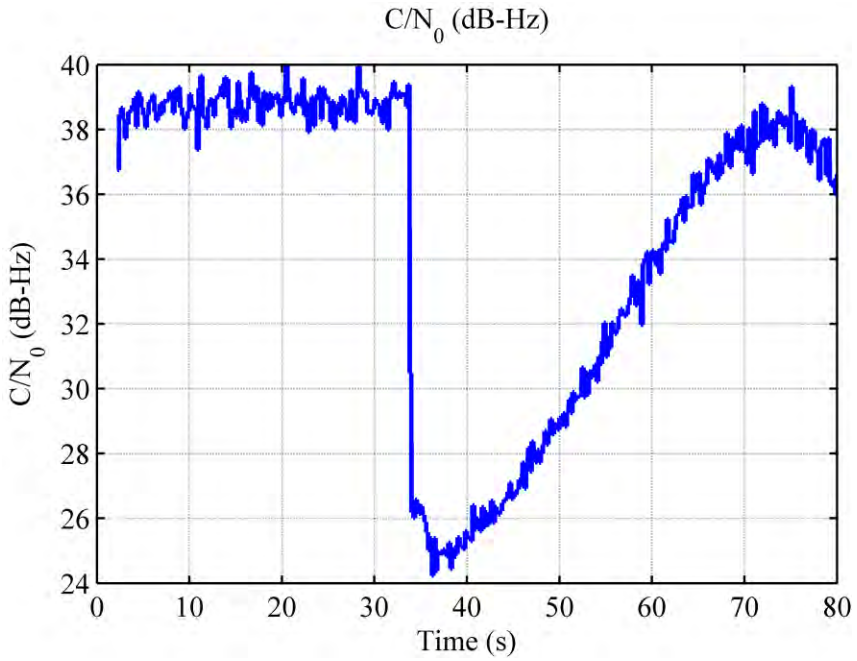

Figure 5-5: C/N_0 estimated for PRN 24 during missile manoeuvres

Figure 5-6 and Figure 5-7 show the estimated Doppler for PRN 24 during the entire scenario's duration and a zoomed version for better illustration, respectively. The Doppler is estimated during signal tracking using KF+INS, FFPLL and FFPLL+INS. Figure 5-8 shows the estimated Doppler standard deviation using the same three algorithms. The same KF design used in Chapter 4 is used here but has been modified to benefit from INS aiding to insure a fair comparison with the INS-assisted FFPLL.

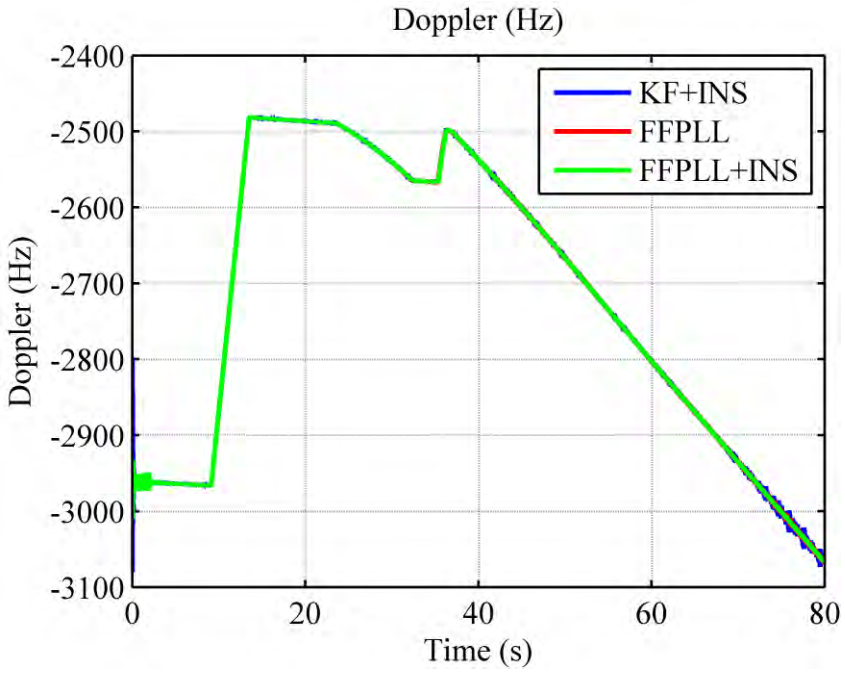

Figure 5-6: Estimated Doppler for PRN 24 using KF+INS, FFPLL and INS+FFPLL

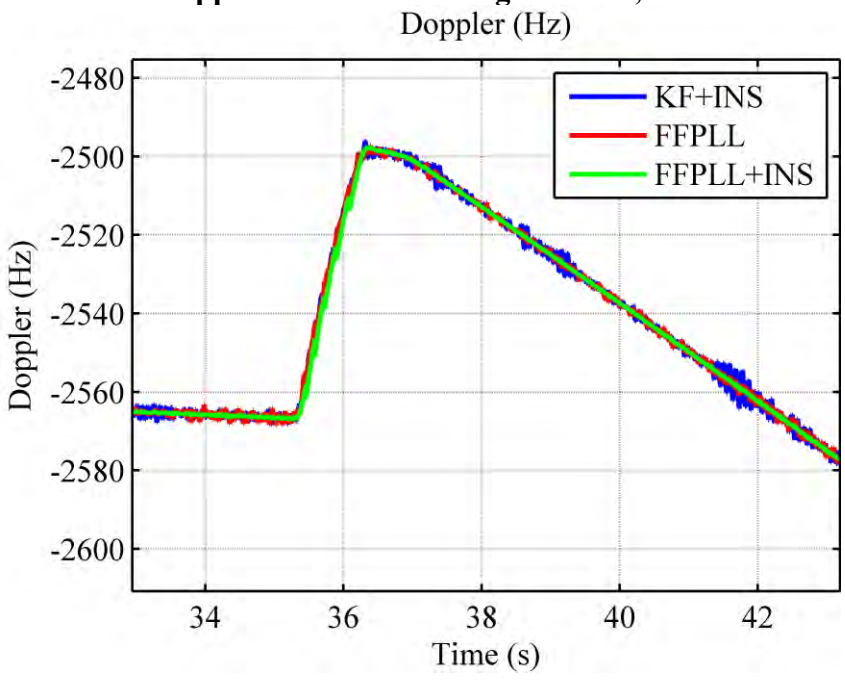

Figure 5-7: Estimated Doppler for PRN 24 using KF+INS, FFPLL and INS+FFPLL (zoom)

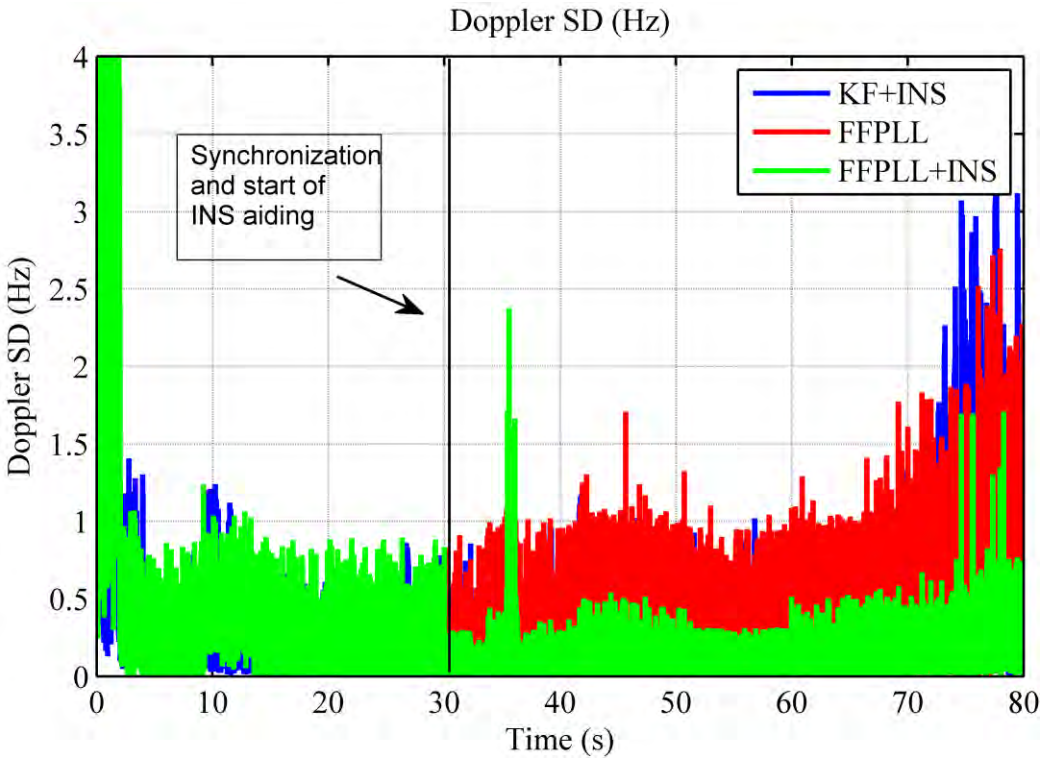

Figure 5-8: Estimated Doppler SD for PRN 24 using KF+INS, FFPLL and INS+FFPLL

From the previous results, it can be seen that the INS-assisted FFPLL algorithm has succeeded to pass the validity test where it is capable of providing continuous tracking during combined incidence of very high dynamics and variable jamming levels. Further more, the estimated Doppler is more accurate than the one estimated using standalone FFPLL, thanks to accurate Doppler estimates from the Litton IMU provided by the simulator. A more and complete assessment of the proposed algorithm is given in the next section where real GPS and IMU signals are used.

5.2.2 Experimental Test Description

In order to test the proposed signal tracking architecture using real GPS and INS data, experimental tests have been conducted in a vehicle. A photo of the testing equipment is shown in Figure 5-9. Testing equipments comprise a GPS antenna and the IMU of the NovAtel SPAN Technology system with a lever arm measured during the experiment. To remain as close as possible to the scope of the research, high dynamics conditions limited by the vehicle capability have been reproduced during the data collection. Logging and control systems were loaded in the vehicle. The complete test setup is illustrated in Figure 5-10.

Rover data was collected with a single antenna using two separate setups. The NovAtel 702 GG antenna was used to collect GPS signals and its output was split between an OEM4 dual frequency GPS receiver, which was connected to a tactical grade IMU (Honeywell HG1700 (Honeywell 2006)), and the National Instruments RF front-end. The front-end was controlled by a PC dedicated to RF samples data logging. The GPS/INS solution was used as a reference for assessing the performance of the INS assisted FFPLL. GPS signals were jammed using a hand-held short range GPS Jammer using a cable connection to the National Instruments RF front-end. The cable connection was used to avoid any possibility of jamming other users. Table 5-2 lists the equipment used for the experiment.

Figure 5-9: GPS antenna mounted on the SUV roof top and IMU with other equipments inside the vehicle

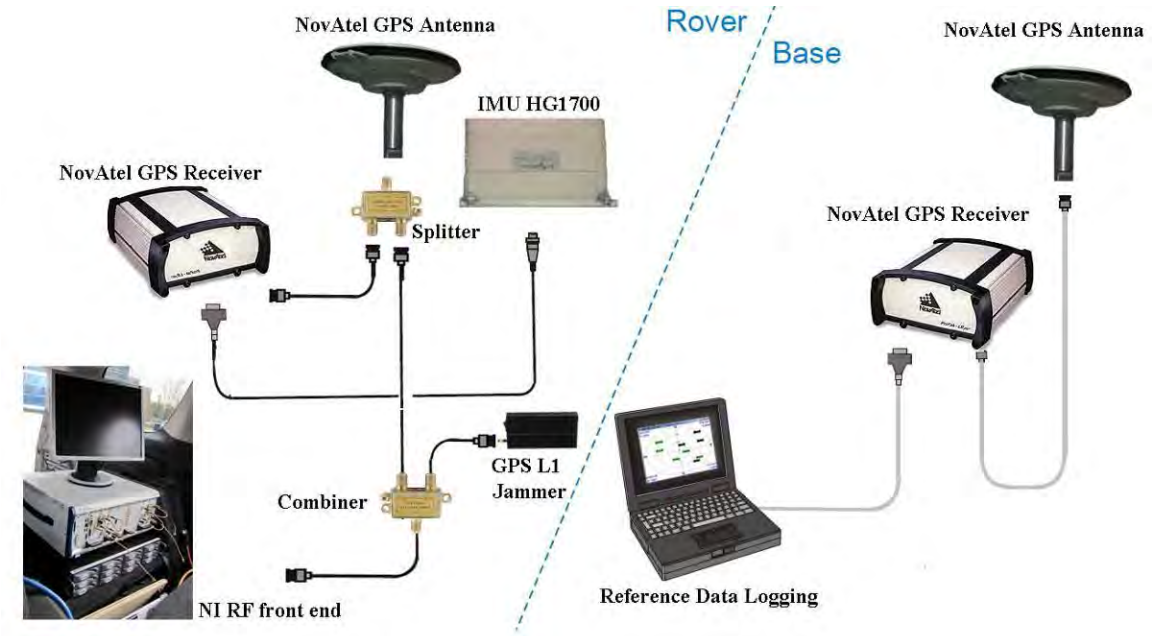

Figure 5-10: Test Setup

Table 5-2: Equipment used for field data collection

Number	Equipment
1	NovAtel GPS receiver (2)
2	IMU Honeywell HG1700
3	National Instruments RF front-end
4	NovAtel GPS antenna (2)
5	Hand-held short range GPS Jammer

5.3 GPS/INS Reference Solution

The IMU of the SPAN system is the Honeywell HG1700 AG58 tactical grade IMU with a 1-degree per hour gyro bias stability. The rest of the IMU system specifications are given in Table 5-3.

Table 5-3: HG1700 IMU system specifications

Output Data Rate	Gyro Input Range	Gyro Rate Scale Factor	Gyro Bias (One Sigma)	Gyro Angular Random Walk	Accel. Range	Accel. Linearity	Accel. Scale Factor	Accel. Bias
100 Hz/ 600 Hz	± 1,000 deg/sec	150 ppm	1 (deg/hr)	0.125 deg/√hr	± 50 g	500 ppm	300 ppm	1.0 mg

INS Doppler values were estimated using post-processed positions and velocities of the rover computed with the off-the-shelf post-processing software Inertial Explorer™ (NovAtel 2011) from Novatel. Tight coupling of GPS dual frequency signals from a stationary base station and a rover receiver with inertial data is performed after solving for initial static GPS/IMU alignment within the software. Furthermore proper stochastic modelling of IMU, i.e. the HG1700 from Honeywell, is set prior to processing. In the tightly coupled approach, only one Kalman filter is used, which enabled filter's update using as little as two satellite measurements. Along the navigation solution, accelerometers bias and gyroscope drift are continuously estimated. The lever arm between the IMU and the GPS rover antenna was surveyed to the centimetre level using a Leica TCR705 reflectorless total station (GlobalSources 2011). The maximum baseline length was about 25 kilometres.

Two approaches have been used for the data post-processing. The first approach is to use differential GPS data with forward and backward smoothing using a Rauch-Tung-Striebel smoother (Jazwinski 1970) to minimize the errors during GNSS outages and to obtain the best possible reference INS solution. Inertial Explorer internal filter accuracy estimation gives mean standard deviations for the position solutions of about 0.01 m with a maximum of 0.01 m, and for the speed about 0.004 m/s with a maximum of 0.005 m/s.

To get as close as possible to the scope of the research where it is very hard to use differential GPS or smoothing in a real time missile application, the INS solution is recalculated through a second approach where only rover GPS data is used in a forward solution using precise point positioning data (PPP). The Inertial Explorer internal filter accuracy estimation for this approach gives mean standard deviations for the position solutions of about 0.17 m with a maximum of 1.16 m and for the speed, about 0.01 m/s with a maximum of 0.09 m/s. The two approaches described above are illustrated in Figure 5-11 and the differences in INS solution estimates for both approaches in terms of position and velocity are shown in Figure 5-12.

As a following step, the INS Doppler is calculated as described earlier and used as an aiding signal for the FFPLL, which is processed separately. An example of INS Doppler difference between the two approaches for PRN 16 is shown in Figure 5-13. The experiment is also described in the stepwise flow diagram shown in Figure 5-14.

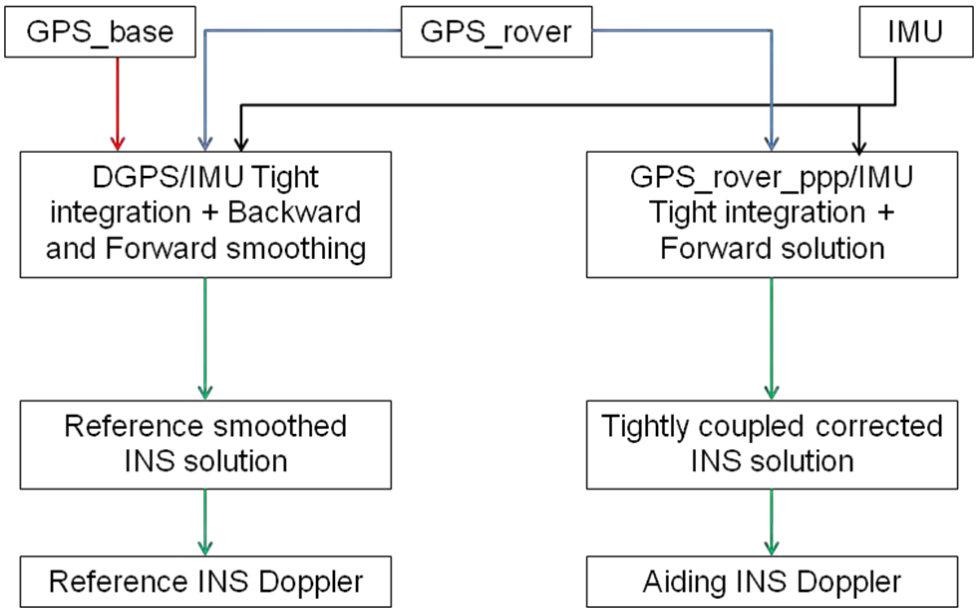

Figure 5-11: Two approaches used to calculate the INS reference and aiding Doppler values

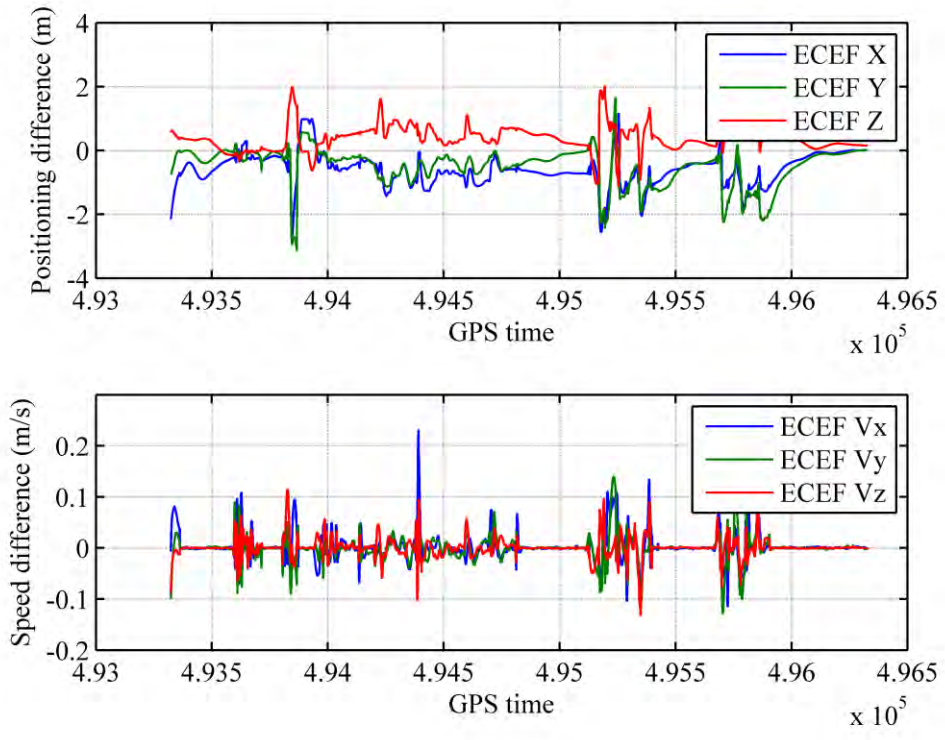

Figure 5-12: Differences between INS solutions using the two approaches

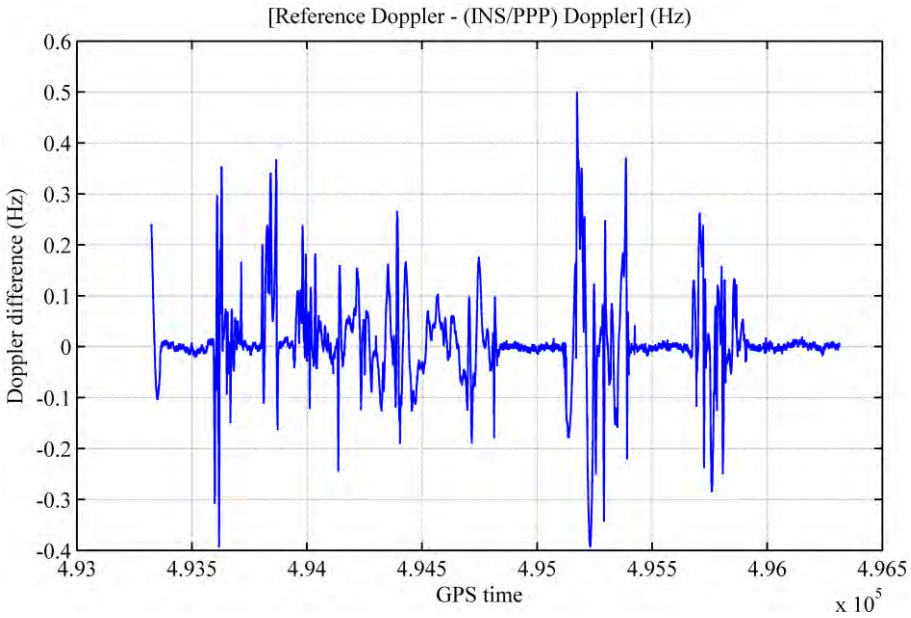

Figure 5-13: Differences between INS Doppler values estimated for PRN 16 using two approaches

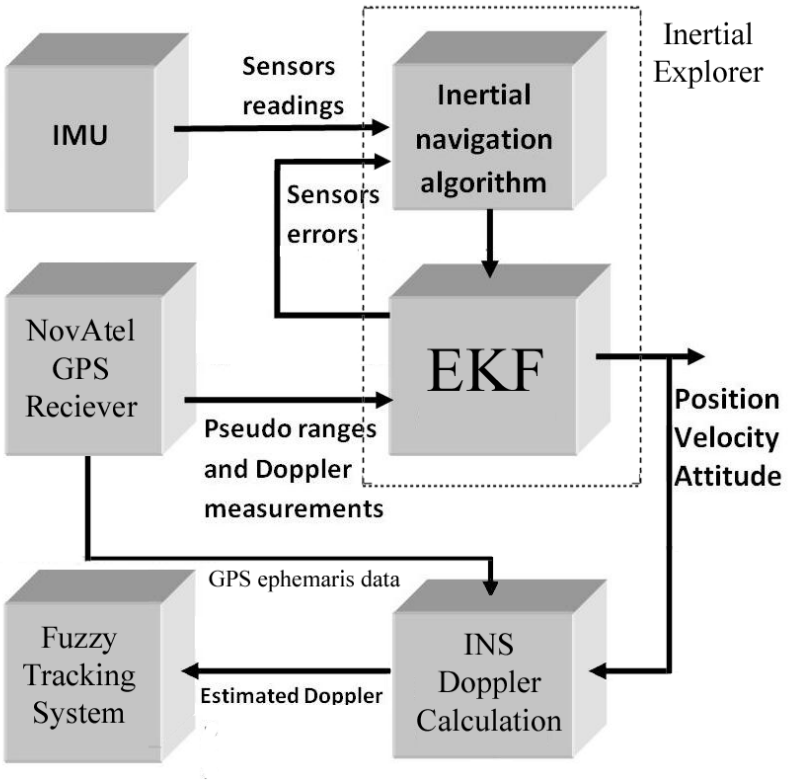

Figure 5-14: Step wise flow diagram and aiding Doppler calculation process

5.3.1 INS Doppler

In order to insure that INS Doppler only were extracted from the tightly coupled solution during jamming periods, artificial outages were simulated in post-processing during the periods of jamming. Indeed the wire GPS jammer perturbed only the RF samples collected by the NI front-end and not the GPS receiver used for the INS equipment. This can be seen in Figure 5-10, where the jammer RF signal is combined with GPS signals only after the splitter used for feeding the NovAtel receiver.

5.3.2 RF Data

The RF data was down converted and saved for post-processing via the National Instruments RF front-end. The GPS signals were collected using complex sampling of frequency $f_s = 5$ MHz at intermediate frequency $f_{IF} = 0.42$ MHz.

5.3.3 Data Collection Site

The test was held on an isolated rural location. The jammer range was below 10 m and had therefore no effect outside the immediate surroundings of the vehicle.

The short range handheld jammer was used through the line connection during short periods of time during the test. This jammer produces a CW signal nearly centered at L1 but with 50 dB higher power than the nominal GPS power. As it was shown previously in Chapter 4, this power is high enough to saturate the receiver amplifier and distort the signal during jamming periods.

The relation between the Free Space Path Loss (FSPL) and the range from the transmitter is governed by the following equation (Saunders & Zavala 2007):

$$FSPL = 20\log_{10}(d) + 20\log_{10}(f) + 32.45, \qquad \textbf{(5.3)}$$

where d is the distance from the transmitter expressed in kilometres and f is the signal frequency in MHz.

As it can be calculated using Equation (5.3), with a 10-metre separation between the jammer and the receiver, more than 50 dB of jamming power are already lost. Therefore this distance is already sufficient enough to get the GPS receiver working properly again and safe for any other GPS receiver outside this small coverage. To increase the safety factor and to avoid any legal issues using free-to-air jammer, the jammer dipole antenna was disassembled and its RF signal was directly combined with the GPS signals as shown in Figure 5-10.

5.4 Data Processing and Results

GPS RF samples were post-processed and tracked using different tracking algorithms as described in Table 5-4. The bandwidths used for classical tracking schemes are increased to their maxima and different to the ones used in Chapter 4 to increase the chance of signal reacquisition after the jamming period.

Table 5-4: Algorithms used for comparative analysis of GPS tracking loops

	Name	Standard Tracking Loop	Kalman Filter Based	Fuzzy Logic	INS assisted
1	PLL (18 Hz)	X			
2	FLL (18 Hz)-assisted-PLL (18 Hz)	X			
3	INS/KF		X		X
4	INS/PLL (18 Hz)	X			X
5	INS/FLL (18 Hz) assisted PLL (18 Hz)	X			X
6	FFPLL			X	
7	INS/FFPLL			X	X

The same criteria as the one described before in Chapter four for assessing the proposed tracking scheme are applied but completed with the new last point as follows:

- Tracking robustness under different dynamic conditions.
- Tracking quality by measuring noise distribution modulated on the estimated carrier Doppler.
- Ability to mitigate signal interference.
- Signal reacquisition ability and time.
- Computational load.

All the previous points of assessment can be investigated by analyzing the estimated Doppler during signal tracking taking into consideration that, when the system is in tracking mode, it tracks the signal phase as well.

During processing, this estimated Doppler is first compared to the INS reference Doppler, calculated using Equation (5.2), to insure that the solution is correct and not biased.

An analysis of the tracking results for two specific GPS signals, PRN code 16 and 13, using standard and non-standard tracking algorithms, is conducted. The associated results are assessed in a concise manner, as all tracking results for the other available GPS signals show consistent results and lead to the same conclusion.

After processing RF data using all the algorithms mentioned in Table 5-4, it was interesting to notice that none of them were able to track the GPS signal phase during jamming periods. Moreover it was observed that standard tracking schemes, even with INS aiding, were not able to reacquire the signal and switch back to tracking mode once jamming ended. For this reason, only non-standard tracking algorithms are shown later in the results analysis. However, an example of standard tracking results will first be shown to illustrate the above.

Figure 5-15 shows the estimated Doppler of PRN 13 during an extract of the scenario. This period started with 55 seconds in static mode followed by acceleration period and then two jamming periods of few seconds. In this figure, a comparison between the standard PLL (BW = 18 Hz) and the original FFPLL is shown. Both tracking loop performance are directly compared with the reference INS Doppler.

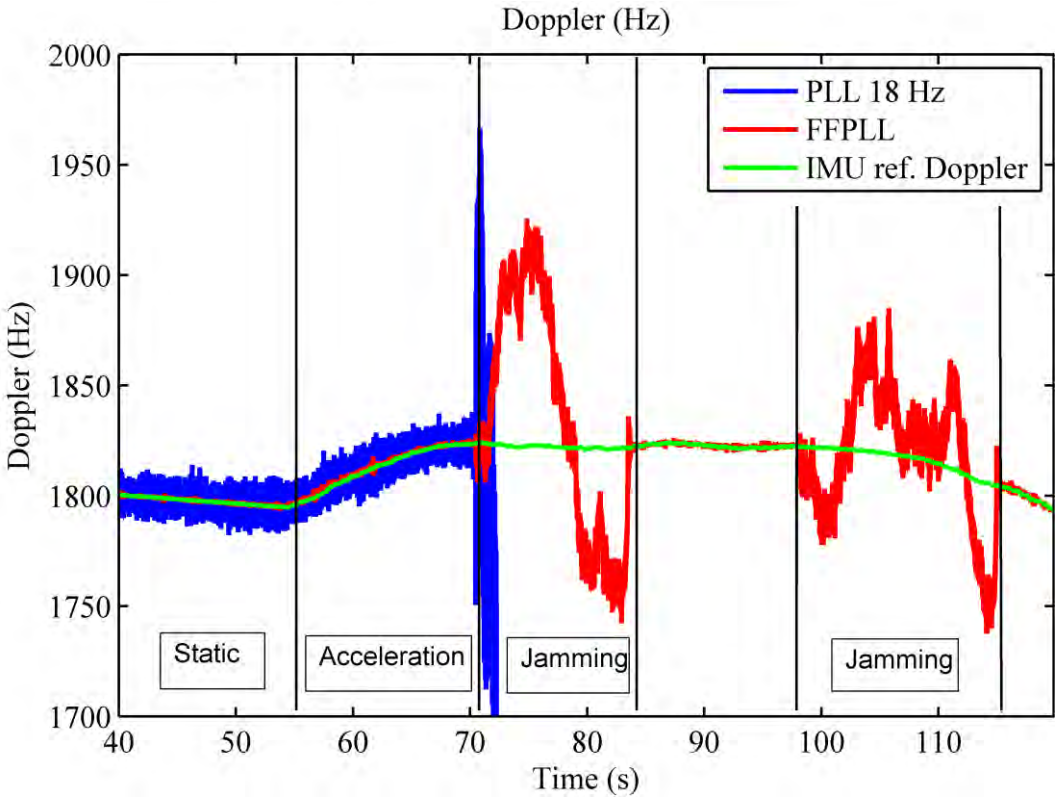

Figure 5-15: Estimated Doppler for PRN 13 using standard PLL 18 Hz and FFPLL

The FFPLL is able to retrieve the tracking mode and its estimated Doppler standard deviation is about 10 times lower than the standard PLL as illustrated in Figure 5-16. These results are consistent with Chapter 4 conclusions in terms of tracking robustness, noise level and signal reacquisition. Standard PLL tracking with wide BW tracking results show that it is not able to reacquire the signal directly during tracking after the signal interference period ends. Indeed in this case, the receiver has to switch back to acquisition mode, which consumes time.

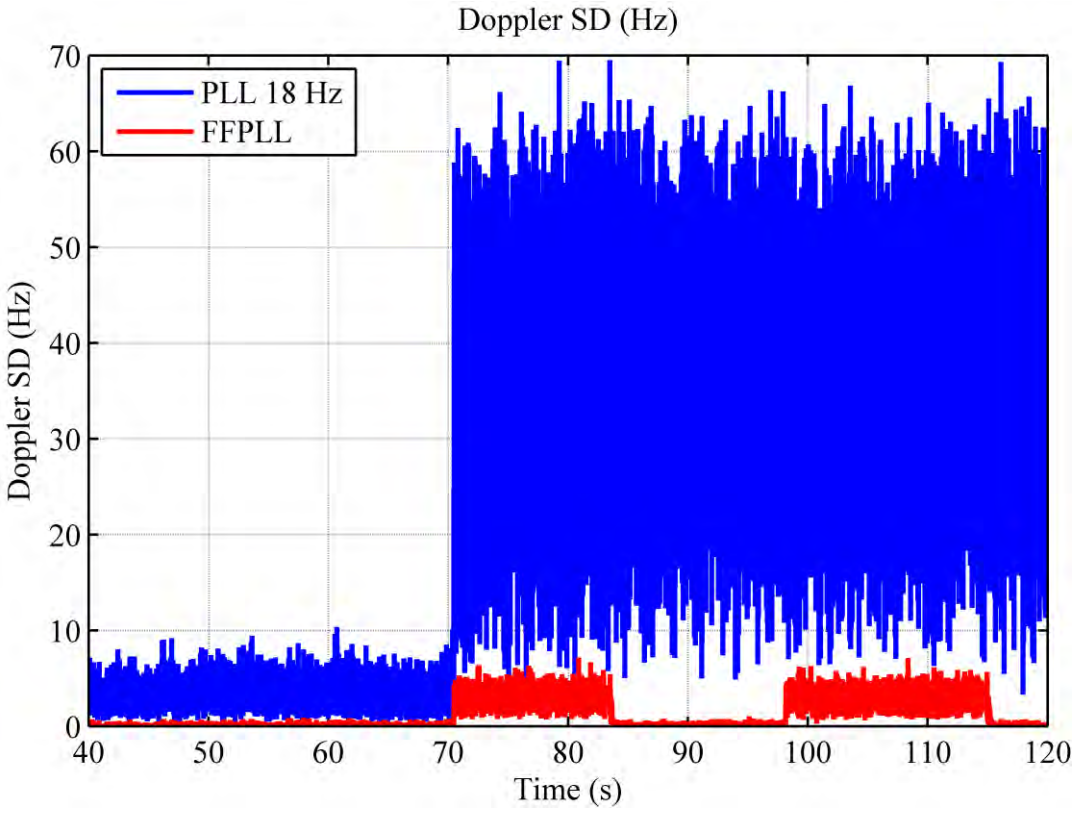

Figure 5-16: Estimated Doppler SD for PRN 13 using PLL 18 Hz and FFPLL

Figure 5-18 and Figure 5-19 show the Doppler calculated for PRN 16 and PRN 13 using KF+INS, FFPLL and INS assisted FFPLL, respectively. The fuzzy algorithms are able to reacquire signal lock after the jamming period. KF signal reacquisition operation is not consistent because it diverges during jamming periods and, if the erroneously estimated frequency is greater than the MAFE as seen previously in Chapter 4, it will not be able to reacquire frequency tracking. Therefore, the model used requires more intensive tuning for this specific problem. In addition, it is observed that the estimated Doppler in the Kalman filter case is diverging to a greater extent than FFPLL during the interference period. In the INS assisted FFPLL case, the estimated Doppler is only oscillating around

the required phase tuning frequency thanks to the Doppler measurements provided by the INS. Furthermore, only nine rules related to the phase input are used, which reduces the calculated processing time by a factor of around three as compared to that of the FFPLL. The computational load measured by processing time is averaged through the simulator and real data experiments and found to be reduced by a factor of about 30% as shown in Figure 5-17.

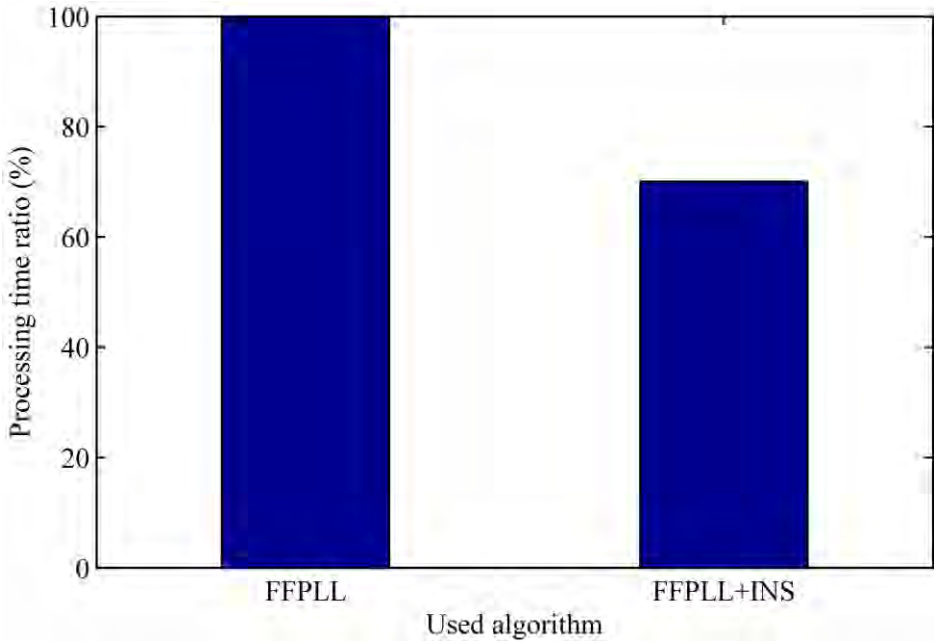

Figure 5-17: Average fuzzy processing time ratio for standalone and assisted FFPLL

Even though the INS aided FFPLL is not able to maintain signal phase lock during the jamming period, its Doppler frequency estimate is much better than the standalone FFPLL. In addition, the transient time required to retrieve the correct signal measurements is much faster as compared to the standalone FFPLL solution. This is illustrated in Figure 5-20 and Figure 5-21 for PRN 16 and PRN 13, respectively. Even

when KF is assisted by INS, its divergence during jamming is obvious due to large and un-modeled noise which was assumed to be following the Gaussian distribution.

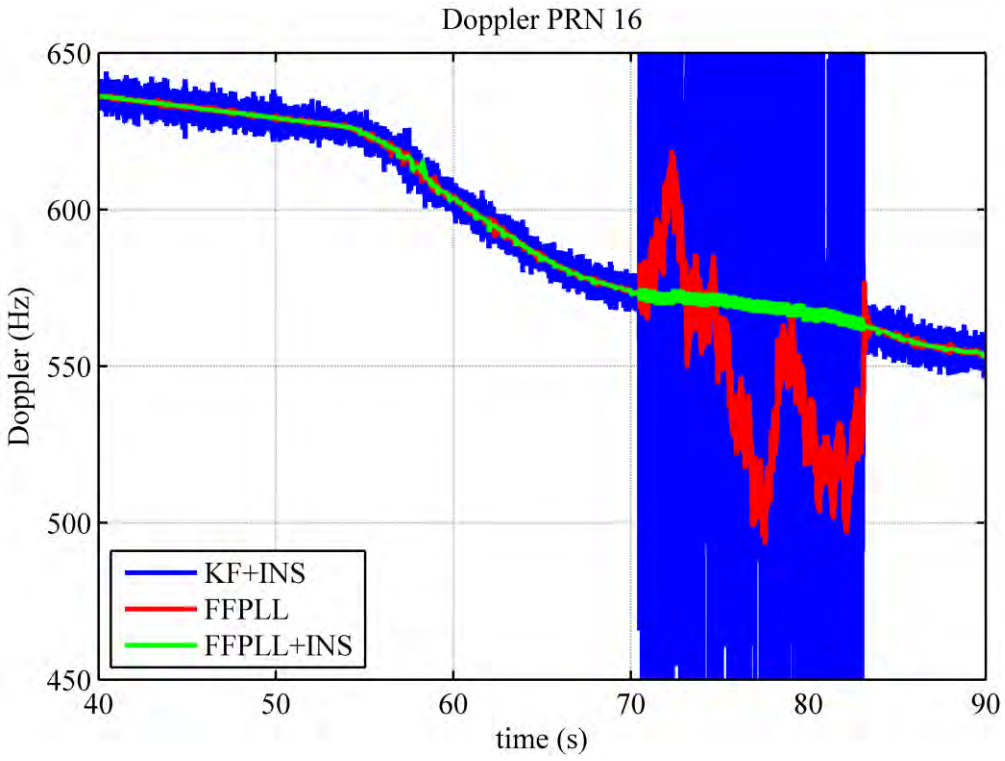

Figure 5-18: Estimated Doppler for PRN 16 using KF+INS, FFPLL, and INS+FFPLL

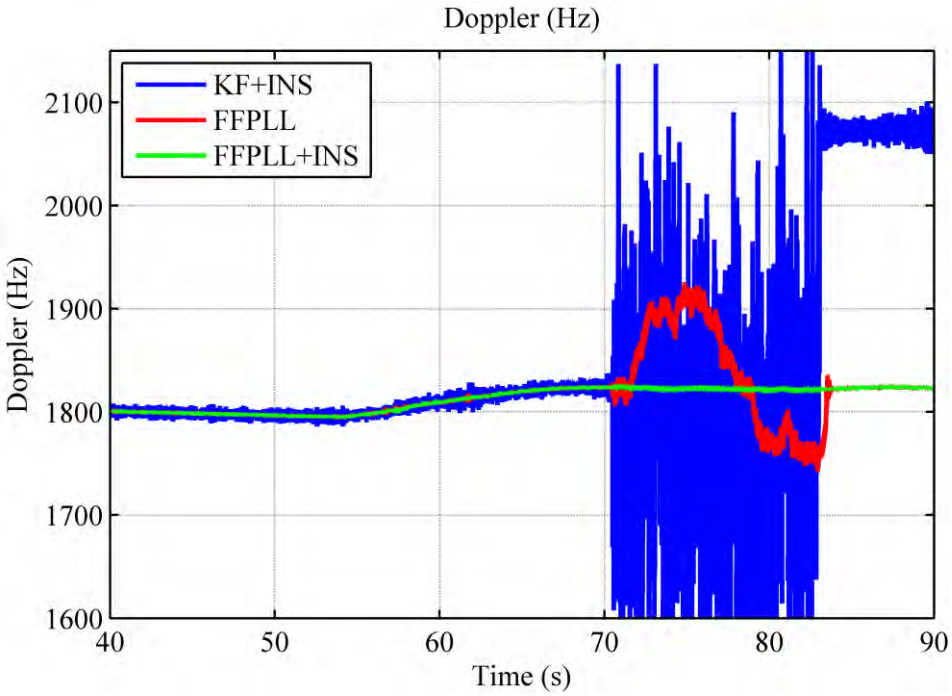

Figure 5-19: Estimated Doppler for PRN 13 using KF+INS, FFPLL, and FPLL+INS

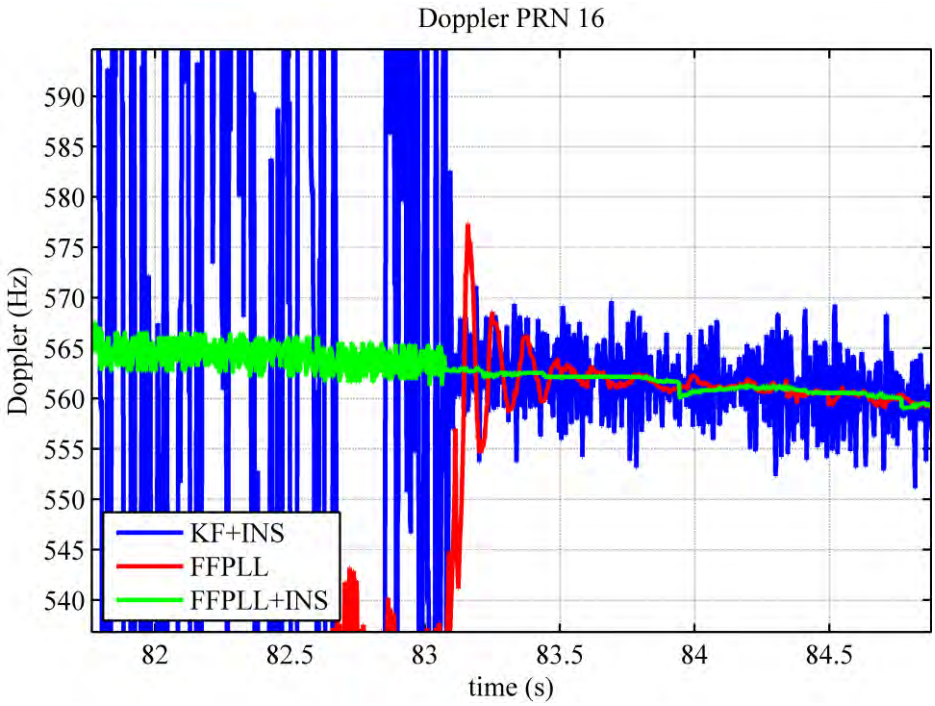

Figure 5-20: Estimated Doppler for PRN 16 using KF+INS, FFPLL, and INS/FFPLL zoomed for transient time illustration

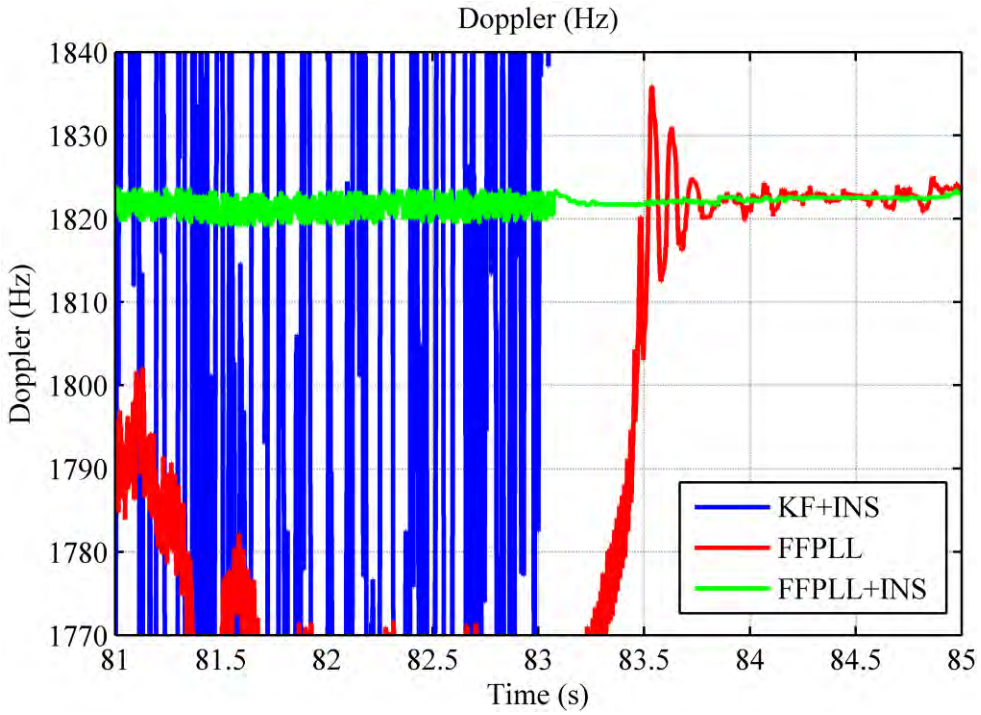

Figure 5-21: Estimated Doppler for PRN 13 using KF+INS, FFPLL, and FFPLL+INS zoomed for transient time illustration

5.5 Summary

In this chapter, a new fuzzy based GPS signal tracking loop is designed and tested. A new approach for GPS/INS ultra tight integration using fuzzy control is also presented as a modification to the original fuzzy tracking system.

By using a good quality IMU, as it is the case onboard of missiles and fighters, the new INS assisted fuzzy tracking is providing better tracking performance as compared to standard and Kalman filter based tracking loops in terms of robustness, quality, and computational load. The system is experimentally tested using live GPS signals in the presence of intentionally jammed signals. The experimental assessment shows that using

INS assistance, a reduction in the computational load by a factor of around 30% is achieved as compared with the originally designed fuzzy tracking system. Furthermore, when the GPS signal is lost during the jamming period, the time required to re-acquire the signal is much faster than the original fuzzy and Kalman filter based tracking systems.

Chapter Six: Design of Dual Frequency FFPLL and System Integration

This chapter explores the possibility of expanding the design of the fuzzy tracking system to include a second GPS frequency. System design of possible integrated configurations, test and analysis are introduced.

6.1 Introduction

Starting from the results in Chapters 4 and 5 the following conclusions are obtained:

- A fuzzy tracking system is able to provide a robust tracking during high dynamics with reduced noise level,
- during low and moderate interference levels, the fuzzy tracking system is able to provide almost the same performance as during interference free conditions,
- during high levels of interference, none of the tracking systems is able to insure signal tracking and an interference resistive alternative has to be provided,
- a high quality INS can be used to aid the fuzzy tracking system to fill the gaps resulting from GPS short outages during high levels of interference,
- a tracking system subjective to longer GPS outages cannot depend on INS aiding because of INS drifting nature and a different aiding approach has to be considered.

If the GPS receiver is assumed to be subjected to a jamming attack on a single frequency, aiding from a second GPS signal can be helpful.

The idea of combining different signals for GPS signal tracking was presented by many researchers. Salem (2010) examined the possibilities of joining L1 and L5 signals through KF for signal tracking mutual aiding purpose. Gernot (2009) also discussed the idea of combining L1 and L2C signals at the discriminator level for aiding purpose and to estimate the phase variations due to ionosphere. Qaisar (2009) has also discussed the idea of Doppler aided tracking loops for the L1 and the L2C signals, where the L2C signal estimated Doppler, which is estimated using a wide bandwidth PLL to cope with dynamics, assists L1 signal tracking using a narrow bandwidth.

Results from the above work have shown that the joint usage of two different GPS signals for tracking purposes provides more robust tracking when compared to each of the two signals separately. Performance of combined signals tracking system is degraded if one of the signals is completely jammed and in this case, it is preferrable to have two separate tracking loops for the two signals. For this reason a second GPS signal is used in this work to aid the fuzzy tracking system in the presence of interference on the primary L1 C/A signal with a separate fuzzy tracking loop for each signal. The L2C signal is chosen for this purpose, although L5 could be used the same manner for further improving the system.

6.2 GPS L2C Signal Overview

L2C is the second civilian GPS signal, designed specifically to meet commercial needs. The name "L2C" refers to the radio frequency used by the signal (1227 MHz, or L2) and “C” is for the fact that it is for civilian use. If L2C signal is combined with L1 C/A in a dual-frequency receiver, accuracy could be increased by resolving the ionospheric delay (Gernot et al 2008), which allows civilians with dual-frequency GPS receivers to enjoy the same accuracy as the military or maybe better, albeit with less resistance to jamming. L2C broadcasts at a higher effective power than the legacy L1 C/A signal, making it easier to receive under trees and even in the indoors. The first GPS IIR(M) satellite featuring L2C was launched in 2005. Every GPS satellite fielded since then has included an L2C transmitter. By 2016, there will be 24 GPS satellites that will effectively broadcast L2C signal (GPS.GOV 2011).

The L2C signal is composed of two codes, namely L2 CM (Moderate) and L2 CL (Long). The L2 CM code is 20 ms long and has 10230 chips while the L2 CL code is 1.5 seconds long and has 767250 chips. The CM code is modulo-2 added to data (i.e. it modulates the data) and the resultant sequence of chips (data channel) is time-multiplexed with the CL code (pilot channel) on a chip-by-chip basis as depicted in Figure 6-1.

The individual CM and CL codes are clocked at 511.5 KHz while the composite L2C code has a frequency of 1.023 MHz. This time-multiplexed L2C sequence modulates the

L2 carrier. The full nature of the L2C signal is defined in the IS-GPS-200 standards document (IS-GPS-200D 2006).

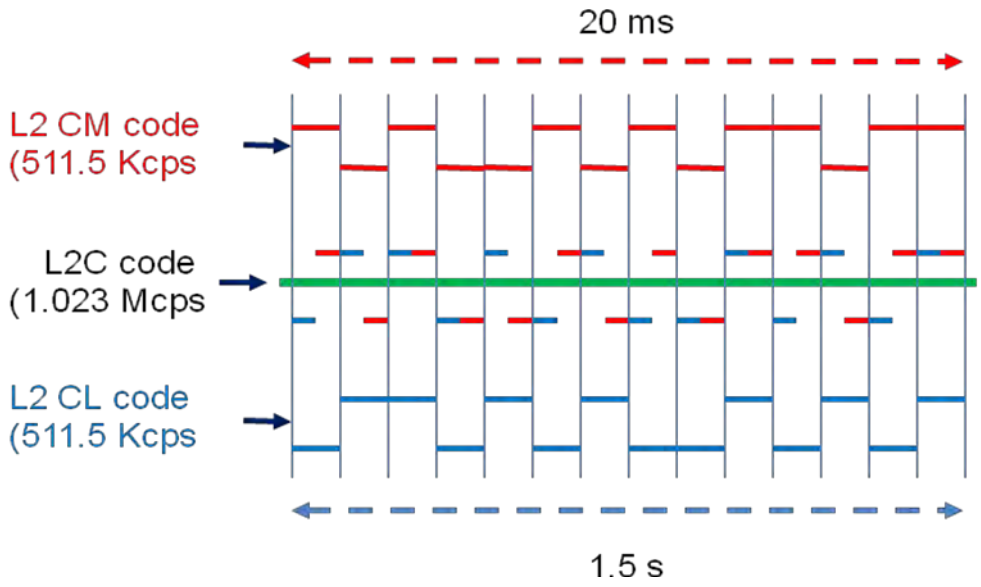

Figure 6-1: GPS L2C signal structure

It has been seen in Chapter 5 that INS Doppler can be used for aiding the phase tracking loop to bridge the tracking gaps resulting from strong jamming attacks. Dependence on the INS estimated Doppler is not a reliable solution if the GPS signal outages are long enough to be affected by INS drifts. If a GPS second frequency is used assuming it is not affected by the applied interference, the Doppler can be estimated for this frequency for the same satellite. Neglecting any ionospheric effects and assuming that the Doppler effect only includes the relative motion between user and satellite, the relation between the two Doppler signals can be written as follows:

$$f_{D1}^{motion} = \frac{f_1}{f_2} f_{D2}^{motion} \tag{6.1}$$

where f_{D1}^{motion} and f_{D2}^{motion} are the motion Doppler values calculated for the frequencies f_1 and f_2 respectively.

Using this approach, the L2C Doppler is used to aid L1 C/A FFPLL with the same design as the one presented in Chapter 5 for INS aiding and as it is further explained in the next sections.

6.3 FFPLL L2C CM Code Tracking and Aiding

It has been seen previously (Chapters 4 and 5) that a FFPLL is able to provide a very good Doppler estimate and improve phase tracking quality for L1 signal. The FFPLL is modified to track the L2C CM code and tested with real L2C data and the same performance as the one reported before for L1 signals is achieved.

Taking advantage of good L2C Doppler estimates, it is possible to use it to aid the L1 FFPLL.

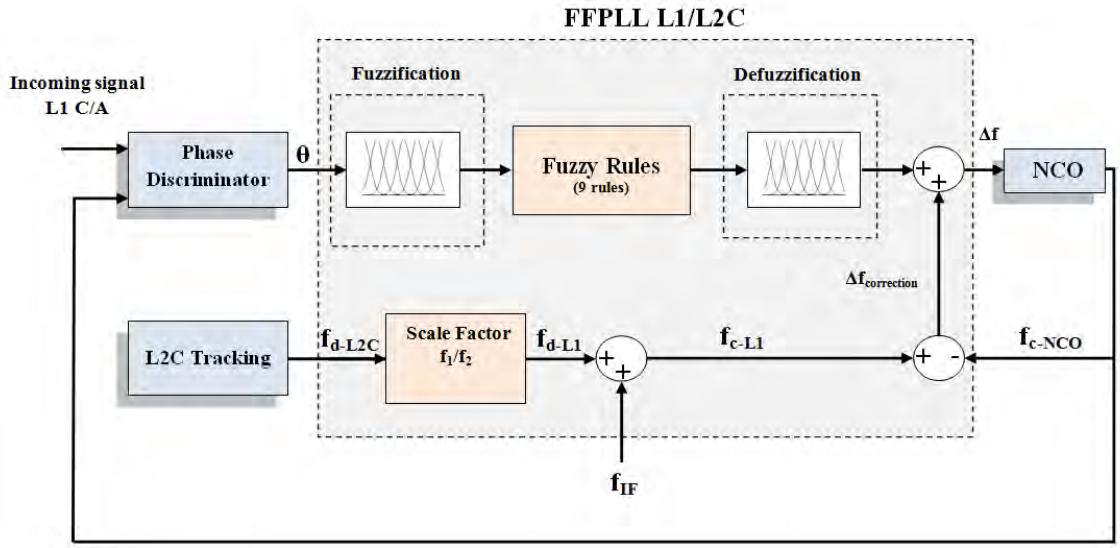

Figure 6-2 shows the modified structure of the L2C Doppler assisted FFPLL. The L2C Doppler has to be scaled with the L1/L2C frequency ratio to reach the level of the L1 Doppler as reported in Equation (6.1).

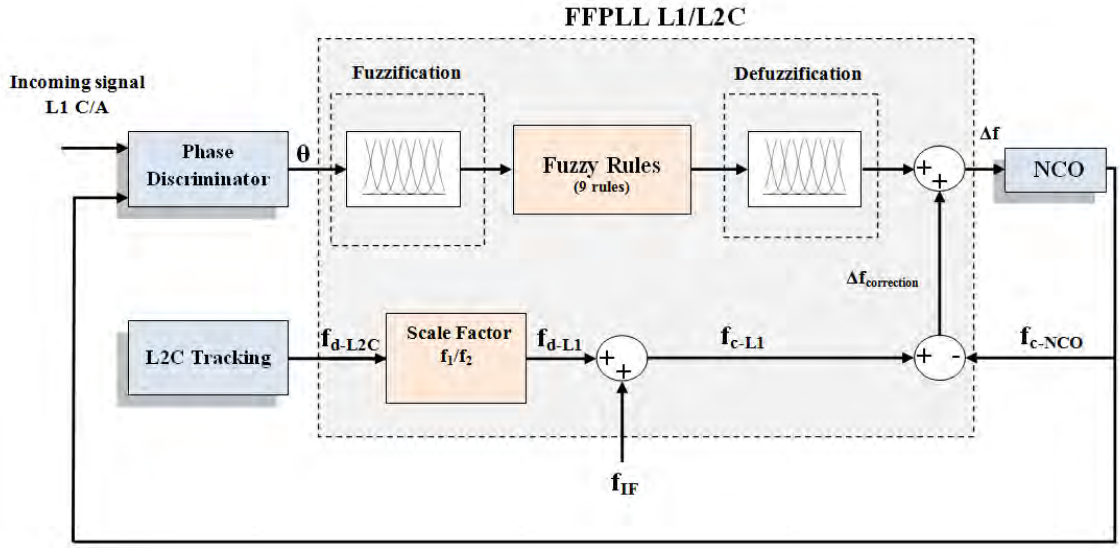

Figure 6-2: L2C Doppler aided L1 FFPLL

Similar to the INS aided FFPLL, the use of the L2C Doppler reduces the complexity of the FFPLL by using only the PD output and the L2C Doppler ($f_{d\text{-}L2C}$) for tuning the frequency. The scaled L2C Doppler ($f_{d\text{-}L1}$) is added to the base frequency (f_{IF}), and then the NCO generated carrier frequency ($f_{c\text{-}NCO}$) is subtracted from it. The resulting frequency corresponds to a frequency correction signal ($\Delta f_{correction}$) that is used to adjust the NCO tuning frequency (Δf). Therefore only nine fuzzy rules corresponding to the phase input, instead of the 81 in FFPLL original design, are used for the input fuzzy sets. The L2C Doppler assisted FFPLL can be used in the presence of jamming on the L1 signal. However if the jamming is on both frequencies, external aiding has to be used. In this case, the tracking system can be integrated by including INS aiding as well. The INS can be used to aid both L1 and L2C tracking loops or just aid one of them, which in turn aids the other. Figure 6-3 shows one of these configurations where INS is used to aid the L2C FFPLL and the resultant estimated L2C Doppler is used to aid L1 FFPLL as shown earlier in Figure 6-2.

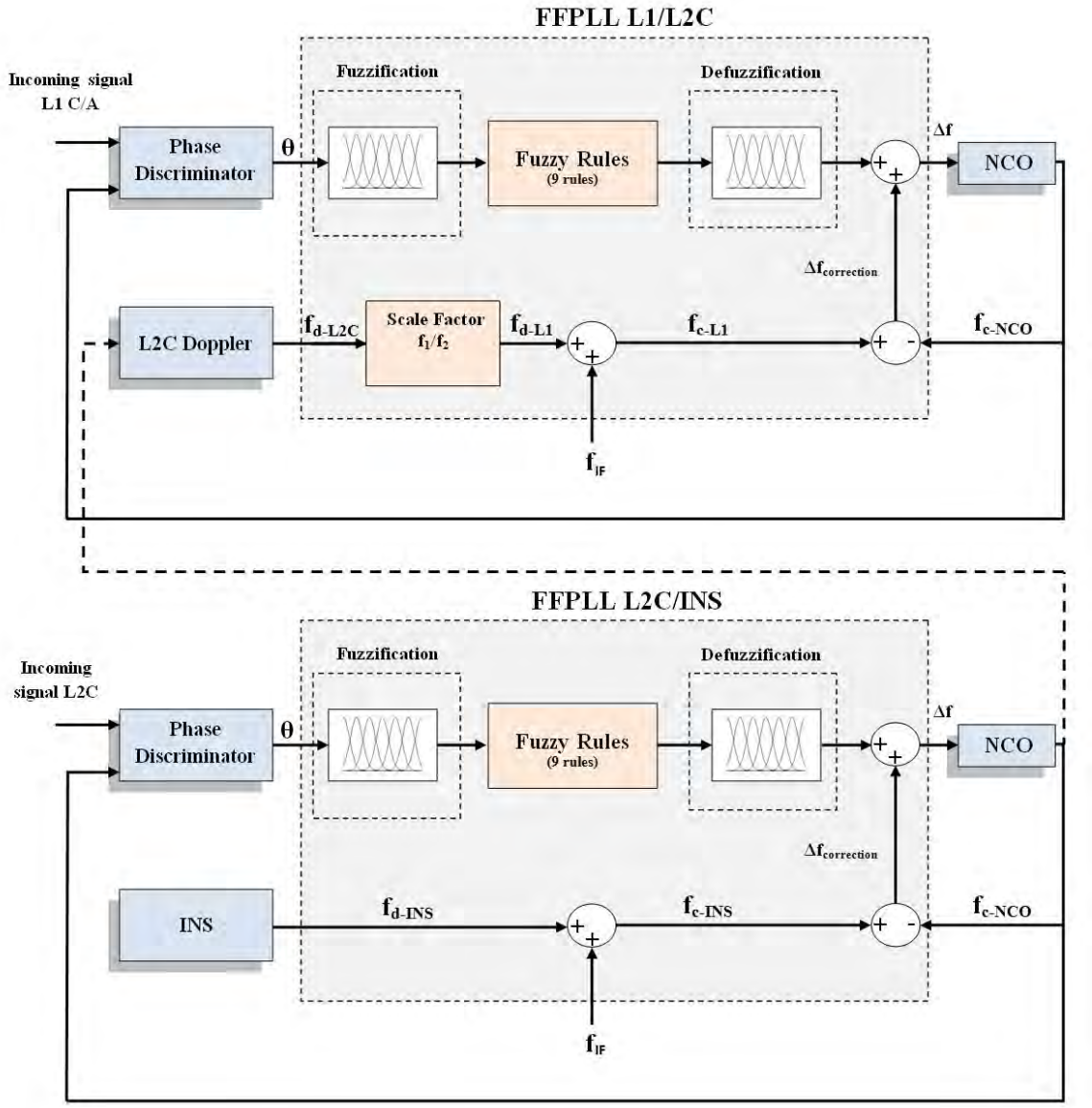

Figure 6-3: Integrated INS/L2C/L1 FFPLL

In this chapter only L2C Doppler aiding is tested during L1 jamming as INS aiding to L1 FFPLL was tested in Chapter 5. Similar results are expected if INS Doppler aiding is applied to the L2C FFPLL.

6.4 Test Results

The GPS hardware simulator is used to generate L1 and L2C RF signals. The collected RF signals are processed using FFPLL tracking and one of the generated scenarios is shown here.

Figure 6-4 shows the estimated Doppler for PRN 5 during a static and interference free scenario. Figure 6-5 shows the estimated C/N_0 for the two frequencies. It can be seen that the L2 signal has a lower quality level than L1 signal, which results in more noise in the estimated Doppler. A CWI jamming signal centered at L1 is applied to the same scenario where J/S = 50 dB started after 16 s. With such a high level of jamming, the FFPLL is not able to track the signal and loss of lock occurs. The L2C Doppler is estimated using the L2C FFPLL in parallel. L2C aiding is initiated after one second of losing lock and the signal tracking is recovered rapidly. The resultant estimated L1 Doppler has a poorer quality than the original one due to the poor L2C estimated Doppler resulting from a lower C/N_0 level. But on the other hand, tracking continuity and robustness is achieved.

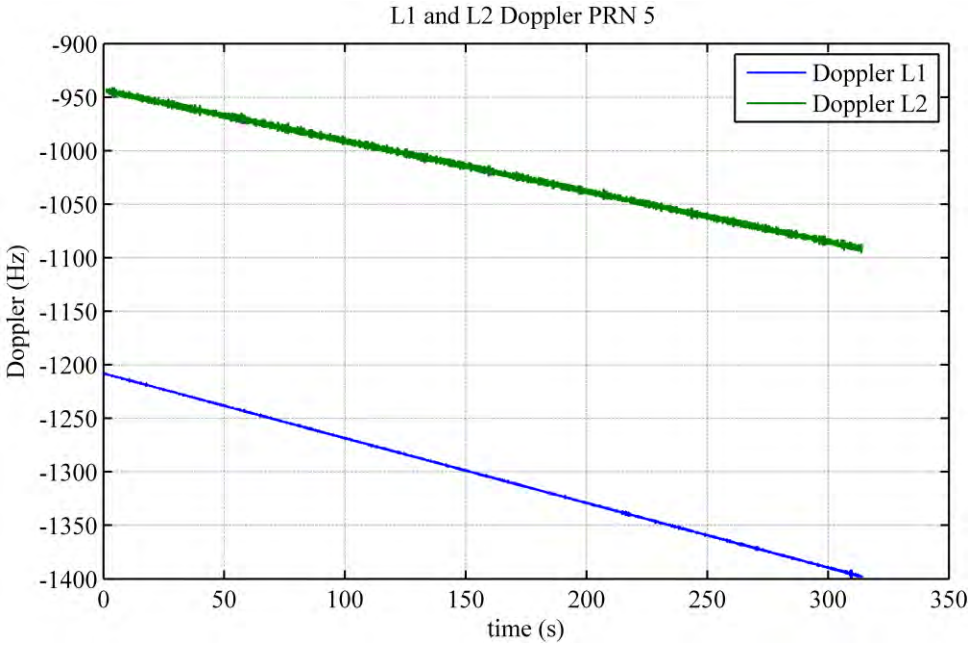

Figure 6-4: L1 and L2 Doppler values estimated for PRN 5

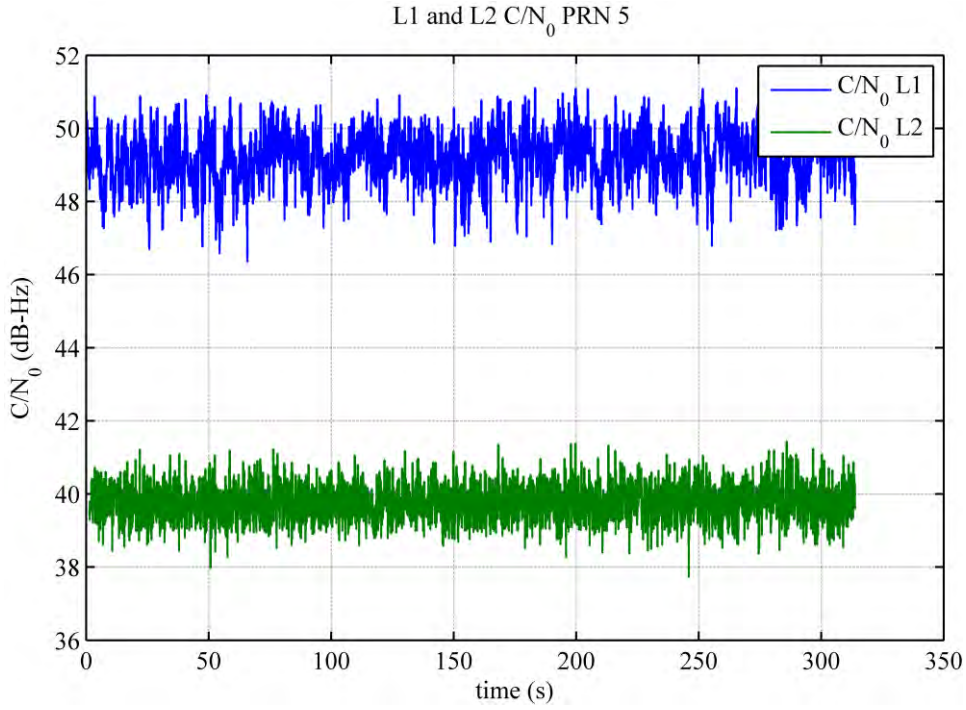

Figure 6-5: L1 and L2 C/N_0 estimated for PRN 5

Figure 6-6 shows the estimated PRN 5 Doppler in interference free condition and when J/S = 50 dB is applied after 16 s. It can be seen that the estimated Doppler is diverging in the second case and loss of lock has occurred. It shows also the ability of recovering signal tracking when L2C Doppler aiding is applied.

Figure 6-7 shows the quality of phase tracking in the same three conditions using the phase lock indicator where phase tracking is re-acquired but with lower quality when L2C Doppler aiding is applied. Phase tracking quality is assessed also by monitoring the prompt correlator output where the navigation data bits are extracted. Figure 6-8 shows the prompt correlator output for the same previous three conditions. It can be seen that the navigation data bits can be extracted again when J/S = 50 dB interference is applied with the aiding of the L2C Doppler.

6.5 System Integration

After a successful design and testing of the FFPLL (L1 and L2C), INS assisted FFPLL, and L2C assisted L1 FFPLL, the three schemes can be integrated to construct a robust GNSS tracking algorithm that can be used for missiles applications. GNSS signals are assumed to be acquired in the clear before launch and no acquisition problems are therefore discussed herein. The L1 and L2C signals are to be tracked in parallel using FFPLL. Depending on the online calculations of J/S as seen earlier in Equation (2.13), a simple decision making processor can select which configuration is perfect for the current situation. If INS data is available and jamming is on both signals, it can be used to aid

both L1 and L2C FFPLLs as reported in Chapter 5. L2C Doppler can be used to aid L1 FFPLL or vice versa. INS can be used to aid one of the loops, which in turn aids the other. The performance of the overall context aware system is dependent on which configuration is chosen where each one of these configurations is tested separately during the thesis progress. The proposed integrated system is shown in Figure 6-9.

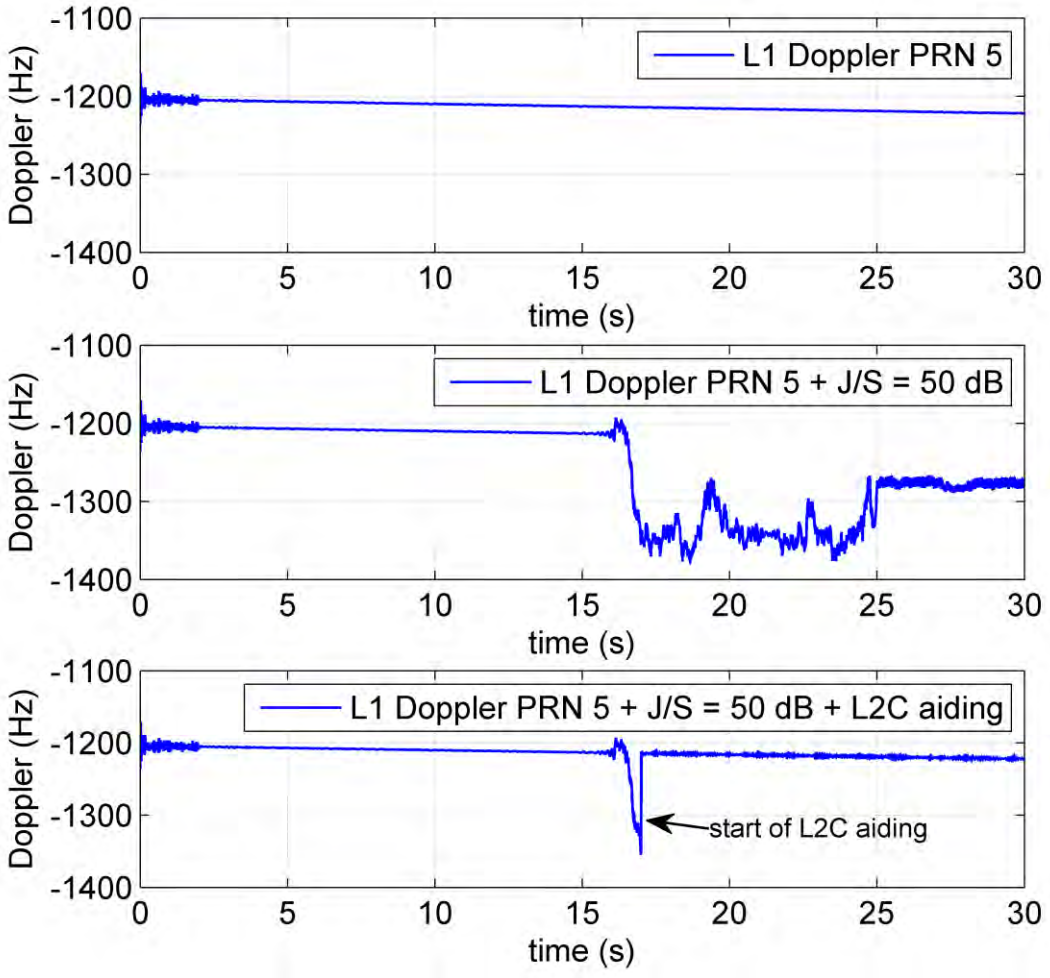

Figure 6-6: Estimated L1 Doppler for PRN 5 using FFPLL in interference free and interference conditions and using L2C Doppler assisted FFPLL in interference condition.

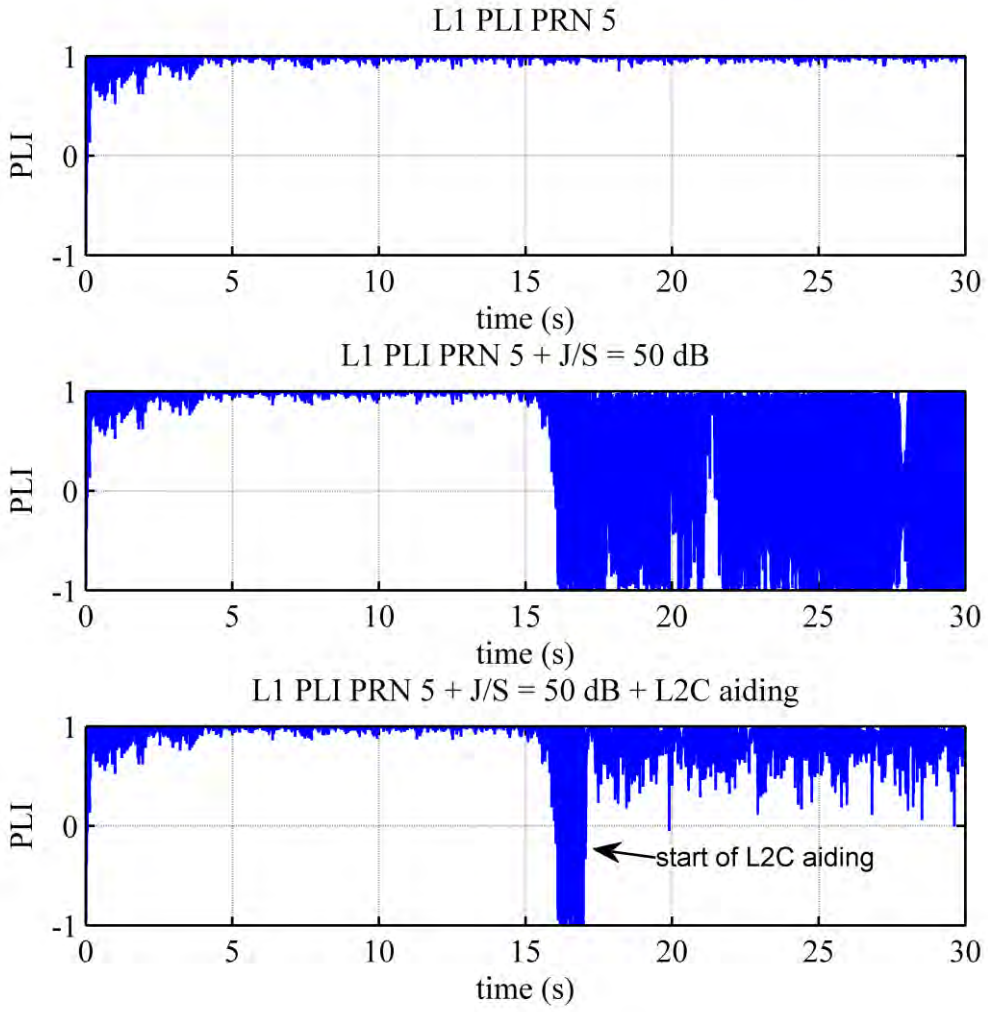

Figure 6-7: Estimated L1 PLI for PRN 5 using FFPLL in interference free and interference conditions and using L2C Doppler assisted FFPLL in interference condition.

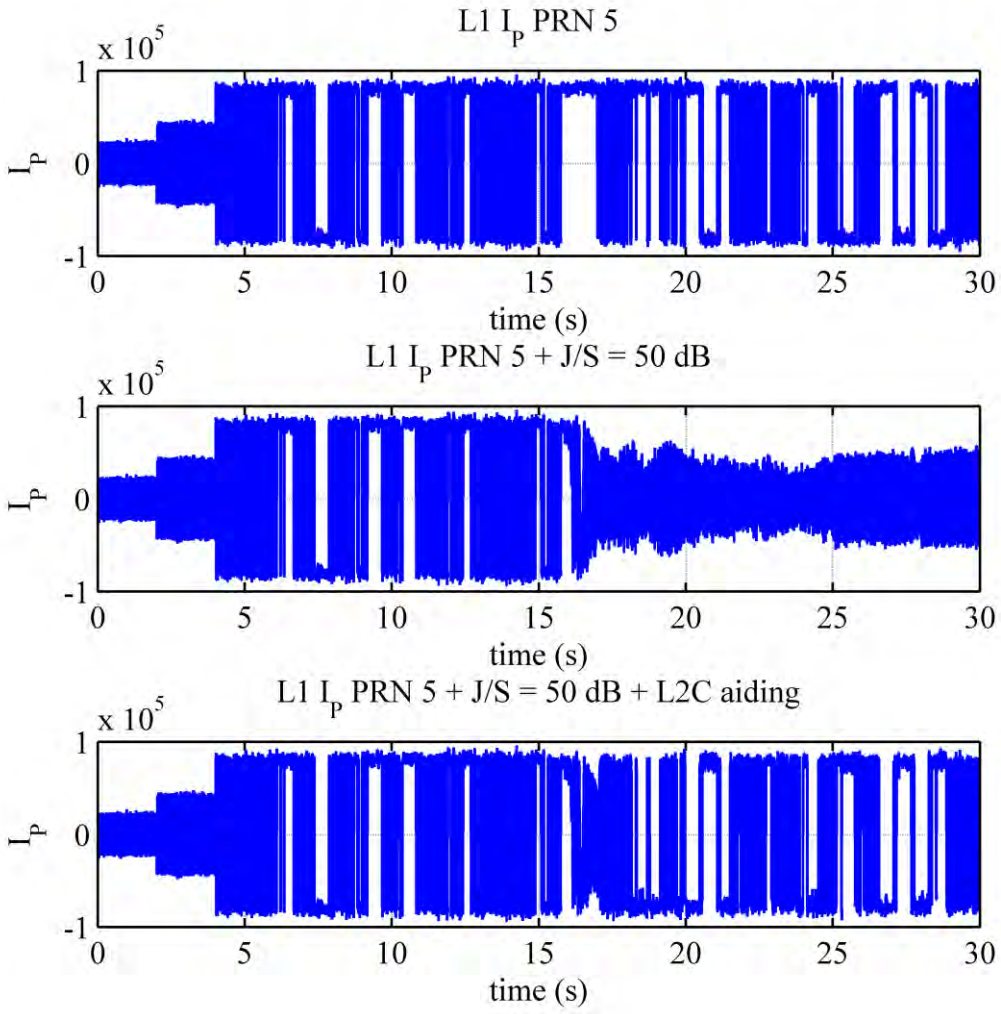

Figure 6-8: Estimated L1 prompt in-phase correlator output (I_P) for PRN 5 using FFPLL in interference free and interference conditions and using L2C Doppler assisted FFPLL in interference condition.

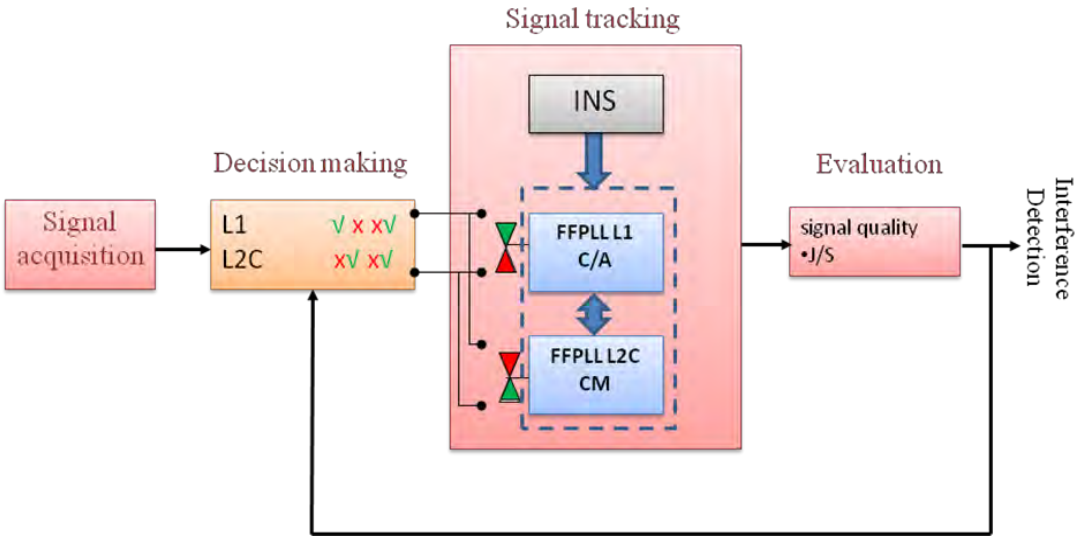

Figure 6-9: Integrated context aware INS aided- dual frequency-FFPLL

6.6 Summary

In this chapter, the fuzzy tracking system is modified to take advantage of the existence of different GPS signals that could be healthy during interference on the primary L1 GPS signal. L2C signal has been chosen to aid L1 FFPLL during its losing lock periods. To do so, L2C CM code tracking is tested using the FFPLL and the same level of performance is achieved. The L2C Doppler is then used after proper scaling using L1/L2 frequency ratio and injected to the single input FFPLL. Phase tuning in this case is the responsibility of the fuzzy processor while frequency tuning is dependent on the estimated L2C Doppler. Test results show that L2C can successfully be used to aid FFPLL for robust signal tracking during high levels of interference. Finally, a proposed context aware

integrated system that comprises all the previously described tracking schemes is introduced.

Chapter Seven: Conclusions and Recommendations

A detailed study of the usage of fuzzy logic techniques to design a robust and efficient signal tracking loop in the presence of combined incidence of high dynamics and signal interference for missiles applications has been presented in this thesis. The main conclusions derived from the thesis are discussed in this chapter. Recommendations for future work are also addressed.

7.1 Conclusions

The objectives of the thesis listed in Chapter 1 included:

- the development of a novel tracking algorithm using artificial intelligence that enable efficient GPS signal tracking under GPS signal interference and high dynamic applications, which is useful for missiles applications,
- using the inertial sensors immunity against RF interference to aid the new tracking algorithms for further performance enhancement,
- investigating the performance of the new tracking algorithms when applied to modern GPS signals such as the GPS L2C signal and studying the benefits of using this signal in a combined scheme with the L1 signal.

The thesis had met these objectives, whereby an innovative signal tracking algorithm based on fuzzy logic control has been proposed, implemented and evaluated. Also, INS

and L2C signal aided tracking for the new system were implemented and evaluated. Experimental results using a GPS hardware simulator and real GPS signals for assessing the proposed system and its alternative configurations have been presented. The conclusions for all proposed tracking loop architectures are recalled below.

7.1.1 System Design and Test Conclusions

An innovative GPS signal tracking system based on fuzzy logic control has been proposed. The design of any fuzzy processor is based on the designer forehand experience of the problem. The problem under investigation is the limited performance of the standard tracking loops in the presence of signal interference and high dynamics. This is why the research started with a theoretical performance assessment of PLLs and FLL-assisted-PLLs in the above challenging conditions. This assessment helped in gaining sufficient experience required to design the new fuzzy tracking system (FFPLL).

Test results of the proposed tracking system lead to the following conclusions:

1- In interference free conditions, the system is tested under a harsh dynamic situation. Test results concluded that the FFPLL is stable and robust under high dynamics conditions. The capability of providing continuous signal tracking without losing lock is achieved. The performance achieved is comparable with those of a standard wide bandwidth PLL in terms of tracking capability in the high dynamics situations. The estimated Doppler noise is compared also to what could be obtained from different bandwidth PLLs. The estimated Doppler noise is

found to be smaller than the estimated Doppler noise from as narrow as a 4 Hz bandwidth PLL. FFPLL performance is also compared to Kalman filter based PLL performance and comparable results are obtained but with the advantage of fuzzy logic based systems simple design.

2- The system is tested under interference conditions focusing on narrowband interference, particularly CW, SCW, and FM. The internal design of FFPLL is modified to cope with discriminators output standard deviation changes due to changing interference level. The modified FFPLL is tested under different interference powers for each type. It is noticed that the system is capable of providing signal tracking up to interference level of J/S= 40 dB with the advantage of providing almost the same Doppler quality as the one obtained in interference free conditions. Higher levels of interference lead to losing signal lock. When the jamming sources are turned off or when the receiver is far enough from these sources, FFPLL is capable of acquiring back the signal without going back to the acquisition stage. This advantage is applicable also even if the receiver is under high dynamic stress. These results were not achievable using standard PLLs.

3- Integration time effects are also investigated during FFPLL performance. Theoretical studies and test results show that increasing integration time will improve the quality of discriminators output and hence the estimated Doppler quality. By increasing the integration time from 4 ms to 10 ms, the Doppler noise is reduced by around 40%, which can be compared to 85% reduction in the case

of standard PLL. This means that by using small integration time value with FFPLL, approximately the same noise level can be reached as if large integration time value is used. Consequently a larger dynamic margin with this small integration time is achieved, putting into consideration that the noise level is much less than the level obtained from standard PLL with the same integration time. Test results also show that FFPLL is capable of sustaining signal tracking during high dynamics at 5 ms of integration time while it can be only sustained using wide bandwidth (10 Hz) PLL at 1 ms integration time.

4- FFPLL pull-in frequency is empirically calculated and compared to other tracking schemes. A maximum allowed frequency error for successfully starting to track signals is found to be equal to 250 Hz. Same frequency error threshold is achieved by Kalman filter based PLL but with longer convergence time required to reach the correct signal frequency.

7.1.2 INS Integration

To cover the gaps resulting from GPS outages due to increased levels of signal interference, inertial navigation is used because of its immunity against signal interference. A test setup was designed to collect live GPS signals with the usage of a tactical grade high quality IMU. The estimated corresponding INS Doppler was used to aid FFPLL, which was modified for incorporating the injected INS Doppler for frequency tuning. The FFPLL design complexity was drastically reduced by only using one input,

which corresponds to the phase error from the PD. Only nine rules were processed simultaneously using the reduced FFPLL, compared to 81 rules in the original design. The reduced rules number was found to reduce the processing time by around 30%. Usage of INS aiding by a good quality INS Doppler helped the tracking loop to reduce the time required to re-acquire the signal. This time was found to be around 14 times faster than the original fuzzy tracking system after the GPS signal is lost during the jamming period.

7.1.3 L2C Aiding

For longer jamming periods, it is not possible to depend on INS only due to its drifting nature. Hence, an alternative has to be provided. The alternative used within the research progress is the GPS L2C signal. Using the GPS hardware simulator, tests that included L1 and L2C with jamming were designed and conducted. FFPLL aiding using the scaled L2C Doppler was performed using the same structure as the one used for INS aiding. Test results showed that during a jamming attack on the L1 frequency with a J/S value of over 40 dB, the FFPLL was losing lock and no data could be extracted. With L2C Doppler aiding and at the same jamming level, the system was found to be robust and loss of lock did not occur with the ability of extracting the navigation data message.

7.2 Recommendations for Future Work

Following the previous conclusions, this section provides some recommendations for future work.

1- Given the high level of performance achieved for the FFPLL, which can be compared to Kalman filter based PLL performance, it worth to conduct tests in real time.

2- The interference tests focused on narrowband interference. However, in reality and especially for military applications the jamming source is expected to be more intelligent and hence the new system should be tested under a larger range of interference types and with more combinations of interference mitigation techniques.

3- Ultra-tight integration with INS was conducted using a tactical grade IMU, which provides accurate readings even when GPS updates are not available for reasonable time duration. It is recommended for the new system to be tested with lower grade IMUs such as MEMS to observe the sensor's error effects on final signal tracking accuracy during harsh jamming attacks.

4- Integration with the L2C signal was proposed on the basis that jamming attacks are concentrated on L1. If the jamming is focused on L2, the design could be reversed and aiding by L1 Doppler is feasible. Testing this design is recommended.

5- Integration with L2C was based on the estimated L2C Doppler obtained during CM code tracking. System performance could be enhanced by tracking both CM and CL codes simultaneously in a combined tracking scheme to increase the C/N_0 level and hence the jamming threshold. On other hand, more accurate and less noisy Doppler estimates will be provided to aid the L1 tracking loop.

6- The system design could be expanded to include the L5 signal as well and increase its robustness during jamming attacks.

7- Finally, although the improvements documented in this work have been achieved at the signal tracking level, it is important to evaluate performance at the position level.

REFERENCES

Alban, S., D. Akos, and S. M. Rock (2003) "Performance Analysis and Architectures for INS-Aided GPS Tracking Loops," *Proceedings of ION National Technical Meeting (NTM)*, 22-24 January, Fairfax VA, 611-622, Institute of Navigation, Fairfax VA

Antonio, L. (2011) *Phase Lock Loops*, http://www.scribd.com/doc/47785355/Phase-Lock-Loops, last accessed 7 August 2011,

Babu, R., W. Jinling, and G. Rao (2008) "Analysis of ultra-tight GPS/INS integrated system for navigation performance," Piscataway, NJ, USA, pp. 234-237, IEEE

Borre, K., D. M. Akos, N. Bertelsen, P. Rinder, and S. H. Jensen (2007) *A software-Defined GPS and GALILEO Receiver, A single frequency Approach*, Brikhauser, Boston

Bourke, M. M. (1995) *SELF-LEARNING PREDICTIVE CONTROL USING RELATIONAL BASED FUZZY LOGIC* DEPARTMENT OF CHEMICAL ENGINEERING University of Alberta, Edmonton

Braasch, M. S., and A. J. van Dierendonck (1999) "GPS receiver architectures and measurements," *Proceedings of the IEEE*, Jan 1999, 48-64, IEEE

Brown, A. (2002) *Performance and Jamming Test Results of a Digital Beamforming GPS Receiver*. NAVSYS Corporation,14960 Woodcarver Road,Colorado Springs,CO,80921

Brown, A., and N. Gerein (2001) "Test Results of a Digital Beamforming GPS Receiver in a Jamming Environment," *Proceedings of ION GPS 2001*, September 2001, Salt Lake City, Utah

Brown, R. G., and P. Y. C. Hwang (1997) *Introduction to Random Signals and Applied Kalman Filtering with Matlab Exercises and Solutions, 3rd Edition*, John Wiley & Sons, New York

Cannon, M. E., R. Nayak, G. Lachapelle, O. S. Salychev, and V. V. Voronov (2001) "Low-cost INS/GPS integration: concepts and testing," *Journal of Navigation*, vol 54, no 1, pp. 119-134

Casbona, M. M., and M. W. Rosen (1999) "Discussion of GPS Anti-Jam Technology," In: *GPS Solutions Vol. 2, No. 3*, 18-23

Chang, C. L., J. C. Juang, and Y. L. Tsai (2004) "Development of neural network-based GPS anti-jam techniques," *Proc. of CACS Automatic Control Conference*, March 2004, Changhua, Taiwan, 1076-1081

Chen, G., and T. T. Pham (2001) *Fuzzy Sets, Fuzzy Logic, and Fuzzy Control Systems*, CRC Press, New York

Cheuk, W. C., M. Trinkle, and D. A. Gray (2005) "Null-steering LMS Dual-Polarised Adaptive Antenna Arrays for GPS " *Journal of Global Positioning Systems*, vol 4, no 1, 2005, pp. 258-267

Crosta, P., and T. Alenia (2009) "A Novel Approach to the Performance Evaluation of an Arctangent Discriminator for Phase Locked Loop and application to the carrier tracking of the Ionospheric Scintillation," *ENC-GNSS 2009*, 3 - 6 May, 2009, Naples, Italy

Dierendonck, A. J. V. (1996) "GPS receivers," [8 8] in *Global positioning system: theory and applications*, Parkinson, B. W., ed., AIAA, Los Altos

Dierendonck, A. J. V., J. B. McGraw, and R. G. Brown (1984) "Relationship between Allan Variances and Kalman Filter Parameters," *Proceedings of the 16th Annual Precise Time and Time Interval (PTTI) Applications and Planning Meeting*, 27 - 29 November, NASA Goddard Space Flight Center, 261-272

El-Sheimy, N. (2007) "ENGO 623 Lecture notes: Inertial Techniques and INS/DGPS Integration," Department of Geomatics Engineering, University of Calgary, Calgary, Canada

Farrell, J. (2008) *Aided Navigation: GPS with High Rate Sensors*, First Ed., Mcgraw-hill

Garnell, P. (1980) "Guided Weapon Control Systems," Elsevier

Gautier, J. D., and B. W. Parkinson (2003) "Using the GPS/INS Generalized evaluation Tool (GIGET) for the Comparison of Loosely Coupled, Tightly Coupled and Ultra-Tightly Coupled Integrated Navigation Systems," *Proceedings of ION 59th Annual Meeting/CIGTF 22nd Guidance Test Symposium*, 23-25 June, Albuquerque, NM, 65 - 76

Gernot, C. (2009) *Development of Combined GPS L1/L2C Acquisition and Tracking Methods for Weak Signals Environments*, Geomatics Engineering, University of Calgary, Calgary

Gernot, C., K. O'Keefe, and G. Lachapelle (2008) "Combined L1 / L2C Tracking Scheme for Weak Signal Environments," *ION GNSS 2008* 16-19 September 2008, Savannah, GA

Gerten, G. (2005) "Protecting the Global Positioning System," *IEEE Aerospace and Electronic Systems Magazine*, vol 20, no 11, pp. 3-8

Giordanengo, G. (2009) *Impact of Notch Filtering on Tracking Loops for GNSS Applications*, Facoltà di Ingegneria dell'infromazione, Politecnico di Torino, Politecnico di Torino, Torino

GlobalSources (2011) *Leica TCR705 Reflectorless [TCR705] product details*, http://www.globalsources.com/gsol/I/Leica-TCR705-Reflectorless-%5BTCR705%5D/p/sm/1025963414.htm,

Golnaraghi, F., and B. C. Kuo (2010) *Automatic Control Systems* 9Ed., John Wiley &Sons

Gormley, D. M., and K. S. McMahon. (1995) "Proliferation of Land-Attack Cruise Missiles:Prospects and Policy Implications," [6 6] in *Controlling the Spread of Land-Attack Cruise Missiles*, American Institute for Strategic Cooperation, California

GPS.GOV (1993) "ICD-GPS-200, Revision C, Initial Release," USA

GPS.GOV (2011) *New Civil Signals*, http://www.gps.gov/systems/gps/modernization/civilsignals/, last accessed 25 May 2011, 2011

Grewal, M. S., and A. P. Andrews (2008) *KALMAN FILTERING Theory and Practice Using MATLAB*, John Wiley & Sons, New Jersey

Groves, P. D. (2008) *Principles of GNSS, Inertial, and Multisensor Integrated Navigation Systems*, ARTECH HOUSE

Honeywell (2006) *HG1700 Inertial Measurement Unit (http://www.honeywell.com/sites/servlet/com.merx.npoint.servlets.DocumentServlet?docid=D7B652202-0601-F56B-1B7F-829F1A7109E4)*, http://www.honeywell.com/sites/servlet/com.merx.npoint.servlets.DocumentServlet?docid=D7B652202-0601-F56B-1B7F-829F1A7109E4,

IS-GPS-200D (2006) "NAVSTAR Global Positioning System Interface Specification IS-GPS-200 revision D," 7 March 2006,

Jazwinski, A. H. (1970) *Stochastic Processes and Filtering Theory*, Academic Press, INC.

Kamel, A. M. (2010) "Design and Testing of an Intelligent GPS Tracking Loop for Noise Reduction and High Dynamics Applications," *ION GNSS 2010*, September, 2010, Portland, Oregon

Kamel, A. M., D. Borio, J. Nielsen, and G. Lachapelle (2011a) "Interference Mitigation for Highly Dynamic GPS Receivers Using Intelligent Tracking Loops," *ION ITM 2011*, 24-26 January, 2011, San Diego, CA

Kamel, A. M., D. Borio, J. Nielsen, and G. Lachapelle (2011b) "Mitigation for Missiles (Fuzzy Logic and Intelligent Tracking Loops Cope with Interference)," In: *GPS World, June 2011*

Kamel, A. M., and G. A. Elsheikh (2004) "A Fuzzy Autopilot for a Semiactive Homing Guided Missile," *ICEENG 2004*, 23-25 November 2004, Military Technical College, Cairo, Egypt

Kaplan, E. D., and C. J. Hegarty (2006) *Understanding GPS: Principles and Applications*, Second Ed., Artech House, INC., Norwood, MA 02062

Kazemi, P. L. (2010) *Development of New Filter and Tracking Schemes for Weak GPS Signal Tracking*, Geomatics Engineering, University of Calgary, Calgary

Knapp, R. B. (2004) *Fuzzy inference systems*, http://www.cs.princeton.edu/courses/archive/fall07/cos436/HIDDEN/Knapp/fuzzy004.htm, last accessed 24 Feb. 2011,

Kosko, B. (1992) *NEURAL NETWORKS AND FUZZY SYSTEMS (A Dynamical Systems Approach to Machine Intelligence)* PRENTICE HALL, Englewood Cliffs, NJ 07632, NEW JERSY

Lewis, D. E. (2003) "Ultra-Tightly Coupled GPS/INS Tracking Performance," *AIAA's 3rd Annual Aviation Technology, Integration, and Operations (ATIO) Tech* 17 - 19 November 2003, Denver, Colorado

Li, P., J. Wang, and C. Rizos (2010a) *GNSS signal re-acquisition with biased Doppler aiding from INS*, http://citeseerx.ist.psu.edu/viewdoc/summary?doi=10.1.1.156.6998,

LI, T., M. PETOVELLO, G. LACHAPELLE, and C. BASNAYAKE (2010b) "Ultra-tightly Coupled GPS/Vehicle Sensor Integration for Land Vehicle Navigation," *Navigation*, vol winter, June 2010,

Lin, T., A. Broumandan, J. Nielsen, C. O'Driscoll, and G. Lachapelle (2009) "Robust Beamforming for GNSS Synthetic Antenna Arrays," *ION GNSS 2009, Session A5*, 22-25 September 2009, Savannah, GA

Malmstrom, J. (2003) *Robust Navigation with GPS/INS and Adaptive Beamforming*, Swedish Defence Research Agency

Mao, W. L., H. W. Tsao, and F. R. Chang (2004) "Intelligent GPS receiver for robust carrier phase tracking in kinematic environments," *IEE proceedings. Radar, sonar and navigation*, vol vol. 151, no no3, pp. pp. 171-180

Milstein, L. B. (1988) "Interference rejection techniques in spread spectrum communications," *Proceedings of the IEEE*, vol 76, no 6, pp. 657-671

Misra, P., and P. Enge (2004) *Global Positioning System Signals, Measurements, and Performance*, Ganga-Jamuna Press

NationalInstruments (2006) *2.7 GHz RF Vector Signal Analyzer with Digital Downconversion*. National Instruments (NI), Data Sheet

NovAtel (2011) *Inertial Explorer® Data Sheet*, http://www.novatel.com/assets/Documents/Waypoint/InertialExplorer.pdf, last accessed 22 May, 2011

Parkinson, B. W., and J. J. Spilker, eds. (1996) "Global Positioning System: Theory and Applications," American Institute of Astronautics and Aeronautics, Washington, DC

Petovello, M., and G. Lachapelle (2006) "Comparison of Vector-Based Software Receiver Implementations with Application to Ultra-Tight GPS/INS Integration," *ION GNSS 2006*, September 2006, Fort Worth TX, 26-29

Petovello, M. G., C. O'Driscoll, and G. Lachapelle (2007) "Ultra-Tight GPS/INS for Carrier Phase Positioning In Weak signal Environments," *NATO RTO SET-104 Symposium on Military Capabilities Enabled by Advances in Navigation Sensors*, Antalya, Turkey, NATO

Phillips, R. E., and G. T. Schmidt (1996) "GPS/INS integration," Neuilly sur Seine, France, pp. 9-1, AGARD

Phocas, M., J. Bickerstaff, and T. Haddrell (2004) "GPS Jamming – the Enemy Inside!," *ION GNSS 17th International Technical Meeting of the Satellite Division*, 21-24 September, 2004, Long Beach, CA

Progri, I. F. (2006) "GPS L5 signal acquisition and tracking under unintentional interference or jamming," Monterey, CA, United states, 112-121, Institute of Navigation

Psiaki, M. L. (2001) "Smoother-Based GPS Signal Tracking in a Software Receiver," *ION GPS 2001*, Sept. 11-14, 2001, Salt Lake City, Utah, pp. 2900-2913

Psiaki, M. L., T. E. Humphreys, A. P. Cerruti, S. P. Powell, and J. Paul M. Kintner (2007) "Tracking L1 C/A and L2C Signals through Ionospheric Scintillations," *ION GNSS 2007*, Sept. 25-28, 2007, Fort Worth, TX, pp. 246-268

Psiaki, M. L., and H. Jung (2002) "Extended Kalman Filter Methods for Tracking Weak GPS Signals," *ION GPS 2002*, 24-27 September 2002, Portland, OR

Qaisar, S. U. (2009) "Performance Analysis of Doppler Aided Tracking Loops in Modernized GPS Receivers," *ION GNSS 2009*, 22-25 September Savannah, GA

Razavi, B. (1996) *Monolithic phase-locked loops and clock recovery circuits: theory and design*, Institute of Electrical and Electronics Engineers, INC., New York

Ross, T. J., J. M. Booker, and W. J. Parkinson (2002) *Fuzzy Logic and Probability Applications*, American Statistical Association Society for Industrial and Applied Mathematics, Alexandria, Virginia

Salem, D. R. (2010) *Approaches for the Combined Tracking of GPS L1/L5 Signals*, Geomatics Engineering, University of Calgary, Calgary

Saunders, S. R., and A. A. Zavala (2007) *Antenna and Propagation for Wireless Communication Systems*, John Wiley & Sons Ltd.

Shanmugam, S. K. (2007) "Narrowband Interference Suppression Performance of Multi-Correlation Differential Detection," *Proceedings of ENC-GNSS 2007*, May 29-31, Geneva, Switzerland

Simon, D., and H. El-Sherief (1994) "Fuzzy phase-locked loops," Las Vegas, NV, USA, 252-259, Publ by IEEE

Siouris, G. M. (2004) *Missile Guidance and Control Systems*, Springer

Spirent (2006) "Signal Generator Hardware User Manual," Spirent Communications

Titterton, D. H., and J. L. Weston (2004) *Strapdown Inertial Navigation Technology*, 2nd Edition Ed., The Institution of Electrical Engineers & The American Institute of Aeronautics and Astronautics

Unglaub, R. A. G., and C.-S. Tsang (1999) "Phase tracking by fuzzy control loop," in *Aerospace Conference, 1999. Proceedings. 1999 IEEE*57-66 vol.55

Ward, P. (1998) "Performance Comparisons Between FLL, PLL and a Novel FLL-Assisted-PLL Carrier Tracking Loop Under RF Interference Conditions," in *Proceedings of the 11th International Technical Meeting of The Satellite Division of The Institute of Navigation*,September 1998, Nashville, TN, pp. pp. 783–795

Ward, P. W. (1994) "GPS receiver RF interference monitoring, mitigation, and analysis techniques," *Navigation. Journal of the Institute of Navigation*, vol 41, no 4, pp. 367-391

Wendel, J., and G. F. Trommer (2004) "Tightly coupled GPS/INS integration for missile applications," *Aerospace Science and Technology*, vol 8, no 7, pp. 627-634

Zadeh, L. A. (1965) "Fuzzy Sets," *Information and Control*, vol 8, no 338-353,

Zoltowski, M. D., and A. S. Gecan (1995) "Advanced adaptive null steering concepts for GPS," *Military Communications Conference, 1995. MILCOM '95, Conference Record, IEEE*, 8 Nov 1995 San Diego, CA 1214 - 1218